



FUNDAMENTAL CHARACTERISATION OF COHERENT STRUCTURES FOR SWIRL COMBUSTORS

BY

ALI SAFA NOURI ALSAEGH

A thesis submitted in partial fulfilment of the requirements for the degree of:

Doctor of Philosophy

in

Mechanical Engineering (Power)

CARDIFF UNIVERSITY

SCHOOL OF ENGINEERING

GAS TURBINE RESEARCH CENTRE

MARCH 2022

TABLE OF CONTENTS

TABLE OF FIGURES	v
TABLES	xiii
NOMENCLATURE	xiv
ABBREVIATION LIST	xix
ACKNOWLEDGEMENT	xxiii
DEDICATION	xxiv
ABSTRACT	xxv
LIST OF PUBLICATIONS	xxvi
CHAPTER ONE:	
1 INTRODUCTION: UK ENERGY SECTOR STATISTICS AND THESIS OBJECTIVES	1
1.1 Introduction	1
1.2 United Kingdom Energy Sector (UKES) in Brief	1
1.2.1 Energy Landscape	2
1.2.2 Decarbonisation of Power Generation.....	6
1.2.3 Emission of Greenhouse Gases (GHGs).....	8
1.2.4 Overall Energy Consumption	11
1.3 Gas Turbine Engines	12
1.3.1 Gas Turbine Components and Principles of Operation	13
1.3.2 Gas Turbine Combustion Chambers.....	15
1.3.3 Gas Turbine Combustion Technologies	16
1.3.4 Gas Turbine Fuels and Fuel Flexibility	17
1.3.5 Gas Turbine Operation Challenges.....	19
1.3.6 Gas Turbine Emissions	20
1.3.7 NOx Control Technologies	22
1.3.8 Turbulent Reactive Flows in Industrial Processes.....	23
1.4 Motivation	23
1.5 Chapter Summary.....	25
1.6 Project Aims and Objectives	26
1.7 Thesis Structure.....	27
CHAPTER TWO:	
2 LITERATURE REVIEW: CHARACTERISTICS OF SWIRLING FLOW	29
2.1 Introduction	29
2.2 Combustion Phenomena in GTs	30

2.2.1	Principles of Combustion.....	30
2.2.2	Turbulent Premixed Combustion and Flame Regimes	32
2.2.3	Type of Flame.....	35
2.3	Flow Characteristics of Swirl-stabilised GT Burners	39
2.3.1	Principles of Swirl Flow	40
2.3.2	Characteristics and Structure of Swirling Flow	46
2.4	Modern Combustion Systems for GTs.....	54
2.4.1	Rich-Burn, Quick-Mix, Lean-Burn (RQL)	54
2.4.2	Trapped Vortex Combustion (TVC)	55
2.4.3	Staged Air Combustion	56
2.5	Lean Premixed Combustion (LPC).....	56
2.6	Flame Stability Issues	57
2.6.1	Lean Blowoff	57
2.6.2	Autoignition	59
2.6.3	Flashback	60
2.7	Alternative Fuels for GTs and Fuel Flexibility	68
2.8	Computational Fluid Dynamics (CFD) Modelling	70
2.8.1	CFD as a Tool for Design and Analysis.....	71
2.8.2	Modelling of Turbulence	71
2.9	Chapter Summary.....	73

CHAPTER THREE:

3	RESEARCH METHODS AND TECHNIQUES	76
3.1	Introduction	76
3.2	Experimental Approach and Facilities	76
3.2.1	The Swirl Burner	76
3.2.2	Non-Intrusive Laser Diagnostics.....	79
3.2.3	Laser Doppler Anemometry (LDA).....	80
3.2.4	Fluid Flow Seeding.....	85
3.2.5	Photography	87
3.3	Numerical Setup	87
3.3.1	The Sequence of CFD Modelling in ANSYS	88
3.3.2	Mathematical Formulation	89
3.3.3	Turbulence	92
3.3.4	Mesh Generation	97
3.4	Chapter Summary.....	100

CHAPTER FOUR:

4 THE HYDRODYNAMIC EFFECTS OF AXIAL AIR INJECTION ON SWIRL FLOW IN TANGENTIAL SWIRL BURNERS	101
4.1 Background and Chapter Objective.....	101
4.2 Experimental Setup.....	104
4.2.1 The Physical Model and Air Injection System.....	104
4.2.2 Test Cases	105
4.3 CFD Analysis	105
4.3.1 The CFD Package.....	105
4.3.2 Computational Domain	106
4.3.3 Mesh Generation	107
4.3.4 Solution Convergence	108
4.3.5 Mesh Independence Analysis	109
4.3.6 Operating and Boundary Conditions	111
4.3.7 Solution Method and Fluent Settings	111
4.4 Results and Discussion.....	113
4.4.1 The CFD Campaign.....	113
4.4.2 The Experimental Work.....	134
4.5 Chapter Summary and Conclusions	137

CHAPTER FIVE

5 IMPROVEMENT OF BLF FLASHBACK RESISTANCE IN SWIRL BURNERS USING NOZZLE WITH SCALLOPED RIBLET MICROSTRUCTURE SURFACE	139
5.1 Introduction	139
5.2 Experimental Setup.....	140
5.2.1 Swirl Burner and Experimental Facilities	141
5.2.2 Nozzle Manufacturing	142
5.2.3 Wire Electrical Discharge Machining (WEDM).....	142
5.3 Results and Discussion.....	144
5.3.1 The Isothermal Tests	144
5.3.2 The Combustion Tests.....	146
5.4 Chapter Summary and Conclusions.....	157

CHAPTER SIX

6 EFFECTS OF DIFFERENT NOZZLE CONFIGURATIONS ON SWIRL FLOW TOPOLOGY AND FLASHBACK PROPENSITY	159
6.1 Introduction	159
6.2 Experimental Setup.....	161

6.3	Results and Discussion.....	162
6.3.1	The Isothermal Experiments	162
6.3.2	The Combustion Tests	166
6.4	Chapter Summary and Conclusions	169
CHAPTER SEVEN		
7	RESULTS AND DISCUSSION	171
7.1	Summary of Discussion	171
7.2	Summary of Results.....	174
CHAPTER EIGHT		
8	CONCLUSIONS AND RECOMMENDATIONS FOR FURTHER WORK	179
8.1	CONCLUSIONS.....	179
8.2	Recommandations for Further Work	179
APPENDIX : (PHOTOGRAPHS AND DIAGRAMS)		181
REFERENCES		184

TABLE OF FIGURES

Figure 1-1: Electricity supplied by fuel type in the UK from 1950 to 2008. Reproduced from [8].	2
Figure 1-2: Shares of UK electricity generated by fuel type in 2019 and 2020. Reproduced from [12].	4
Figure 1-3: The transition of energy sector out to 2040: (A) primary energy consumption by fuel, (B, C) shares of primary energy. Reproduced from [14].	5
Figure 1-4: Proportion of UK energy supplied from low carbon sources from 2000 to 2020. Reproduced from [12].	6
Figure 1-5: Energy and carbon ratios in the UK from 1990 to 2020. Reproduced from [12].	7
Figure 1-6: UK territorial greenhouse gas emissions, 1990-2019. Reproduced from [19].	8
Figure 1-7: Trends of emissions in the UK. Reproduced from [6].	10
Figure 1-8: (A) Final energy consumption, actual and temperature corrected; (B) Total consumption in primary energy equivalents. Reproduced from [24].	11
Figure 1-9: Europe GT market size (US\$ Million), by application in 2017 and predicted for 2024. Reproduced from [28].	13
Figure 1-10: Components of a GT (SGT-750 GT developed by Siemens): 1- compressor rotor, 2-horizontal and vertical split casing, 3- guide vanes, 4- multi-stage compressor, 5- bearing and balancing planes, 6- combustor, 7- multi-stage compressor turbine, 8- online monitoring, 9- multi-stage power turbine. Reproduced from [29].	14
Figure 1-11: Illustration of two common combustor types: (A) tubo-annular combustion chamber arrangement, (B) annular combustion chamber. (Rolls Royce plc.). Reproduced from [30].	15
Figure 1-12: GT combustion concepts: (A) pre-mixed flame, (B) pre-mixed combustion system design. Reproduced from [30][32][33].	17
Figure 1-13: Range of gaseous fuel used in GT power plants. Reproduced from [33].	18

Figure 1-14: Effects of high levels of combustion instabilities, (A) new burner assembly, (B) damaged burner due to excessive combustion dynamics, (C) flashback damage. Reproduced from [35][41].	20
Figure 1-15: The effect of flame temperature on emissions. Reproduced from [30].	21
Figure 2-1: Combustion regimes (Borghi diagram) for turbulent premixed combustion. Reproduced from [69].	34
Figure 2-2: Combustion regime classification as a function of the reactant introduction scheme: (A) non-premixed (diffusion) flame, (B) mixing device and premixed flame. Reproduced from [72].	35
Figure 2-3: Schematic showing the structure of a laminar non-premixed (diffusion) flame. Adapted from [71].	36
Figure 2-4: Schematic showing the structure of a laminar premixed flame. Adapted from [72].	38
Figure 2-5: Schematic of: (A) radial-tangential swirler geometry ($Sg = 0.8$), (B) axial swirler geometry.	44
Figure 2-6: Coherent swirl flow structures of a typical confined swirl burner (radial-tangential swirler). Reproduced from [119].	46
Figure 2-7: (A) Process of the development of the CRZ in unconfined swirl flows, (B) the tangential velocity profiles within the CRZ. p is the centrifugal pressure, r is the radial distance from the burner centreline, w is the tangential (or azimuthal) velocity and u is the axial velocity. Reproduced from [88][120][122].	48
Figure 2-8: Visualisations of the PVC: (A) PVC and CRZ pairing, (B) PVC helical nature. Adapted from [88][102].	50
Figure 2-9: Differences between the levels of the fluctuating pressure caused by the PVC under different conditions: (A) isothermal, (B) combustion. Reproduced from [137].	51
Figure 2-10: Shear layer propagation in a swirling flame: (A) the full flame, (B) indication of the mixing and shear layers. Adapted from [102].	53
Figure 2-11: Rich-Burn, Quick-Mix, Lean-Burn (RQL) combustor: (A) combustor description, (B) NO _x rout. Adapted from [149].	55
Figure 2-12: Flow and flame configuration model (2D) at the onset of laminar boundary layer flashback (BLF). Adapted from [189].	62

Figure 3-1: Sketch of the burner, (not-to-scale). Reproduced form [121].....	77
Figure 3-2: Schematic top view of the swirl burner with 25%-25% inserts, (not-to-scale).....	78
Figure 3-3: Optical measuring systems employing light scattering. Reproduced from [229].	79
Figure 3-4: Test rig diagram and backscatter LDA system measurement setup. Reproduced from [232].	81
Figure 3-5: The parallel planes of high light intensity (the fringes). Reproduced from [232].	83
Figure 3-6: Doppler frequency to velocity transfer function for a frequency shifted LDA system. Reproduced from [63][232].	84
Figure 3-7: LDA measurement of the axial velocity profile for two different Al ₂ O ₃ seeding particle size.	87
Figure 3-8: Cell types employed for grid generation in ANSYS: (a) 2D model, (b) 3D model. Reproduced from [223].....	97
Figure 3-9: Skewness calculation explanation shape and its relation to mesh quality. Reproduced from [95].	99
Figure 4-1: Flame effects on centre-body under flame flashback. Adapted from [63].	102
Figure 4-2: Data movement paths between CFD predictions and experimental work during this study.....	103
Figure 4-3: Experimental setup of the modified burner design, (not-to-scale): (A) detailed view of central axial air injector; (B) the dual air/fuel injection technique.	104
Figure 4-4: Different burner configurations investigated in the CFD campaign with a swirl number (S_g) of 0.913.	106
Figure 4-5: CFD computational mesh of the burner (not-to-scale).....	107
Figure 4-6: Scaled residuals versus number of iterations of the numerical solution adopted for one of the simulated cases.	108
Figure 4-7: Velocity magnitude monitoring. Conditions: 600 l/min tangential flow rate without axial air injection.	109
Figure 4-8: Local swirl numbers (S) at different axial air jet flowrates.	114

Figure 4-9: Velocity vectors coloured by axial velocity (m/s) at burner mouth for tangential flow rate (400 l/min) with 50 l/min axial air jet represented in both axial and radial planes.	115
Figure 4-10: Axial velocity contours (m/s), isothermal flow, for (200 l/min) inlet tangential flow rate and $L_o=150$ mm (a) without axial air injection, and (b) with 50 l/min axial air injection.....	116
Figure 4-11: Axial velocity contours (m/s), isothermal flow, for (200 l/min) inlet tangential flow rate and $L_o=29$ mm (a) without axial air injection, and (b) with 50 l/min axial air injection.....	117
Figure 4-12: Axial velocity contours (m/s), isothermal flow, for (200 l/min) inlet tangential flow rate and $L_o=0$ mm (a) without axial air injection, and (b) with 50 l/min axial air injection.....	117
Figure 4-13: Axial velocity contours (m/s), isothermal flow, for (300 l/min) inlet tangential flow rate and $L_o=150$ mm (a) without axial air injection, and (b) with 50 l/min axial air injection.....	118
Figure 4-14: Axial velocity contours (m/s), isothermal flow, for (300 l/min) inlet tangential flow rate and $L_o=29$ mm (a) without axial air injection, and (b) with 50 l/min axial air injection.....	118
Figure 4-15: Axial velocity contours (m/s), isothermal flow, for (300 l/min) inlet tangential flow rate and $L_o=0$ mm (a) without axial air injection, and (b) with 50 l/min axial air injection.....	119
Figure 4-16: Comparison of axial velocity (m/s) measured by LDA with the CFD results for tangential flowrate of 600 l/min without axial air jet, $L_o=150$ mm at P_2	120
Figure 4-17: Comparison of axial velocity (m/s) measured by LDA with the CFD results for tangential flowrate of 800 l/min without axial air jet, $L_o=150$ mm at P_2	121
Figure 4-18: Comparison of axial velocity (m/s) measured by LDA with the CFD results for tangential flowrate of 600 l/min with 50 l/min axial air jet, $L_o=150$ mm at P_2	121
Figure 4-19: CFD results, the effect of axial air injection on the axial velocity defect downstream of the burner mouth, tangential flowrate 400 l/min, $L_o=150$ mm, at level $P_2=5$ mm.	122

Figure 4-20: CFD results, the effect of axial air injection on the axial velocity defect downstream of the burner mouth, tangential flowrate 600 l/min, $L_o=150$ mm, at level $P_2=5$ mm.	122
Figure 4-21: CFD results, the effect of axial air injection on axial velocity defect downstream of the burner mouth, tangential flowrate 800 l/min, $L_o=150$ mm, at level $P_2=5$ mm.	123
Figure 4-22: CFD results, the effect of axial air injection on the axial velocity defect downstream of the burner mouth, tangential flowrate 400 l/min, $L_o=29$ mm, at level $P_2=5$ mm.	123
Figure 4-23: CFD results, the effect of axial air injection on the axial velocity defect downstream of the burner mouth, tangential flowrate 600 l/min, $L_o=29$ mm, at level $P_2=5$ mm.	123
Figure 4-24: CFD results, the effect of axial air injection on the axial velocity defect downstream of the burner mouth, tangential flowrate 800 l/min, $L_o=29$ mm, at level $P_2=5$ mm.	124
Figure 4-25: CFD results, the effect of axial air injection on the axial velocity defect downstream of the burner mouth, tangential flowrate 400 l/min, $L_o=0$ mm, at level $P_2=5$ mm.	124
Figure 4-26: CFD results, the effect of axial air injection on the axial velocity defect downstream of the burner mouth, tangential flowrate 600 l/min, $L_o=0$ mm, at level $P_2=5$ mm.	124
Figure 4-27: CFD results, the effect of axial air injection on the axial velocity defect downstream of the burner mouth, tangential flowrate 800 l/min, $L_o=0$ mm, at level $P_2=5$ mm.	125
Figure 4-28: CFD results, the effect of axial air injection on the axial velocity defect downstream of the burner mouth $L_o=150$ mm, at level $P_2=5$ mm.....	125
Figure 4-29: CFD results, the effect of axial air injection on the axial velocity defect downstream of the burner mouth $L_o=29$ mm, at level $P_2=5$ mm.....	126
Figure 4-30: CFD results, the effect of axial air injection on the axial velocity defect downstream of the burner mouth $L_o=0$ mm, at level $P_2=5$ mm.....	126
Figure 4-31: CFD results, effect of axial air injection on the axial velocity defect downstream of the burner mouth at 1000 l/min flowrate $L_o=150$ mm, $P_2= 5$ mm.	127

Figure 4-32: CFD results, effect of axial air injection on the axial velocity defect downstream of the burner mouth at 1200 l/min flowrate $L_o=150$ mm, $P_2=5$ mm.	127
Figure 4-33: CFD results, effect of axial air injection on the axial velocity defect downstream of the burner mouth at 1400 l/min flowrate $L_o=150$ mm, $P_2=5$ mm.	128
Figure 4-34: Axial velocity component at different distances from burner dump plane (P_y), 600 l/min, $L_o=150$ mm.	128
Figure 4-35: CFD results, Axial velocity contour for 600 l/min, $L_o=150$ mm (a) with air injection, (b) without air injection.	129
Figure 4-36: Effect of axial air injection on turbulence intensity values, 400 l/min, $L_o=150$ mm, $P_2=5$ mm.	130
Figure 4-37: Effect of axial air injection on turbulence intensity values, 600 l/min, $L_o=150$ mm, $P_2=5$ mm.	131
Figure 4-38: Effect of axial air injection on turbulence intensity values, 800 l/min, $L_o=150$ mm, $P_2=5$ mm.	131
Figure 4-39: Effect of axial air injection on turbulence intensity values, 1000 l/min, $L_o=150$ mm, $P_2=5$ mm.	131
Figure 4-40: Effect of air injector position (L_o) on turbulence characteristics, 400 l/min and 50 l/min, $P_2=5$ mm, central air injection.	132
Figure 4-41: Effect of air injector position (L_o) on turbulence characteristics, 600 l/min and 50 l/min, $P_2=5$ mm, central air injection.	132
Figure 4-42: Effect of air injector position (L_o) on turbulence characteristics, 800 l/min and 50 l/min, $P_2=5$ mm, central air injection.	133
Figure 4-43: Effect of air injector position (L_o) on turbulence characteristics, 1000 l/min and 50 l/min, $P_2=5$ mm, central air injection.	133
Figure 4-44: Turbulent intensity contours (600 l/min), $L_o=150$ mm (a) with central air injection; (b) without central air injection.	134
Figure 4-45: Burner stability operation region (effect of using central air injection), $L_o=0$ mm.	135
Figure 4-46: Flame flashback trends at different central injector positions (L_o).	136

Figure 4-47: Stability map of the burner under the effect of 50 l/min axial air injection.	137
Figure 5-1: The tangential swirl burner with the new fitting (microstructured surface nozzle).....	141
Figure 5-2: Working principles of WEDM. Reproduces from [265].	143
Figure 5-3: The geometry of scalloped riblet microstructure surface on the nozzle wall.	144
Figure 5-4: Axial velocity distribution downstream the burner rim (a) nozzle with scallop riblet, (b) smooth nozzle.....	145
Figure 5-5: Effect of microstructure on turbulence intensity at the nozzle outlet. ...	146
Figure 5-6: Effect of using scalloped riblet microstructure nozzle on the outer boundary layer propagation, no axial air injection.	147
Figure 5-7: Flame structure of the scalloped riblet burner nozzle (no axial air) for stable operation at different Reynolds number (Re) and equivalence ratios (Φ).	149
Figure 5-8: Flame stability map of the microstructured nozzle, $h_n=25$ mm - central injector technique (i.e., no axial air injection).....	151
Figure 5-9: Effect of using microstructured nozzle on the stability map, $h_n=25$ mm – central injector technique (i.e., no axial air injection).	152
Figure 5-10: Flame shape of scalloped riblet microstructure nozzle; (a) without axial air, (b) with 50 l/min axial air injection.	153
Figure 5-11: Flame stability map of the microstructured nozzle, $h_n=25$ mm - axial injector technique (50 l/min axial air jet).	154
Figure 5-12: Effect of using microstructured nozzle on the stability map, $h_n=25$ mm – axial injector technique (50 l/min axial air jet).....	155
Figure 5-13: The stability map of the burner the microstructured nozzle (no axial air injection) versus that of the smooth nozzle with 50 lpm axial air injection. ...	156
Figure 6-1: Nozzle inner surface with 316 stainless steel woven wire as a liner....	161
Figure 6-2: The geometry of the Microsurfaces.....	162
Figure 6-3: LDA results, axial velocity for different nozzle heights ($h_n=25, 70$ mm), 800 l/min tangential flowrate.	163

Figure 6-4: LDA results, axial velocity for different nozzle heights ($h_n=25, 70$ mm), 1000 l/min tangential flowrate.	164
Figure 6-5: Turbulent intensity for different nozzle lengths (h_n) and different inlet tangential flowrates with air injection.....	164
Figure 6-6: Axial velocity downstream the burner nozzle for different surface roughness length strip.....	165
Figure 6-7: Contour of axial velocity downstream the dump plane (a) lining grid length (25 mm) (up left), (b) lining grid length (70 mm) (up right).....	166
Figure 6-8: Flame stability map of the long nozzle, $h_n=70$ mm - central injector (i.e., no axial air injection).	167
Figure 6-9: Effect of using the long nozzle on the stability map, $h_n=70$ mm – central injector technique (i.e., no axial air injection).....	168
Figure 6-10: Flame structure for stable operation at equivalence ratios (ϕ).	169

TABLES

Table 1-1: Annual electricity generated from renewable sources in the years 2000 to 2020. compiled from [12].	4
Table 1-2: Electricity capacity in the UK from 1996 to 2016. Compiled from [25].....	12
Table 1-3: NOx control technologies used for GTs. Compiled from [43].....	22
Table 2-1: GT's fuels Classification. Compiled from [217].	69
Table 2-2: Gas quality limits for entry into the UK NG system. WI values referenced at $P_2 = 0.101$ MPa and $t_1, t_2 = 288$ K. Compiled from data in [218][122].	70
Table 2-3: Turbulence models overview used in turbulence modelling [223].....	72
Table 3-1: Geometrical swirl number (Sg) values for different inserts.....	78
Table 3-2: The key features of RANS $k-\epsilon$ Turbulence Models available in ANSYS Fluent [223].....	94
Table 4-1: Air injector positions with respect to the burner baseplate.....	105
Table 4-2: Mesh size statistics.	110
Table 4-3: Numerical setup discretization for the RANS simulation of the isothermal swirl flows.	112

NOMENCLATURE

Greek Symbols

A_t	= Total area of tangential inlets	m^2
$C_{1\epsilon}$	= Model constant in k - ϵ equation	-
$C_{2\epsilon}$	= Model constant in k - ϵ equation	-
CV	= Fuel volumetric calorific value	J/m^3
D	= Characteristic length (exhaust diameter of swirl burner)	m
d_c	= The characteristics of an obstacle	m
d_d	= Diameter of the particle	m
D_e	= Exit burner diameter	m
D_s	= Burner sleeve diameter	m
d_f	= The fringe distance or spacing	μm
D_H	= Hydraulic diameter	m
D_{inj}	= Axial air injector diameter	m
D_t	= The inner diameter of tangential inlet	m
f	= Oscillation frequency (vortex shedding)	$1/s$
f_d	= Doppler (shift) frequency	Hz
f_s	= Frequency shift in LDA system	Hz
g	= Gravity	m/s^2
G_b	= The generation of turbulence kinetic energy due to buoyancy	m^2/s^2
G_k	= The generation of turbulence kinetic energy due to the mean velocity gradient	m^2/s^2
G_θ	= Axial flux of tangential momentum	$kg \cdot m/s$
G_x	= Axial momentum flux	$kg/m \cdot s$
H	= Distance to the stagnation point	m
k	= The mean kinetic energy per unit mass associated with eddies in turbulent flow	m^2/s^2
l_o	= The integral turbulent length	m

N	= The number of image pairs applied in the PIV tests	-
P	= The static pressure	in. wc
Q	= The total flow rate	m ³ /s
r	= The radial component of the swirl flow	-
r _e	= Characteristic radius (the exit nozzle radius of the tangential burner)	m
Re	= Reynolds number	-
R _{eff}	= Effective burner radius	m
Ri	= Richardson number	-
r _i	= Radius of burner plenum	m
S	= Local swirl number	-
S _g	= Geometrical swirl number	-
S _{g,comb}	= Geometrical swirl number under combustion conditions	-
S _{g,iso}	= Geometrical swirl number for isothermal conditions	-
S _T	= Turbulent flame speed	m/s
S _l	= Laminar flame speed	m/s
Ś	= The modulus of the mean rate-of-strain tensor in realizable <i>k-ε</i>	-
S _k	= User-defined source terms in <i>k-ε</i> equation	-
S _ε	= User-defined source terms in <i>k-ε</i> equation	-
S _{Mi}	= The gravitational body force in i-direction	kg/m.s
Sr	= Strouhal number	-
Ś _r	= Strouhal number as a function of the swirl number	-
S _g	= Geometrical swirl number	-
Stk	= Stokes number	-
t	= Time	s
T _{int}	= Relative turbulence intensity	%
T _{inlet}	= The inlet temperature of the fluid	K
T _{outlet}	= The outlet temperature of the fluid	K

u	= Velocity components in x direction (axial)	m/s
U	= Mean velocity value	m/s
U_b	= Average bulk burner exit axial velocity	m/s
\bar{u}	= Mean velocity at burner exit nozzle	m/s
u'_a	= Fluctuating axial velocity	m/s
u'_t	= Fluctuating tangential velocity	m/s
\acute{u}	= Fluctuating velocity value.	m/s
u_τ	= The wall friction (shear) velocity	m/s
u_i	= Instantaneous velocity component	m/s
u_{RMS}	= Root-mean-square velocity value	m/s
v	= Velocity components in y	m
\vec{V}	= Velocity vector	m/s
VB_{crit}	= Vortex Breakdown critical conditions for appearance	-
w	= Velocity components in z (tangential)	m
WI	= Wobbe Index	MJ/Nm ³
y	= The tangential component of the swirl flow	m
y^+	= The y mesh value at the wall	m
Y_M	= The contribution of the fluctuating dilatation in compressible turbulence to the overall dissipation rate	-

Latin Symbols

Φ	= Equivalence ratio	-
β	= Thermal expansion coefficient	1/K
Ω_{ij}	= Represents the mean rate-of-rotation tensor viewed in a moving reference frame with the angular velocity	-
λ_{LDA}	= The LDA laser wavelength	nm
ρ_d	= Seeding particle density	kg/m ³
μ_t	= The turbulent (eddy) viscosity	kg/m.s

μ_{to}	= The turbulent viscosity value calculated without the swirl modification	kg/m.s
μ_f	= Dynamic viscosity of the fluid	kg/m.s
δ_l	= The laminar flame thickness	mm
\emptyset	= The unknown variable in the general transport equation	-
α	= Thermal diffusivity	m ² /s
σ_k	= Realizable k - ε turbulence model constant	-
σ_ε	= Realizable k - ε turbulence model constant	-
ν	= Kinematic viscosity	m ² /s
ρ	= Fluid density	Kg/m ³
Γ	= The diffusion coefficient in the general transport equation	-
τ_m	= The flow time scale	s
τ_c	= The chemical time scale	s
ε	= The dissipation of the kinetic energy of turbulence	m ² /s ³
θ	= Angle between laser beams in the LDA system	degree
η_k	= The Kolmogorov length scale	Mm
ΔT	= Temperature difference	K
τ_{ij}	= Viscous stress component acts in the j-direction on a surface normal to i-direction	N/m ²
τ_s	= Seeding particle relaxation time	s
ϑ	= The stress tensor	-

Subscripts

Act	= Actual
e	= Exit of the burner
eff	= Effective
g	= Geometrical
i	= Inner
stoicio	= Stoichiometric

t = Tangential

inj = Injection

pos = Positive

neg = Negative

Chemical Compounds

C_3H_8 = Propane

CH_4 = Methane

CO = Carbon monoxide

CO_2 = Carbon dioxide

H_2 = Hydrogen

H_2O = Water

H_2S = Hydrogen sulfide

N_2 = Nitrogen

NH_3 = Ammonia

ABBREVIATION LIST

BFG	Blast furnace gas
BLF	Bounday layer flashback mechanism
BSI	The British Standards Institution
CAD	computer aided design
CCGT	Combined cycle gas turbine
CCS	Carbon capture and storage
CFD	Computational fluid dynamics
CIVB	Combustion induced vortex breakdown flashback mechanism
CPU	Central processing unit
CRZ	Central recirculation zone
DES	The detached eddy simulation turbulence method
DLE	Dry low emissions
DNS	Direct Numerical Simulations turbulence model
DZ	The dilution combustion zone
EDF	Energy company
EPR	Third generation pressurised water nuclear reactor
EU	The European Union
FR	Fuel reburning
FBN	Fuel bound NO _x pathway
FDM	The finite difference method
FEM	The finite element method
FFT	Fast Fourier transform
Fps	Frame per second
FVM	The finite volume method
G8	The eight highly industrialised nations
GHG	Greenhouse gas emissions

GS(M)R	Gas Safety (Management) Regulations (UK)
GW	Gigawatt
GWP	Global warming potential
GT	Gas turbine
GTRC	Gas turbine rsearch center of Cardiff University
HCV	The higher calorific value
HENG	Hydrogen enriched natural gas
HMFR	High momentum flow region
HSP	High-speed photography
hydro	The hydroelectric renewable energy source
IA	Interrogation area
IC	Internal combustion
Ktoe	Kilotonne of oil equivalent
LBO	Lean Blowoff
LCV	The lower calorific value
LES	Large eddy simulation turbulence model
LDA	Laser Doppler Anemometry
LDI	Lean direct injection technology
LED	Light emitting diode
LNB	Low NOx burners
LNG	Liquefied natural gas
LPC	Lean primixed combustion
LPM	Lean premixed mixture
LPP	Lean pre-vaporized premixing
MtCO ₂ e	Million tons of CO ₂ equivalent
NG	Natural gas
NGR	Natural gas reburning
NMVOCs	Non-methane volatile organic compounds

NTPR	Non-thermal plasma reactor
OEMs	Original equipment manufacturers
ORZ	Outer recirculation zone
PISO	Pressure-velocity correction algorithm
PIV	Particle image velocimetry
PLF	Premixed laminar flame
POD	Proper orthogonal decomposition
PZ	Primary combustion zone
PV	Solar photovoltaics
PVC	Precessing vortex core
RAM EDM	Electrical Die Sinking
RANS	The Reynolds Averaged Navier-Stokes turbulence model
RD	Relative fuel density
RHS	Right hand side
RQL	Rich–burn quick-mix lean-burn combustion
rpm	Revolutions per minute
SCR	Selective catalytic reduction
SIMPLE	Pressure-velocity correction algorithm
SIMPLEC	Pressure-velocity correction algorithm
SL	Shear layer in swirling flow
SNCR	Selective non-catalytic reduction
SGS	Subgrid-scale model
TTL	Transistor-transistor logic
TVC	The trapped vortex combustor
TWh	Terawatt hour
UHC	Unburned hydrocarbon
UK	The United Kingdom
UKES	United Kingdom energy sector

USA	The United States of America
VBD	The vortex breakdown in the swirl flow
VG	Variable geometry
VLES	The very large eddy simulation turbulence model
WEDM	Wire Electrical Discharge Machining
WI	Wobbe index
YOY	Year on year

ACKNOWLEDGEMENTS

First and foremost, I would like to praise and thank GOD for always being with me, in good and bad times, always being the sunshine when the skies are dark, guiding me to the best that I can give and helping me complete this thesis. Second, I would like to share my most enormous thanks for my country and many heroes who have sacrificed their lives to protect Iraq and keep it safe.

I wish to express my gratefulness to my supervisors, Dr. Agustin Valera-Medina and Prof. Phil Bowen, for allowing me to do my PhD under their supervision. Thank you for all the advice, recommendations, suggestions, patience in my inquiries, valuable feedback, and constructive criticism, which motivated me to do my best.

I would like to thank the staff of the School of Engineering, the staff of the Gas Turbine Research Centre (GTRC), and the staff of the Research Office for all the help over the last few years. Special thanks for whom I will never forget going to the following: (Mrs. Aderyn Reid, Mrs. Chris Lee, Mrs. Jeanette Whyte). Special thanks to the academic and industrial partners in the Flex-E-Plant Consortium, in particular Mr. David Abbott from Uniper Technologies and Dr. Suresh Sadasivuni from Siemens. My great thanks extended to all laboratory technicians for their help in offering me the facilities to complete my experiments. Finally, I sincerely appreciate the help of the technical team of the Mechanical Engineering Workshop, especially Mr. Malcom Seaborne and Mr. Paul Malpas. Their technical knowledge contributed to the successful completion of this work.

Special thanks should be given to my wife (Dr. Najlaa Alboshmina) for her enduring love, for believing in me and for sharing my wish to reach the goal of completing this task, thanks for your constant care and kindness in the most challenging days. My deepest thanks to my lovely kids, Nawar, Hussein and Summer (my new-born baby that I have never seen yet); you inspired me with your patience and love, even as you bore my permanent activity. Extraordinary thanks to my mother (the hero of Viber and WhatsApp). I did it mum and hope I could tell you all about it; I will miss you until the day we meet again. My deepest thanks, love, and gratitude for all my family, brothers (Ahmed and Zaid), sister (Shaimaa), my auntie (Suaad) and friends who have had never let me feel alone over these years; thanks for your calls and incredible messages.

I want to extend my thanks to the Iraqi Government for sponsoring my PhD study, and many thanks to the staff of the Iraqi cultural attaché in London for their help during my stay in the UK.

I could not have done this without you all, and my journey from Iraq to Cardiff would have remained simply a dream.

DEDICATION

This thesis is dedicated to the memory of my father,

Safa Nouri Marzoog Alsaegh,

the man who taught me to perform all of life's tasks no matter how big or small, to the best of my ability and without complaint. He is the man I will always aspire to be.

ABSTRACT

Swirl combustors have demonstrated that they can effectively stabilise flames across a wide range of operating conditions due to established, widely known but not fully understood swirl coherent structures. Unfortunately, their use in lean premixed (LP) modes as occurs with the introduction of alternative fuels, particularly blends with a relatively high hydrogen content can result in unstable combustion. An important such instability is a flame flashback which can cause considerable hardware damage to the combustion system as well as significantly increasing pollutant levels. Combustion Induced Vortex Breakdown (CIVB) and Boundary Layer Flashback (BLF) which are a result of interaction between swirl structures and burner geometry is an important modes of flashback instabilities because they can occur even when the velocity of the combustible mixture is greater than the flame speed. This project is part of the attempts to improve burner geometry and control swirl flows to increase resistance to these modes of flashback.

This investigation used numerical and experimental methods to ascertain the effect of a range of burner designs on flame flashback processes. Experiments were carried out on a 150-kW tangential swirl burner operating in a premixed mode to demonstrate practically the effectiveness of the flame flashback resistance methods techniques for premixed fuels. The flow field characteristics were simulated by the ANSYS Fluent code. The experimental work was carried out using a 1D LDA system which provided the required measurements for the swirl flow.

First hydrodynamic parameters were investigated with the intention of enhancing resistance against CIVB flashback. Initially, by replacing the central fuel injectors by axial air injection. The effects were assessed using ANSYS Fluent code. It was confirmed that axial air jets had good possibilities for improving flame stability, producing a wider range of stable operations than did central fuel injectors. In addition, the increase in stability occurred with equivalence ratio and tangential inlet velocity. The use of these air jets also promised lower maintenance costs because the working environment of the combustor would not be so harsh. Unfortunately, reducing the likelihood of CIVB can increase the likelihood of a different flashback mechanism, Boundary Layer Flashback (BLF).

Thus, the second part of the research programme was to experimentally combine techniques that increased CIVB resistance (e.g., using central air injection) while at the same time evading BLF (e.g., by modifying the characteristics of the wall boundary layer). The former technique was achieved by applying a scalloped riblet geometry to the nozzle surface. Results confirm that combining these techniques is very promising regarding achieving a wider range of stable operations, enabling swirl combustors to burn a wider variety of fuel blends efficiently and safely.

Then the work was extended to investigate the effects of different burner nozzle heights on the characteristics of the swirl flow. Finally, a new technique to reduce Boundary Layer Flashback (BLF) using biomimetic engineering methods has been established and tested. A stainless-steel woven wire mesh liner has been used with different heights to modify the internal surface roughness of the longest smooth burner nozzle. It was confirmed that inserting the mesh as a liner changed the structure of the flow adjacent to the burner wall, increasing resistance to Boundary Layer Flashback. It was demonstrated that the likelihood of Boundary Layer Flashback was reduced by using the designed micro-surfaces, the shorter the woven wire mesh liner, the better effect. It is suggested that by combining the different flow manipulation techniques, there is the potential for increasing the fuel flexibility of GTs.

LIST OF PUBLICATIONS

Ali Alsaegh, Agustin Valera-Medina, Najlaa Alboshmina, M. A. Al-Fahham, Fares A. Hatem, Chong C T: Effects of different nozzle configurations on swirl flow topology in tangential swirl burners. Energy Procedia, 2019, Vol. 158, pp. 2317-2322.

DOI: [10.1016/j.egypro.2019.01.269](https://doi.org/10.1016/j.egypro.2019.01.269).

Ali Alsaegh, F.A. Hatem, Agustin Valera-Medina: Visualisation of Turbulent Flows in a Swirl Burner under the effects of Axial Air Jets. Energy Procedia, 2017, Vol. 142, pp. 1680-1685.

DOI: [10.1016/j.egypro.2017.12.549](https://doi.org/10.1016/j.egypro.2017.12.549).

Ali Alsaegh, F.A. Hatem, Agustin Valera-Medina: CFD Simulation and Validation of Hydrodynamic Instabilities Onset in Swirl Combustors. The 8th European Combustion Meeting (ECM), Dubrovnik, Croatia, 2017, pp.1507-1512.

URI: <http://orca.cardiff.ac.uk/id/eprint/99265>.

Najlaa Alboshmina, Agustin Valera-Medina, **Ali Alsaegh**: Ammonia- hydrogen combustion in a swirl burner with reduction of NOx emissions. Energy Procedia, 2019, Vol. 158, pp. 2305-2310.

DOI: [10.1016/j.egypro.2019.01.265](https://doi.org/10.1016/j.egypro.2019.01.265).

F.A. Hatem, **Ali Alsaegh**, M. Al-Faham, Agustin Valera-Medina, C.T. Chong, S.M. Hassoni: Enhancing flame flashback resistance against combustion induced vortex Breakdown and Boundary Layer Flashback in swirl burners. Applied Energy, 2018, Vol. 230, pp. 946-959.

DOI: [10.1016/j.apenergy.2018.09.055](https://doi.org/10.1016/j.apenergy.2018.09.055).

F.A. Hatem, **Ali Alsaegh**, M. Al-Faham, Agustin Valera-Medina: Enhancement flame flashback resistance against CIVB and BLF in swirl burners. Energy Procedia, 2017, Vol. 142, PP. 1071-1076.

DOI: [10.1016/j.egypro.2017.12.358](https://doi.org/10.1016/j.egypro.2017.12.358).

M. Al-Faham, F.A. Hatem, **Ali Alsaegh**, Agustin Valera-Medina, Samuel Bigot: Experimental study to enhance resistance for boundary layer flashback in swirl burners using microsurfaces. ASME Turbo Expo 2017: Turbomachinery Technical Conference and Exposition, Charlotte, North Carolina, USA, 2017. Paper number GT2017-63367.

DOI: [10.1115/GT2017-63367](https://doi.org/10.1115/GT2017-63367).

F.A. Hatem, **Ali Alsaegh**, Agustin Valera-Medina, Nick Syred: Experimental investigation of the Effect of Air Diffusive injection on premixing swirl flames. 55th AIAA Aerospace Sciences Meeting, Grapevine, Texas, 2017. Paper number AIAA 2017-0778.

DOI: [10.2514/6.2017-0778](https://doi.org/10.2514/6.2017-0778).

F.A. Hatem, **Ali Alsaegh**, Agustin Valera-Medina: Experimental and numerical investigation of the effect of diffusive air injection on turbulence generation and flashback propensity in swirl combustors. The 8th European Combustion Meeting (ECM), Dubrovnik, Croatia, 2017, pp.59-64.

URI: <http://orca.cardiff.ac.uk/id/eprint/99196>.

F.A. Hatem, M. Al-Faham, **Ali Alsaegh**, Zaid Al-Dulami, Agustin Valera-Medina: Experimental investigation of the effects of bluff-body size and axial air injection on blowoff limits of swirl burners. Journal of Engineering Science and Technology, 2021, Vol. 16, pp. 2202-2214.

URI: <http://orca.cardiff.ac.uk/id/eprint/142516>.

Chapter 1

Introduction:

UK Energy Sector

Statistics and Thesis

Objectives

CHAPTER ONE:

1 INTRODUCTION: UK ENERGY SECTOR STATISTICS AND THESIS OBJECTIVES

“To raise new questions, new possibilities, to regard old problems from a new angle, requires creative imagination and marks real advance in science”

Albert Einstein, German Physicist (1879-1955)

1.1 Introduction

This chapter starts with a presentation of global and local (UK) statistics concerning energy usage, energy resources and pollutants from energy generating plants. In addition, relevant details of selected gas turbines (GTs) and combustion technologies are also introduced. After that, a brief description of the motivation for undertaking the present, work, followed by the aims of the project, research questions to be answered, and research methods are presented. Finally, the chapter ends with the layout of the thesis.

1.2 United Kingdom Energy Sector (UKES) in Brief

The United Kingdom energy sector (UKES) in particular, and the global energy sector generally, are subject to systemic challenges in both generation and consumption, represented by the unavailability of revolutionary new technology or fantastic new energy resources except the fracking process and the using of shale gas in power generation sector which is still controversial. In the UK, fracking and shale gas appear to promise bountiful supplies estimated a possible a trillion cubic metres in the Bowland Shale Formation, north-west England alone [1]. Fracking in the United States (USA) doubled natural gas (NG) production in about ten years [2]. Significant obstacles might be faced to maintain the current energy resources through and beyond the current century.

As modern societies need ever-increasing amounts of energy from an ageing traditional fuel supply (fossil fuel) and the slow growth of the renewable energy sector, the near future will witness an international conflict among geologic depletion and technological developments [3]. In the next sub-sections, all statistics and figures are

for the UK only (except [Figure 1-3](#)) and exclude Crown Dependencies and Overseas Territories to emphasise a reduction in unwanted emissions, increased efficiency to reduce running costs and flexibility regarding the use of different fuel gases.

1.2.1 Energy Landscape

The UK economy needs a vast and continuous power supply. Learning from the lessons of the past, it is necessary to develop new energy technologies to increase efficiency and flexibility when consuming known resources [\[4\]](#). In general, the supplied electrical energy can be categorised according to its source and fuel. In the meantime, different sources are using in the UK to meet the requirements of the day and those range from fossil fuels, to low-carbon sources, to others [\[5\]](#). In the UKES, NG, coal and oil represent the carbon sources, while the low carbon sources are nuclear and renewables such as wind, biofuels, solar photovoltaics (PV) and hydro [\[6\]](#).

Historically, the primary public electricity supply in the UK was generated by hydropower, but was soon displaced by coal as the primary fuel for power generation, in 1950 the energy output from coal-based power stations was 97% of the total energy production in the UK [\[7\]](#). Coal continued to dominate power generation, but by 1970 oil had passed hydro to be the second largest source of energy, accounting for 16% of all power generation in the UK. At this time NG made only a minimal contribution. The early 1970s was a peak in oil use while the second peak in oil usage occurred around 1990, see [Figure 1-1](#) [\[8\]](#).

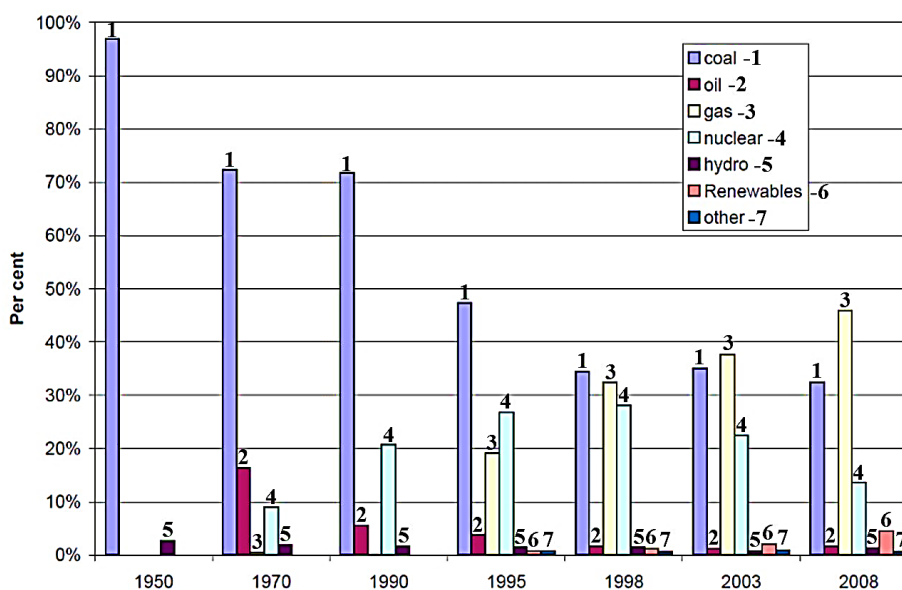


Figure 1-1: Electricity supplied by fuel type in the UK from 1950 to 2008. Reproduced from [\[8\]](#).

Post-1990, in the UK, it can be seen in [Figure 1-1](#) a steady and rapid increase in gas-fired power stations with the installation of efficient combined-cycle gas turbines (CCGT) [8]. This was accompanied by a clear decrease in coal powered generation. In 1999 gas usage exceeded that of coal [9]. The decline in coal-fired power and the growth of gas have been the most marked characteristic in electrical power generation, post 2000. Gas has represented the primary fuel for power generation in the UK since the millennium and is seen as a clean and efficient fuel. In the first quarter of 2018, the gas-based electricity generated about 40% of the total electrical power produced in the UK [10].

Concerning nuclear power generation, in 1970, nuclear energy began its challenge to the dominant position held by coal, increasing from 9% to 21% between 1970 and 1990, and rising to 28% in 1998. However, public apprehension fuelled by the disasters at Chernobyl in 1986 and Fukushima in 2011 meant that as nuclear power stations came to the end of their working lives, they were not replaced by the end of 2008. The percentage supplied by nuclear had dropped to 13% as shown in [Figure 1-1](#) [8].

The nuclear option might generate strong opinions but just how much energy does it generate. In the meantime, there are 15 reactors left in the UK and by 2035 all these will have been retired. So, what is next for nuclear in the UK? British Government plans to have EDF Energy company build two EPR nuclear reactors (a third-generation pressurised water reactor) at Hinkley Point in Somerset. This project will be finished in 2025 as expected, and it will hope to bring about 7% of the UK energy needs. However, it is still some doubts about what nuclear energy really looks like in the future [11].

Due to the reduction in electricity demand caused by Covid-19 pandemic, the total electricity generated in the UK decreased by 3.6% between 2019 and 2020. The electricity generated from coal dropped a further 0.3 percentage points from 2.1% to 1.8%, continuing a long-term downwards trend. The share of electricity generation from gas declined from 40.7% to 35.7%, while the percentage from nuclear decreased from 17.4% to 16.1% as illustrated in [Figure 1-2](#) [12].

Regarding renewable energy, wind, waste and hydro, following 2000, there was a noticeable development in the generation and by 2008 renewable power was contributing 5.5% of total electricity generation, return to [Figure 1-1](#) [8]. Continuous investments in this sector helped by governmental tax incentives and “feed-in”

subsidies [13], meant renewable power provided 30.1% of the total electricity generated in the UK in the first quarter of 2018 [10].

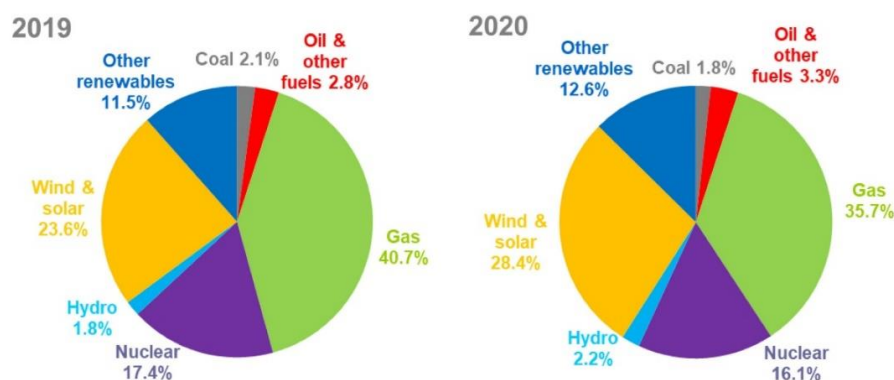


Figure 1-2: Shares of UK electricity generated by fuel type in 2019 and 2020. Reproduced from [12].

In 2020, the decline in electricity supplied from fossil fuels was enabled by increased generation from renewables, which increased its share of generation from 36.9% in 2019 to a record 43.2% in 2020 [12], see Figure 1-2 and Table 1-1.

Table 1-1: Annual electricity generated from renewable sources in the years 2000 to 2020. compiled from [12].

	TWh				
	2000	2010	2018	2019	2020
Onshore wind	0.9	7.2	30.4	31.8	34.7
Offshore wind	-	3.1	26.5	32.0	40.7
Solar PV	-	0.0	12.7	12.6	13.2
Hydro	5.1	3.6	5.5	5.9	6.8
Landfill Gas	2.2	5.2	3.9	3.6	3.5
Other Bioenergy	1.7	7.0	31.1	33.7	35.8
Total Renewables	9.9	26.2	110.1	119.5	134.6

Table 1-1 shows the electricity generated from renewable sources in the years 2000 to 2020 [12]. The increase in renewables' generation in 2020 came after unusually high wind speeds and the increase in average rainfall during the year. Total wind generation increased by 18% to a record 75.4 TWh thanks to exceptionally strong wind speeds; within this, offshore wind generation rose by over 27% in 2019 to 40.7 TWh in 2020, surpassing onshore wind at 34.7 TWh. Wind generation was particularly high during Quarter 1 of 2020, when storms Clara and Dennis hit the UK. Average onshore wind speeds in 2020, at 9.1 knots, were 0.8 knots higher than in 2019. Hydro generation increased by 15% in 2020, largely due to an increase in average rainfall,

which was up by 23% on 2019. Generation from solar PV increased by 4.6% in 2020 as compared with 2019, following a small increase in capacity and average sun hours (up 0.2 hours in 2020). Generation from bioenergy and waste (excluding landfill gas) increased by 6.3% between 2019 to 2020 [12].

Finally, for a complete understanding of the UK power generation sector position compared with the worldwide trend, an overview of the future global direction of the energy generation sector needs to be briefly mentioned. To have a clear conception about the global primary energy generation by fuel type and the shares of primary energy in the next decades out to 2040, see Figure 1-3 [14]. This figure shows the path of energy transition out to 2040 and what likely to happen for the energy sector in the future not only in the UK but in the world. NG is the wave of the future of electricity production in the globe with no other power source even close to matching NG's potential in the future. It is an on-demand energy source that essentially decreases air pollution as compared to coal. A 45% increase has been expected in global NG use by 2040. The expected growth in global NG power is attached to its value in reducing air pollution rather than an anticipated cost as compared with the other fossil sources [14].

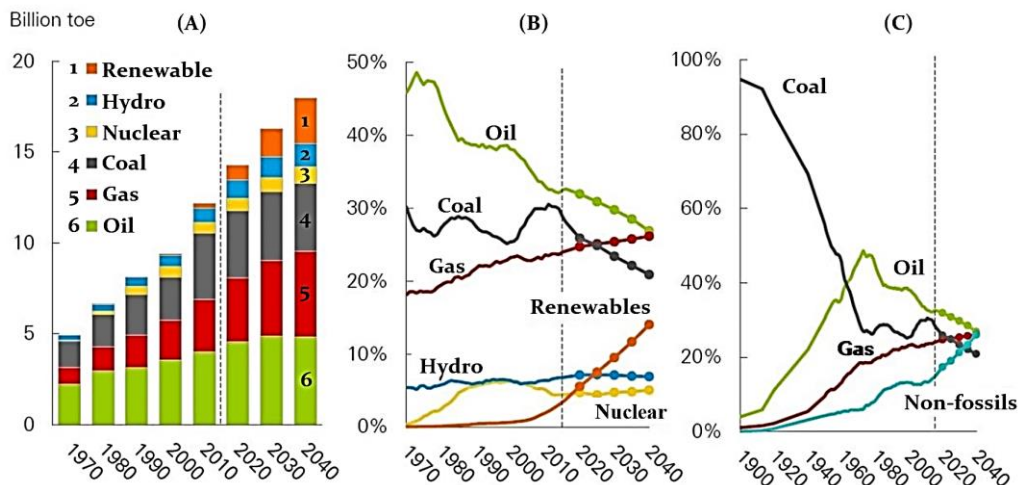


Figure 1-3: The transition of energy sector out to 2040: (A) primary energy consumption by fuel, (B, C) shares of primary energy. Reproduced from [14].

However, government policies, social preferences and new technologies will change how energy is generated and used in the future in ways which are difficult to predict now. In any case, the gas-fired electrical power generation will continue as a major contributor to the global supply and in that context, there is a need to ensure that the gas turbines used are as efficient and as flexible as possible. This trend in power

generation will be different in the UK as the government targets no gas power generation and the renewables will become dominant in the energy market certainly beyond 2035 [12].

1.2.2 Decarbonisation of Power Generation

The UKES is embarking on possibly its most significant step towards decarbonisation to reduce greenhouse gas (GHG) emissions, which are widely accepted to accelerate adverse global climate change. The goals also include (i) to secure energy resources sufficient to meet required needs, (ii) to produce efficiently to meet the environmental standards of the day and (iii) to ensure a reliable and affordable energy supply [15]. Both consumers and government are expecting the energy industry to play an important and essential role in the path towards a low carbon economy.

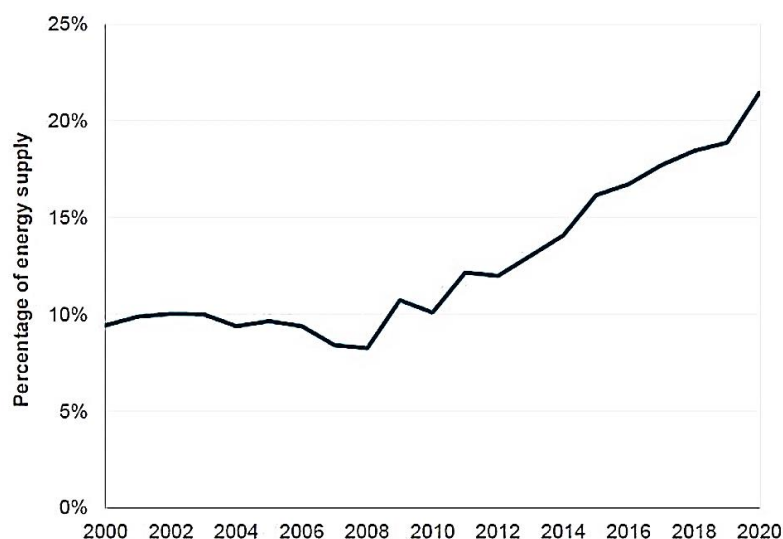


Figure 1-4: Proportion of UK energy supplied from low carbon sources from 2000 to 2020. Reproduced from [12].

The marked increase in low carbon energy produced in the UK that occurred after 2008 has continued until now, as shown in Figure 1-4 [12]. The UK played an essential role in the 2015 Paris agreement, which builds upon existing UK legislation that aims to reduce the GHG 1990 emissions levels by 50% ahead of 2030 and 100% before 2050 [16]. In this international agreement, 195 countries have committed to work together as a team to minimise the effect of the energy generation sector, to reduce the GHG emissions and hence mitigate climate change. Following the Paris 2015 agreement, the UK participated in international efforts, and there have been noticeable increases in carbon reduction targets. In 2020 the UK obtained 21.5% of

its primary energy from low carbon sources, with 37% of this from bioenergy, 31% from nuclear, and 18% from wind. From 2019 to 2020, the energy supplied from biofuels increased by 3.9% and wind energy increased by 18% with capacity up by 2.5%, whilst solar was up by 4.4% reflecting increased capacity; however, the supply of nuclear fell by 11% due to numerous outages at all 8 of the UK's power stations during 2020 [12].

The latest data in a survey by BP of energy and carbon emissions showed that in the group of highly industrialised nations (G8) the energy ratio is falling [14]. The energy ratio is found by dividing temperature corrected primary energy consumption (primary supply less non-energy use) by gross domestic product (GDP) at constant prices, with the carbon ratio similarly calculated by dividing CO₂ emissions by GDP.

Figure 1-5 illustrates that both energy ratio and carbon ratio in the UK have dropped steadily over the period of the survey, 1990-2020 [12]. This trend is expected to be the same for the EU and continue until 2040, at which date the countries of the present EU will consume the same amount of energy, in total, as they did in 1975. This was possible due to continuous improvements in the efficiency of the energy sector [14]. Figure 1-5 shows that the energy ratio declined by around 2.5% per year, and the carbon ratio dropping at a faster pace of just over 3.5% per year, despite the level of GDP continuously increasing.

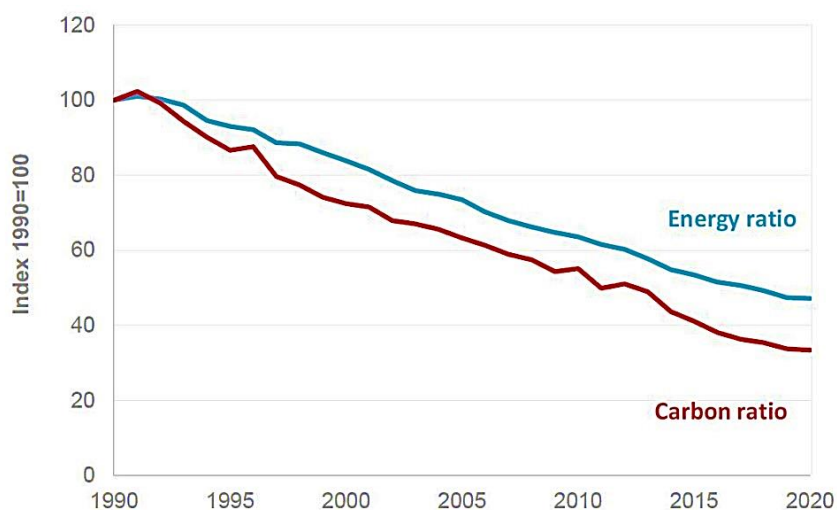


Figure 1-5: Energy and carbon ratios in the UK from 1990 to 2020. Reproduced from [12].

These downward trends for both energy and carbon ratios are due to enhancements in energy efficiency and the reduction in the relative importance of energy-intensive

industries, such as steel. The additional improvement in carbon ratio has been achieved due to using more renewables and carbon efficient fuels. Currently, the UK leads the transition to a lower carbon economy and it is estimated to have the lowest energy ratio in the EU [17].

1.2.3 Emission of Greenhouse Gases (GHGs)

Air pollution is a local, regional, and global challenge produced by the emission of pollutants. It is a global dilemma as the air pollutants emitted in any one place may be transferred within the atmosphere, sharing harmful consequences across the globe. These pollutants can be emitted directly or can be formed through chemical reactions with other contaminants and the environment that lead to a negative impact on ecosystems and the health of individuals. Knowledge of the sources and estimations of the effects of different pollutants released into the air aids the development of policies and strategies to minimise air pollution generated by human activities and hence diminish its impact on the environment and our health [18]. In 2019, net territorial emissions in the UK of the basket of seven greenhouse gases covered by the Kyoto Protocol were estimated to be 454.8 million tonnes carbon dioxide equivalent (MtCO₂e), a decrease of 2.8% compared to the 2018 figure of 468.1 million tonnes and 43.8% lower than they were in 1990 as shown in Figure 1-6. Carbon dioxide made up around 80% of the 2019 total [19].

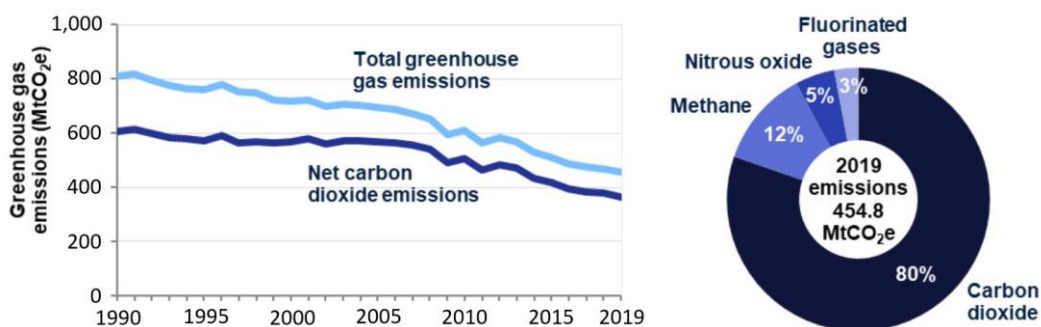


Figure 1-6: UK territorial greenhouse gas emissions, 1990-2019. Reproduced from [19].

In the UK, the dominant sectors in terms of total emissions of GHGs are the transport and the energy sectors, almost entirely through carbon dioxide (CO₂) emissions. The transport sector was the most significant source of emissions in 2019, accounting for 27% of total GHG emissions (mainly CO₂ emissions) in the UK. The transport sector consists of emissions from road transport, railways, domestic aviation, shipping, fishing, and aircraft support vehicles. About 8.14% of transport sector emissions in

2019 came from civil aviation while road transport, in particular passenger cars, is by far the highest emitter accounting about 70% of all GHG emissions from this sector. The total emissions from the transport sector in the UK decreased only by around 5% between 1990 and 2019, as increased road traffic has largely offset improvements in vehicle fuel efficiency of both diesel and petrol vehicles. In the future, most fuels used for mobility would require to be of a non-fossil source to achieve a decline in GHG emissions. However, the use of liquefied natural gas (LNG) in lorries and shipping can diminish emissions of different air pollutants [19]. Emissions from the energy sector over the same period was equal to 21% of total GHG emissions in the UK and have declined by 65.5% since 1990 due to changes in the energy policy in the UK, the phasing out of coal-fired power stations. Carbon dioxide (CO₂) being by far the most prominent gas for this sector (94%). The main source of emissions from this sector remains the use of coal and gas in electricity generation. Of course, the sources of air pollution, include not only transport and energy generation, but also businesses and residential which are sharing equally about 32% of the total GHG emissions in 2019 in the UK [19].

Air pollution statistics are required to support and justify the efforts of organisations and governments in addressing major environmental issues such as air pollution, tropospheric ozone destruction and GHGs to mitigate climate change effects. The most well-known emissions were reported in the Kyoto Protocol [20], the first six are GHGs: carbon dioxide (CO₂), methane (CH₄), hydrofluorocarbons (HFCs), nitrogen oxides (NO_x), perfluorocarbons (PFCs) and sulphur hexafluoride (SF₆), sulphur dioxide (SO₂), non-methane volatile organic compounds (NMVOCs), carbon monoxide (CO), ammonia (NH₃), and particulate matter (PM₁₀, PM_{2.5}) [21]. For every GHG, a Global Warming Potential (GWP) has been specified to indicate its ability to trap heat in the atmosphere and how long it exists in the atmosphere as compared to CO₂ (used as reference). Accordingly, GWP-weighted emissions can be presented in a million tons of CO₂ equivalent (MtCO_{2e}). GHGs with a higher GWP contribute more to “warming the Earth” as they absorb more energy per unit mass [22].

1.2.3.1 Impacts of Air Pollution

The most significant impacts of air pollution on our ecosystems are acidification, eutrophication, and ground-level ozone. Acidification is due to chemical reactions between air, water, and pollutants NO_x, NH₃ and SO₂. These reactions create acidic droplets that accumulate in irrigation systems and the ground through the acidic rain, impacting negatively on soil, plants, and constructions [6]. Eutrophication is producing

by the nitrogen-based pollutants (NO_x and NH₃) and is due to the ability of nitrogen to accumulate in aquatic systems which changes nutrient levels, boosting algae growth in reservoirs and water channels which can de-oxygenate the water. Ground-level ozone is formed by chemical reaction between NO_x and NMVOCs that creates ozone. A GHG, ozone (O₃) contributes to global warming and increases the damage risk to plants, vegetables, and forests [6][18].

1.2.3.2 Statistics of Gas Emissions

Net CO₂ emissions in 2017 were estimated as equal to 80.4% of total UK anthropogenic GHG emissions; 366.9 Mt, some 3.3% less than in 2016. Between 1990 and 2017, UK net CO₂ emissions decreased by nearly 40%, with the main reason, once again, the reduction in the use of coal in power generation and increased use of renewables [17][18]. Figure 1-7 shows the long-term reduction in the emissions of air pollutants; NH₄, NO_x, NMVOCs, PM₁₀, PM_{2.5} and SO₂ [6].

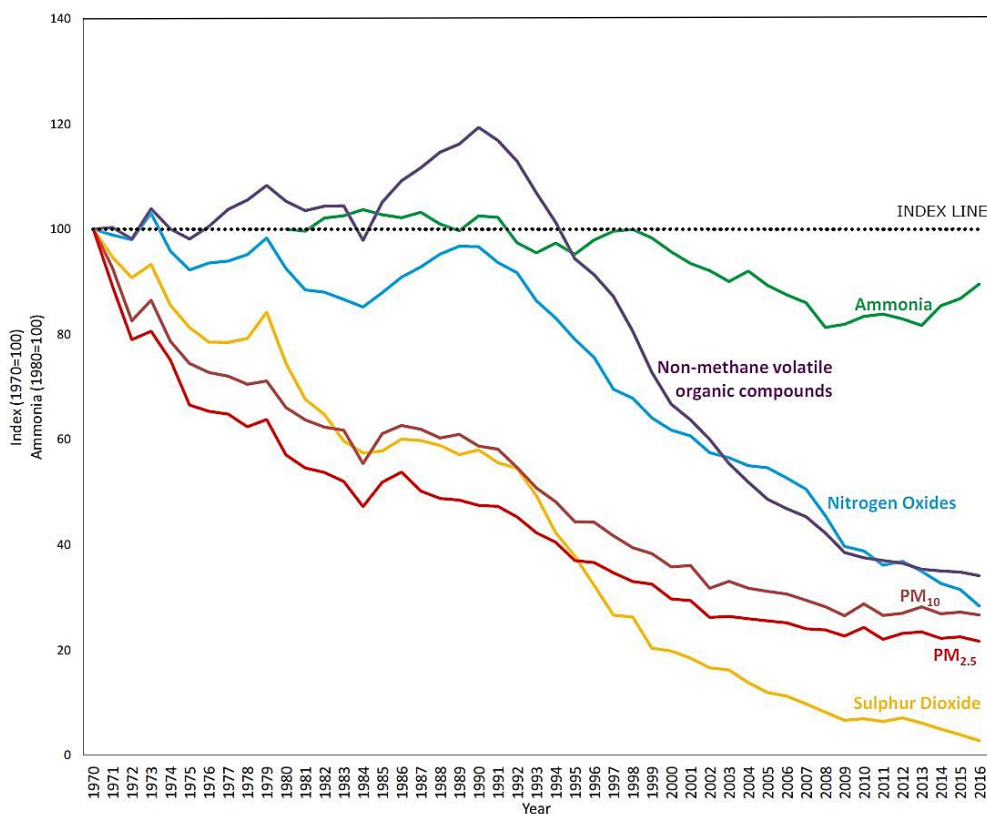


Figure 1-7: Trends of emissions in the UK. Reproduced from [6].

It can be seen that between 2015 and 2016; NO_x emissions reduced by 10%, SO₂ emissions decreased by 29% to their lowest recorded level, and PM₁₀ and PM_{2.5} levels dropped by 2% and both reached their lowest recorded levels. We see the emissions

of NMVOCs was most pronounced, reached a peak in 1990 and have declined ever since. However, there was an increase of about 3% in the level of NH₃ emissions between 2015 and 2016. These statistics demonstrate that the UK met the EU and the international emissions ceilings as permitted under the EU National Emission Ceilings Directive and the Gothenburg Protocol 2016 [6][23].

1.2.4 Overall Energy Consumption

The overall electricity consumption is the final energy consumption by consumers excluding non-energy uses (not been used directly to supply energy). As depicted in Figure 1-8 (A), since 2002, both actual and temperature corrected consumptions have dropped by about 10% in the UK. The temperature corrected consumption is consumption adjusted to exclude the effect of changes in the external air temperature and to identify underlying trends. During 2002-2017, actual consumption varied year on year (YOY), though temperature corrected consumption declined gradually between 2002 and 2014, but in the three years 2014-2017 there has been a marked upward trend [24].

Primary energy equivalent is the summation of the energy consumed by the user, the energy consumed in transforming the primary fuel to electricity, any losses in transportation, and any other losses in the system. Figure 1-8 (B) shows the long-term fuel consumption in primary equivalents. It is clear that electricity consumption rose to a peak in 2001 at 236,856 (ktoe). However, by 2017, primary energy consumption has fallen by 19% to 192 (ktoe). The reduction in electricity consumption was essentially because of lower gas consumption in the domestic sector due to the warmer mean temperatures, specifically in the key heating season [24].

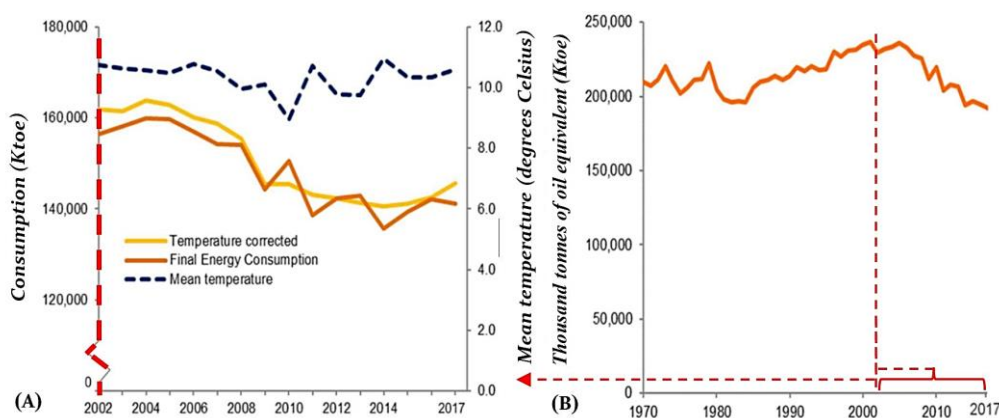


Figure 1-8: (A) Final energy consumption, actual and temperature corrected; (B) Total consumption in primary energy equivalents. Reproduced from [24].

Table 1-2 indicates the data for electricity capacity in the UK per technologies from 1996 to 2016. The installed capacity in the UK has developed steadily between 1996 and 2016, from 73.6 GW to 97.8 GW. Overall, there has been a drop in conventional steam power (includes coal, non-CCGT gas, oil and mixed/dual fired), outweighed initially by an increase in CCGT and more latterly by the growth in renewables [25]. From Table 1-2, It could be observed that in 2016 the electricity capacity from CCGT only is counting about 32% of the total electricity capacity in the UK.

Table 1-2: Electricity capacity in the UK from 1996 to 2016. Compiled from [25].

	1996	2000	2005	2010	2015	2016
Conventional Steam	43.0	39.7	37.1	37.1	22.3	18.1
CCGT	12.7	21.1	25.9	34.0	31.7	31.8
Nuclear	12.9	12.5	11.9	10.9	9.5	9.5
Pumped Storage	2.8	2.8	2.8	2.7	2.7	2.7
Renewable	2.3	3.0	4.5	9.3	30.9	35.7
Total (GW)	73.6	79.0	82.1	94.0	96.5	97.8

1.3 Gas Turbine Engines

Combustion (gas) turbines are complex machines used in a wide area of applications such as aviation, electrical energy generation, oil and gas industries, process plants, marine and many others. The principle of operation is like that of the internal combustion (IC) engine; they employ the energy of combustion to generate mechanical power (rotational) that is used for different purposes. Modern GTs were first promoted as aero engines but were rapidly used in land-based applications including natural-gas-fuelled power plants. It took a long time to develop the high standards of performance now available and make it a heavy-duty machine to dominate the power plant industry. GTs were first used at the end of the 19th century; however, simple cycle GT for power generation was first tested successfully in 1939 in a local power station in Switzerland [26].

GTs were first introduced into the power sector after the Second World War (1939-1945). Until the 1980s most GT engines were relatively small and inefficient [27]. However, by 2017, GTs for power generation were receiving the greatest share of GT investment compared to other applications. The conversion of power generation to advanced gas-fired power stations is due to the continuing efforts to curb emissions and will nurture the GTs market growth in the future. The same trend as presented in Figure 1-9 is a forecast of Europe GT market size for 2024 [28].

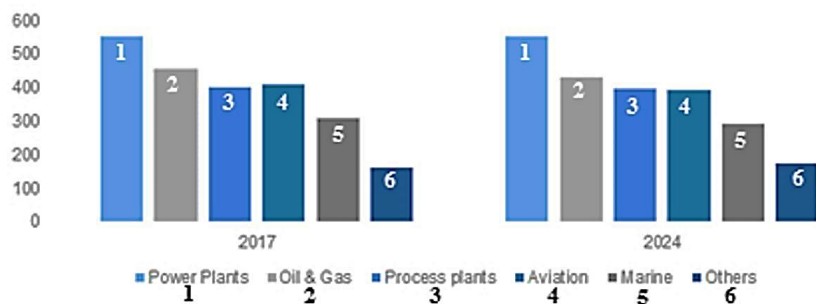


Figure 1-9: Europe GT market size (US\$ Million), by application in 2017 and predicted for 2024. Reproduced from [28].

Increasingly, network operators are giving dispatch priority to renewable energy. Due to these industry changes, GT operators are taking on an additional new role: switching from providing baseload to providing power at times of peak demand. Plant flexibility is critical for on-call GT generation. GT plants that can be dispatched within minutes are essential assets for balancing electric system loads and maintaining grid reliability. As a result, renewable energy and natural gas are the big winners in the race to meet the global demand for power over the next 25 years, according to the 2018 World Energy Outlook. The rapid growth in renewables (notably wind and solar power) is changing the electricity supply landscape and how GTs are being called on to generate to the grid. The modern power grid needs intelligent resources able to ramp up and down swiftly, efficiently, and repeatedly [3].

1.3.1 Gas Turbine Components and Principles of Operation

Figure 1-10 shows the detailed cross-section of a typical land-based GT engine, [29], GTs comprise two main sections: the gas generator with a high-pressure turbine (the cold flow zone) on the left of Figure 1-10, and the power or low-pressure turbine (the hot flow zone) on the right of Figure 1-10.

GT components are usually fixed on one continuous shaft or multiple shafts. The flow domain within these two main stages is connected via the combustion system (the combustors) while the power turbine is directly connected to the electrical generator through the power shaft. An external drive starts the engine, in the stationary GT case it is an electrical motor which drives the shaft connected to the high-pressure turbine and the multi-stage axial compressor mounted on it. The starting system is disengaged once the high-pressure turbine rotational speed approaches the self-driving speed (about 50% of full speed) when the generated power is enough to run the compressor and maintain the combustion process [29][30].

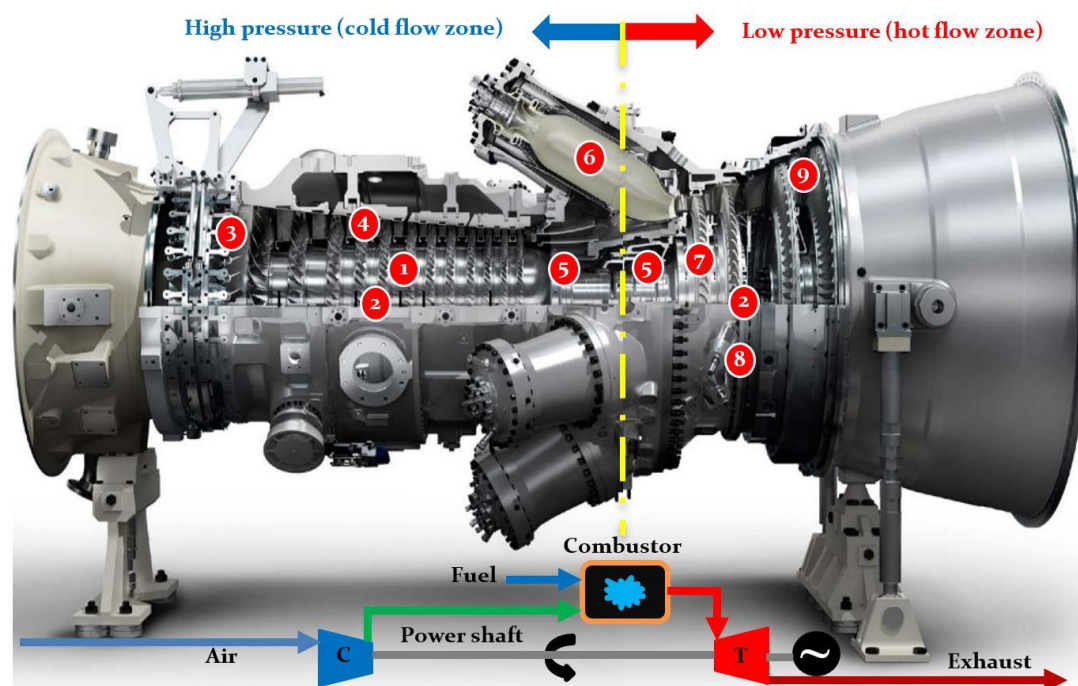


Figure 1-10: Components of a GT (SGT-750 GT developed by Siemens): 1- compressor rotor, 2- horizontal and vertical split casing, 3- guide vanes, 4- multi-stage compressor, 5- bearing and balancing planes, 6- combustor, 7- multi-stage compressor turbine, 8- online monitoring, 9- multi-stage power turbine. Reproduced from [29].

The compressor driven by the high-pressure turbine draws air into the GT, compresses it, raises its temperature and feeds it to the combustion system at an increased flow velocity [30]. Turbine speed depends on the manufacturing company and the GT design, varying from 2000-10000 rpm. There are two general types of compressors, axial and centrifugal. The first type is more common for their higher flow rates.

Advanced combustors premix the fuel gas with the compressed air to produce a homogeneous air/gas mixture before it is fed into the combustion chambers where it is ignited by the ignition system and burns. Ignition systems for gas-turbine engines consist of three main components: the exciter box, the ignition lead, and the igniter. The exciter box sends high-voltage current to the ignition lead, which transfers the high voltage to the igniter. The products of combustion are many times the volume of the air/gas mixture due to the heat produced by the combustion process. The expanding hot exhaust gases flow at high speed first through the multiple-rows of blades of the high-pressure turbine and then through the lower-pressure power turbine that drives the power shafts. The shaft of the power turbine is connecting to the machine to be driven such as an electrical generator. The exhaust gases flow

through a diffuser into the outlet casing, shown on the right of [Figure 1-10](#), these are at a temperature which can be higher than 750 K and can be utilised to generate steam as part of an energy recovery programme [27].

1.3.2 Gas Turbine Combustion Chambers

GT combustion chambers are where the combustion process takes place and the energy released to drive the entire GT. Modern GT combustion chambers consist of two main parts, the primary cylinder and coaxial liner cylinder locating inside it. The fuel-air mixture is injected inside the inner cylinder (the liner) by the burner nozzle while a separate air flow is introduced between the two cylinders which acts to cool down the liner of the combustor and in so doing experiences an increase in temperature. The secondary air enters the combustion chamber(s) through dilution air holes along the liner of the combustor to dilute the very hot combustion products, reduce their temperature and hence minimise wear of GT burners and turbine blades and extend hardware life. The combustion products expand and accelerate to form a uniformly heated gaseous stream suitable for all GT operating conditions. In general, GT combustion chambers can be classified according to the design of the GT, the purpose for which the GT will be used and the space available for the combustion system. There are three different types of the combustion chamber, tubo-annular, annular and tubular. The two most common combustion chambers are shown in [Figure 1-11](#) [30].

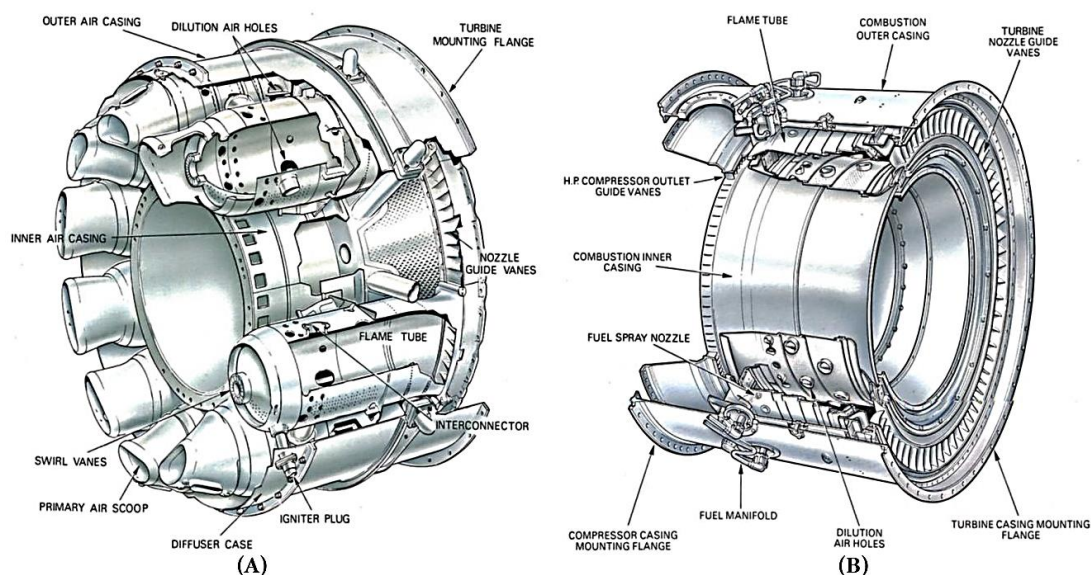


Figure 1-11: Illustration of two common combustor types: (A) tubo-annular combustion chamber arrangement, (B) annular combustion chamber. (Rolls Royce plc.). Reproduced from [30].

GT combustors need to meet the following essential requirements: high-combustion efficiency, reliable and smooth ignition, wide stability margins, low emissions, minimum cost, low-pressure loss, GT turndown ratio and, most crucial, fuel flexibility. Turndown ratio refers to the width of the operational range of a GT and is defined as the ratio of the maximum capacity to minimum capacity. The implementation of the turndown upgrade is designed to help increase efficiency for combined cycle plants in part load operation with a reduced minimum part load with lower carbon monoxide emissions and almost constant gas turbine exhaust temperature [31].

1.3.3 Gas Turbine Combustion Technologies

There are two main combustion concepts applied in GT combustion systems, the non-premixed and the lean premixed. Both combustion systems are offered in both turbo-annular or annular combustion chambers.

The first GT combustion systems employed a non-premixed, diffusion flame to generate the required heat energy. In a diffusion flame, the fuel-air mixing process and combustion happen at the same time in the primary combustion zone (PZ). In general, this combustion system has been more flexible and used with fuel of all types with widespread fuel concentrations. The rich primary combustion of non-premixed flame produces a very high flame temperature (for methane burning in air, the temperature will be close to 2500 K) as the fuel-air mixture is near stoichiometric. One of the main drawbacks of diffusion flames is the generation of high levels of NO_x emissions due to the high burning temperature. On the other hand, the diffusion flame can give stable and efficient combustion, wide operating envelopes and more flashback resistance [30][32][33].

The second combustion technology (lean pre-mixed (LPM)) is shown in [Figure 1-12 \(a, b\)](#). Today, most GTs operate with LPM staged flame technology aimed at producing low levels of emissions because in a lean burn system the combustion takes place at a relatively low temperature. GT combustors which utilising this system are also known as Dry Low Emission (DLE) combustors. DLE combustors consist of four main features: Fuel/air injection unit, stability device, pre-mixed zone and flame stabilisation zone. In DLE systems, fuel and air are fully mixed before the PZ to produce a homogeneous LPM mixture which passes to the reaction zone where the combustion process takes place as presented in [Figure 1-12 \(a\)](#) [32][34].

DLE combustors provide adequate residence time and high turbulence for the fuel/air premixing. A pilot fuel injector is locating in the PZ to keep the operation stable at

partial load. The reacting mixture is diluted by air in the last section of the combustor as in the conventional diffusion combustion system. An example of a typical DLE combustor design can be seen in Figure 1-12 (b) [32][34].

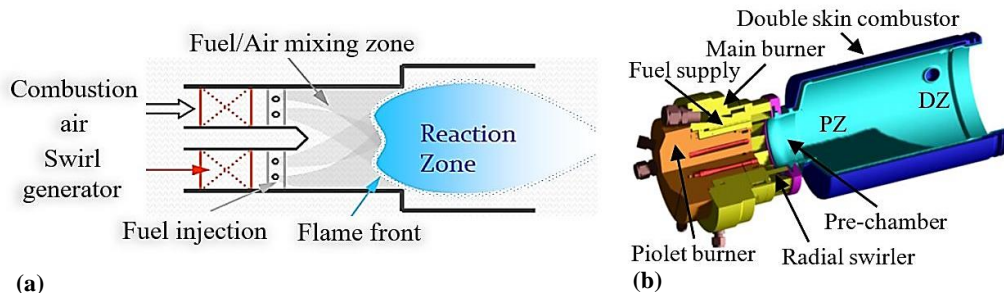


Figure 1-12: GT combustion concepts: (a) pre-mixed flame, (b) pre-mixed combustion system design. Reproduced from [30][32][33].

Compared with diffusion flame combustion, the DLE system has lean combustion giving low NO_x emissions. However, the main system drawbacks are dynamic issues such as flame stability problems, the potential for flashback, and the need for careful combustion tuning [32][34].

1.3.4 Gas Turbine Fuels and Fuel Flexibility

Modern low emissions GTs are sensitive to fluctuations in NG composition. Throughout the EU, the growing dependency on NG imports is driving to extended gas composition variation in the distribution system. Because of the increasing diversification of NG supply, differences in the gas composition have the potential to be very fast. It is anticipated that the variation in fuel composition a rising problem in the next decades. Recently, the UK has imported increasing quantities of LNG, with various compositions and combustion characteristics than a conventional NG. The LNG contribution to the gas supply in the UK has grown from almost zero to higher 25% after 2008, and the Norwegian gas is also a significant contributor while the North Sea gas production will maintain to decrease. LNG is expected to compensate any shortfall in UK gas supply and could provide over 50% by 2030 [35]. Consequently, developing fuel-flexible GT combustors is essential to achieve fuel flexibility and variability in GT power plants, while minimising combustion emissions, combustion dynamics and the impact on revenues and components life. Knowledge of local emission regulations, fuel composition (hydrocarbon species, inert species, contaminants, water vapour), and the principal combustion characteristics of the fuel itself, are the main criteria for selecting the fuel for GT power plants.

At present, DLE technology fundamentally focuses on NG as a fuel, and while there is some variation across the EU, NG is mainly methane (CH_4). However, concerns about energy security have motivated the study of the effects of different fuel compositions on GT combustors' operability, and the use of other energy sources such as landfill gas, syngas (from coal, biomass, and wastes), and gases containing a high proportion of H_2 , such as refinery gases. Theoretically, GTs, in general, are capable of firing any combustible gas, but any given GT can allow only limited variations in gaseous fuel composition and properties, as some gases will have serious operability issues and may adversely affect GT component life. It is not only the fuel gas composition and flammability limits that must be considered, all fuels entering the GTs must be of a high standard (allowable ranges for physical properties, constituents and contaminants [36]) to achieve stable and clean combustion across a wide range of loads and operating conditions [37]. Figure 1-13 lists the compositions of gaseous fuels that have been used in GTs for power generation [33].

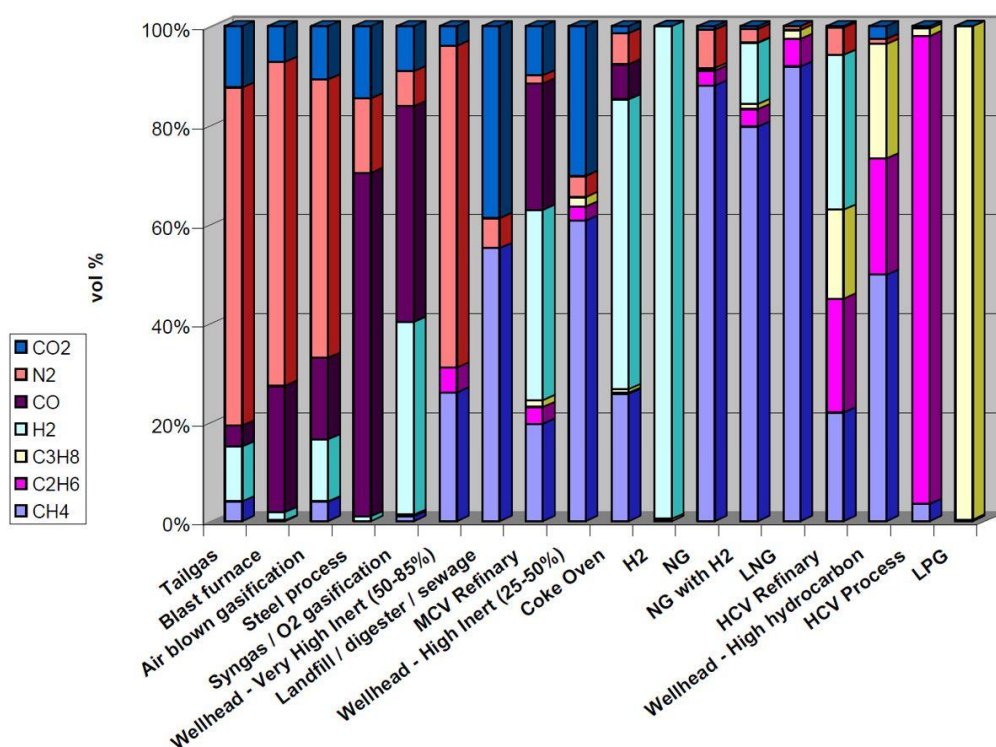


Figure 1-13: Range of gaseous fuel used in GT power plants. Reproduced from [33].

In addition to the gaseous fuel presented Figure 1-13, unconventional shale gas is expected to dominate the world's NG supplies. The shale gas composition (in average) is as follows: 87% light hydrocarbons- CH_4 (C_1), 7% C_2H_6 (C_2), 2% C_3H_8 (C_3), 1.5% CO_2 and 2.5% N_2 [38].

A primary parameter used to characterise gaseous fuel composition is the Wobbe Index (WI), which gives a measure of fuel heat content. It is equal to the net volumetric calorific value (CV) divided by the square root of relative fuel density (RD), for methane the WI is typically about 50 MJ/Nm³. The WI provides a direct comparison of various fuels based on their heating value. However, fuels with different compositions may have the same WI and hence the same heat value. Fuel composition represents the second main parameter that directly affects GT operability and emissions.

Variation in WI can lead to operational issues such as flashback, increasing NO_x with increasing WI, flame stability problems with reducing WI, part load and dynamics CO issues, and GT de-load trips [35][39]. However, the WI does not address the consequences of changes in other fuel features, such as combustion chemistry or flame speed, that affect the stability of LPM GT combustion systems. If the WI diverges from the designed conditions, a modification to the whole GT fuel system could be required [34].

1.3.5 Gas Turbine Operation Challenges

Implementing modifications on GT combustors to achieve efficient combustion is challenging due to the many operational issues such as instabilities, low reaction rates, extinctions, mixing issues and reduced heat release [40]. The main operational challenges to GTs are represented by the variation of WI and fuel composition (fuel quality), e.g., increasing the WI can lead to flame stability problems and incomplete combustion. Addressing these issues is done by giving careful attention to the GT combustion system design, to control sudden changes in the fuel quality, and stabilise the combustion processes.

Combustion instabilities, also known as unsteady flow oscillations, have appeared frequently in GTs and hindered the improvement of LPM combustors. These oscillations may attain enough amplitude as to interfere with GT operation, and in extreme cases, produce a system hardware failure because of dangerous levels of vibration (and heat transfer) in the combustion chamber. Figure 1-14 (A, B) shows a burner assembly damaged by combustion oscillations as compared to the new burner [41].

Figure 1-14 (C) was associated with elevated levels of the higher hydrocarbons. For the burner shown, GT manufacturers have increased flashback resistance to eliminate this issue. Nevertheless, there is still the potential for flashback on some

burners particularly with elevated levels of higher hydrocarbons or by adding hydrogen (with its fastest flame speed of any gas) to the natural gas transmission system [35].

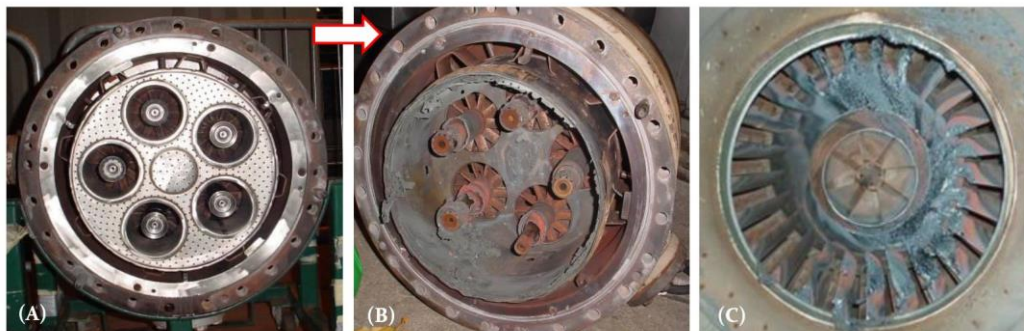


Figure 1-14: Effects of high levels of combustion instabilities, (A) new burner assembly, (B) damaged burner due to excessive combustion dynamics, (C) flashback damage. Reproduced from [35][41].

In summary, better control over the fuel quality, and continuous modifications to GT combustion systems using experimental and numerical investigations are essential to eliminate GT operational issues.

1.3.6 Gas Turbine Emissions

One of the main challenges in the power generation sector is to meet ever more stringent emission regulations. To satisfy future requirements of reduced emissions from GT power plants, while maintaining satisfactory combustion stability and performance, better knowledge of pollutant formation mechanisms is required. The concentration of pollutants in the GT exhaust is directly linked to the operating conditions (temperature and pressure) within the GT combustors, and to the residence time in different combustion regions. Achieving effective gaseous fuel mixing with the primary combustion air, and the subsequent admittance of secondary air into other combustor zones have a substantial effect on the level of emissions [42].

There are a wide variety of emissions from GT power plants; however, the primary pollutants are NO_x, CO and UHC. There are three pathways for NO_x formation; (FBN) fuel bound NO_x nitrogen (appears from the oxidation of the already-ionised nitrogen contained in the fuel like coal), prompt NO_x (formed from oxidation of the nitrogen molecules in air and fuel in the fuel-rich conditions and becomes NO_x during combustion) and the more dominant thermal NO_x generation (controlled by the

nitrogen and oxygen molar concentrations and the temperature of the combustion) [43].

FBN is an important consideration for liquid fuel but does not really exist for gaseous fuel. However, with the increasing demand to lower the CO₂ emissions worldwide, pure ammonia (NH₃) combustion or co-combustion with a conventional fuel is an alternative solution in GTs. The major challenges with the use of NH₃ as a fuel are lowered heat flux and increased NO_x emissions. Therefore, special techniques to reduce NO_x emission are essential for GT combustors which burn NH₃ [44]. For GT combustors burning liquid fuel FBN formation can yield (0.5-10 ppm) of NO_x depending on the fuel nitrogen content. Prompt NO_x formation can happen under fuel rich conditions. NO_x is formed essentially by the thermal (Zeldovich) NO_x formation mechanism, which starts to form at temperatures above 1700 K. Above this threshold, the thermal NO_x formation will increase exponentially [32][33]. However, CO follows the opposite behaviour and occurs at relatively low temperatures with lower reaction rates and limited oxidation of CO to produce CO₂. UHC emissions are a consequence of rich combustion as the fuel will not be fully burned with the excess ejected in the exhaust gases. Figure 1-15 shows the pollutants CO and NO_x in ppmv emitted from GT combustors as a function of primary temperature and equivalence ratio (ϕ) [30].

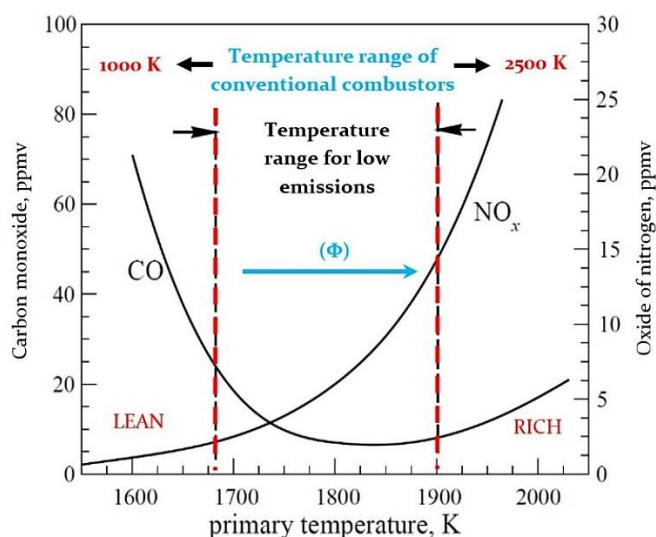


Figure 1-15: The effect of flame temperature on emissions. Reproduced from [30].

It appears that while low flame temperature is desirable for NO_x reduction, the CO formation shows a sharp increase. It is also observed that UHC emissions in GTs follow the same general trend as CO emissions. As a result, for low emissions, GT combustors should work within the range of equivalence ratios (ϕ), where the CO,

UHC and NO_x emissions are maintained within the boundaries required by current legislation [45].

1.3.7 NO_x Control Technologies

Energy industries in the UK contribute about 20% of the total NO_x that is emitted in 2020 [46]. GTs employ the Brayton Cycle with a burner to raise the temperature of gas following compression and before expansion within the turbine. GTs essentially use reducing high burning temperature and decreasing residence time methods to minimise NO_x emissions [43].

There are many technologies used for low NO_x emissions from GT engines: lean pre-vaporized premixing applied for liquid fuel, lean direct injection (LDI), variable geometry VG (constant equivalence ratio), lean premix combustion system (LPM), rich–burn quick-mix lean–burn combustion (RQL) (see section 2.4.1 for more details), water or steam injection, catalytic combustion and staged combustion with multi-steps of fuel injection or air added in series or parallel (see section 2.4.3 for more details). The addition of particles to air flow entering the GT would accelerate the erosion of turbine blades. As a result, sorbent particles can be introduced to flow after it leaves a GT after the expansion to control the NO_x [45].

The well-known NO_x control systems for modern GT power plants to keep NO_x emissions at under 5 ppm (the optimistic value [47]) are DLN (dry low-NO_x which burns the fuel gas near its lean limit) or DLE combustion systems. The use of DLN and DLE increase the bulk of the system. The NO_x control technique chosen for a given GT will depend on the size (volume and mass) of the NO_x control technology being acceptable. For instance, a GT used for land-based power stations does not have the limitations on weight and volume as, for example, applications like marine propulsion. See Table 1-3 for the most important NO_x control technologies employed for GTs in the meantime [43].

Table 1-3: NO_x control technologies used for GTs. Compiled from [43].

NO _x control principle	Technologies	Efficiency
Reducing peak temperature	Natural gas reburning (NGR), low NO _x burners (LNB), inject water or steam, reduced air preheat, and catalytic combustion	70-85%
Oxidation of NO _x with subsequent absorption	Non-thermal plasma reactor (NTPR)	No data
Reducing residence time and peak temp.	Air staging of combustion and inject steam	70-80%

Table 1-3: Continued.

NOx control principle	Technologies	Efficiency
Chemical reduction of NOx	Fuel reburning (FR), low NOx burners (LNB), selective catalytic reduction (SCR), selective non-catalytic reduction (SNCR)	70-90%
Using a sorbent	Sorbent in ducts	60-90%
Removal of nitrogen	Ultra-low Nitrogen fuel	No data

1.3.8 Turbulent Reactive Flows in Industrial Processes

Most reacting flows in industrial applications are turbulent, e.g., in engines, turbomachines, GT burners and many others. Turbulence in GT combustion represents a regime where the flow is disturbed and excited by random fluctuations in pressure, velocity and temperature. These fluctuating components have a big influence on flame shape, flame behaviour, and stability of the reacting flow inside the GT combustors as they are very sensitive to flow fluctuations. The appearance of turbulence in the flow allows an increase in the burning rate as it leads to an enhanced, turbulent, flame speed. This behaviour is essential for industrial purposes since the output power density is proportionally scaled with the combustion rate. However, too much turbulence should be avoided as it can produce flame instability or quenching, in addition to many other operational issues. As a result, the aim of GT original equipment manufacturers (OEMs) and researchers is to use the turbulent characteristics of reacting flows to achieve optimal performance from GT burners regarding a balance of power generation, pollutant emissions and efficiency. This suggests more investigations are needed for a better understanding of turbulent combustion, where both numerical simulation and experimental enquiry will be necessary.

1.4 Motivation

A fundamental difficulty facing the decarbonisation of the energy supply chain is that any changes must ensure energy supplies remain reliable and affordable to the consumers. Despite the significant development of the renewable energy sector, there is still considerable interest in GT power generation. Today, the biggest problem is how to provide cheap energy from GT power plants while meeting emission mitigation trends. Despite extensive modifications to GT combustion systems having been carried out and good results achieved, there remains a need for both

experimental and numerical investigations to increase fuel flexibility and ensure the stable operation of LPM GT combustors.

The current focus is on NG flames; swirl burners and their operation LPM conditions with the expectation of a major step towards attaining significant improvements in GT combustion systems, with low emissions and flame stability over a wide range of equivalence ratios. The study of swirling flow combustion received significant attention in the previous decade when it was investigated in order to better understand combustion chemistry and fluid dynamics. Such understanding of the swirl flow structure did lead to better design of GT combustors, better control of combustion and reduced cost of engine maintenance. However, implementing modifications to swirl burners to achieve more efficient GT combustors is a serious challenge because of the many combustion issues that have to be overcome, including flame extinction, reduced heat output, lower reaction rates, flame stability issues, and harmful emissions [48].

Future GTs will be expected to operate over a wide range of alternative fuels with low-cost engine modifications enabling the change from one fuel to another, to accommodate price and availability. These alternative fuels will have a wide range of flame speeds, heating values, and compositions ranging from syngas with a high hydrogen (H_2) and carbon monoxide (CO) content, to landfill and digester gases that are mainly composed of methane (CH_4), carbon dioxide (CO_2), and nitrogen (N_2) [49]. Consequently, many researchers are strongly motivated to develop the burner design of GT power plants capable of being powered by alternative gaseous fuels in order to produce stable flames and low levels of unwanted emissions.

The combustion system in GTs has to be developed and designed to meet many requirements each of which is essential; with efficiency, reliability, and low emissions the main criteria for assessing the performance of a GT engine [50]. Flame stabilisation of high-intensity combustion in swirl GT combustors is essential for efficient and stable operation with low emission levels. Turbulent combustion in GTs, in general, is the consequence of the interaction of turbulent hydrodynamic flow and chemical reactions, each of which is complicated and which, combined, produce behaviour that is not yet fully understood. These interactions will produce turbulence in the combustion process or, possibly, diminish it and hence affect the combustion stability of GT burners [51].

Numerous techniques can be employed in developing a burner design. The first is by improving the aerodynamics of the swirling flow field in the combustion chamber to

widen the stability limits [52]. The flame stabilisation in swirl burners is made possible by the vortex breakdown (VBD) that happens when the geometric swirl number is quite enough [53]. Latterly, the efforts of GT manufacturers have been concentrated on manipulating and characterising the aerodynamics of the flow processes in swirl combustors for isothermal conditions [54]. The flow turbulence is continuously altering the swirl flow structure which has an effect on the combustion process, including flame stability issues such as blowoff and flashback [8,9]. A second direction is employing alternative fuels (including hydrogen blends) to minimise the impact of the products of combustion on the environment [10-12].

The flow field generated in GT swirl burners has a major impact on the performance of the combustion process. However, the combustion process in GTs has already reached its highest possible efficiency using conventional fuels, but still has a long way to go to provide pollutant free combustion [58]. As a result, particular attention should be given to the hydrodynamics and the flow characteristics of the swirl flow field to stabilise and modify the combustion phenomena, this represents the main motivation of this work.

For the reasons given above, this work intends to enhance the operability of swirl burners by adopting different design modifications and study their impacts on swirl flow behaviour and coherent structures to ensure the stable operation of these swirl burners and produce a fuel-flexible, and variable design GT burner.

1.5 Chapter Summary

A better knowledge of swirl flow structures in swirl burners behind different configurations will permit GT OEMs to design better combustors with increased control over the structures, allowing more efficient combustion and more powerful combustors. This will be especially true for those operating on alternative fuels with high hydrogen content and redesign to meet the anticipated change in fuel composition with the future gas fuel supply.

LPM combustion employing swirling flame is widely used in GT combustion systems for its low emissions. Obstacles that stand out involve flame stability issues due to the combustor geometry and the fuel features. Accordingly, this work has adopted both numerical and experimental approaches to characterise the flow structures in swirl burners under the effects of different configurations and focusing on their influence on the swirl flow and hence the flame instabilities, especially flame flashback mechanisms.

1.6 Project Aims and Objectives

Interest in LPM combustion of fuels utilising swirl burners is growing due to this combination's ability to emit low levels of NO_x. As presented previously, fuel flexibility is crucial for the use of GTs. The addition of hydrogen (H₂) to enrich the conventional gaseous fuel is being considered as a way of reducing the emission of unwanted GHGs. However, advanced fuel presents several disadvantages, i.e., flame flashback. Consequently, better stabilisation techniques are required. Furthermore, comprehensive knowledge about swirling flow phenomena in GT burners close to these requirements is needed.

Therefore, this project provided an important opportunity to advance the understanding of flame flashback mechanism in GT swirl burners for different stabilisation techniques. The main aim of this study is to develop the flashback resistance in tangential swirl burners (typically used in GTs) for both flashback mechanisms; combustion induced vortex breakdown (CIVB) and boundary layer flashback (BLF).

To meet the aim of this thesis, three specific objectives need to be performed:

- Employing ANSYS Fluent code to predict the flow field characteristics in a tangential swirl burner subject to injection of an axial air jet to determine if CIVB flashback resistance is enhanced. The effects of different axial air injection positions relative to the burner base plate were investigated. Laser Doppler Anemometry (LDA) measurements were used to validate the CFD findings. The numerical and experimental investigations were conducted on a 150-kW tangential swirl burner constructed at Cardiff University. The flow characterisation was based on the extent to which the flow velocity and turbulence downstream of the burner exit was affected by the proposed axial air injection system.
- Focusing on a further mitigation of the BLF flashback phenomenon employing nozzle with scalloped riblet microstructure surface in conjunction with the axial air injection system. The effects of using this microstructure on the swirl flow characteristics were investigated experimentally using 1D LDA system. In addition, the flashback resistance technique for both BLF and CIVB mechanisms were examined simultaneously.
- Examining another mitigation technique of the flashback phenomenon employing different smooth nozzle configurations. The effects of varying the

height of the burner nozzle on swirl flow characteristics were studied experimentally using laser diagnostic system. Furthermore, this technique has been extended to study the flashback resistance technique for both BLF and CIVB mechanisms simultaneously. This involves utilising microstructured surfaces for the improvement of flashback resistance. Different strip heights of a wire woven mesh were employed as a liner on the long smooth nozzle to change its surface roughness and improve and control the BLF flashback.

1.7 Thesis Structure

The present thesis consists of eight chapters as follows:

- **Chapter One:** Presents an introduction to the thesis. Background, the energy sector statistics and challenges, motivations, objectives of the study, as well as the methods used to perform the research, are summarised in this chapter.
- **Chapter Two:** Provides a comprehensive review of previous investigations of different swirl flow structures such as the central recirculation zone (CRZ) and the Precessing Vortex Core (PVC) carried out by the academic and the industrial research communities. Chapter two also reports on theoretical knowledge concerning the different flashback mechanisms, fuel flexibility in GTs, GT emissions, swirl flame stabilisation techniques, combustion technologies, LPM combustion technology in GTs and the laser diagnostic system used in GT studies.
- **Chapter Three:** Provides details of the experimental equipment, the techniques used to measure the flow structures and the methodologies employed in this work for both experimental and numerical approaches.
- **Chapter Four:** The CFD results will be presented regarding the effects of the axial air injection system on flow field characteristics downstream the burner exit with the correlation with experimental data required to validate the CFD findings. In addition, the effects on the flame stability map have been discussed in the chapter as well.
- **Chapter Five:** This chapter is dedicated to the experimental work related to the flow velocity and turbulence characterisation, and their influence on the BLF flashback resistance employing nozzle with scalloped riblet microstructure surface.

- **Chapter Six:** Describes the impact of different heights of nozzles with and without micro-structured surfaces on the flame flashback in tangential swirl burner.
- **Chapter Seven:** Merges and discuss all the numerical and experimental results obtained during the study.
- **Chapter Eight:** Presents, conclusions, recommendations, and suggestions for further work.

Chapter 2

Literature Review:

Characteristics of

Swirling Flow

CHAPTER TWO:

2 LITERATURE REVIEW: CHARACTERISTICS OF SWIRLING FLOW

“Science knows no country, because knowledge belongs to humanity, and is the torch which illuminates the world”

Louis Pasteur, French scientist (1822-1895)

2.1 Introduction

Swirl burners are an intrinsic part of the combustion processes used in almost every industry, wherever there is the need to stabilise high-intensity flames [59][60]. Swirl burners have the great advantage of being able to burn a wide variety of fuels with a range of calorific values and specially designed swirl burners and multi-inlet cyclone combustors have been developed to burn fuels with low calorific values (1.3 - 1.4 MJm⁻³) without the need for auxiliary fuel [61].

Research into the use of swirl burners in gas turbines GTs has been ongoing for two, or more, generations, and there is a large body of relevant literature available. Today the emphasis is on clean, efficient systems as the expectation is that combustion-based systems will continue to produce most of the energy to meet human needs for some time yet [28]. Manufacturers have become aware that many of the emissions GTs are pollutants that are environmentally damaging [30], and there is now considerable effort being made to reduce the adverse effects of GTs. The efficient production of clean energy is a major challenge for those developing enhanced combustion systems with the target of ultra-low (or even zero) levels of polluting emissions.

During and after World War II (1939-1945), the technological development of GTs was phenomenal, in design methods, turbine performance and manufacturing techniques [27][28]. Issues encountered and overcome ranged from fuel type and availability to component manufacture using new materials.

Interest in lean combustion of premixed fuels using swirl burners is increasing due to this combination's ability to emit low levels of NO_x. The addition of hydrogen (H₂),

supplied as a by-product of other industries (e.g., coke oven gas) or even in a pure form, to enrich the original fuel (e.g., natural gas) is being considered as a way of reducing the emission of unwanted greenhouse gases. The addition of hydrogen to the fuel for GTs raises the questions of combustion instabilities (e.g., blowoff and flashback), limited fuel interchangeability, and flame temperature.

There are significant areas of the GT combustion process that are still not fully understood, one of the most urgent for swirl burners are the flow patterns which show large coherent structures in the combustion process and have not yet been explained theoretically, nor successfully modelled using even the most advanced computers and software. Obviously, the conceptualisation of these phenomena will require the development of more advanced ideas on combustion aerodynamics.

This chapter briefly describes previous research carried out and which acts as a foundation for the present project. It also introduces the more important phenomena that affect swirl combustor performance.

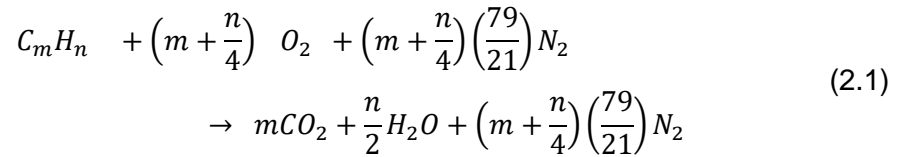
2.2 Combustion Phenomena in GTs

2.2.1 Principles of Combustion

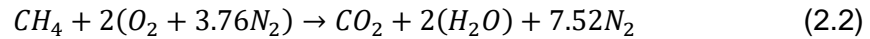
The combustion of fossil fuels generates over 60% of the world's current energy needs, a pattern that is likely to continue for this century [10]. Combustion – an exothermic chemical reaction between oxidizer and fuel – is the basis of heat and power generation in numberless systems ranging from a simple hob on which to boil a kettle to the most advanced rocket engines [62]. GT combustion is a continuous process taking place at a temperature above that of the melting point of the metal composing the burner. The flows of air and fuel necessary for combustion are engineered to form a stable flow pattern that adequately mixes the fuel and air, with sufficient time in the combustion chamber for the combustion process to be completed. However, there remain a host of unknowns concerning this process.

The basis of combustion is the chemical reaction between an oxidizer, commonly air (oxygen), and the combustible fuel to generate heat. For complete combustion of the fuel (f), a minimum amount of oxidiser must be supplied. The minimum amount of oxidiser required for complete combustion is termed the stoichiometric value, $\left(\frac{f}{a}\right)_{stoic}$, where a is air. This ratio is an important parameter used to describe the combustion process. However, since mixing of fuel and oxidiser is rarely perfect in

real systems, more oxidiser than the stoichiometric ratio is required to fully burn the fuel. The stoichiometric reaction for any arbitrary fuel can be written as [63]:



For CH₄ – air (strictly, oxygen in the air), the stoichiometric combustion reaction is:



Thus, the stoichiometric ratio of fuel to air is:

$$\left(\frac{f}{a}\right)_{stoic} = \frac{\text{Mass of the fuel}}{\text{Mass of the air required for complete combustion}} \quad (2.3)$$

The equivalence ratio, ϕ , is the ratio of oxidiser actually supplied compared to the stoichiometric value [64]:

$$\phi = \frac{\left(\frac{f}{a}\right)_{act}}{\left(\frac{f}{a}\right)_{stoic}} \quad (2.4)$$

The useful heat energy obtained from such a reaction will be the “gross heating value” (GHV) of the fuel, less the energy expelled in the exhaust gases after combustion. Different fuels will, of course, have different GHVs depending on their chemical composition. However, fuels tend to be rated according to their “lower calorific value” (LCV), the heat generated when unit mass of the fuel is completely burned and the water vapour produced during combustion is exhausted without being condensed. A second term, “higher calorific value” (HCV), is sometimes used, this has a slightly higher value than LCV, as it does not subtract the heat required to evaporate the water generated during combustion, see Equation (2.2).

The equivalence ratio (ϕ) as expressed in Equation (2.4), can be used to classify the combustion:

When $\phi = 1 \equiv$ Stoichiometric combustion, ideal state,

$\phi < 1 \equiv$ Lean combustion, and

$\phi > 1 \equiv$ Rich combustion.

However, some researchers have used “air excess ratio” ($\lambda = \frac{1}{\phi}$) to define the status of the combustion [63].

Both fuel and products of combustion contain the wide variety of species, each of which should be considered, as they could have significantly different thermodynamic characteristics. Lighter fuel fractions break down faster than heavier, while straight-chain molecules take less time than branched molecules. Combustion is a staged process; long molecules are continuously broken into shorter ones until combustion is complete. The colour of flames can be used to identify the radicals and combustion products, e.g. a blue colour is an indication of the combustion of a fairly simple fuel of low molecular weight, a yellow colour tends to show soot formation, while a green colour suggests the existence of radicals [64].

2.2.2 Turbulent Premixed Combustion and Flame Regimes

Because of their industrial importance in, for example, GT power generation, premixed, turbulent flames are of great interest. Turbulence improves the mixing process giving turbulent flames burning rates that are noticeably superior to those of laminar flames. Thus, GT combustors with laminar flame combustion (LFC) at high levels of turbulence can attain efficient combustion in a small volume. However, the presence of turbulence makes the combustion process substantially more complex [65].

The reaction zone of premixed laminar flames (PLFs) is often sub-divided into an initial preheat zone, a reaction zone where the fuel is consumed, and an oxidization zone. The air/fuel mix is heated in the preheat zone to the temperature at which combustion can take place. The heat energy for this comes from hot radicals diffusing from the reaction zone, where fuel and oxidizer are consumed by a complex pattern of chain branching and chain propagating reactions. The oxidization zone completes any remaining reactions between intermediate species [66].

Laminar flames are relatively simple and are described in terms of the thermochemical properties of the fuel/air (oxidizer) mix. Two significant parameters used to describe PLFs are δ_l (flame thickness) and S_l (flame speed). δ_l is the thickness of the reaction zone in which most of the combustion reactions occur. S_l is equal to; δ_l divided by the time taken for the flame to travel that distance [65].

Some eighty years ago, Damköhler proposed that the flame front, or “combustion wave”, wrinkles when impacted by large-scale turbulence. Depending on the flow characteristics, the flame front, or wave, could be distorted but remain continuous with an increased area. The consequence of increasing the area of the flame front would be to increase the rate of combustion above that for laminar conditions [64][67].

Quantifying the laminar flame speed, S_l , is not easy as it requires determining both flame front surface area and thickness under turbulent conditions [68].

Turbulence, without a flame present, will interact with the flow structure adding complex arrays of length and time to the flow structure in ways that are still not fully understood. The presence of a flame will add further complexity to the processes, in the form of sharp density, temperature, velocity and viscosity gradients across the flame. Thus, premixed turbulent flames will show markedly different characteristics from PLFs.

One method to characterize interactions between turbulence and the flame structure in premixed turbulent flames is to compare the turbulent and chemical length and time scales. However, it is usual to use the known properties of laminar flames to define and determine the additional thermal and chemical processes taking place in the turbulent combustion.

Three dimensionless numbers are commonly used to separate premixed turbulent flames into diverse regimes. The Damköhler number (Da) and Karlovitz number (Ka) both relate to flow and chemical time characteristics [69].

The Damköhler number (Da) is used to assess how turbulence affects a combustion wave. The Da is the non-dimensional ratio of the turbulent mixing time, τ_m , and the chemical reaction rate, τ_c [70]:

$$Da = \frac{\tau_m}{\tau_c} \quad (2.5)$$

Valera-Medina [64] and Dawson [67] have defined the turbulent mixing time, τ_m , “as the integral turbulent length l_o divided by the turbulence intensity of the incoming flow, \bar{u} ”, and the chemical reaction rate, τ_c , as “the laminar flame thickness δ_l divided by the laminar burning velocity, S_l ” and can be used to describe “the reaction time over a flame thickness”. Thus Equation (2.5) can be written:

$$Da = \frac{\tau_m}{\tau_c} = \frac{l_o S_l}{\bar{u} \delta_l} \quad (2.6)$$

Large Da represents a fast reaction with “perfectly stirred reactor” conditions, implying the mixing is instantaneous and no spatial variations in concentration and temperature. This implies that the reaction zone is of minimal thickness. Small Da represents slow reactions, with thicker flame fronts and possible spatial variations in temperature and concentration [64][67]. Under certain conditions, if the flame speed

becomes fast enough the combustion wave travels at supersonic velocity and there will be a detonation [63].

The Karlovitz number (Ka) is the ratio of the chemical time scale, τ_c , to the smallest turbulence time scale, the Kolmogorov time scale (τ_η) [69]:

$$Ka = \frac{\tau_c}{\tau_\eta} = \frac{\delta_l u_\eta}{\eta S_l} = \left(\frac{l_o}{\delta_l}\right)^{-\frac{1}{2}} \left(\frac{\dot{u}}{S_l}\right)^{\frac{3}{2}} \quad (2.7)$$

The remaining number is the turbulent Reynolds number (Re_{l_o}) which associates the inertial and viscous forces, and is defined using \dot{u} , l_o and ν (the kinematic viscosity of the fluid (m^2/s)):

$$Re_{l_o} = \frac{\dot{u} l_o}{\nu} \quad (2.8)$$

Depending on the relative values of these three dimensionless numbers, the Borghi diagram shown in Figure 2-1 will indicate the type of flame. Figure 2-1 illustrates that the flame will be laminar at Reynolds numbers less than unity.

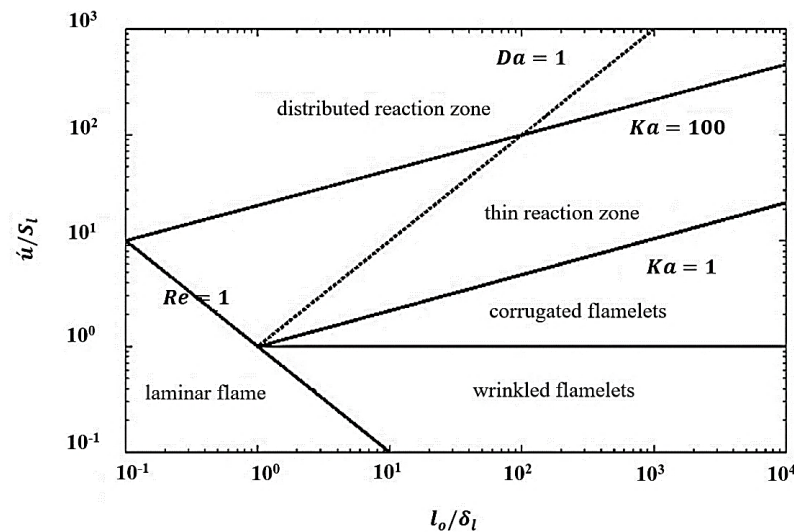


Figure 2-1: Combustion regimes (Borghi diagram) for turbulent premixed combustion. Reproduced from [69].

The line $Da = 1$ is the boundary at which chemical and turbulence time scales are equal, above this line τ_c will be less than τ_m , so the turbulence time scale will be shorter than chemical time scale. If $Da < 1$, τ_c will be greater than τ_m , and the chemical reactions will be slower than the turbulent mixing. Here combustion will be controlled by chemical considerations rather than by turbulence. $Da < 1$ is, therefore, termed a perfectly stirred reactor regime.

For $Ka < 1$, only those turbulent structures in the flow which are larger than the thickness of the flame front will affect the flame, wrinkling the flame front but not penetrating the preheat or inner reaction zones. Here, if the turbulence intensity of the incoming flow is less than the laminar flame speed ($\bar{u} < S_L$), we have wrinkled flames, conversely if $\bar{u} > S_L$, we have corrugated flamelets. The larger the Karlovitz number the more the effect of turbulence on the flame structure [65][69].

In the range $1 < Ka < 100$, we have the “thin reaction zone” where the smallest turbulence structures can penetrate into the preheat zone but not the inner reaction zone of the premixed flame. The smallest turbulence scales are so small they will interact with the flame’s inner reaction zone. At $Ka > 100$, the flame’s inner reaction zone will so thin that even the smallest turbulence structures will perturbate it. However, for large enough Ka the flame front will no longer be identifiable and we have a “distributed reaction zone” [65].

In reality GTs will be operated with very high levels of turbulence, and correspondingly high Reynolds numbers. Laboratory scaled combustors generally operate at lower Reynolds numbers with Karlovitz numbers around unity [66].

2.2.3 Type of Flame

Commonly, combustion is divided into three groups; premixed, non-premixed and partially premixed [71]. This division is dependent on how the reactants and oxidiser are introduced into the combustion zone, a process which is one of the main ways of controlling the combustion regime, see Figure 2-2 [72].

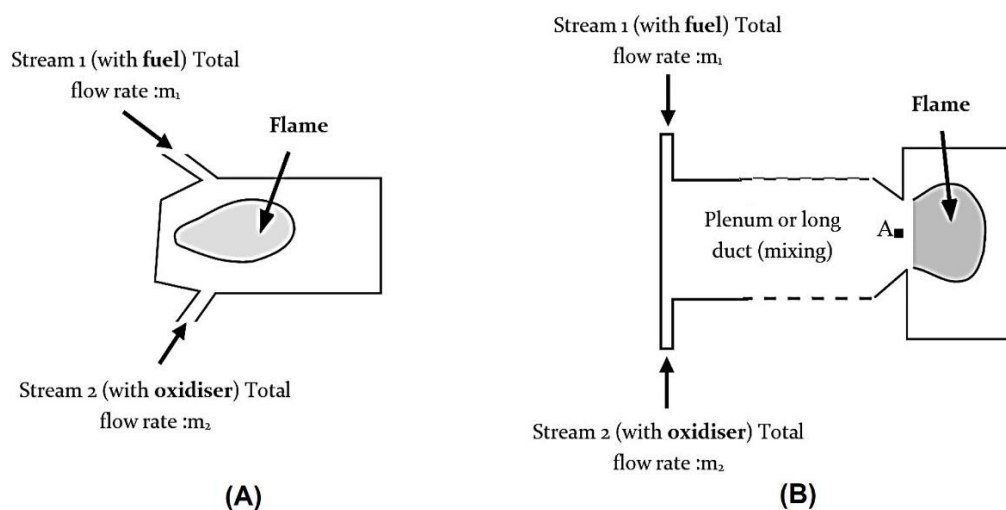


Figure 2-2: Combustion regime classification as a function of the reactant introduction scheme: (A) non-premixed (diffusion) flame, (B) mixing device and premixed flame. Reproduced from [72].

Oxidiser and fuel can be entered the combustion zone independently, mixing as they react (diffusion, or non-premixed flames, see [Figure 2-2 \(A\)](#)) or mix before combustion (premixed flames, see [Figure 2-2 \(B\)](#)). Partially premixed combustion is a premixed flame with a non-uniform mix of fuel and oxidizer [\[71\]](#).

2.2.3.1 Non-premixed Flame

In diffusion or non-premixed, combustion of the fuel and oxidiser enter the reaction zone in distinct streams, see [Figure 2-2 \(A\)](#) for an idealised representation. A non-premixed flame is unable to spread into stream 1, because stream 1 contains no oxidizer, ditto for stream 2, which contains no fuel.

Air and fuel in the correct proportions can be injected at high velocities into the combustion chamber, the jets of gaseous fuel and air mix rapidly, the conditions for large Da , considerably increasing the chemical residence time [\[72\]\[73\]](#). These conditions mean it is possible for the fuel to combust at a prescribed distance from the burner nozzles as might be determined by flame stabilisation/anchorage devices [\[63\]](#). [Figure 2-3](#) is a sketch of the structure of a one-dimensional laminar non-premixed flame, assuming that the streams of oxidiser (air) and fuel streams are at the same temperature. GTs traditionally use diffusion flames, where oxidiser and fuel mix by turbulent diffusion and the combustion zone is located in the “locus of the stoichiometric mix”. The flame, in fact, is contained in the region where fuel and oxidizer are in combustible proportions. Reactant temperature can reach 2000 °C, and the combustor walls and turbine blades are protected by a thin layer of air injected for that purpose [\[71\]](#).

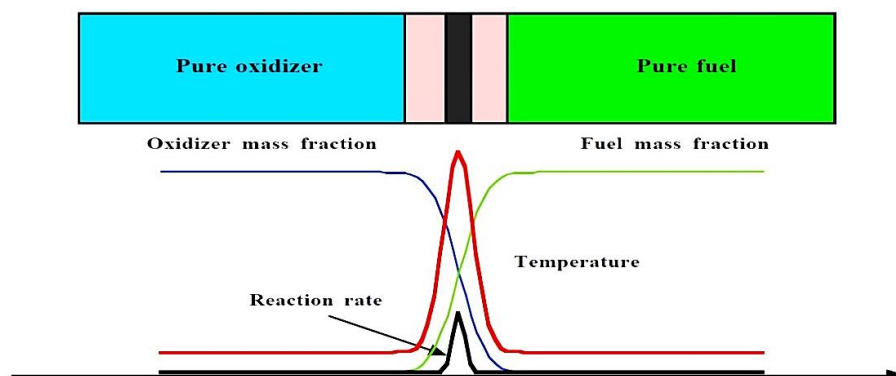


Figure 2-3: Schematic showing the structure of a laminar non-premixed (diffusion) flame. Adapted from [\[71\]](#).

Non-premixed combustion gives greater flame stability in GT combustors than premixed flames but produce high levels of NO_x due to the higher temperature of

combustion. Soot formation, which is largely governed by the combustion parameters, is another undesirable feature of diffusion flames [74][75]. It has been demonstrated that soot formation can be decreased by using oxygen rather than air as the primary oxidant, and adding CO₂ to either oxidiser or fuel [75]–[77]. However, diffusion-controlled combustion is less efficient because oxidiser and fuel mix by molecular diffusion before combusting, with maximum flame temperature occurring when oxidiser and fuel are in stoichiometric proportions. This cannot be easily controlled.

Turbulence enhances the combustion processes in diffusion flames. When the jet becomes turbulent due to increased flow rates, the length of the diffusion flame does not change, indicating increased intensity of combustion [78]. Excessive flow rates will cause the flame first to “lift-off” – stabilise itself some distance downstream of the burner – and then to “blow-off” and extinguish.

2.2.3.2 Premixed Flames

Premixed flames are confined to gaseous phase combustion, not liquid fuel droplets nor solid particles. Until now such commercial combustors have been largely limited to NG. Other fuels are usually burned using diffusion systems or non-premixed combustion systems with special burner designs [79][80]. With premixed combustion, the oxidiser and fuel, whether fuel-lean, stoichiometric or fuel-rich, are taken to be perfectly mixed prior to entering the combustion zone, see [Figure. 2-2\(B\)](#).

Premixed combustion systems can operate at a relatively low ϕ value, such that the flame temperature and, hence production of thermal NO_x is less than for a comparable diffusion system. Dry Low NO_x (DLN) systems use fuel-lean pre-mixed combustion to lower flame temperature, but these have the disadvantage of relatively poor flame stability, which increases the lower the ϕ value.

Premixed flames propagate towards the fresh fuel/oxidiser mix largely by diffusion: the heat released by the combustion process increases the temperature of the unburned reactants until they ignite. [Figure 2-4](#) shows a one-dimensional, pre-mixed, laminar flame propagating into a combustible gaseous mix, in which there is excess oxidizer, at speed S_l . S_l is a function of the reactants, their temperature and pressure. For typical, gaseous, hydrocarbon, premixed laminar flames the preheat zone, is between about 0.1 to 1 mm, but the reaction zone only one tenth that [71].

When the flows of air and fuel gas are increased until they become turbulent, the flame “brush” thickens and the flame speed appears to increase. This turbulent flame

speed (S_T) is substantially greater than S_l [67]. Numerous simple expressions have been suggested for the relation between S_T and S_l , via the turbulence intensity, \hat{u} , of the fuel/gas flow at the flame front. From the phenomenological arguments of Damköhler, theoretical analyses such as [81], and the experimental observations of [69][82] we obtain:

$$\frac{S_T}{S_l} = 1 + \alpha \left(\frac{\hat{u}}{S_l} \right)^n \quad (2.9)$$

Where α and n are parameters of the order of unity.

Equation (2.9) is in agreement with experimental observation that S_T increases with increase in \hat{u} until just before flame extinction, when a small decrease in S_T is observed. This small decrease is commonly termed the “bending effect”. However, S_T is not well-defined [83]. Its dependence on, e.g., flow parameters and chemistry characteristics is not yet fully understood. In practice, when tested against wide ranges of \hat{u} and ϕ values, Equation (2.9) and similar relations exhibit rather poor agreement with measured data [84]. This may suggest that there is no unique turbulent flame speed.

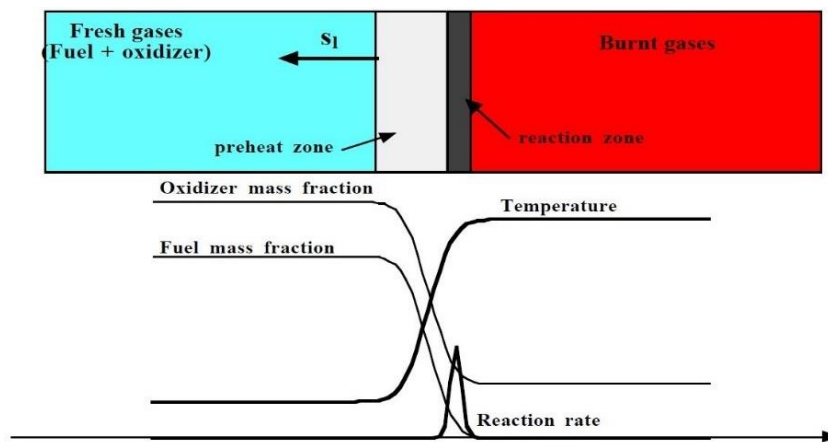


Figure 2-4: Schematic showing the structure of a laminar premixed flame. Adapted from [72].

Premixed flames provide efficient combustion as the reactants are mixed prior to combustion. The temperature of the combustion products which plays an important role in pollutant formation can be controlled by the proportion of fuel gas injected into the mix. But design of combustors for such flames may be difficult because the reactants should be mixed in well-defined proportions (oxidizer/fuel mixtures burn only for a limited range of fuel mass fraction). A premixed flame may also develop as soon as the reactants are mixed, leading to possible safety problems [71].

2.2.3.3 Partial Premixed Flame

Partially premixed combustion is a useful compromise when it is necessary to have the operation features of both premixed and non-premixed mixtures. Note that the descriptions offered above for premixed and non-premixed flames relate to idealised conditions. In practice, perfect premixing of oxidiser and fuel cannot be achieved. Indeed, to reduce pollutant emission or fuel consumption imperfect premixing can be deliberate [71]. In practice with so-called non-premixed flames, the oxidiser and fuel must mix in order to burn, which means partially premixed combustion zones.

Partially premixing can be used to reduce emissions and/or increase flame stability. In such systems, a proportion of the air or fuel is injected axially as a premixed blend, with the remainder of both air and fuel injected separately and mixed by turbulence [62]. The combustion process can be beneficially altered by such partial diffusion injection which can ensure ignition at the injection plane while simultaneously reducing pressure fluctuations [85]. However, from a practical point of view, several primary and essential issues regarding partially premixed combustion need to be resolved. Two such problems are how reactant composition inhomogeneities affect the laminar and turbulent flame speeds and how the burnt gas temperature varies as a function of these inhomogeneities. Knowledge of the flame speed is critical in optimizing combustion performance, and the minimization of pollutant emissions relies heavily on the temperature in the burnt gases [86].

2.3 Flow Characteristics of Swirl-stabilised GT Burners

Despite its wide use, and research into swirl combustion for over 70 years by many talented researchers, the combustion processes associated with swirling flows contain many poorly understood phenomena. Swirl combustion is a means of flame stabilisation, maintaining a flame seated on the burner within specified limits – the flame neither extinguishes nor spontaneously re-ignites [87]. Other methods of flame stabilisation include the use of pilot flames at the base of the flame, or a bluff body in the combustible stream downstream of the fuel injection system. The stabilisation mechanisms used will depend upon the application.

Flames “blow off” when the local flow velocity exceeds the flame speed of the combusting mixture. Bluff bodies and swirlers maintain the presence of a flame by generating zones where the local velocity of the combusting fluid is less than the flame speed.

With swirl burners the fuel flow velocity is expected to be a maximum as it passes through the burner nozzles. With distance downstream, the tangential velocity will progressively decrease, and there will also be a corresponding loss of radial pressure [88]. The ideal situation is where the flame sits at the nozzle exit, i.e., the burner design is such that the fluid velocity and turbulent flame speed match in that region. Should the flame speed decrease it is expected that the turbulent flame will stabilise at some point downstream. If, however, the decrease in flame speed is too large then the flame will not stabilise and it will “lift off” and “go out”.

2.3.1 Principles of Swirl Flow

Swirling flow is a flow simultaneously subject to both tangential and axial vortex motions [89]. These swirling components are generated by the flow of the fuel through the geometry of the burner which produces a spiralling or swirling motion in the flow. This tangential velocity component will affect the combustion process and be affected by the combustion process. A common parameter for characterising swirl flow is the swirl number [90].

The three most commonly used methods to produce swirl flow are [91]:

- Tangential entry (axial-tangential entry swirl generator).
- Guide vanes (swirl vane pack or swirler).
- Direct rotation (rotating pipe).

Here, tangential entry was used to generate swirling flow, see [Figure 3-1](#) in Chapter Three.

2.3.1.1 Swirl Number

Swirl number (S) is defined as “the ratio of axial flux of the tangential momentum to the product of axial momentum flux and characteristic radius” [92], see [Equations 2.10, 2.11 and 2.12](#). S is the dominant similarity criterion for specifying the intensity of swirling flows generated by geometrically similar swirl generators [93].

$$S = \frac{G_{\theta}}{G_x \cdot r_e} \quad (2.10)$$

Given that:

$$G_{\theta} = \int_0^x (\rho \cdot u \cdot w + \rho \dot{u} \cdot \dot{w}) r^2 dr \quad (2.11)$$

$$G_x = \int_0^x [\rho \cdot u^2 + \rho \dot{u}^2 + (p - p_\infty \cdot r^2)] dr \quad (2.12)$$

In [Equations 2.10, 2.11 and 2.12](#): G_θ is the axial flux of tangential momentum (kg·m/s), G_x is the axial momentum flux (kg/m·s), u is the axial velocity (m/s), \dot{u}_a is the Fluctuating axial velocity (m/s), w is the tangential velocity (m/s), \dot{u}_t is the fluctuating tangential velocity (m/s), ρ is the density (kg/m³), r is the radius (m), and r_e is the characteristic radius (m).

S is strongly affected by both the geometry of the combustor and the flow profile [\[94\]](#). Burner geometry is unchanged during any given test, but the combustion process will change the temperature of the flow both within the burner and within the combustion zone in ways that could affect the coherency of the flow structures and significantly influence the flow field [\[64\]](#). These fluctuations make the determination of the integrals shown in [Equations 2.2 and 2.3](#) exceptionally difficult. It follows that determining swirl number via [Equation 2.10](#) will also be extremely difficult as it involves evaluating both pressure and velocity profiles under different flows/ temperatures which could mean different values of S at different points in the flow field [\[64\]\[95\]](#).

Being able to specify a single value for S without having to obtain velocity measurements would be immensely beneficial. The geometric swirl number for radial-tangential swirl burners, (S_g) is a more easily obtainable representation of swirl imposed on the air-fuel flows. S_g is determined using only combustor geometry and inlet conditions, which means that changes in flow pressure can be disregarded [\[63\]](#).

Here we assume that the axial flux of angular momentum, G_θ , and axial momentum, G_x , are conserved in isothermal swirling flows [\[64\]](#), hence:

$$G_\theta = \int_{r_1}^{r_2} 2\pi \cdot \rho \cdot u \cdot w \cdot r^2 dr = const. \quad (2.13)$$

$$G_x = \int_{r_1}^{r_2} 2\pi \cdot (p + \rho \cdot u^2) r dr = const. \quad (2.14)$$

Syred and Beér [\[92\]](#), and Fick [\[96\]](#), agree that for constant density (isothermal conditions) and neglecting pressure variations across the flow, it is possible to evaluate a number (S) for the swirl burner as:

$$S = \frac{\pi \cdot r_e \cdot R_{eff}}{A_t} \left[\frac{\text{Tangential flow rate}}{\text{Total flow rate}} \right]^2 \quad (2.15)$$

In [Equation 2.15](#): r_e is the exit radius (m), R_{eff} is the radius at which the tangential inlets are attached with respect to the central axis of the burner (m), and A_t is the total area of the tangential inlets (m^2).

For radial-tangential swirl burners, the tangential and total flow rates are one and the same, and [Equation 2.15](#) simplifies to [Equation 2.16](#) [96]:

$$S_g = \frac{\pi \cdot r_e \cdot R_{eff}}{A_t} \quad (2.16)$$

Combustion will increase the temperatures of the fuel gas exiting from the combustor nozzle, and for swirl burners this will take place after tangential momentum has been added to the flow. This means the increase in temperature and consequent increase in volume of the gases will serve to reduce the level of swirl due to the relative increase in axial momentum with respect to tangential momentum of the flow [96]. $S_{g,comb}$, which allows for combustion effects may be expressed as [Equation \(2.17\)](#):

$$S_{g,comb} = S_{g,iso} \left(\frac{T_{inlet}}{T_{outlet}} \right) \quad (2.17)$$

In [Equation 2.17](#): T_{inlet} is the inlet temperature of the fluid (K), T_{outlet} is the outlet temperature of the fluid (K), $S_{g,comb}$ is the combustion swirl number, and $S_{g,iso}$ is the Swirl number at isothermal conditions (can be calculated using [Equation 2.15](#)).

S_g is not a measure of the flow swirl number of the flow exiting the nozzle. It is a measure of the flow into the burner and effect of burner geometry. Syred and Beér [92], and Beer and Chigier [97] have found the onset of the Central Recirculation Zone (CRZ) will take place at $S_g < 0.6$. Others [98][99] have reported obtaining CRZs even at very low values of S_g .

The value of the swirl number is the determining factor for the beginning of vortex breakdown (VBD), and thus the shape and size of the CRZ. Swirl is often divided into strong, weak and very weak [91][63]. $S_g \leq 0.2$ corresponds to very weak swirl and the adverse pressure gradient generated is insufficient to produce axial recirculation. $S_g \leq 0.4$ corresponds to weak swirl. For $0.2 \leq S_g \leq 0.4$, the velocity profiles normal to the jet axis are Gaussian in form, with maximum velocity along the jet axis. However, when $S_g \geq 0.5$ the maximum velocity is displaced from the jet axis and a recirculation zone is formed [97]. For strong swirl, $S \geq 0.6$, both the axial and radial pressure gradients are of sufficient magnitude to generate a recirculation zone.

2.3.1.2 Strouhal Number

The Strouhal number (S_r) is a dimensionless number that is weakly related to the Reynolds number (Re) and is useful for characterising flows. S_r is defined in numerous texts as “representing the ratio of inertial forces due to the unsteadiness of the flow or local acceleration to the inertial forces due to changes in velocity from one point to another in the flow field” [100]. S_r represents the unsteadiness of the flow and can be used in combination with other dimensionless numbers such as Reynolds (Re) and swirl numbers (S) to help characterise important aspects of swirling flows, such as the Precessing Vortex Core (PVC) [88][101]. The Strouhal number (S_r) is defined by [64]:

$$S_r = \frac{f \cdot D}{U_b} \quad (2.18)$$

In Equation 2.18: f is the oscillation frequency (vortex shedding) or precessing frequency (1/s), D is the characteristic length (exhaust diameter of swirl burner) (m), and U_b is the average bulk burner exit axial velocity (m/s).

To correlate the frequency of the system with the swirl number, S_r is used, this is related to the Strouhal number (S_r) [64]:

$$S_r = \frac{f D_e^3}{Q} \quad (2.19)$$

Where Q is the total flow rate through the burner.

2.3.1.3 Swirl Burner Configurations

In swirl burners, normally the flow is directed by an arrangement of vanes placed either radially or axially [41], see Figure 2-5. Actual GTs systems use both single and multiple arrangements to give the fuel/air distribution required for efficient combustion.

Radial swirl geometries have their inlets perpendicular to the burner’s central axis to produce the required swirl, see Figure 2-5 (A) [102]. The value of S_g for such burners is easily found, refer to section 3.2.1 in chapter three. Such burners can be readily adapted to vary the value of S_g and, thus, have been the subject of considerable research into swirl combustion [64][89][90][103]–[105]. Figure 2-5 (A) is a schematic of a simple radial swirl arrangement where air is injected through tangential inlets so arranged as to generate a flow that rotates around an axial injector through which fuel can be injected into the burner. Alternatively, the fuel can be premixed with air.

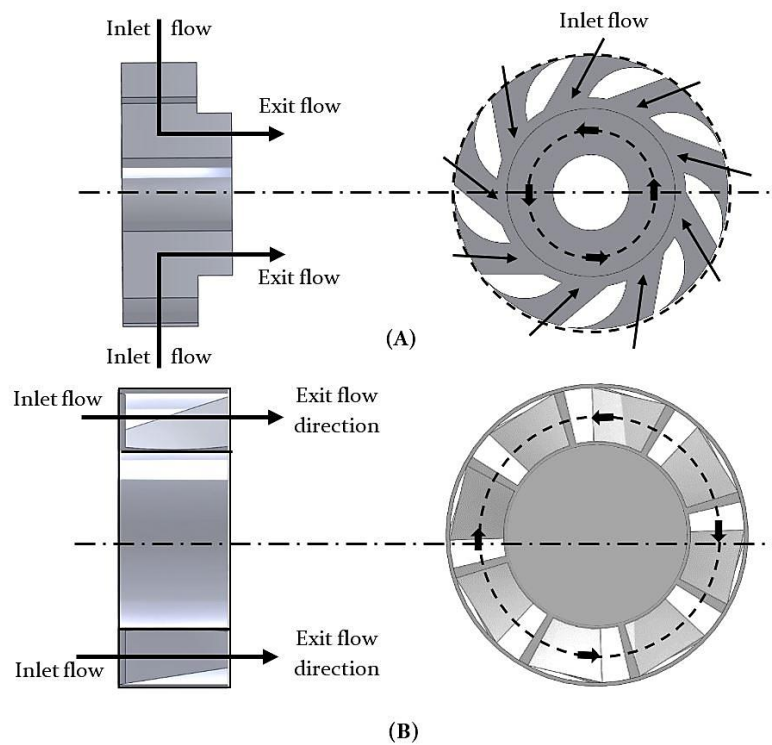


Figure 2-5: Schematic of: (A) radial-tangential swirler geometry ($S_g = 0.8$), (B) axial swirler geometry.

The axial swirl arrangement, as shown schematically in [Figure 2-5 \(B\)](#) [102] generates the swirl by using an arrangement of vanes that redirect the air flow and give a tangential momentum. This arrangement is not applicable to the geometric swirl number [Equation 2.16](#).

2.3.1.4 The Vortex Breakdown (VBD)

It is claimed [91][99] that swirl burners can create zones of reverse flow that are controllable and able to produce stable combustion due to a region of high turbulence and shear, called Vortex Breakdown (VBD). VBD occurs when S_g becomes greater than a particular threshold value and there is an abrupt disruption of the intact vortex core and, at the same time, flow retardation/reversal around the centreline [50]. Depending on the value of S , Re , and geometry of the combustor, VBD can be asymmetric or axisymmetric [106].

Axisymmetric VBD is distinguished by reverse axial flows round the centreline. Spiral VBD continues to present positive axial flows round the centreline, but with an off-axis volume of reverse flows. As the value of S approaches the threshold value, the flow remains axisymmetric. The onset of VBD appears either with an abrupt change

in the core as a spiral pattern with vigorous turbulence, or as a three-dimensional recirculating bubble of fluid, ovoid in shape, which sits in the flow just above the burner exit. A CRZ forms downstream of the burner, see [Figure 2-6](#), and remains in place over a wide range of flow conditions. The vortex core starts precessing with a constant frequency determined by burner geometry and flow conditions [\[91\]](#). The overwhelming majority of GT combustion systems use swirl generation with CRZ for flame stabilisation [\[107\]](#).

For swirl burners the VBD is very important because it is the major mechanism stabilising the flame. Characteristic of the VBD are reverse flows and stagnation points [\[108\]–\[111\]](#). Over the past five decades, many investigations on VBD phenomenon have been done. However, until now, no consensus has been reached on the basic mechanisms that produce the breakdown [\[112\]](#).

At first, as the value of S begins to increase, only bubble breakdown is seen. However, as the value of S increases the bubble moves upstream until it meets a solid boundary. If S is increased even further, the CRZ may form a reverse flow, columnar vortex which extends along the entire axis. According to Schuermans et al., [\[113\]](#), the velocity profile of the flow upstream of the VBD is similar to that of a jet with a maximum velocity which can be three times that of the mean. The conditions under which such effects appear are [\[114\]\[115\]](#):

$$VB_{crit} = \frac{1}{u^2} \int_0^\infty \frac{w^2}{r} dr + \frac{gH\beta\Delta T}{u^2} \equiv S + Ri \geq \frac{1}{2} \quad (2.20)$$

In [Equation 2.20](#): VB_{crit} is the Vortex Breakdown critical conditions for appearance, u is the axial velocity (m/s), r is the radius (m), g is the gravity acceleration (m/s²), H is the distance to the stagnation point (m), β is the thermal expansion coefficient (1/K), ΔT is the temperature difference (K), Ri is the Richardson number, ratio of potential to kinetic energy (-), and S is the swirl number (-).

The critical swirl number has been cited as $Sc = 0.6$ [\[101\]](#), above this value VBD definitely occurs. Compared to total flow rates only a small proportion is recirculated from the upstream core. On current theory, VBD is an accumulation of small-scale perturbations that build to create a large-scale disturbance to the flow. Paschereit and Gutmark [\[116\]](#), claim that Kelvin-Helmholtz instabilities are the source of the coherent structures formed in the separating shear layer. These vortices grow exponentially with roll-up of the shear layer, and a similar process occurs with the turbulence near the breakdown region. Logically, given that the level of turbulence is a measure of the

energy of the flow, a change in the state of the flow will show itself in a change in the energy spectrum of the turbulence [64][117].

Considering the VBD in more depth, it has been observed that the VBD redistributes the azimuthal velocity close to the envelope of the ovoid bubble. Initially, fluid near the burner axis, and moving in the direction of the burner axis, carries little angular momentum. However, to travel around the bubble it must move radially outwards. Conservation of angular momentum requires a decrease in tangential velocity. This means that in the region immediately exterior to the bubble the tangential velocity will be very low.

In some turbulent approach flows, the magnitudes of the swirl velocities within the CRZ do not diminish and the direction of spin of the swirl components inside the CRZ are in the same direction as the external flow. The transfer of circumferential velocity to the bubble is likely the result of turbulent diffusion [118].

2.3.2 Characteristics and Structure of Swirling Flow

With vortex breakdown, coherent flow structures form downstream of the swirl generating mechanism. Figure 2-6 presents an idealised picture of the downstream flow structures generated by the swirl burner of a typical GT [119].

Three distinct features can be discerned in the flow field: a VBD-induced CRZ downstream of the injector, the PVC surrounding the CRZ, and shear layers initiated at the outer rim of the inlet annulus [97]. It has been established [120] that in swirl flow a CRZ must be in place before a PVC can be formed. These structures significantly affect burner flame stability in both desirable and undesirable ways.

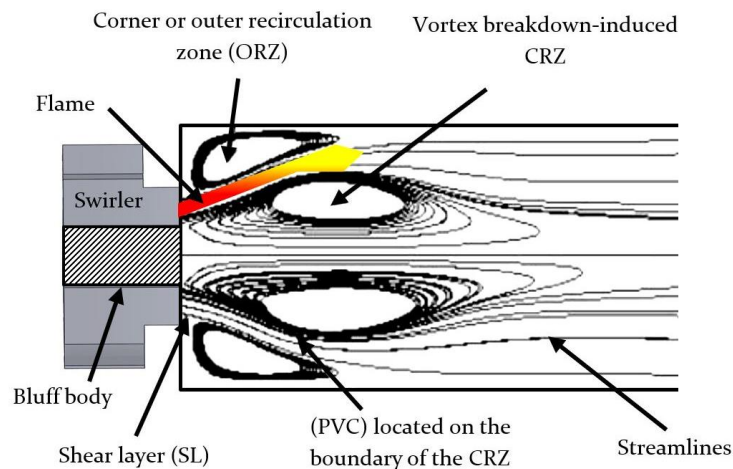


Figure 2-6: Coherent swirl flow structures of a typical confined swirl burner (radial-tangential swirler). Reproduced from [119].

2.3.2.1 Central Recirculation Zone (CRZ) and Velocity Profile

With increase in axial distance from the burner nozzle, the flow expands in both radial and tangential directions. At a critical value of swirl number S , the interaction of the tangential velocity profile of the swirl flow with a bluff body can create a reduction in velocity, and a zone of low or even negative pressure along the central axis of the burner [120]. The reduction in tangential velocity with distance along the central axis means there will be a corresponding reduction in the radial component of the centrifugal pressure gradient. There will be a consequent flow of fluid from the higher pressure to the zone where the fluid is at a lower pressure, this will create a recirculation zone with a net flow toward the nozzle, this is the CRZ.

The CRZ, see Figure 2-7, forms a low-pressure, low-velocity region, near the exit of the burner and re-circulates both active chemical species and thermal energy, increasing mixing rates especially near the boundaries of the recirculating zone, enhancing flame speed to match the turbulent flow velocity and stabilising the flame, all of which significantly reduce the flame length [64][92][120]. The formation and form of the CRZ are controlled by factors which include; equivalence ratio, flow field characteristics at the burner exit plane, and swirl strength [121]. Additional and very important factors are the burner configuration and the confinement imposed by the presence of the combustion chamber, both of which have considerable effect on the flow structure and hence on the shape and volume of the CRZ [64]. The volume of the CRZ tends to increase when the burner/flame system is confined due to the difference in the axial decay of the tangential velocity compared with the unconfined case [88].

Figure 2-7 (A) is a flow schematic showing the formation of a CRZ in unconfined swirling flow [88]. The CRZ formation, as observed is described by the radial momentum as expressed in Equation 2.21 [107], which uses the variables presented in Figure 2-7 (A) with the addition of ρ , the density of the flow. Close to the burner exit, we observe a rather rapid change in tangential velocity with radial distance which combines with the centrifugal force to produce a low-pressure region along the central axis.

The rate of change of tangential velocity, w , decreases with distance along the central axis, and pressure is recovered, creating a negative pressure gradient at the central axis. The combination of this pressure gradient and the low-pressure region at the burner exit centreline can generate reverse flow along the central axis in this region,

which is the CRZ. Of course, the swirl component must be large enough for this pressure distribution to form [88][107][122].

$$\frac{\delta p}{\delta r} = \frac{\rho w^2}{r} \quad (2.21)$$

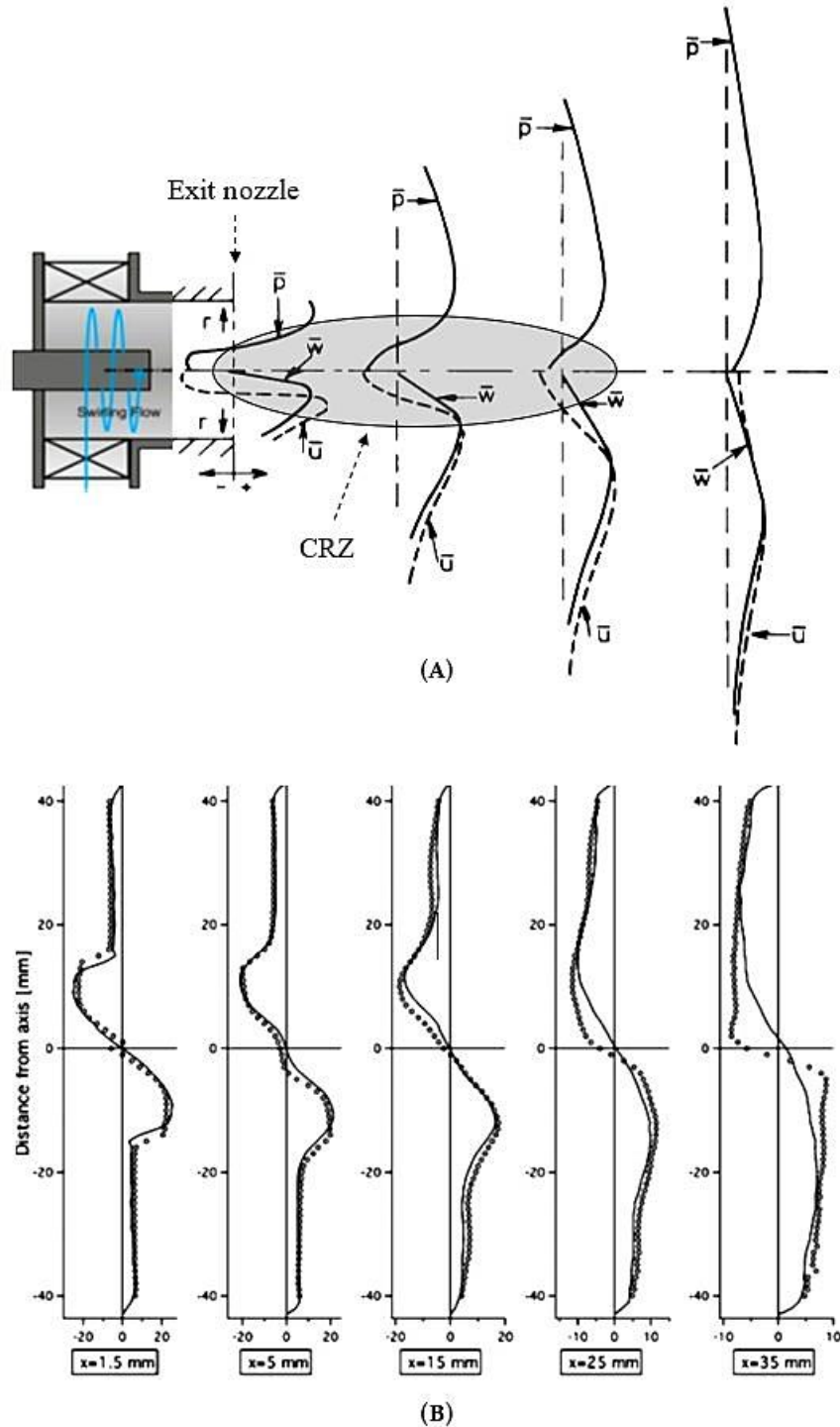


Figure 2-7: (A) Process of the development of the CRZ in unconfined swirl flows, (B) the tangential velocity profiles within the CRZ. p is the centrifugal pressure, r is the radial distance from the burner centreline, w is the tangential (or azimuthal) velocity and u is the axial velocity. Reproduced from [88][120][122].

Figure 2-7 (B) shows that downstream of the burner, w has a Rankine distribution. We see a steady increase from the central axis, rising to a maximum value at the forward shear layer (forced vortex), then a gradual decrease to a minimum value at the walls (free vortex). This pattern continues with distance downstream, though in this case the maximum levels showed a sharp decrease with distance downstream [88].

2.3.2.2 Precessing Vortex Core (PVC)

Syred and Beér were the first to report the presence of the precessing vortex core (PVC) in GT turbulent swirl combustors [92]; a 3-D asymmetric, unsteady, flow structure, the existence of which has since been reported many times [41][123]–[132].

The formation of the PVC usually occurs in flows with high Reynolds number and is linked to VBD and formation of a recirculation zone. Syred and Beér [94] noted that PVCs are usually located on the boundary of the CRZ between the zero velocity and zero streamline, see Figure 2-6. In combustion systems, the presence of the PVC will have a strong effect on both flow and flame evolution. Any displacement of the vortex core will push the flow field towards the chamber wall, conservation of angular momentum will cause a substantial increase in tangential velocity in the region where the flow is squeezed.

Figure 2-8 (A) shows how a PVC can distort the shape of the CRZ. We see that the profile of the CRZ becomes crescent shaped, rather than circular. The PVC and CRZ rotate around the central axis of the burner and system, see Figure 2-8 (A) and note that their direction of rotation is the same as that of the dominant swirl [88][102]. The presence of a PVC also helps explain the occurrence of instantaneous negative azimuthal velocity in the region near the centreline of the chamber.

A number of studies [88][104][133] have demonstrated that loss of tangential momentum and velocity with distance downstream from the burner means the PVC presents a helical structure about the central axis, see Figure 2-8 (B). The precession frequency will increase in direct proportion to the flow rate, and will be a function of chamber dimensions and S [88].

The PVC can enhance combustion efficiency by improving mixing and turbulence intensity, but it adds the unwanted possibility of coupling with low-frequency resonant modes present in GT combustors, and which can have serious adverse effects [88][121]. Many researchers have investigated mechanisms to minimise or eliminate

these undesirable oscillations, It was found that it possible to change the PVC frequency by changing the downstream configuration of a cyclone combustor [134], and that the PVC could be enhanced or delayed by such changes. Other researchers have shown distortions of the PVC occurred when the burner nozzle was changed [64][96]. Other techniques, such as multi-annular configurations of swirl injectors, and modulation of swirl strength have been suggested as means to suppress PVC oscillations in swirl combustors [123].

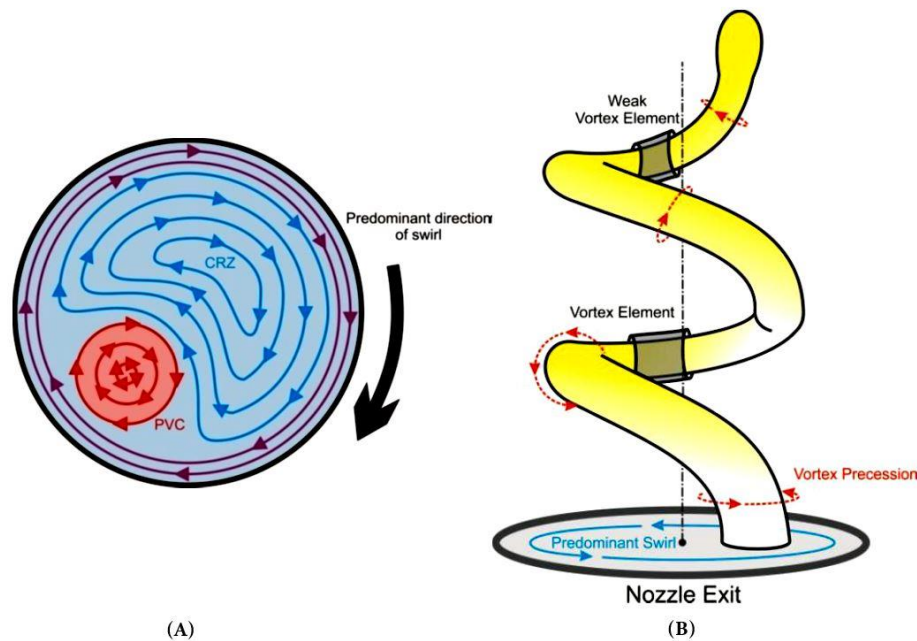


Figure 2-8: Visualisations of the PVC: (A) PVC and CRZ pairing, (B) PVC helical nature. Adapted from [88][102].

Wang et al., [128] carried out a Large Eddy Simulation (LES) study of the CFM56GT axial jet entry swirl burner using liquid fuel. Initially, the CRZ was found to align with the central axis, in a region immediately downstream of the fuel nozzle. However, after the stagnation point it moves away from the centreline taking a spiral form as it progressed downstream, the spiral twisted in a direction against the main flow rotation, but the structure as a whole followed the main flow. Consistent with reports by Syred and Beer [41], the induced low-pressure core was found to be exterior to the zone where the axial velocity was zero. Wang et al., also found that periodically large-scale vortices would peel off from the spiral core and be convected downstream.

The processes by which the PVC is manifested are not known for certain, but theories exist. Lieuwen and Yang [135] claim it is the result of a series of small eddies

generated by the CRZ. Paschereit and Gutmark [116] have suggested that Kelvin-Helmholtz vortices, produced by non-linear fluctuations in momentum and density, found a common path energized by the CRZ. Alekseenko et al., [136] have argued that the PVC is a symptom of a compression-expansion mechanism in the inner part of the vortex structure. Sarpkaya [134] investigated the nature of the VBD by exploring the possibility of two PVCs precessing around the recirculation zone.

Selle et al., [129] and Roux et al., [130] studied a Siemens swirl burner with pre-mixed fuels, under both reacting and non-reacting (isothermal) conditions. For the non-reacting flows a strong PVC was observed. However, for the given operational conditions considered, the PVC disappeared with combustion. This may have been due to the increase in viscosity and volume of the gases after being burnt [41]. If the PVC is severely diminished by the combustion process this would have a significant effect on any consequent pressure fluctuations. Syred et al., [137] used a radial swirl burner to demonstrate how a PVC could be affected by combustion, they compared measured pressure fluctuations under combustion and isothermal conditions. Figure 2-9, which shows typical comparisons between RMS pressure fluctuations for isothermal and combustor flows (NG fired through a central injector located on the back wall of the combustor).

Figure 2-9 (A) shows that when fuel is injected axially the amplitude of pressure fluctuations of the PVC are reduced significantly, by up to a factor of 15 when moving from isothermal to combustion conditions. Figure 2-9 (B) [137] shows the results for a similar test but with the fuel/air pre-mixed. We see that, premixing increases the sound level slightly over most of the spectrum of interest, but there is still a dampening effect at the peak frequency [102].

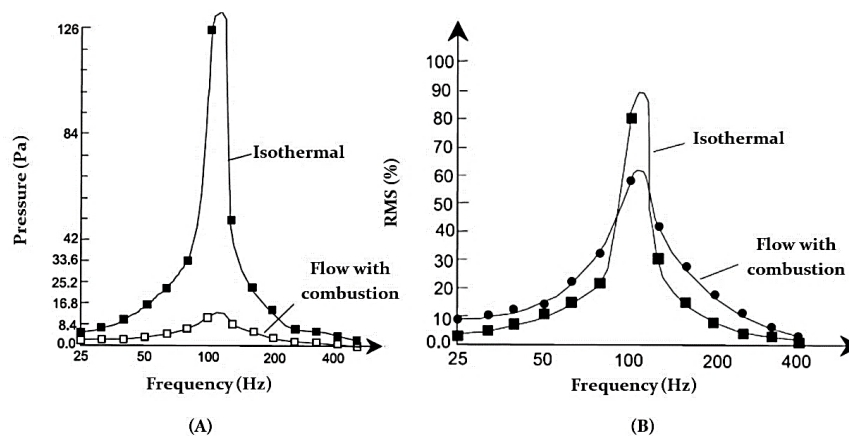


Figure 2-9: Differences between the levels of the fluctuating pressure caused by the PVC under different conditions: (A) isothermal, (B) combustion. Reproduced from [137].

Many investigators have attempted to explain the interaction between the PVC and the CRZ in swirling flow, one of the most comprehensive studies was by Syred [88]. Syred's study correlated known information on the formation of CRZ and PVC with swirl number (S) and burner geometry. Syred reported that the higher S , the stronger the CRZ. However, it is known that there is a lower limit to S , for VBD, coherent swirl structures normally begin to form for $S \geq 0.6$.

The frequency of the PVC can be characterised by Strouhal (S_r) and swirl (S) numbers, by the flow momentum and fluctuations in pressure [64][92][120][137]–[139]. Fick [96] has demonstrated that a pressure sensor mounted on a burner nozzle has shown that the PVC generated pressure fluctuations at the same frequency that it rotates around it. The PVC can be visualised with surfaces of constant pressure and vorticity, swirl strength λ and the λ_2 criterion [41][104][128][130][140]–[143].

Visualisation techniques including Chemiluminescence, Laser Doppler Anemometry (LDA), Particle Image Velocimetry (PIV) and High-Speed Photography (HSP) have been used effectively to investigate different types of swirling flows and coherent structures [104]. Valera-Medina, et al., [104] used these techniques to visualise and identify new structures in a tangential swirl burner with isothermal flow. The manner in which the CRZ and PVC co-exist, their shapes, sizes and interactions all depend on the flow regime and burner geometry. An interesting finding of this study was the observation of a channel formed by the PVC on the side of the CRZ and which was taken as evidence of interaction between them. In addition, this paper also demonstrated the formation of a secondary central recirculation zone (CRZ₂), subject to confinement conditions. Generally, the formation of these regions depended upon burner configuration, flowrate, location of the flame front, mixture ratio, and swirl number.

Extensive numerical studies based on Large Eddy Simulation (LES) have been used to give a visual representation of the PVC and definitively explain its manifestation [128]. Comparison of an actual PVC image obtained experimentally for a premixed flame with a CFD/LES visualisation clearly shows the LES model produced an exaggerated PVC representation [96].

2.3.2.3 Shear Layer and Coherent structure

The flow is expelled from the burner and travels downstream; because of the difference in velocities between the jet flow and the ambient fluid strong shear layers develop, see Figure 2-10. Of course, the presence of a bluff body in the flow is another means of generating shear layers. Within the shear layers it is possible that large-

scale coherent structures are generated and, due to Kelvin–Helmholtz instabilities, they can be shed and travel downstream [116]. These vortices generate fluctuations in the mixing of air, fuel and hot products of combustion and in this way can exert a significant influence on the combustion process [41].

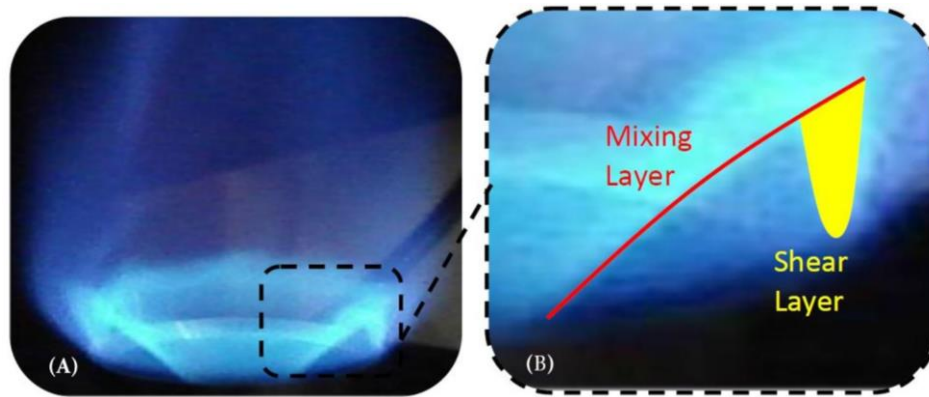


Figure 2-10: Shear layer propagation in a swirling flame: (A) the full flame, (B) indication of the mixing and shear layers. Adapted from [102].

Disturbances generated by the PVC and shear layers also play a role in the propagation, quenching, re-ignition, and stabilisation of flames in strong swirling flows. Stöhr et al., have reported that these disturbances can cause quasi-periodic flame roll-up, influencing ignition along the swirling shear layer by enhancing the mixing of hot products and fresh reactants, [143]. Stöhr et al., also claim to have created a time-varying stagnation point in the region of the swirler exit, where flame ignition and propagation are inherently unsteady and unstable [144].

There will be strong shear layers when high speed swirling flow encounters the relatively slow-moving fluids present in the combustion chamber, conditions under which flame can propagate backwards towards the nozzle of the combustor. The greater the distance from the burner, the less the fluid velocity and the greater the thickness of the shear layer, see Figure 2-10 (A) and (B) [102]. The mixing layer is where the flame front meets the un-ignited air/fuel mixture. Across the flame front there is a velocity gradient which is important for flame stability [145]. Figure 2-10 (B) shows the flame front's mixing layer.

2.3.2.4 Outer Recirculation Zone (ORZ)

An Outer Recirculation Zone (ORZ), see Figure 2-6, also referred to the corner external recirculation zone, is generated by the rapid expansion of the flow out of the nozzle into a combustion chamber of greater diameter (contained combustion), which

generates low-pressure ORZs in addition to the CRZ. The ORZ helps retain and stabilise the flame by re-circulating hot unburned gases into the reactant mixture [88][146]. Suitable design of the combustor can avoid the formation of the ORZ by avoiding the presence of corners where low-pressure zones can form [102].

Return to Figure 2-6; it presents a time-averaged representation of the ORZ for a confined flame. It also shows the flame, shear layers and CRZ, the coherent flow structures found with confined swirl flames [122]. However, swirl flames occur in unsteady, highly turbulent flows with reaction zones that are typified by the formation of flow vortices, followed by their dissipation. Swirl flame also exhibit reaction chemistry that takes place on a number of different temporal and spatial scales [41][122][147].

2.4 Modern Combustion Systems for GTs

It is expected that the next generation of GTs will work at higher turbine inlet temperatures and higher-pressure ratios, which would be expected to escalate emissions of NO_x. To satisfy likely future clean air standards, lower NO_x emissions will be required and that means new combustion technologies. Here, a number of possible combustion systems are briefly introduced.

2.4.1 Rich-Burn, Quick-Mix, Lean-Burn (RQL)

Two techniques for low NO_x emissions presented in the literature are “Lean direct injection” (LDI) and “rich-burn/quick-quench/lean-burn” (RQL) [148]. LDI, as its name implies, has lean primary combustion so that flame retention has to be used. RQL refers to a system with three stages of combustion; the first is a fuel rich primary combustion zone, downstream there is a rapid shift to a lean mixture by the speedy injection of sufficient air in the Quench zone for the final combustion to be fuel lean see Figure 2-11 (A) [149].

Both RQL and LDI avoid stoichiometric conditions, so the combustion is at a relatively low temperature and this reduces production of pollutants. However, the two systems are fundamentally different, the main combustion/heat release regions are very different, and one requires flame retention. The RQL system was first proposed in 1980 as a means of reducing NO_x emissions [148], and today, RQL is of great interest for stationary, power generating GTs because these are better able to process complex fuels.

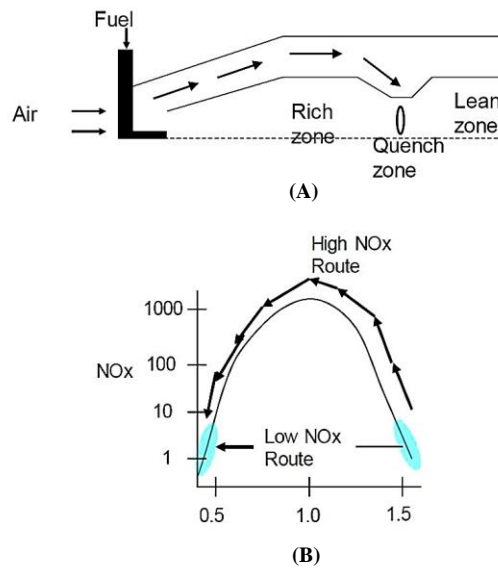


Figure 2-11: Rich-Burn, Quick-Mix, Lean-Burn (RQL) combustor: (A) combustor description, (B) NOx rout. Adapted from [149].

The primary zone of a GT combustor is most effective with fuel rich mixtures which enhance flame stability by producing high concentrations of active hydrogen and hydrocarbon radicals. Additionally, rich burn minimises the generation of NO_x, this is because of the low population of oxygen containing intermediate species, and relatively low combustion temperatures [149]. The success of the RQL in reducing NO_x emissions depends crucially on carefully controlling the rich and lean conditions (equivalence ratios, ϕ) and obtaining the required cooling rates so that the combustion moves rapidly and smoothly from fuel rich to fuel lean without passing through the high NO_x production region, see Figure 2-11 (B). Typical values of the equivalence ratio, ϕ , for fuel rich and lean combustion zones are 1.2-1.6 and 0.5-0.7 respectively. The drawback of RQL is the complexity of the system and the extra hardware needed [148].

The injected air must mix rapidly and smoothly transition the conditions from rich to lean-burn, in particular by reducing the temperature sufficiently to avoid NO_x production while maintaining it sufficiently high to avoid CO and unburned hydrocarbons (UHCs). To satisfy the relevant emission standards the value of ϕ for the lean-burn zone must be selected carefully [149].

2.4.2 Trapped Vortex Combustion (TVC)

The “trapped vortex combustor” (TVC) is a promising approach to reducing pollutant emissions and pressure drop across the combustor. The TVC generates a stable

vortex by means of cavity stabilisation, which acts as a pilot flame for the main flow of the fuel/air mix. Researchers have been investigating such schemes since the early 1990's [150] and have tended to concentrate on liquid fuel and aircraft combustors [148].

TVC offers a number of advantages for GTs: the most important of which is its capacity for burning a range of fuels, with calorific values from low to medium with enhanced flame stability, and extended flammability limits. But TVCs can also function with very lean fuel/air mixes which can reduce the possibility of flashback. TVCs can also produce very low NO_x emission levels without post-combustion treatment since it can be operated as a staged combustor if the fuel is injected into both the cavity and the main airflow. Generally, staged combustion systems have the potential of achieving about 10 to 40% reduction in NO_x emissions [151], see the next section.

2.4.3 Staged Air Combustion

Sequential, contiguous combustion stages with recirculation within the combustion chambers have been shown to produce stable combustion with low CO and NO_x emissions. Experimental results have demonstrated that such a combustion system can attain a clean exhaust; a European Commission research project was able to reduce NO_x emission to 2-4 ppm and CO emission to < 7 ppm, using an air/fuel ratio of 2.5 [148][152]. To optimise a particular aspect of the GT's performance staged combustion can be arranged to be either axial or radial, as appropriate [149].

2.5 Lean Premixed Combustion (LPC)

Lean premixed combustion (LPC) is used in numerous applications, including GTs, and IC engines [95], with high levels of excess air resulting in $\phi \ll 1$. Premixed, lean fuel is widely believed to be a promising approach to reduce unwanted emissions from GT combustion [153][154]. Some researchers have suggested NO_x levels < 10ppm are possible [149].

With LPC, NO_x formation is directly affected by residence time and local flame temperature with lower flame temperatures meaning lower NO_x emission; and in most lean premixed flames the fuel is combusted at a lower temperature than in typical, normal combustors [155]. But lower flame temperatures mean slower chemical reaction rates, requiring more time to completely oxidise CO into CO₂. Hence, lean premixed flames, may well emit higher levels of CO and UHCs, thus combustors

intended for lean premixed flames need to be designed to meet CO and NOx emission standards. This has been achieved by controlling flame temperatures by regulating ϕ [63].

Flame “blowoff” is an inherent and common problem with lean combustion [156], another is flashback [157]–[160]. The latter is more likely the faster the flame speed, i.e. the greater the concentration of hydrogen in the fuel blend [89][161]–[163]. Additionally, the low frequency, thermo-acoustic, combustion instabilities produced from swirl flow structures can be coupled with the natural frequencies of the combustion system equipment producing resonance and damages [88][164].

LPC technology is widely used with GT swirl burners to reduce harmful emissions [41][165][166]. However, the generation of such coherent structures as CRZs and PVCs will directly affect combustion stability and the combustion processes due to the lack of damping mechanisms relative to diffusion flames [104][167]–[169].

2.6 Flame Stability Issues

For efficient combustion which produces few or no greenhouse gases (particularly NOx and CO₂), a complex balance must be preserved between reaction chemistry and energy transport in a highly turbulent flow field. With swirl-stabilized flames such a combination can generate non-steady processes affecting flame stability [50], and this has been an important area of research in modern GT combustors with the use of LPC to reduce greenhouse gas emissions [94]. We note that combustion instabilities can cause serious damage to GT combustion systems [35][122].

2.6.1 Lean Blowoff

GT combustors operating under LPC deliver the benefit of reduced emissions, but when operated near lean blowoff are intrinsically prone to low frequency, high amplitude, pressure oscillations [88]. These fluctuations in pressure are the result of higher values of τ_c , and lower values of τ_m . For $\phi < 1$, lean flames are typified as having a low adiabatic flame temperature and poor combustion efficiency. These can appear in the combustion process as periodic flame extinction and re-ignition [122][170]. Lean blowoff is flame extinction that occurs when the flame leaves its anchor and moves downstream where it is extinguished. In GT combustors such an event is most likely to happen under part-load conditions or transient operation such as GT start-up. A common technique for avoiding blowoff is stabilisation using a pilot flame which is supplied with a richer fuel/air mix than for the main flame, or maybe a

diffusion flame. However, such pilot flames will have a higher combustion temperature than the main flow and this could increase the formation of NO_x. In practice, it is preferable to avoid blowoff through accurate control of the combustor's blowoff limits [65].

Two theoretical approaches are currently being used to describe blowoff [171][172]. The first assumes that blowoff takes place when the residence time in the combustor is too short for the necessary chemical reactions to take place. The chemical time scale τ_c is approximated using S_l and thermal diffusivity of the mixture (α) see Equation 2.22 [65][172][173].

$$\tau_c = \frac{\alpha}{S_l^2} \quad (2.22)$$

The chemical time scale (τ_c) and residence time are compared based on flow properties and combustor dimensions.

A second means of estimating the chemical kinetic time τ_c is to determine the residence time for the lean blowoff in a perfectly stirred reactor, using the ratio of flame and flow speed. Flamelet-like combustion behaviour is assumed; blowoff takes place when the speed of the flow is greater than the flame speed at certain critical sites inside the combustor [174].

In both methods, prediction of blowoff is possible only with knowledge of the characteristic kinetics of the mixture [175], and the flow field in the combustor [65].

The flame holder is vital for ensuring a stable flame, and numerous papers have reported using bluff bodies as the flame holders and their effects on blowoff limits. Lieuwen, et al. [176] investigated the effect of varying the geometry of bluff-bodies, emphasising that vortex shedding from the bluff-body plays a key role in determining gas expansion across the flame and hence the blowoff mechanism. Roychowdhury and Cetegen [177] related flame strain rate with turbulent intensity and found that as the one increased so did the other, which inevitably led to areas of local extinction on the flame's surface. Other researchers have also reported that ϕ at blowoff is affected directly by upstream flow extinction [177].

Radhakrishnan et al. [173] developed a relationship for flame extinction for premixed CH₄-air swirl flames based on the Damköhler number [178]. The authors considered the contending influences of increasing τ_c with decreasing τ_m , at near-lean and lean blowoff conditions under high pressures and temperatures [122]. The resulting relationship, Equation 2.23, shows flame extinction takes place when the product of

$\tau_c (= v/S_l^2)$, and reciprocal of, $\tau_m (= \bar{u}/D_{lance})$ exceeds a certain value (R) which would be in the order of unity at extinction. This assumes that the three constants A , C_1 , and C_2 , obtained from flow, geometric, and turbulence scale considerations hold their values [178].

$$\frac{1}{Da} = \left[\left(\frac{C_1}{C_2} \frac{15}{A} \right) \left(\frac{\bar{u}}{D_{lance}} \right) \left(\frac{v}{S_l^2} \right) \right]^{\frac{1}{2}} > R \quad (2.23)$$

Where D_{lance} was diameter of the instrumentation (pilot lance bluff body). At lean blowoff, increasing mean burner exit nozzle velocity (\bar{u}), would result in a reduction in τ_c coupled with an increase in τ_m [122].

2.6.2 Autoignition

Autoignition has been defined as the “spontaneous ignition of a fuel/oxidizer mixture in the absence of any concentrated source of ignition such as a flame or spark” [50]. It is happening when the residence time in the premixing section exceeds the ignition delay of the mixture. Autoignition can seriously detract from GT performance and inflict substantial damage on the system, particularly in GTs where the fuel and oxidiser (air) are mixed prior to entering the combustor. Autoignition usually occurs when there is a sudden increase in the reaction rate of a combustible mixture, such an increase can be due to either: the heat of combustion increases and with it the temperature of the reaction, which then accelerates the reaction rate; or the exponential multiplication of reactive species (radicals) through chain branching reactions accelerates the reaction rate [65].

Ignition delay (assumed to be the inverse of the reaction rate, τ) of a given fuel/oxidizer mix will depend on its temperature, pressure and the value of Φ , in the form of an Arrhenius equation for the reaction rate [65]:

$$\tau = Ap^{-n}\Phi^{-m} \exp\left(\frac{E}{R_u T}\right) \quad (2.24)$$

In Equation 2.24: A , n and m are constants which are determined experimentally, p is the pressure (Pa), E is the activation energy, R_u is the universal gas constant and T is the initial temperature of the fuel/air mixture.

Both chemical reactions and a number of physical processes (including turbulent mixing and heat loss to the walls) are involved in autoignition of fuel/air mixtures in a GT combustor. This is especially true when flow is present, where the interaction

between the physical aspects (fluid mechanics) and chemical effects will affect the ignition delay of the given fuel/air mix [65].

Natural gas (or CH₄) is the favoured fuel for GTs used for electrical power production, and has reasonably weak autoignition behaviour at low temperatures [179]. However, if H₂ is added, the proportion of H₂ in the mix has a substantial impact on autoignition. The more H₂, the more the chemistry of hydrogen dominates the ignition of the mix [180].

In GTs using swirling combustion, where aerodynamic effects dominate (e.g., fast flow rates, strong swirling motion) they are directly linked to autoignition time. On the other hand, weak aerodynamic effects make the systems more disposed to flashback. This means that the ignition delay time of the fuel/air mix being used and local aerodynamic conditions need to be taken into account when designing a premixer to preclude autoignition [34].

2.6.3 Flashback

Flashback is a particular feature of premixed flames, whereby the turbulent flame speed exceeds the local flow velocity and the flame front moves from a previously stable location downstream against the fuel/oxidizer flow and towards the zone where the fuel/oxidizer were mixed. Unfortunately, in GTs with LPC, this location is usually inappropriate for flame stabilisation (e.g. swirl vanes or a mixing plenum) [122][147]. However, experimental studies reported in the literature have demonstrated that in swirling flows, flashback is not simply a competition between flame speed and flow velocity [154][162][163][181][182]. Flashback has been shown to be very much dependent on the characteristics of the fuel/oxidiser flow and the flame stabilisation device used. We have seen that for $\phi < 1$ the blowoff of lean flames is related to decreasing τ_c and increasing τ_m . However, for $\phi < 1$, flashback generally occurs for increasing τ_c and decreasing τ_m [122]. Lean flame flashback, due to variation in the fuel/oxidiser composition has been noted in GTs, especially where H₂ was added to the fuel gas [122][183], but enhanced C₂₊ levels can have a similar effect [35].

It is natural to associate flashback with turbulent burning velocity, S_T , which is larger than the laminar burning velocity, S_L . Beerer et al. [183] found that for pure methane, S_T was directly related to the fluctuating axial velocity (\dot{u}). Of course, adding a gas such as H₂ with a very fast flame speed will increase S_L . Thus flashback must be considered, when blending H₂ with CH₄ [122].

It has been noted that flame movement during flashback will often follow boundary layers. Within a swirling flow field these will include the shear layers between the CRZ and ORZ, see [Figure 2-6 \[122\]\[147\]](#), because these layers have a lower velocity than the mean flow. Four flashback mechanisms will be discussed in the next section [\[154\]\[166\]\[175\]\[184\]](#).

2.6.3.1 Flame Propagation in High-Velocity Core Flows

In turbulent swirl flows, the link between S_T and magnitude of the turbulence fluctuation is essential for determining flashback. In such flows, local flow velocities can be significantly lower than the mean velocity in the combustor; such an event will pose the possibility of flame propagation upstream from the combustor towards the mixing zone. Such flashback is, therefore, highly dependent on turbulent velocity fluctuations [\[65\]](#). Consequently, a basic design parameter for swirl burners is to ensure that fuel/oxidant mixes are always subject to axial flow velocities that are everywhere greater than S_T [\[79\]](#).

Despite measurement of S_T being difficult because of the very complex chemical interactions caused by turbulence there have been many publications published on measurement of turbulent flame speeds [\[185\]](#). To propagate, the turbulent flame speed must be greater than the characteristic fluctuations in turbulent velocity. In the swirl burners the strength of the turbulence fluctuation in the mixing zone is determined by swirl strength [\[79\]](#). Swirl flames are both wrinkled and corrugated (see section 2.2.2) which means a substantial increase in flame surface area and S_T being higher than S_L . The S_T is constant but the wrinkling means a greater flame front area and so the rate at which the mix is burned increases. With such a relation between S_T and S_L , one could conclude that to achieve effective resistance to flashback, low turbulence burners are better suited for fuels having high values of S_L than swirl burners [\[185\]](#).

Lipatnikov and Chomiak [\[186\]](#) found that decreasing the Lewis number (Le) (the ratio of thermal to mass diffusivity) which depends on the composition of the fuel, the turbulent flame velocity increased. Kobayashi, et al. [\[186\]](#) compared measured values for S_T for syngas flames burned with air ($CO/H_2/CO_2/air$) using Hydroxyl Planar Laser Induced Fluorescence and flame radiation for methane/air flames. They reported that the ratio (S_T/S_L) for the $CO/H_2/CO_2/air$ flame was greater than that for CH_4/air flames. LDA technique was used to measure local flame displacement and so measure S_T for H_2/CH_4 flames for a low swirl burner for different gas ratios and levels of turbulence intensity [\[63\]\[183\]](#).

2.6.3.2 Boundary Layer Flashback (BLF)

Having assumed a no-slip wall boundary condition, the axial flow velocity will increase from zero at the wall boundary to the free stream velocity. Boundary layer flashback (BLF) is where a flame propagates through the regions of low flow velocity close to the wall, see [Figure 2-6](#), into the premixing zone. However, the flame speed will also decrease close to the wall because within a distance known as the “quenching distance” heat loss to the wall quenches the chemical reactions. Flashback can occur in the boundary layer only if the boundary layer is more than the quenching distance from the wall, and the local flame speed is greater than the flow velocity [\[65\]](#). This explanation of the BLF was originally proposed for laminar flames by Lewis and von Elbe [\[187\]](#) some eighty years ago.

Wohl [\[188\]](#) extended and emphasised quenching effects. His model defined the limits on flashback in terms of a critical velocity gradient, g_c . The velocity of a near-wall layer, flowing parallel to the wall was $u(y)$, where (y) represented the wall - normal coordinate. The flame speed was $S_f(y)$ at the quenching distance d_q from the wall.

From [Figure 2-12](#) for equilibrium between $u(y)$, and $S_f(y)$, we see g_c at the wall can be used as a measure of the laminar wall flashback limit [\[189\]](#) and can be represented by [Equation 2.25](#) [\[63\]](#):

$$g_c = \frac{\partial u}{\partial y} = \frac{S_f(y)}{d_q} \quad (2.25)$$

In [Equation 2.25](#): g_c is the critical velocity gradient (s^{-1}), $S_f(y)$ is the flame speed (m/s), and d_q is the quenching distance (m).

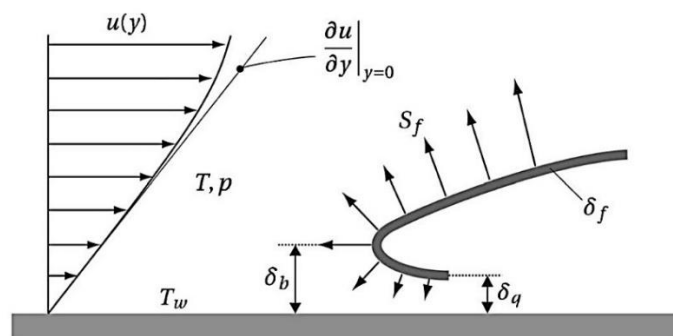


Figure 2-12: Flow and flame configuration model (2D) at the onset of laminar boundary layer flashback (BLF). Adapted from [\[189\]](#).

Generally, g_c will depend on wall temperature, fuel-oxidiser kinetics, local pressure and temperature, Φ , and the local geometry. Equation (2.25) suggests flashback can take place when the velocity gradients at a distance d_q from the wall become lower than the flame speed. In another word, that if $S_f(y)$ is greater than the local velocity and the distance from the wall is $> d_q$ flashback is possible. Lewis and Von Elbe [187] suggested the critical velocity gradient, g_t , for laminar poiseuille flow in circular pipes as:

$$g_t = \left. \frac{\partial u}{\partial r} \right|_{r=R_t} = \frac{4U_b}{\pi r^3} \quad (2.26)$$

In Equation 2.26: r is the radial coordinate (m), R_t is the radius of the tube (m), and U_b is the bulk flow velocity (m/s).

Lin, et al. [190] suggested a method of relating propensity for boundary layer flashback with S_T for hydrogen rich gases for measurement of critical velocity of the flame and flow characteristics as follows:

$$g_c = \frac{S_T}{(Le \cdot \delta_{l0})} \quad (2.27)$$

In Equation 2.27: g_c is the critical velocity gradient of the flame (s^{-1}), R_t is the Lewis number which represents the ratio between thermal diffusivity to mass diffusivity (-), and δ_{l0} is the (un-stretched) laminar flame thickness (m).

They suggested Equation 2.28 as representing the critical velocity gradient of the flow:

$$g_f = 0.03955 * U_b^{\frac{7}{4}} * \nu^{\frac{-3}{4}} * d^{\frac{1}{4}} \quad (2.28)$$

In Equation 2.28: g_f is the flow velocity gradient (s^{-1}), U_b is the bulk velocity at the combustor inlet (m/s), ν is the kinematic viscosity of the combustible mixture (m^2/s), and d is the diameter of combustor inlet (m).

Equations (2.27) – (2.28) suggest that flashback takes place when g_c exceeds g_f . Although Equation (2.25) has been used extensively to describe BLF, it omits consideration of flame-flow interaction. Additionally, the local flame speed might be significantly affected by heat transferred from flame to combustor wall in addition to any flame stretch effects. This means g_c must be measured experimentally for the fuel being used [147].

BLF for turbulent flames was investigated by Yamazaki and Tsuji [191] who suggested that the flashback limit could not be adequately explained by the notion of velocity gradient because, in turbulent flows, the boundary layer was very thin. Fine reported [192] that the critical boundary velocity gradient for turbulent flashback was significantly larger than that for laminar flashback. He proposed that in near flashback conditions, a turbulent flame could be stabilised in the laminar sub-layer much closer to the boundary wall than could be attained by a laminar flame. This was put down to the fact that the heat transfer coefficient in the presence of turbulence decreased from the turbulent core toward the wall.

Many studies have investigated different mechanisms to reduce or avoid wall BLF. Eichler and Sattelmayer [189] attempted a 2-D exploration of flashback in hydrogen rich mixtures flowing over a flat plate. They found considerable differences with results reported for tube burners. This was ascribed to adverse pressure gradients in the boundary layer, producing a totally different interaction between flame and flow. Two years later Eichler and Sattelmayer [158] confirmed that the limits of wall BLF are governed by flame tip quenching in a “backflow region” upstream of the flame front generated by the interaction of boundary layer and a pressure increase ahead of the flame front.

Al-Fahham et al. [193] originated a novel technique encouraged by biomimetic engineering; to enhance resistance to BLF in swirling flows through the use of micro-surfaces consisting of a fine (of the order of 10^{-5} m) woven steel mesh. The addition of these biologically inspired shapes successfully stabilised flows and gave added control of the boundary layer, reducing outflow drag and enhancing system resistance to BLF. Combustion stability maps showed an extended operational region when the micro-surfaces were used.

2.6.3.3 Flashback Caused by Autoignition

Flashback caused by autoignition occurs when a flame autoignites in the premixing section, usually because the residence time of the fuel-air mixture exceeds the time necessary for autoignition. Plee and Mellor [194] and Sayad [65] have observed that autoignition can occur in the premixing zone of the combustor, even under conditions where the mean-flow residence time is an order of magnitude shorter than the ignition time predicted by chemical-kinetics for the given fuel-air mixture. Beerer and McDonnell [195] determined experimentally the autoignition times for hydrogen in an environment comparable to those of a GT premixing zone. They noted that on occasion autoignition did not occur even with high temperatures along the walls of

the reactor [195]. The authors explained this delay as due to increased residence time of the reactants along the wall, combined with catalytic reactivity at the walls [65].

2.6.3.4 Combustion Induced Vortex Breakdown (CIVB)

Combustion Induced Vortex Breakdown (CIVB) can be, but should not be, confused with Vortex Breakdown (VBD). VBD is the root cause of the CRZ, but CIVB is the reason for its destruction [102]. Therefore, for stable flames, CIVB should be forestalled and prevented.

In swirling combustion CIVB is a source of rapid flame transition and a flashback mechanism in which a recirculation zone with strong backflow of hot gases becomes a mechanism for flame stabilisation. The relative strengths of the incoming flow and the backward flow in the recirculation zone will determine the position of that recirculation zone. This balance is a dynamic one and can be disturbed by interactions between the recirculation zone and the flame, causing the recirculation zone to travel out of the combustor and into the premixing zone. This generates a region of low velocity upstream of the flame, which allows the flame to move into the premixing zone. Numerous studies agree that the CIVB can occur even when the turbulent flame speed is lower than the flow velocity [154][185][196]–[199].

The earliest study of CIVB was by Kröner, et al. [184] who investigated flashback limits for LPC with swirl burners, with a cylindrical premixing section without centre-bodies. It can be debated whether VBD plays a role in turbulent flame propagation by augmenting the position of the flame in a way that makes them happen more readily [200].

Valera-Medina et al. have observed that the CRZ is closely connected to system stability, its curvature, shape and strength all being of great importance for resisting blowoff and flashback [64][121][201][202]. The interaction between recirculation zone and flame can be explained by considering the azimuthal vorticity transport equation, Equation 2.29 [203]:

$$\frac{D\omega}{Dt} = \frac{\partial}{\partial t}(\vec{\omega}) + (\vec{U} \cdot \nabla)\vec{\omega} = (\vec{\omega} \cdot \nabla)\vec{U} - \vec{\omega}(\nabla \cdot \vec{U}) + \frac{1}{\rho^2}(\nabla\rho * \nabla p) \quad (2.29)$$

In Equation 2.29: $\vec{\omega}$ is the azimuthal vorticity (m/s), \vec{U} is the velocity vector (m/s), ρ is the flow density (kg/m³) and p is the static pressure (Pa).

Equation 2.29 describes how, according to Lenz's law the change in azimuthal vorticity, ω , will produce a velocity component moving in a direction against the main flow [204]. Azimuthal vorticity is enhanced by heat energy from the flame and this can

affect the location of the CRZ. In Equation 2.29 the last terms on the RHS correspond to baroclinic torque and the last but one term represents the volume, both generated by the combustion process. Baroclinic torque generates an azimuthal vorticity which induces an axial velocity in a direction that acts to push the flame upstream towards the premixing zone [198]. The volume expansion, on the other hand, produces an azimuthal vorticity that reduces the induced axial velocity acting against the incoming flow. Thus, the density change across the flame is important in determining the position of the flame and the likelihood of its flashback into the premixing zone.

It has been found that a dominant factor in determining flashback limits is the quenching achieved by chemical reactants, and that flame propagation is largely governed by mutual interaction of the flow of fuel/oxidiser and chemical reactions [185]. Thus, flashback is very sensitive to flow patterns in the vortex core, where chemical reactions lead to changes in pressure conditions at the combustion chamber inlet, which promote the propagation of VBD. The study demonstrated that significant mechanisms resistant to flashback are possible when using axial jets but will change the levels of swirl. Konle and Sattelmayer have also investigated the effects of axial jets [199]. They reported that increasing diameter of the axial jet generated thicker vortex cores, which shifted the VBD downstream, improving flame stability and widening the window of useful burner operation.

Similar findings have been reported by [198][205] who found that axial injection widened the vortex cores and so produced lower pressure gradients which reduced baroclinic torque, and increased resistance to CIVB flashback. Mayer, et al. [206] improved flashback resistance using axial injection of fuel relative to trailing injection, achieved by having injector holes inserted along four trailing edges of a vaned swirler.

The fuel or blend type is important for CIVB flashback, for example, adding H₂ to a gaseous fuel can greatly increase the likelihood of CIVB [89][162][207]. A number of studies [162][175] [208] agree that the behaviour of fuel mixes can be very different from that of the constituent parts.

Swirl flow characteristics and local values of ϕ will affect the flow interactions at the burner mouth and thus the conditions governing CIVB flashback. Researchers have explored the effect of degree of mixing and swirl strength on flashback, Baumgartner and Sattelmayer [209] report that at low swirl intensities flashback changes from BLF to CIVB as ϕ increased. Sayad, et al. [210] found that BLF took place at lower swirl intensities than CIVB flashback.

Investigation of the influence of combustor geometry on CIVB flashback has found that different geometries can considerably enhance resistance to CIVB flashback. The presence of a centrally placed bluff body (or lance) has been shown to be very useful in avoiding CIVB flashback and upstream flame propagation, and is widely used in swirl burners [63]. Other researchers have found axial injection can improve resistance to flashback, though at the cost of working with lower swirl numbers and partial premixing. Reichel, et al. [161] showed that the injection of large quantities of axial air changed the character of the axial velocity sufficiently to move the zone where VBD took place and so enhanced resistance to CIVB.

Lewis, et al. [165] investigated how the axial injection of CO₂, CH₄, and air affected the coherent structures found in swirling flames, and found significant changes which varied with the gas injected. They suggested there was a correlation between effect of the high momentum flow region (HMFR) and the CRZ, according to which, CIVB flashback takes place as and when the CRZ is squeezed by the region of high momentum. Another study, by Sattelmayer, et al. [80], found that placing a diffuser between mixing tube and combustor can change the flashback mechanism from CIVB to BLF. They also found that for a particular swirl combustor, similar limits for BLF and that initiated by CIVB could be attained by adjusting the aerodynamics of the combustor and claimed that this represented the optimum means for flashback resistance. However, even small deviations from the optimum aerodynamics produced lower flashback resistance to both CIVB or BLF, actually worsening flashback limits [63].

Hatem et al. [211] have confirmed experimentally that increasing resistance to CIVB can increase the likelihood of BLF. However, resistance to CIVB was increased by, for example, repositioning the central injector and using central air injection, and BLF was avoided by simultaneously adding microspheres of woven steel mesh to the boundary wall of the burner nozzle, changing the boundary layer characteristics. Results showed that combining these techniques widened the range of stable operation for the swirl combustors tested and enabled them to safely burn a wider variety of fuel blends.

However, although much work has been undertaken to deepen our understanding of the mechanisms of CIVB, there remain many unknowns such as the quantitative effects of changed combustor geometries and different fuels on flashback phenomena [63].

2.6.3.5 Flashback Due to Combustion Instabilities and Coherent Structures

Thermo-acoustic instabilities occurring inside a combustion chamber can be sufficiently intense as to cause the flame to propagate upstream in both turbulent core and boundary layer, producing flashback. Such instabilities take place when there is a periodicity in the heat release rate which couples with a resonant mode of the combustor [168][212]. Swirling combustion, especially the PVC is a possible source of unsteadiness or fluctuating combustion, triggering the formation of radial eddies and small fluctuations in the patterns of rich and lean combustion which are oscillations in the combustion process [88]. These fluctuations inside the combustor can develop as part of a feedback loop, where the fluctuations in heat release rate feed into an acoustic field, which can increase in intensity to produce high levels of acoustic pressure and corresponding velocity fluctuations which can trigger corresponding oscillations in flame front and ϕ , producing further fluctuations in heat release rate and closing the feedback loop [169].

2.7 Alternative Fuels for GTs and Fuel Flexibility

A positive feature of heavy-duty GTs is that they can function relatively efficiently when using a wide range of fuels that are by-products of industrial processes, including; petroleum distillates, gas produced from coal or biomass, gas condensates, alcohols. Molière reviewed the influence of fuel on the energy and combustion performances of GTs, including thermodynamic performance, combustion efficiency and gaseous emissions [213].

More recent research projects have assessed, and will continue to assess, the combustion performances of GTs on alternative fuels for the efficient production of clean energy, including the appropriation and storage of the CO₂ produced by burning fossil fuels [214][215][216]. Another objective of this research is to extend the ability of “dry low-emission GT technology” to burn fuels with relatively low heat values such as bio-gas when enriched with H₂ [155]. Adding H₂ to NG decreases the calorific value, but at the cost of increased flame speed and some very fast chemical reactions [216].

To classify GT’s fuels, a simple way is to split them between gas and liquid fuels, and within the gaseous fuels, to divide by their calorific value (LHV) as presented in Table 2-1 [217].

Table 2-1: GT's fuels Classification. Compiled from [217].

FUEL	TYPICAL COMPOSITION	LHV KJ/NM ³	TYPICAL SPECIFIC FUELS
ULTRA/LOW LHV GASEOUS FUELS	H ₂ < 10% CH ₄ < 10% N ₂ +CO > 40%	< 11,200	Blast furnace gas (BFG), Air blown IGCC, Biomass gasification
HIGH HYDROGEN GASEOUS FUELS	H ₂ > 50 C _x H _y = 0-40%	5,500-11,200	Refinery gas, Petrochemical gas, Hydrogen power
MEDIUM LHV GASEOUS FUELS	CH ₄ < 60% N ₂ +CO ₂ = 30-50% H ₂ = 10-50%	11,200-30,000	Weak natural gas, Landfill gas, Coke oven gas, Corex gas
NATURAL GAS	CH ₄ = 90% C _x H _y = 5% Inert = 5%	30,000-45,000	Natural gas (NG), Liquefied natural gas (LNG)
HIGH LHV GASEOUS FUELS	CH ₄ & higher hydrocarbons C _x H _y > 10%	45,000-190,000	Liquid petroleum gas (butane, propane), Refinery off-gas
LIQUID FUELS	C _x H _y , with x > 6	32,000-45,000	Diesel oil, Naphtha, Crude oils, Residual oils, Bio-liquids

NG quality is crucial as numerous industrial GT combustion systems are adjusted for a specific NG composition local to the GT installation. The UK will become increasingly dependent on gas imports to oppose decreasing domestic production and potential short-to-medium term growths in gas-fired power generation. Given the high variability between international and domestic gas compositions, the UK restricts the quality of gas admissible into the NG grid through the Gas Safety (Management) Regulations (UK) [GS(M)R], affecting industrial and domestic gas users. One gas quality issue of particular importance is the acceptable Wobbe Index (WI) range. This is specifically essential for industrial GTs as variation in H₂ content in NG can remarkably decrease the WI while the higher hydrocarbons presence can increase the WI. WI is usually employed in the gas industry to calculate the energy delivery of NG fuel to a combustion device [122]. It is an estimated value based on a group of reference conditions (combustion and metering temperature, t_1 and t_2 , and pressure, P_2) as described in Equation 2-30:

$$WI [t_1, V(t_2, P_2)] = \frac{\tilde{H}[t_1, V(t_2, P_2)]}{\sqrt{d(t_2, P_2)}} \quad (2.30)$$

Where \tilde{H} is the real higher (gross) calorific value of the natural gas mixture and d is the real relative density of the mixture with respect to air, with the “real” values differing from the “ideal” values by incorporating a compression factor, Z , as described

in the British Standards Institution (BSI) document for the calculation of calorific values, density, relative density and WI from NG composition, BS EN ISO 6976:2005 [122]. All NG which enters the UK gas transmission system must meet the standards shown in Table 2.2 [218][122]. These limits also impact the operation and emissions of industrial users of the NG pipelines, including GT power generators.

Table 2-2: Gas quality limits for entry into the UK NG system. WI values referenced at $P_2 = 0.101$ MPa and $t_1, t_2 = 288$ K. Compiled from data in [218][122].

PARAMETER	
Wobbe Index (Mj/m ³)	47.20 - 51.41
Total Sulfur (mg/m ³)	50 (max)
Hydrogen Sulfide (H ₂ S) + Carbonyl Sulfide (COS) (mg/m ³)	5 (max)
Oxygen (O ₂) (% vol)	0.2 (max)
Hydrogen (% VOL)	0.1
Incomplete Combustion Factor	0.48 (max)
Soot Index	0.60 (max)

While the present GS(M)R limits define the useful energy content supplied to industrial GT burners through the WI, it does little to give any sign of the actual chemical composition of the NG in the distribution system, which can enormously affect the resulting combustion behaviour of those gases at elevated pressure and temperature conditions. Accordingly, while fuel flexibility has been emphasised as a key consideration in future GT operations, GT operators, many GT OEMs, GT operators and combustion researchers are presently examining the technological barriers to achieving high efficiency, low emissions combustion as the composition of NG varies [122].

2.8 Computational Fluid Dynamics (CFD) Modelling

Numerical modelling has been employed as a tool to help the discussion of the fundamentals of turbulent swirling flows. The CFD prediction of this kind of complex flow is a challenging topic because of anisotropic turbulence structures in the CRZ. An extensive early review of the numerical modelling studies on swirling flows was [118] which illustrates the challenges and complexity of CFD approaches to swirling flows in GT combustors. This difficulty still exists for the flow dynamics of both

isothermal (cold) and reacting (combustion) swirling flows. Various numerical approaches have been extended for the solution of different fluid flow problems [219].

2.8.1 CFD as a Tool for Design and Analysis

Prototyping and experimental investigation of GT combustion systems are expensive and time-consuming due to the complexity of the system. Therefore, CFD simulation is a critical enabling technology for designing better combustion and after-treatment systems. Combustion engineers have integrated simulation up front into the design processes to increase GT efficiency and reduce emissions. Currently, CFD codes utilising different software packages are used widely in industrial design for many reasons: CFD simulations are relatively convenient and easy to use, CFD is an inherently more flexible way to investigate a change in operating conditions as the change to computer code is quicker and cheaper than designing and conducting experimental tests, which may require the redesign, manufacture and testing of modified components. The continuous improvements in CPU capabilities and hard drive capacity offers the generalisation of CFD modelling and numerical analyses and allow them to be used as an advanced modelling tool. In this thesis, ANSYS Fluent R19.2 CFD Academic code employed to achieve some of the study objectives.

2.8.2 Modelling of Turbulence



Currently, there are three numerical techniques available for solving Navier-Stokes equations to determine the characteristics of turbulent cold flow (isothermal flow) and combusting flow (reacting flow). They are Direct Numerical Simulations (DNS), where a problem is solved in space and time, presenting the exact time course of the monitored flow parameters. Reynolds Averaged Navier-Stokes (RANS) derives mean (time-averaged) fields, but gives the mean value only [220]. When it is permissible to consider only the larger vortices and ignore small perturbations, Large Eddy Simulation (LES) can be used. This is much less computationally expensive than DNS but achieves this advantage by low-pass filtering, the outcome of which is a smoothed signal [221]. However, LES is almost expensive in terms of computing tools and time needs as compared to the classical RANS approach.

A hybrid model which is a combination of both methods (LES and RANS) is a technique to determine some part of the computational domain with RANS and the rest with the LES model. The purpose of this is to estimate the part of high computational load with RANS so that the whole computational load is decreased while maintaining the advantages of the LES model. There are various hybrid models

with different calculation methods, the Detached Eddy Simulation (DES) and the Very Large Eddy Simulation (VLES). This model is perfect for near wall calculations [222].

Table 2-3 presents a summary and overview of the level of complexity, and accuracy/cost of the computational approaches. RANS and LES turbulence modelling techniques are available in ANSYS Fluent software, but DNS is not [223].

Table 2-3: Turbulence models overview used in turbulence modelling [223].

Model	Computational Approaches Overview	Computational Cost
RANS	<ul style="list-style-type: none"> Solves ensemble-averaged (or time-averaged) Navier-Stokes equations. Can model all turbulent length scales. The most widely used approach for calculating industrial flows. 	 <p style="text-align: center;">Increase in computational cost per iteration</p> 
LES	<ul style="list-style-type: none"> Solves the spatially averaged N-S equations. Large eddies are directly resolved but eddies smaller than the mesh are modelled. (But RANS, DNS and LES all model flow patterns). Less expensive than DNS, but the amount of computational resources and efforts are still too large for most practical applications. 	
DNS	<ul style="list-style-type: none"> Theoretically, all turbulent flows can be simulated by numerically solving the full N-S equations. Resolves the whole spectrum of scales. No approximations are required. But the cost is too prohibitive! Not practical for industrial flows 	
NOTE !!	<ul style="list-style-type: none"> There is not yet a single, practical turbulence model that can reliably predict all turbulent flows with sufficient accuracy. DNS is not available in ANSYS Fluent. 	

The RANS (Reynolds time- and space-averaged equation) approach “flattens” the local flow components, as it calculates only the overall elements of turbulent flows. The RANS method significantly reduces the computation burden as it calculates the flow parameters by sub-dividing the parameters into a mean (average) element and a fluctuating element. For example, the mean flow describes the main flow, while the fluctuating element is calculated by the turbulence model. The results are strongly affected by the CFD model chosen to simulate the turbulence [224]. Thus, the instantaneous velocity is decomposed into two parts, a time-invariant mean and a time-varying fluctuating element, see Equation 2.31, which represents the basis of most mathematical descriptions of turbulence [225]:

$$U(x, t) = \bar{U}(x) + u(x, t) \quad (2.31)$$

The DNS method directly solves the Navier-Stokes equations without including any turbulence models. Therefore, the DNS requires very fine computational meshes and substantial computer resources to address the Kolmogorov turbulence scale (smallest scale). Currently, DNS is not used for complex flows at even moderately high flow Reynolds number, and is far from application to real engineering problems [226].

Latterly, LES has been widely adopted in engineering applications because of the rapid development of computer computational capacity. However, LES remains almost as expensive, in terms of computations and time needed, as the classical RANS approach. The fundamental concept behind LES is to decompose the flow components into small-scale parameters and large-scale parameters by applying a “cutoff” filter function. LES simulates the larger eddies but parameterises the smaller eddies employing a subgrid-scale (SGS) model, by which it gives precise results for length-scales greater than the cut-off threshold in a complex fluid flow [227].

The LES method has been found to be a powerful numerical tool, consistently able to produce predictions which compare well with experimental measurements. Such a model can be utilised even in situations where no previous experimental data exists. In many engineering applications, the engineers do not normally require precise data exactly matching real measurements, reasonable predictions with moderate computational costs, as obtained from models which employ RANS and LES, are acceptable.

2.9 Chapter Summary

This chapter has presented a review of previous research related to swirl-stabilised GT combustion, including GT combustion systems, combustion problems associated with swirl burners, fuel flexibility and alternative fuels for GTs.

Swirl-stabilised combustors were developed to meet increasingly strict pollution standards while maintaining GT operational efficiency. LPC using alternative fuels has been shown to be an important development. However, combustion stability issues that include autoignition, blowoff, and flashback remain common. Unfortunately, LPC makes swirl combustors more prone to such instabilities, especially when using alternative fuel blends high in hydrogen (H₂).

Flame flashback has long been thought of as an intrinsic operational issue with premixed swirl combustors and can severely damage system hardware; four mechanisms are responsible for flashback; BLF, CIVB, combustion instabilities and turbulent core flashback. Investigations of CIVB flashback and BLF mechanisms represent state of the art research because they are not yet completely understood compared to other types of flashback. Such investigations are important because these mechanisms can be initiated even under apparently stable operating conditions. Further research is needed to deepen our understanding of this phenomenon in order to develop techniques that can reduce or totally eliminate these serious instabilities.

To better understand the various flashback mechanisms, intense numerical and experimental research is needed. Such investigations need to consider modifications to both system hardware and flow fields. A number of techniques are known to efficiently reduce CIVB Flashback and successfully fix the CRZ downstream of the burner by making a modification to system geometry and/or changing the patterns of flow. Placing a bluff body in the flow can act to stabilise the flow, while altering the pattern of fuel flow by changing the fuel injector can move the position of the vortex breakdown further downstream and so reduce the likelihood of CIVB flashback.

Nevertheless, useful as these techniques are they cannot fully solve the problem of flashback and have potential drawbacks. Inserting a bluff body (or central injector) in the presence of high-temperature combustion processes for extended periods of time could produce material degradation and increase maintenance costs. The use of a central fuel injector could increase NO_x emissions and downgrade the fuel/air mixing process. The injection of air into the central core of the vortex to reduce negative axial velocity and turbulence characteristics is another possible way of mitigating CIVB flashback. In the present context this appears to have the significant benefits of avoiding any increase in pollutant levels which providing the required flame stabilisation.

The turbulent combustion in GTs, in general, is the sequence of two central interactions, the very complicated hydrodynamics and the chemical reactions. This interaction can enhance or reduce the combustion turbulence and hence affect the combustion stability. Improvements of burner geometries and manipulation of swirl flows can produce good resistance against CIVB flashback. However, increase flame flashback resistance against CIVB can lead to an increase in the propensity of another flashback mechanism, BLF. Thus, this work presents an experimental and

numerical approach that allows the increase in CIVB resistance by using axial air injection and simultaneously avoid BLF by changing the wall boundary layer characteristics using microstructure surfaces as a liner for the nozzle wall. Using combined techniques together has promising potentials regarding wider stable operation for swirl combustors, enabling them to burn a great variety of fuel blends safely.

Efficient configuration and operation of GT burners can be significantly facilitated by measurements attained from parallel experimental and modelling investigations. Such studies merge experimental and theoretical combustion aerodynamics with advanced CFD and its development and use will decrease the cost of improvement programs noticeably. Of course, there are still many facets of swirl burners that remain poorly understood, particularly in the important areas of coherent structures, flashback, and system instabilities. This thesis is intended to contribute to the understanding of the flashback processes occurring in GT combustors that are not yet fully understood.

Chapter 3

Research Methods

&

Techniques

CHAPTER THREE:

3 RESEARCH METHODS AND TECHNIQUES

“When we try to look only at one thing in Nature, we find it connected to everything else”

John Muir, American naturalist (1838-1914)

3.1 Introduction

This chapter presents and discusses the experimental methods and numerical techniques employed in this study. All the findings presented were obtained in the Cardiff School of Engineering using purpose designed test rigs and equipment available in the combustion laboratory.

Accurate measurements of swirl flow in GT burners are essential in order to address problems concerning their operation. However, swirling flows are so complex that despite great advances in CFD codes, precise solutions require a combination of CFD analyses and experimental tests. The test rig should have substantially similar characteristics to those of a real GT combustion system and able to simulate both stable and unstable operation. In general, these experiments included a tangential swirl burner as usually used in GTs, Laser diagnostic systems, and other apparatus needed for average measurements. At the end of this chapter, the CFD simulation technique, code setup and numerical models used provide an initial prediction of swirl flow behaviour for different burner configurations.

3.2 Experimental Approach and Facilities

3.2.1 The Swirl Burner

Combustion and isothermal experiments were performed in a 150-kW steel-scaled versions of a 2-MW swirl burner. The tangential generic swirl burner used in this study is depicted in [Figure 3-1](#), this burner had been used on previous investigations of different flame flashback mechanisms and swirling flow stability as reported in [\[121\]\[166\]](#). The burner exit diameter ($D_e=2R_o$) at the outlet can be changed using different nozzle configurations, in this study the exit nozzle diameter is equal to $0.8D_s$ (61 mm) as recommended in previous work [\[64\]](#). A burner sleeve diameter (D_s) of

76 mm has been used in this study as a reference length to which all other dimensions are referred. The inner radius of the burner plenum chamber (r_i) is twice that of the burner sleeve ($r_i = 2r_s = D_s$). The burner consists of two tangential inlets of 67.4 mm inner diameter ($D_t = 0.89D_s$). However, the cross-sectional area of these two inlets can be varied using inserts. The two inlet areas were maintained equal at 25%, 50%, 70% and 75% of the original area. This made it possible to vary the original geometric swirl numbers (0.573- no insert case) to 0.913 and up to 3.65, depending on the insert used. The air to these inlets was supplied by a centrifugal fan via flexible hoses and two banks of rotameters for flow rate control. Another bank of rotameters monitored the injection of NG. The errors in air and gas rotameters readings were $\sim 3\%$. For the combustion trials, the burner was designed to operate under atmospheric pressure with no air preheating, using NG (90% CH₄, N₂, C₂₊ hydrocarbons, CO₂, H₂S, and noble gases, refer to Figure 1-3). Fuel to be added in premixed mode (i.e., being premixed where the tangential inlets met plenum) and diffusive mode (i.e., through the central injector, just for burner start-up). The mixture enters the burner plenum circumferentially through the tangential inlets. This produces a robust azimuthal velocity component generating a high degree of a swirl. This burner was developed to meet the aim of the present study by adding axial air injection system, details will be mentioned in Chapter Four.

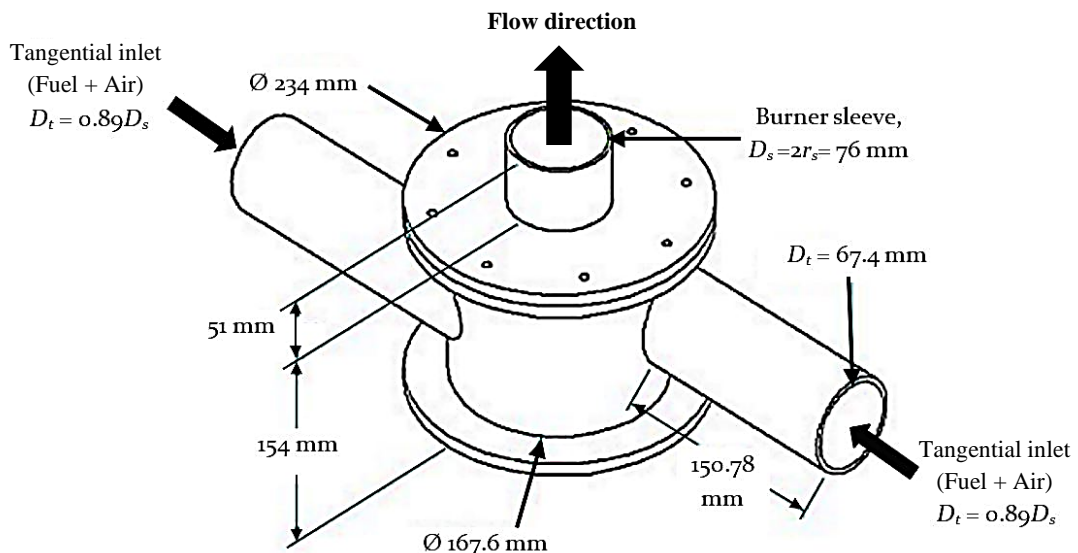


Figure 3-1: Sketch of the burner, (not-to-scale). Reproduced from [121].

Some of the complexities of swirling flows, were firstly recognised in the middle of the nineteenth century and as a result the swirl number (S), Strouhal number (S_r) and Reynolds number (Re) are usually used to characterise these flows. Full derivation of

swirl number can be found elsewhere [120]. Equation 2.16 discussed in section 2.3.1.1 of Chapter Two provides a direct method for determining the geometrical swirl number S_g for the burner described above (tangential burner) [64][104][205].

The way of calculation R_{eff} is shown in Figure 3-2. A_t is the total free area of the tangential inlets, [$A_t = \left(\frac{\pi D_t^2}{4}\right) * \text{Insert \%}$]. As configuration (25%-25%) at $S_g=0.913$ showed the most stable results in [121] for the same burner, this was used for all the combustion and isothermal cases in this work. Figure 3-2 shows that both tangential inlets have their areas reduced by 25%.

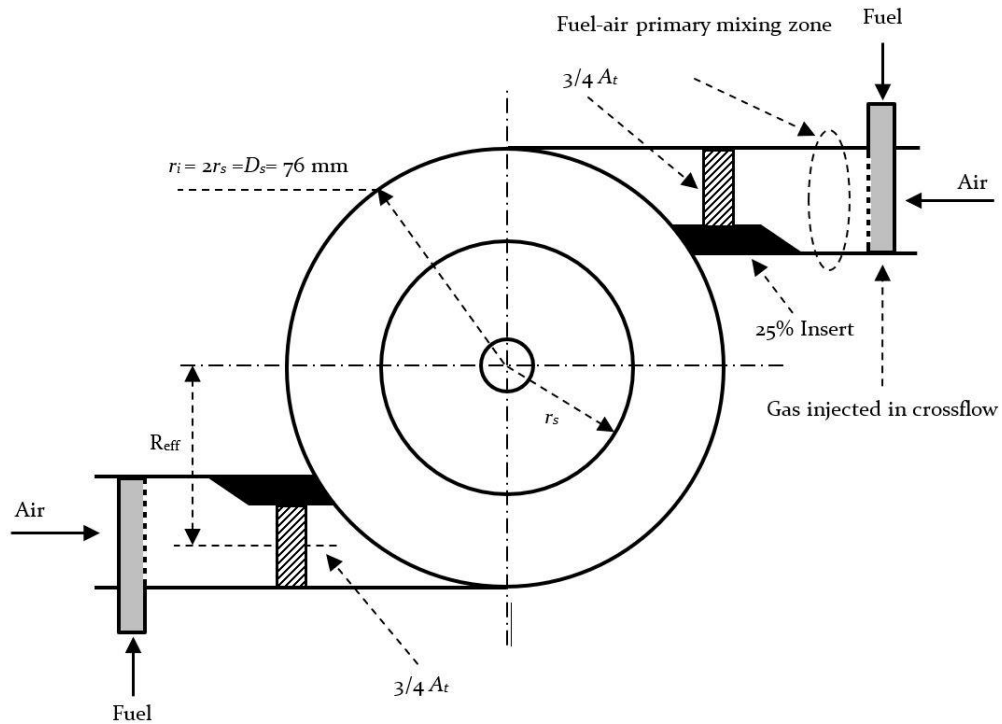


Figure 3-2: Schematic top view of the swirl burner with 25%-25% inserts, (not-to-scale).

Table 3-1 presents for the effect of the four inserts on R_{eff} , A_t and S_g . In general, vortex breakdown and the development of a central recirculation zone happen when the swirl number is between 0.5-0.6 [88].

Table 3-1: Geometrical swirl number (S_g) values for different inserts.

Insert [%]	Tangential inlet area [%]	R_{eff} [mm]	Total air inlet area $2A_t$ [m ²]	S_g
0-0	100	42.79	0.00714	0.573
25-25	75	51.22	0.00536	0.913
50-50	50	59.64	0.00357	1.956
70-70	30	66.38	0.00214	2.961
75-75	25	68.07	0.00179	3.643

3.2.2 Non-Intrusive Laser Diagnostics

Swirl flow diagnosis has been critical for the improvement of GT combustion systems and the development of GT combustors. Conventional measurement techniques have proved incapable of capturing the actual flow behaviour and the need for improved high-precision measurement and diagnostic systems for GT combustor design is now imperative. Over the past three decades, laser diagnostics techniques have snowballed and are being used to estimate different parameters of isothermal and combustion swirl flow fields, including temperature, velocity, turbulence and flow fluctuations, with high space and time resolution [228]. The laser beam or sheet used for combustion or cold flow diagnostics retains its coherence, intensity and monochromatic properties even when scattered from particles seeded in the fuel or air flows. There are numerous optical measuring techniques based on light diffusion that have the advantage of being non-intrusive, see Figure 3-3 [229].

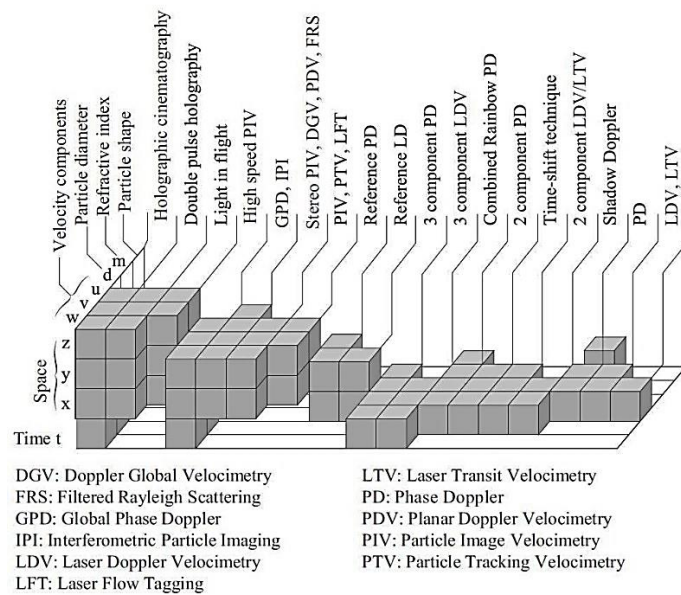


Figure 3-3: Optical measuring systems employing light scattering. Reproduced from [229].

In addition to the laser diagnostic systems presented in Figure 3-3, a novel technique for point flow velocity measurements utilising the displacement of laser-induced plasma has been introduced at the Imperial College London, which does not need the introduction of any tracer (seeding or any other substances) in the flow field [230].

Laser diagnostic systems have the major advantage over conventional contact devices that they do generate disturbances and have very limited impact on the flow field. Laser measurement tools are capable of changing the traditional point

estimation to linear or planar measurements and to give detailed information about the transient behaviour of the swirling flow. Laser Doppler Anemometry (LDA), also known as Laser Doppler Velocimetry (LDV), is an optical technique ideal for non-intrusive 1D, 2D, and 3D point measurement of velocity and turbulence distribution in both free flows and internal flows. LDA is a widely accepted tool for fluid dynamic investigations in gases and liquids and has been used as such for more than three decades. It is a well-established technique that gives information about swirl flow characteristics. The measurement results are essential steps in fine-tuning the GT burners designs to improve aerodynamic efficiency, quality, and safety. The method's particular advantages are non-intrusive measurement, high spatial and temporal resolution, no need for calibration, and the ability to measure reversing flows. As this study investigates the change in swirl flow characteristics (axial velocity and turbulence) behind different burner configurations, the LDA was chosen between the other laser diagnostic systems.

The next subsections provide brief descriptions of a common and highly accurate laser measurement technique that been used in this research programme: the Laser Doppler Anemometry (LDA). Also included are details of how this system will be employed to meet the aims of this work.

3.2.3 Laser Doppler Anemometry (LDA)

LDA is a non-intrusive, low weight, small size and directionally sensitive flow measurement system, making it convenient for applications such as measurements of swirling flows, investigations of reversing flows, combustions and chemically reacting flows, and even rotating machinery, where positioning of real sensors is challenging and signals are difficult to interpret. LDA is a single point optical tool that needs tracer particles (seeding) in the flow field to be measured and needs to be manipulated to estimate velocity values and turbulent intensities of the particles carried by the gases or liquids. The main advantages of the LDA system are: no calibration is required (it is an absolute measurement technique), capable of measuring reverse flow (especially useful in swirl flow characterisation), with high spatial and temporal resolution due to small measurement volume and non-intrusive nature of the measurements [231][232].

3.2.3.1 LDA System Setup and Configuration

The LDA system, in general, consists of the following different essential components as presented in [Figure 3-4 \[232\]](#).

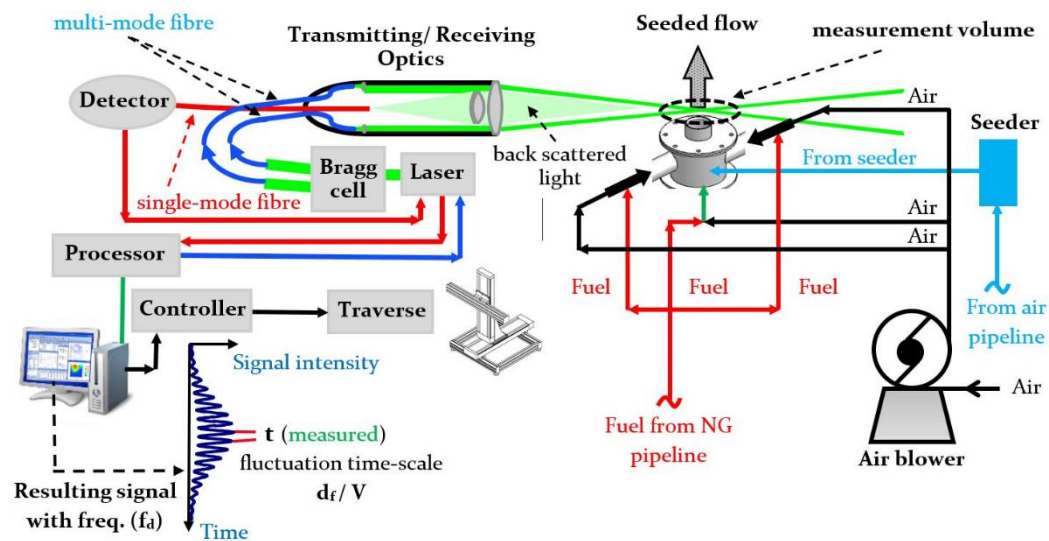


Figure 3-4: Test rig diagram and backscatter LDA system measurement setup. Reproduced from [232].

As the axial velocity is the dominant velocity component in the swirling flow, a one component FlowLite (Dantec) LDA system operating in backscatter mode was used in this study to measure the instantaneous axial velocity component and velocity fluctuations downstream of the burner exit. The light source for this system consists of an argon ion laser with 500 mm focal length of the lens. Its simplicity and reliability made it the best choice for these experiments. The system offered a calibration uncertainty of 0.067%. The burst signal was processed using a BSA F60 processor and Dantec BSA Flow Software v5.20 to yield the mean and RMS velocities at the control volume location.

The configuration of the FlowLite Dantec LDA system used in this work consisted of the following essential elements which are generally the same for any 1D LDA system:

- **Continuous wave laser:** The Dantec Dynamics backscatter LDA system used in this study was a neodymium-doped yttrium aluminium garnet; $\text{Nd:Y}_3\text{Al}_5\text{O}_{12}$, commonly known as an Nd:YAG laser. It is a coherent, linearly polarised, monochromatic, Gaussian intensity distribution with low divergence (collimator) laser. This backscatter system utilizes a 200 mW constant wave Nd:YAG laser (532 nm) split to produce two beams by a Bragg cell.
- **Brag cell:** Also known as an acoustical-optical modulator, is used as a laser beam splitter and operating at 40 MHz, dividing one beam into two, one of

which is frequency shifted under the effect of this cell. It is a glass crystal with a vibrating piezo crystal attached. Applied vibration via the piezo-electric crystal causes the crystal to behave as an optical grid. The beam separation is equal to 38 mm.

- **Transmitting/ receiving optics:** A single device, suitable placed will combine the functions of receiving and transmitting the laser light to a photo-diode together with the detected signal produced by particles traversing the control volume.
- **Photodetector:** Collects the back-scattered light.
- **LDA probe:** A focusing lenses and interference filter to pass only the selected wavelength.
- **Signal processor:** Involves spectrum analyser, counter, correlator, and tracker.
- **Personal computer (PC):** Windows XP operating system installed to be compatible with the Dantec BSA Flow Software v4.5. The results can be exported for additional post-processing utilising third-party software such as Tecplot 360 and MATLAB, or for CFD results validation.
- **Traverse system:** Frequently, the swirl flow measurements require mapping of the flow velocity and turbulence in a large space. Accordingly, these values should be measured at many points in the flow field. Traverse system control ensures precise movement by the LDA probe and hence gives the flow information at multiple points in a matrix form. Dantec traverse X, Y, Z system with traverse controller has been utilised to measure the axial velocity and the turbulence intensity values at different points in the swirl flow. The BSA Flow Software installed in the PC controlled the traverse system through the traverse controller that is connected to the PC by a serial interface, see photograph in appendix. The flow field was divided into many sub-regions (levels) according to the distance from the burner mouth. The starting point (the datum) was specified using a laser target sheet where both laser beams met. During the traverse, the movement is stepped in all three space coordinates Δx , Δy and Δz , and the software included a calibration factor so target sheet and the actual space have identical space coordinates.
- **Seed generation:** Seeding material and seed generator.

3.2.3.2 LDA Measuring Fundamentals

The fundamental method of the LDA system is the frequency variation (shift) of the light returned from a moving seeding and collected by a stationary receiver. This is known as the Doppler effect. LDA systems have undergone many developments, particularly with respect to signal processing, since 1964, when the LDA was invented by Yeh and Cummins, [233]. LDA has become widely available and is used extensively in fluid mechanics, especially for measurements in turbulent reacting flows (combusting flows). Light intensity is modulated because of interference between the laser beams, and as a result, high-intensity parallel fringes will be generated, see Figure 3-5 [232]. The LDA probe size is usually several millimetres long.

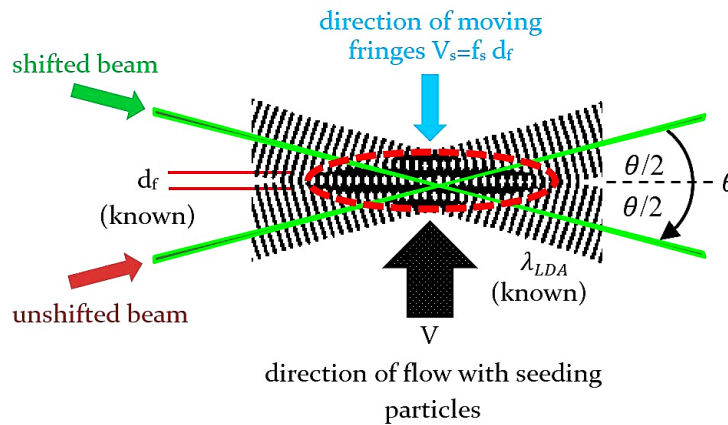


Figure 3-5: The parallel planes of high light intensity (the fringes). Reproduced from [232].

The fringe peak-to-peak distance (d_f) will depend on the laser wavelength and the magnitude of the angle separating the laser beams, Equation 3.1 [233]:

$$d_f = \frac{\lambda_{LDA}}{2 \sin\left(\frac{\theta}{2}\right)} \quad (3.1)$$

Each seeding particle crossing the laser beam scatters light equivalent to the local light intensity. The velocity magnitude of the flow field is derived from the light scattered by the particles carried in the flow when they pass across the measurement volume. The scattered light includes a Doppler shift, the Doppler frequency (f_d) depends on the velocity component perpendicular to the laser beam's bisector. A lens collects the scattered light and concentrates it onto a photo-detector [234]. An interference filter is mounted so that it transmits only the required wavelength so no

other light wavelength reaches the detector. The tangential velocity component can be estimated by rotating the laser probe 90°, conventionally in a clockwise direction.

The photodetector converts the fluctuating light to an electrical signal (the so-called Doppler burst) which is sinusoidal with a Gaussian envelope because of the intensity profile of the laser beam. The Doppler bursts are separated from background noise and amplified in a signal processor, which also estimates the Doppler frequency (f_d) for each seed particle, usually by employing a robust Fast Fourier Transform (FFT) algorithm. The fringe spacing (d_f) can represent the distance travelled by the seeding particle, while the Doppler frequency (f_d) gives information about the time scale of the flow fluctuations (where, $t = 1/f_d$). The flow velocity can be calculated from Equation 3.2 [232]:

$$V = d_f \cdot f_d = \frac{\lambda}{2 \sin\left(\frac{\theta}{2}\right)} \quad (3.2)$$

As shown in Figure 3-6, the LDA system can determine the sign of the flow direction [63][232].

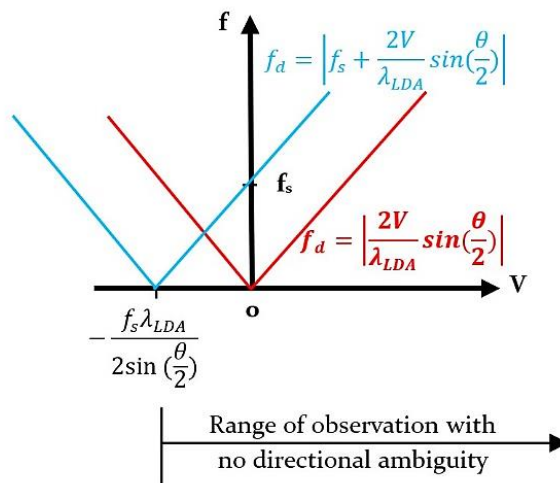


Figure 3-6: Doppler frequency to velocity transfer function for a frequency shifted LDA system. Reproduced from [63][232].

The frequency shift (f_s) produced by the Bragg cell creates the fringe pattern which moves at a constant velocity (V_s). Seeding particles which are moving cause a shift frequency. The negative and positive velocities, V_{neg} and V_{pos} , create f_{pos} and f_{neg} signal frequencies, respectively, so the flow direction can be specified. However, without such a frequency shift, the LDA system cannot distinguished the flow direction or measure zero velocity [232].

3.2.3.3 LDA System Settings

The LDA settings for the isothermal conditions are quite different from those for combustion, due to the great differences between the flow structures in the two cases. It has been demonstrated that the number of acquired samples during the LDA acquisition process for combusting flow is less than that for the isothermal conditions [211]. The expander ratio during the isothermal test was equal to 1.0, and the probe volume dimensions were ($d_x = 0.338$ mm, $d_y = 0.388$ mm and $d_z = 8.919$ mm). However, to increase the data rate during the combustion test when needed, the expander ratio must be increased to 1.5, and hence the probe volume need to be decreased ($d_x = 0.225$ mm, $d_y = 0.226$ mm and $d_z = 3.968$ mm) [63].

For isothermal conditions, the LDA system has been recently calibrated by controlling the seeding rate to operate with 50,000 measuring particles (data capture rates) or 30 s capture time before moving to the next measuring point [63]. The velocity and turbulence intensity values were estimated using Dantec BSA Flow software by taking the average values for all particle passing through the measuring volume for each point in the flow field.

3.2.4 Fluid Flow Seeding

The seeding particles (tracers) are an essential element of laser diagnostic systems such as PIV and LDA, since they rely on the tracking of illuminated particles suspended in the flow field. It is assumed these particles are adequately buoyant to follow any flow pattern at the test flow conditions [122]. The particle size and type need to be selected carefully and will depend on the fluid flow behaviour under consideration. Otherwise, they will not be able to match and visualise the flow components adequately. Typical seedings are fog, smoke, metal dioxides or water droplets [64].

Perfect tracer particles will have about the same density as the fluid system being tested while choice of particle size and type will depend on the characteristics of the flow field and the fluid flow system. The refractive index of the seeding particles should be different from that for the fluid flow as the laser light incident on the flow field must be reflected from them towards the CCD camera. A compromise between decreasing the seeding particle size to enhance flow tracking and increasing the particle size to enhance light scattering must be made in each case, and is a significant decision [235]. The degree to which the seeding particles follow the fluid flow dynamic is not precise and is described by the Stokes number (Stk), Equation 3.3, which is a

dimensionless parameter related to the behaviour of particles carried by the fluid flow [102]:

$$Stk = \frac{\tau \cdot U}{d_c} \quad (3.3)$$

Where:

- d_c = The characteristics dimension of an obstacle (m)
- U = Velocity (m/s)
- τ = Particle relaxation time (s)

Which is determined as:

$$\tau = \frac{\rho_d \cdot d_d^2}{18 \cdot \mu_f} \quad (3.4)$$

Where:

- ρ_d = Particle density (kg/m³)
- d_d = Diameter of the particle (m)
- μ_f = Dynamic viscosity of the fluid (m²/s)

The smaller the Stokes number the better the precision of the trace. When Stk is higher than unity the particles will separate from the flow, especially under heavy acceleration. However, when Stk is less than unity the seeded particles will tend to follow the flow streamlines. If the Stk is less than 0.1, the tracking accuracy will be better than 99% [236]. Considering all the above requirements, the highly reflective, micro-scale diameter calcined aluminium oxide powder (Al_2O_3) was chosen for this work from the variety of seeding particles available for LDA experiments. To test the effect of particle size on the accuracy of the results, an LDA isothermal experiments was carried out under the same operating conditions, using two different sized particles of Al_2O_3 powder; F800 5.5-7.5 μm , and 1 μm from Logitech. It was found that the axial velocity profile at the burner nozzle exit was very much the same for both sizes, see [Figure 3-7](#).

As a result, the air flows in all LDA experiments in this study were seeded with Al_2O_3 particles with Sauter mean diameter of approximately 1 μm , using powder supplied by Logitech and introduced into the burner plenum using a pressurised seeder vessel. The seeding device was designed so that seeding of the flow was homogenous and sufficient, without overly disturbing the flow. It was also desirable that the seeding

particles be non-corrosive, non-toxic, non-volatile, non-abrasive and chemically inert [102].

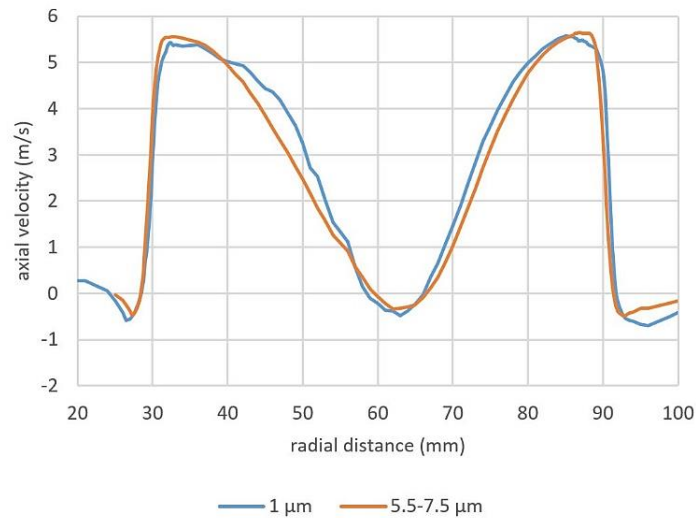


Figure 3-7: LDA measurement of the axial velocity profile for two different Al_2O_3 seeding particle size.

3.2.5 Photography

A 24.2-megapixel Nikon digital single-lens reflex camera (DSLR) camera model D7200 with 18-105mm VR Nikon lens was used to take photographs whenever needed, see camera setup in Appendix. The sensitivity of the camera's sensor (ISO) range of 100-25600 made it a good choice to capture a usable photograph no matter the light strength. The main feature of this camera is the shutter speed of 1/8000-30 s with 6 fps continuous shooting which is necessary to capture unsteady flow behaviour.

3.3 Numerical Setup

In addition to the experiments undertaken in this work, CFD simulation with ANSYS Workbench R19.2 Academic with solver Fluent cod was also used as a first step to providing some predictions about the techniques to be used in the experimental work, and to correlate with experimental data. ANSYS Fluent R19.2 code was employed in this study as it generates accurate and reliable fluid simulation results. It is software that has been extensively validated across a wide range of applications. With ANSYS Fluent, advanced physical models and analysis of various fluids phenomena can be created in a customizable and intuitive space. Ansys Fluent contains the best-in-class

physics models and can accurately and efficiently solve large, complex models. This includes internal and external flow, single-phase and multiphase flow, chemical reaction, combustion, noise prediction, heat transfer, radiation, turbomachinery flows, and many more fluid flow related models.

CFD modelling of experimental conditions was used to provide significant support to the experimental findings and vice versa. Numerical modelling has been employed as a tool to help the discussion of the fundamentals of turbulent swirling flows [118]. Various numerical approaches have been extended for the solution of different fluid flow problems [219]. For isothermal flows, CFD has grown to be the conventional engineering tool and many commercial CFD solvers are available [219]. In this section, the numerical approach adopted in this study is discussed in detail.

3.3.1 The Sequence of CFD Modelling in ANSYS

Every CFD modelling process using the ANSYS Fluent R19.2 code goes through three successive steps: pre-processing, problem solving and post-processing. The Pre-processing step including the input of the flow problem to a CFD code through an operator-friendly interface in terms of suitable forms to be used by the solver. The main activities in the pre-processing stage include: defining the computational model, grid generation, selecting the method of solution (which depends on the simulated problem), defining the thermo-physical properties of the fluid flow and finally specifying the boundary conditions [237].

The second step is the solution method from the different numerical solution techniques employed within the CFD codes (such as the finite difference method (FDM), the finite element method (FEM) and the finite volume method (FVM)) [226][238]. The principal differences between these methods are associated with the approximation procedure for the flow variables and the discretisation process. ANSYS Fluent commercial code employs the FVM method as a discretisation process, with a suitable approach to linearise and solve the discretised flow equations [237]. The FVM solutions necessarily satisfy the conservation laws: e.g., mass, energy, momentum, and species. This is done for any one control volume, for any number of control volumes and even the entire computational domain. Even a poor (coarse) grid solution can show accurate integral balances [238].

The post-processing in ANSYS Fluent is mainly related to result presented and data exported. Fluent is equipped with a handy data visualisation tool to display the grid,

the computational domain and the results in terms of, for example, line, contour, and surface plots.

3.3.2 Mathematical Formulation

It is necessary to have a computational model capable of capturing the main physical effects, that govern the hydrodynamics of the swirl flows. Fluent solves the conservation equations for mass and momentum for the swirl flow, using the finite volume approach to solve the governing Navier-Stokes equations which are derived from the conservation of mass and momentum [223]. Fluid flow governing equations were used to represent mathematical descriptions of the conservation laws of physics with the following assumptions [238][239]:

- The rate of change of momentum equals the sum of the forces on a fluid particle (Newton's second law).
- The fluid mass is conserved.
- The rate of change of energy is equivalent to the sum of the rate of heat addition and the rate of work applied on a fluid particle (First law of thermodynamics).

The continuity equation, or equation for conservation of mass, can be represented in compact vector notation as follows [224]:

$$\left(\begin{array}{c} \textit{The rate of} \\ \textit{the change in} \\ \textit{time of the} \\ \textit{density (mass per} \\ \textit{unit volume)} \end{array} \right) + \left(\begin{array}{c} \textit{"the convective term"} \\ \textit{the net flow rate} \\ \textit{of mass across} \\ \textit{the element} \\ \textit{boundaries} \end{array} \right) = 0 \quad (3.5)$$

Then:

$$\frac{\partial \rho}{\partial t} + \nabla \cdot (\rho \vec{V}) = 0 \quad (3.6)$$

Equation 3.5 states that the rate of mass increase in a fluid element corresponds to the net rate of mass flow into the fluid element. This can be represented in the detailed form as:

$$\frac{\partial \rho}{\partial t} + \frac{\partial(\rho u)}{\partial x} + \frac{\partial(\rho v)}{\partial y} + \frac{\partial(\rho w)}{\partial z} = 0 \quad (3.7)$$

Where:

ρ = Fluid density

t	=	Time
u, v, w	=	Velocity components in x, y, and z respectively
\vec{V}	=	Velocity vector

Regarding **the momentum equation**, Newton's second law states that the rate of momentum change of a fluid particle is equal to the sum of the forces acting on it. We considered two kinds of forces: the surface forces (viscous forces and pressure) and the body forces (centrifugal, gravity, Coriolis, and electromagnetic) [95].

Applying this to a fluid moving through a fixed and infinitesimal control volume produces the conservation of momentum equation in an inertial reference frame which is defined in compact vector notation as [224][239]:

$$\rho \frac{\partial \vec{V}}{\partial t} + \rho(\vec{V} \cdot \nabla)\vec{V} = -\nabla p + \rho \vec{g} + \nabla \cdot \tau_{ij} \quad (3.8)$$

Where ($\rho \vec{g} = S_{Mi}$) is the gravitational body force, and τ_{ij} is the stress tensor that is related to the strain rate, as described in Equation 3.9 [238]:

$$\tau_{ij} = \widetilde{\tau}_{ij} + \overline{\tau}_{ij} \quad (3.9)$$

The components of the momentum equation in x, y, z directions are [238][239]:

The x-component of the momentum equation:

$$\rho \frac{Du}{Dt} = \frac{\partial(-p + \tau_{xx})}{\partial x} + \frac{\partial \tau_{xy}}{\partial y} + \frac{\partial \tau_{zx}}{\partial z} + S_{Mx} \quad (3.10)$$

The y-component of the momentum equation:

$$\rho \frac{Dv}{Dt} = \frac{\partial \tau_{xy}}{\partial x} + \frac{\partial(-p + \tau_{yy})}{\partial y} + \frac{\partial \tau_{zy}}{\partial z} + S_{My} \quad (3.11)$$

The z-component of the momentum equation:

$$\rho \frac{Dw}{Dt} = \frac{\partial \tau_{xz}}{\partial x} + \frac{\partial \tau_{yz}}{\partial y} + \frac{\partial(-p + \tau_{zz})}{\partial z} + S_{Mz} \quad (3.12)$$

Where:

P	=	The static pressure
τ	=	Viscous stress
τ_{ij}	=	Viscous stress component acting in the j-direction on a surface normal to i-direction
S_{Mi}	=	The gravitational body force in i-direction

The pressure sign is opposite to that associated with the normal viscous stress as the standard sign convention takes tensile stress to be the positive normal stress so that the pressure, which is a normal compressive stress, has a minus sign. On the other hand, the consequences of the surface stresses are estimated explicitly; the source terms, S_{Mx} , S_{My} and S_{Mz} are body forces only. As a result, the body force due to gravity, for example, would be expressed by $S_{Mx} = 0$, $S_{My} = 0$ and $S_{Mz} = -\rho g$.

In a Newtonian fluid, the viscous stresses are equivalent to the rates of deformation. The three-dimensional form of Newton's law of viscosity for a compressible flow includes two constants of proportionality: the dynamic viscosity (μ), to describe stresses to linear deformations, and the kinematic viscosity (λ) to describe stresses to the volumetric deformation. The viscous stress is associated with both μ and λ . Introducing the values of viscous stress into the momentum equations gives the well-known **Navier-Stokes equations** [238][239]:

$$\rho \frac{Du}{Dt} = -\frac{\partial p}{\partial x} + \nabla \cdot (\mu \nabla u) + S_{Mx} \quad (3.13)$$

$$\rho \frac{Dv}{Dt} = -\frac{\partial p}{\partial y} + \nabla \cdot (\mu \nabla v) + S_{My} \quad (3.14)$$

$$\rho \frac{Dw}{Dt} = -\frac{\partial p}{\partial z} + \nabla \cdot (\mu \nabla w) + S_{Mz} \quad (3.15)$$

A *general transport (conservation) equation* can be introduced to generalise the mathematical model in the numerical simulations. This type of equation illustrates how a scalar is transported in space. Typically, it is used in the transport of a scalar field such as material properties, temperature, or chemical concentration within an incompressible flow. Mathematically, the transport equation is also known as the convection-diffusion equation, which is a first order partial differential equation. The convection-diffusion equation is the foundation for most recent transportation models, as a result, the conservative pattern of all fluid flow equations can usefully be expressed in the following form:

$$\begin{aligned} & \left(\begin{array}{c} \text{Rate of increase} \\ \text{of } \Phi \text{ in a fluid} \\ \text{element} \end{array} \right) + \left(\begin{array}{c} \text{Net rate of flow} \\ \text{of } \Phi \text{ out of the fluid} \\ \text{element} \end{array} \right) \\ & = \left(\begin{array}{c} \text{Rate of increase of} \\ \Phi \text{ due to} \\ \text{diffusion} \end{array} \right) + \left(\begin{array}{c} \text{Rate of increase} \\ \text{of } \Phi \text{ due to} \\ \text{other sources} \end{array} \right) \end{aligned}$$

Or:

$$\frac{\partial(\rho\phi)}{\partial t} + \nabla \cdot (\rho\phi V) = \nabla \cdot (\Gamma \nabla\phi) + S_\phi \quad (3.16)$$

Equation 3.16 is defined as the transport equation of the unknown variable ϕ . It highlights the numerous transport processes: the diffusive term (Γ : diffusion coefficient) and the source term respectively are on the right-hand side and the rate of change term and the convective term are on the left-hand side of the equation.

3.3.3 Turbulence

3.3.3.1 Turbulence Characteristics

Turbulence is a common flow phenomenon in engineering applications. Study of turbulence which directly influences the accuracy of prediction of many engineering applications continues to be a hot topic for research. It is somewhat easier to characterise the turbulent flows than provide an exact and precise definition. Turbulent flow happens when instabilities in a flow are not adequately damped by viscous action and all the flow parameters display random fluctuations [66]. This kind of flow is composed of multiple eddies with a multitude of length and time scales. Generally, the flow configuration geometry determines the size of the largest eddies, which extract energy from the mean flow and feed it to smaller scales through a cascading process. The energy contained in the smallest scales is dissipated due to viscous effects. The size of the smallest of these eddies is given by the Kolmogorov length scale (η_k), defined by the amount of energy transferred down the energy cascade towards the smallest eddies and by the fluid molecular kinematic viscosity [240].

Turbulent flows, which occur at high Reynolds numbers (Re), are characterised by random fluctuations in velocity and pressure in both space and time. These fluctuations cause other transported quantities such as energy, momentum, and species concentration to fluctuate as well. Such fluctuations can be small scale and high frequency and are computationally expensive to simulate directly. Alternatively, the fundamental instantaneous governing equations can be averaged in many ways to eliminate the small scales appearing in a set of equations, which makes them less time and resource consuming to solve [239].

3.3.3.2 Turbulence Computational Technique

Chapter Two section 2.8.2 presents four turbulence modelling methodologies: DNS, LES, RANS and hybrid (LES and RANS) models. Reynolds Averaged Navier Stokes (RANS) calculations require a small fraction of the computational resources required

for DNS and LES and thus, remain the choice for most industrial CFD users. As such, the predictive capability of RANS-based models must be continually assessed by researchers in the turbulence community. The RANS equations are primarily used to describe turbulent flows. These equations can be used with approximations based on knowledge of the properties of flow turbulence to give approximate time-averaged solutions to the Navier–Stokes equations [241]. In the present work, computational solutions are obtained using the Reynolds-averaged Navier-Stokes (RANS) approach.

To this end, part of the present work will evaluate the performance of a classical RANS technique to produce a reliable model capable of predicting the flow field characteristics of swirl flow with acceptable accuracy. Similar investigations have been completed using two-dimensional (axisymmetric) RANS modelling, as described in [88][242], however, the literature search revealed not a single study to assess the performance of a three-dimensional RANS model using this design of burner with an axial air injection system. Another motivation for using such a turbulence model is that extensive experimental work has been carried out on this burner during this study or done by previous researchers [63][64][95][211]. That experimental data can now be compared to the RANS based numerical findings. On the other hand, using a reliable RANS model to make predictions before manufacturing a burner could suggest modifications to the burner which would be useful in saving time and minimise the cost of trial-and-error system modifications.

3.3.3.3 RANS Based Turbulence Model in Fluent Code

ANSYS Fluent includes different RANS-based turbulence modelling techniques to satisfy the requirements of individual classes of problems. The selection of the turbulence model depends on available computational resources, the level of accuracy required, and the necessary turnaround time. The RANS based turbulence models available in ANSYS Fluent R19.2 are [223]:

- ❖ One-Equation Models:
 - Spalart-Allmaras model.
- ❖ Two-Equation Models:
 - $k-\varepsilon$ model.
 - Standard $k-\varepsilon$.
 - RNG $k-\varepsilon$.
 - Realisable $k-\varepsilon$.

- $k-\omega$ model.
 - Standard $k-\omega$.
 - SST $k-\omega$.

❖ Reynolds Stress Model.

Table 3.2 describe the key features of the RANS based turbulence model contained in the methods library of the ANSYS Fluent code [223].

Table 3-2: The key features of RANS $k-\varepsilon$ Turbulence Models available in ANSYS Fluent [223].

Model	Features and Notes
Standard $k-\varepsilon$ (SKE)	<ul style="list-style-type: none"> • The most widely used engineering turbulence model for industrial applications. • Robust and reasonably accurate. • Contains sub-models for compressibility, buoyancy, combustion, etc. • Limitations: <ul style="list-style-type: none"> ▪ The ε equation contains a term which cannot be calculated at a containing. Therefore, wall functions must be used. ▪ Generally, performs poorly for flows with strong separation, large streamline curvature, and large pressure gradient.
Renormalizable (RNG) $k-\varepsilon$	<ul style="list-style-type: none"> • Constants in the $k-\varepsilon$ equations are derived using renormalisation group theory. • Contains the following sub models: <ul style="list-style-type: none"> ▪ Differential viscosity model to account for low Re effects. ▪ The analytically derived algebraic formula for turbulent Prandtl / Schmidt number. ▪ Swirl modification. • Performs better than SKE for more complex shear flows, and flows with high strain rates, swirl, and separation.
realizable $k-\varepsilon$ (RKE)	<ul style="list-style-type: none"> • The term realisable is used to mean that the model satisfies certain mathematical constraints on the Reynolds stresses, consistent with the physics of turbulent flows. <ul style="list-style-type: none"> ▪ Positivity of normal stresses: $\overline{u_i' u_j'} > 0$. ▪ Schwarz' inequality for Reynolds shear stresses: $(\overline{u_i' u_j'})^2 \leq \overline{u_i'^2} \overline{u_j'^2}$. • Neither the standard $k-\varepsilon$ model nor the RNG $k-\varepsilon$ model is fully realisable. • Benefits: <ul style="list-style-type: none"> ▪ Relatively accurate prediction of the spreading rate of both planar and round jets. ▪ Likely to provide superior performance for flows involving rotation, separation, recirculation, boundary layers under strong adverse pressure gradients.

The RANS approach to turbulence modelling has been one of the most prevalent due to the straightforward, efficient use of resources; mainly, the $k-\varepsilon$ model is widely used. Moreover, it has been used with a reasonable agreement with experimental data. It has been noted that the modified (Realizable) $k-\varepsilon$ model is more efficient in the swirl

flow than the unmodified (Standard) k - ϵ model. This is due to the way the dissipation of turbulence energy is calculated. The Realizable k - ϵ model is designed to mitigate several issues with the Standard model, mainly how the eddy dissipation is modelled. This was addressed in the Realizable k - ϵ model via a new eddy-viscosity formula and a new dissipation equation [243]. As a result, in this study, the Realizable k - ϵ turbulence model was used to study the turbulent isothermal flow behaviour in the tangential swirl burner described above.

The realizable k - ϵ turbulent model is a popular turbulence model used to solve the swirl flow that attempts to allow a new eddy-viscosity equation including a variable C_μ and a new model formula for dissipation rate ϵ based on the dynamic equation of the mean-square vorticity fluctuation, which will be discussed in detail below.

The realizable k - ϵ turbulence model is derived from the instantaneous Navier-Stokes equations. The analytical derivation produces a model with model constants unlike those in the standard (k - ϵ), and further functions and terms in the transport equations for k and ϵ . The realizable (k - ϵ) turbulence model has the following form:

$$\frac{\partial}{\partial t}(\rho k) + \frac{\partial}{\partial x_j}(\rho k u_j) = \frac{\partial}{\partial x_j} \left[\left(\mu + \frac{\mu_t}{\sigma_k} \right) \frac{\partial k}{\partial x_j} \right] + G_k + G_b - \rho \epsilon - Y_M + S_k \quad (3.18)$$

and:

$$\begin{aligned} & \frac{\partial}{\partial t}(\rho \epsilon) + \frac{\partial}{\partial x_j}(\rho \epsilon u_j) \\ &= \frac{\partial}{\partial x_j} \left[\left(\mu + \frac{\mu_t}{\sigma_\epsilon} \right) \frac{\partial \epsilon}{\partial x_j} \right] + \rho C_1 S \epsilon - \rho C_2 \frac{\epsilon^2}{k + \sqrt{\nu \epsilon}} + C_{1\epsilon} \frac{\epsilon}{k} C_{3\epsilon} G_b + S_\epsilon \end{aligned} \quad (3.19)$$

Where:

$$C_1 = \max \left[0.43, \frac{\eta}{\eta + 5} \right], \quad \eta = S \frac{k}{\epsilon}, \quad S = \sqrt{2 S_{ij} S_{ij}} \quad (3.20)$$

and:

G_k = The generation of turbulence kinetic energy due to the mean velocity gradient (refer to Equation 3.21)

G_b = The generation of turbulence kinetic energy due to buoyancy for nonzero gravity force and a non-isothermal flow. $G_b=0$ for isothermal flow.

Y_M	=	The contribution of the fluctuating dilatation in compressible turbulence to the overall dissipation rate. It is typically neglected in the incompressible flows modelling.
S_k, S_ϵ	=	User-defined source terms
$C_{1\epsilon}$	=	Model constant, equal to 1.44
C_2	=	Model constant, equal to 1.68
σ_k	=	Model constant, equal to 1.0
σ_ϵ	=	Model constant, equal to 1.2

The turbulence kinetic, G_k , due to the mean velocity gradient is calculated as:

$$G_k = -\rho \overline{u_i u_j} \frac{\partial u_j}{\partial x_i} \quad (3.21)$$

To estimate G_k in a way compatible with the Boussinesq hypothesis:

$$G_k = \mu_t \dot{S}^2 \quad (3.22)$$

The parameter (\dot{S}) represents the modulus of the mean rate-of-strain tensor, calculated from:

$$\dot{S} \equiv \sqrt{2S_{ij}S_{ij}} \quad (3.23)$$

Turbulence, in general, is influenced by swirl in the mean flow. The realizable turbulence model in ANSYS Fluent represents a good choice for a wide range of flows such as rotating shear flows, channel and boundary layer flows, free flows including jets and mixing layers and separated flows [223]. The eddy viscosity μ_t is computed from:

$$\mu_t = \rho C_\mu \frac{k^2}{\epsilon} \quad (3.24)$$

The difference between the realisable model and the other RANS based models is that C_μ is no longer constant and it is computed from Equation 3.25. However, it is equal to 0.09 for inertial sublayer in an equilibrium boundary layer.

$$C_\mu = \frac{1}{A_0 + A_s \frac{kU^*}{\epsilon}} \quad (3.25)$$

Where:

$$U^* \equiv \sqrt{S_{ij}S_{ij} + \overline{\Omega_{ij}}\overline{\Omega_{ij}}} \quad (3.26)$$

and:

$$\overline{\Omega_{ij}} = \epsilon - 2\epsilon_{ijk}\omega_k, \quad \Omega_{ij} = \overline{\Omega_{ij}} - \epsilon_{ijk}\omega_k \quad (3.27)$$

Where $\overline{\Omega_{ij}}$ represents the mean rate-of-rotation tensor viewed in a moving reference frame with the angular velocity. The model constants and are given by:

$$A_0 = 4.04, \quad A_s = \sqrt{6} \cos\phi \quad (3.28)$$

Where:

$$\phi = \frac{1}{3} \cos^{-1}(\sqrt{6}W), \quad W = \frac{S_{ij}S_{jk}S_{ki}}{S^3}, \quad \tilde{S} = \sqrt{S_{ij}S_{ij}}, \quad (3.29)$$

$$S_{ij} = \frac{1}{2} \left(\frac{\partial u_j}{\partial x_i} + \frac{\partial u_i}{\partial x_j} \right)$$

3.3.4 Mesh Generation

The ANSYS Workbench R19.2 Academic meshing programme was used to determine the mesh for the computational domain of the tangential swirl burner. There are several meshing methods and techniques in numerical analysis that can be used for three-dimensional simulation in the ANSYS code; including hexahedrons (usually structured), tetrahedrons (unstructured), pyramids (where hexahedrons and tetrahedrons cells meet) and Prisms (created when a tetrahedron mesh is extruded). See Figure 3-8 for cell geometries used to mesh the computational domain within ANSYS Fluent R19.2 [223].

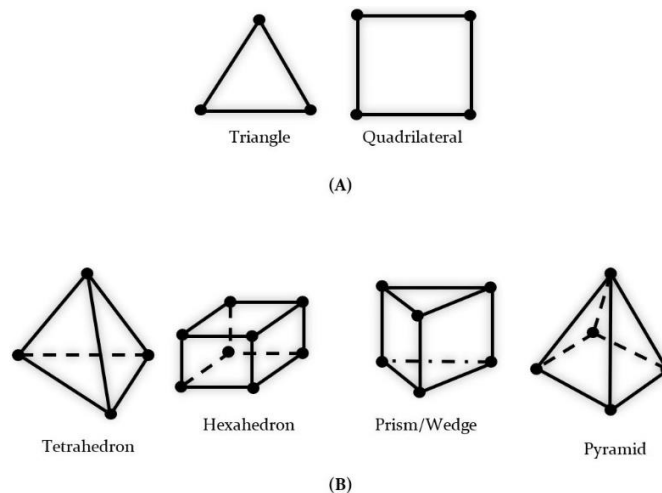


Figure 3-8: Cell types employed for grid generation in ANSYS: (a) 2D model, (b) 3D model. Reproduced from [223].

The structured mesh is usually generating manually. On the other hand, unstructured grid is creating automatically including several element types, the majority of them being tetrahedrons. A structured mesh typically provides the modeller with better control over the generated mesh and enables denser node concentrations in certain regions where better resolution is wanted. Every cell is used to define nodes where fluid properties are estimated [223].

For axisymmetric problems, simplification or two-dimensional simulation, triangular and quadrilateral cells are acceptable. The shapes and numbers of elements will determine the accuracy of the model. The greater the number of mesh elements contained in the geometry, the higher the accuracy of the CFD. Nevertheless, this will increase the required computational time, and corresponding expense [237].

The CFD simulation near walls (in this case the burner walls) requires a specific criterion within the mesh, termed y^+ , which is a non-dimensional distance, closely related to the distance of the first node from the wall (see Equation 3.25), and is considered essential in turbulence modelling when deciding the proper size of the mesh cells near domain walls. The laws governing the turbulence model place limits on the y^+ value at the wall. The y^+ value depends on the wall shear stress, i.e., on the velocity gradient near the wall. For turbulence modelling, the width of the shear layers should be at least 10 mesh cells deep, fewer than this and the model will not be capable of giving its expected performance [244] particularly for free shear flows whose position is not known during the mesh generation [244]. The viscous layer grid y^+ can be calculated from the following equation:

$$y^+ = \frac{yu_\tau}{\nu} \quad (3.30)$$

Where:

- y = Distance of the first node from the wall
- u_τ = The wall friction (shear) velocity
- ν = Kinematic viscosity

The characteristics associated with mesh quality are skewness, aspect ratio, node point distribution and smoothness. The skewness and aspect ratio are related to the shape of the cells and have a critical impact on the accuracy of the CFD simulation. Highly skewed cells can reduce accuracy and destabilise the numerical solution. The skewness can be described as the difference between the cell's shape in the mesh and that of an equilateral cell of similar volume. There are two approaches to defining the skewness [95][223][239]:

- According to the equilateral volume deviation:

$$skewness = \frac{\text{optimal cell size} - \text{actual cell size}}{\text{optimal cell size}} \tag{3.31}$$

The above equation applies only to tetrahedral and triangular cell shapes.

- According to the normalised angle deviation:

$$skewness = \left(\frac{\theta_{max} - \theta}{180 - \theta} \right) \left(\frac{\theta - \theta_{min}}{\theta} \right) \tag{3.32}$$

Equation 3.32 applies to cell face shapes and is used for pyramids and prisms; where:

- θ = The equiangular face/cell (60° for tetrahedrons and triangles, and 90° for quadrilaterals and hexahedrons)
- θ_{max} = The maximum angles (in degrees) between the edges of the element
- θ_{min} = The maximum and minimum angles (in degrees) between the edges of the element

It is obvious that the best mesh resolution is related to low skewness values, see Figure 3-9 [95]. The mesh generation technique and the grid size adopted in the present work will be mentioned in Chapter Four.

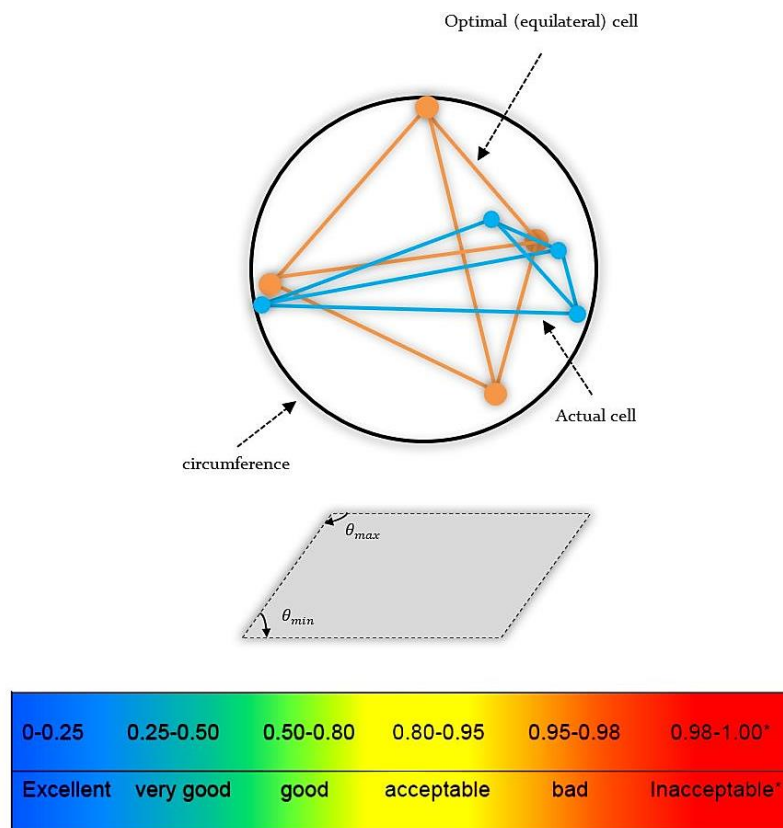


Figure 3-9: Skewness calculation explanation shape and its relation to mesh quality. Reproduced from [95].

3.4 Chapter Summary

Over the past decades, the use of laser diagnostic systems to the study of swirl flow has advanced our understanding of combustion phenomena in swirl burners regarding the interaction of turbulence, flow behaviour and chemistry. The measurement technology can provide an in-depth understanding of the flow phenomena, regardless of how complex the system under consideration. These kinds of experiments have also significantly improved the availability of detailed data sets that can be used for validation of CFD simulation findings [242]. This study adopted the LDA to obtain experimental observations.

Most mathematical descriptions of turbulence, decompose the velocity field into two parts: a time-invariant mean and a time-varying fluctuating component. LDA is an important a technique for investigating turbulent flows, it measures the instantaneous velocity as a single point, from which the time-invariant mean value and time-varying fluctuating velocity can be easily derived.

The present study will perform an assessment of the RANS technique to predict the flow field structure of swirling flow under the effect of different burner configurations using the ANSYS Workbench with Fluent solver R19.2 code which gives a wide flexibility to the CFD component of this work.

Chapter 4

The Hydrodynamic Effects of Axial Air Injection on Swirl Flow in Tangential Swirl Burners

CHAPTER FOUR:

4 THE HYDRODYNAMIC EFFECTS OF AXIAL AIR INJECTION ON SWIRL FLOW IN TANGENTIAL SWIRL BURNERS

“There are in fact two things, science and opinion; the former begets knowledge, the latter ignorance”

Hippocrates, Greek Scientist (460-370 BC)

4.1 Background and Chapter Objective

In most practical combustion systems achieving high flashback resistance depends on flame stabilisation which relies on an equilibrium, both in magnitude and direction, between flame speed and incoming flow velocity at the reaction zone. This balance, in turn, is a function of different parameters such as burner configuration, degree of mixing, and fuel type. Furthermore, swirl combustion, the most used technology in current GT burners, generates three-dimensional structures that further complicates the balance [121]. However, avoiding flame flashback by controlling the equilibrium between incoming flow velocity and flame speed is not always manageable [79], and flashback can lead to dramatic consequences when extremely turbulent fuels with high flame speeds are used [245]. The phenomenon is particularly important in swirling flows, which are characterised as highly complex phenomena because of their inherent three-dimensional time-dependent structures.

Many studies have investigated flame flashback mechanisms in swirl combustors, suggesting many techniques for mitigating flame flashback either by using some geometrical enhancements or by promoting flow field patterns [246]. One of these mechanisms, CIVB [184], is considered a fast acting flashback mechanism that appears in swirl burners as a consequence of the formation of the CRZ [185], see Section 2.6.3 for more details. Flame flashback due to CIVB has received particular attention amongst other flashback mechanisms since it is one of the prevailing flashback mechanisms in swirl combustors and represents an obstacle to developing combustion systems, especially those fed by high flame speed, highly reactive fuels [209]. Motivated by this issue, this chapter presents a new method (the axial air

injection system) to mitigate the propensity for CIVB flashback, performing an analysis using a CFD approach.

Of particular interest in reducing flashback, central fuel injectors and bluff bodies have proved their ability to anchor the CRZ downstream of the burner nozzle [247] with a considerable flame flashback resistance, especially against CIVB. Most investigations in this context have concentrated largely on the effect of bluff body geometries on blowoff limits [70][248][249]. The high complexity of swirling flows under lean conditions generate phenomena still not entirely understood, that can propagate through the flow field to produce either blowoff or flashback [94]. For example, some studies [250] have investigated the effect of position and geometry of bluff-bodies on flow aerodynamics and flashback resistance. However, employing bluff-bodies in GTs does not fully mitigate the risks of flashback [174]. Moreover, one of the main drawback of using centre-body devices is material degradation due to the harsh environment produced by high temperature flames, especially when high hydrogen content blends are used [89][251], see Figure 4-1 [63].

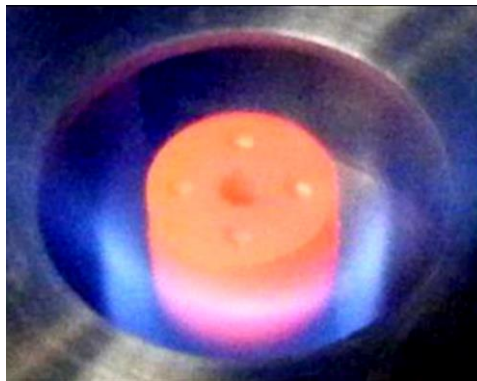


Figure 4-1: Flame effects on centre-body under flame flashback. Adapted from [63].

Therefore, flow field manipulation has been considered as an effective technique that can inhibit flame flashback propagation [252]. An axial fuel injector with variable orifices was employed to enhance the flashback resistance in swirl burners [185]. Others [199] used unswirled core flows (axial injection) with different jet diameters to control the position of swirling coherent structures. It was concluded that increasing axial fuel jet diameter produces a more coherent and stronger axial jet flow, which in turn pushes the vortex breakdown downstream, optimising flashback resistance. However, whereas injecting fuel axially in the centreline demonstrated a wider operability for improving CIVB flashback resistance, the technique can lead to significant increase in the level of NO_x emissions [80]. Moreover, central fuel injection

cannot completely mitigate flame flashback as most of the previous applications suffered considerable degradation of mixing.

Using central air injection is considered a suitable alternative to central fuel injection to reduce NO_x, where distributed reaction conditions in the combustor can be achieved by controlling the air injection velocity [253], though this can lead to mixing degradation. However, this state-of-the-art technique has been barely investigated for flashback resistance. It was found that injecting a large high amount of air centrally could influence the position of the CRZ and improve flashback resistance and provide a considerable reduction in NO_x levels [161]. This technique can produce significantly wider operation stability maps in GTs [63], a critical requirement regarding the possibility of switching to different blends for flexible power plants. Central air injection can also be employed in colourless distributed combustion (CDC) [254], where air jets can support dilution of the blends to enable lower temperatures and highly distributed reactions, consequently reducing emissions [73], even with high hydrogen content blends [255] that tend to raise temperature profiles over the combustion processes. This area of research, however, appears to have been investigated uniquely by Reichel et al. [161].

Thus, due to the need for improving flashback conditions in swirl burners, this chapter seeks to fill gaps of knowledge directly linked to these phenomena. This chapter reports the implementation of isothermal CFD simulations employed in the consequences of axial air injection on the three-dimensional isothermal swirl flow characteristics of a 150-kW tangential swirl burner. The numerical approach of this thesis was carried out in parallel with an experimental programme carried out at Cardiff University [63] to determine the effects of changing the burner configuration and boundary conditions. The CFD work gave a primary prediction to validate, and compare with, the experimental work [63] as depicted in the schematic diagram, Figure 4-2.



Figure 4-2: Data movement paths between CFD predictions and experimental work during this study.

The CFD work is based on isothermal conditions due to the limitation of the ANSYS Fluent partial premixed combustion model to simulate the modified burner design.

4.2 Experimental Setup

Brief descriptions of the experimental setup of the axial air injection system will be presented here. Details of the burner setup were presented in Chapter Three.

4.2.1 The Physical Model and Air Injection System

The design of the burner, refer to [Figure 3-1](#), was developed to allow the positioning of an axial air injector, D_{inj} of 23 mm outer diameter that could move up and down vertically to position (L_o) inside the plenum with respect to the base plate as shown in [Figure 4-1](#). This injector is allowing an axial air jet of diameter (19 mm).

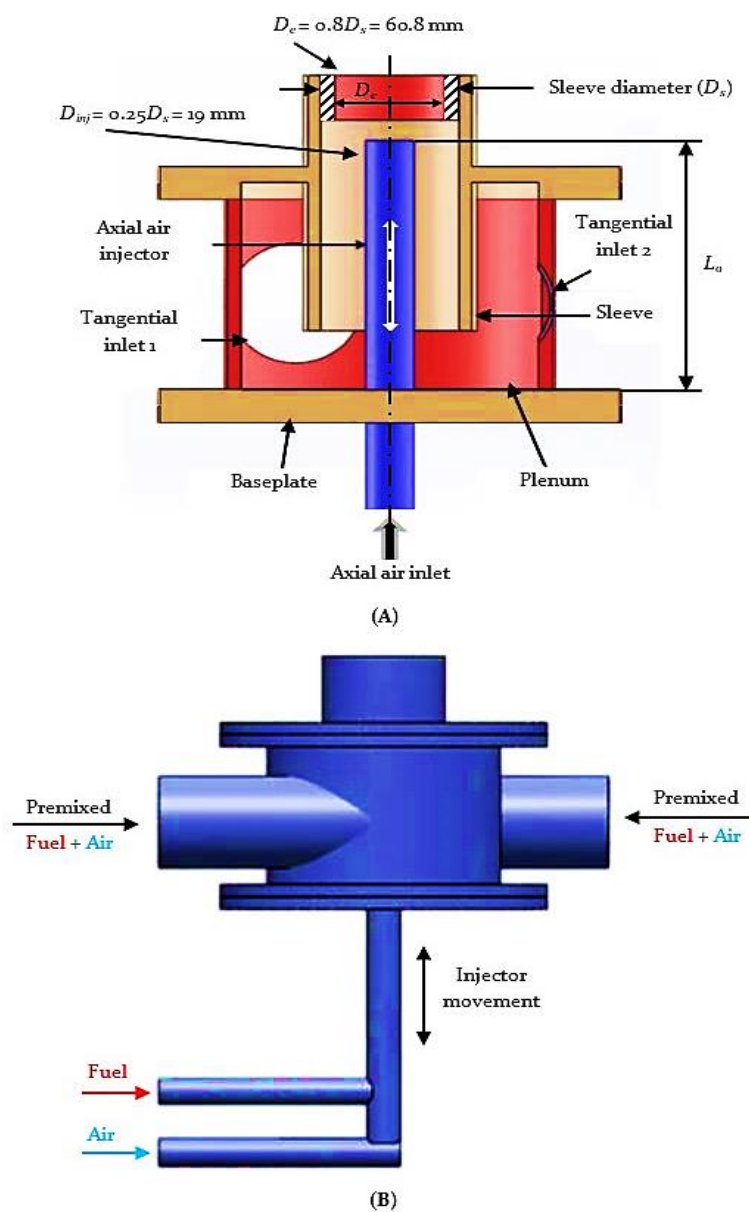


Figure 4-3: Experimental setup of the modified burner design, (not-to-scale): (A) detailed view of central axial air injector; (B) the dual air/fuel injection technique.

The diameter of the central air injector was chosen based on a previous study [256] where this diameter set the flashback transition from Wall Boundary Layer Flashback (BLF) to Combustion Induced Vortex Breakdown (CIVB) flashback. The modified configuration, as schematically depicted in Figure 4-3 (A), has been employed to facilitate central air injection from the burner plenum bottom instead of the central fuel injector. Therefore, the original baseplate which holds the central fuel injector in the original design (central injector) has been changed to one that allows axial air injection in addition to the fuel, Figure 4-3 (B).

4.2.2 Test Cases

In the CFD programme two main burner configurations were used with each injector position (L_o), the swirl burner had no axial air jet (central body only) and that under the effects of axial air injection. Three axial air injector positions (L_o) for each configuration were investigated numerically as shown in Table 4-1.

Table 4-1: Air injector positions with respect to the burner baseplate.

No.	Distance from the base plate (L_o) (mm)	Distance from the burner outlet (mm)
1	0	205
2	29	176
3	150	55

The distance L_o is measured from the tip of the axial air injector to the burner's base plate. The zero distance refers to the case of the axial air injection without a central air tube to examine the effect of a simple axial jet injected at the base plate on the swirl flow characteristics, while the insertion length of 29 mm refers to the maximum turbulence case where the axial and tangential streams meet in the same plane but with different flow directions. The 150 mm distance is when the tip of the axial air injector is nearest to burner dump plane to avoid the material degradation of the injector due to the high flame temperature.

4.3 CFD Analysis

4.3.1 The CFD Package

Different numerical approaches have been developed for the solution of fluid flow problems. For isothermal flows, computational fluid dynamics (CFD) is now the conventional engineering tool and many commercial codes are available [51]. ANSYS Fluent R19.2 CFD finite volume solver has been used in this study to simulate the isothermal swirl flow in the 150-kW tangential swirl burner. This package is comprised

of three sub-programmes. The first is responsible for the drawing of the computational domain. The second is used to generate the mesh, define the different computational zones and boundaries of the model. The third is employed to identify the boundary and operating conditions, the solver parameters, the material properties, and the numerical model, and also includes the fluid mechanics solvers. The ANSYS Fluent CFD code accommodates a sophisticated user interface to input the test parameters, conditions and output the results.

4.3.2 Computational Domain

The configuration of the system of interest must be performed in ANSYS Workbench R19.2 Code. However, the geometry could be imported from computer aided design (CAD) software. Due to the complexity of the adopted geometry, SolidWorks 2017 software has been used to draw the computational domain for the tangential swirl burner under consideration. Then the generated file from the SolidWorks exported to the design modeller (the pre-processing step) of Ansys Workbench R19.2 in (XT) extension file format. Different burner configurations as mentioned in Table 4-1 above have been investigated with the same nozzle geometry (exit diameter $D_e=0.8D_s=60.8$ mm and height of 25 mm).

Figure 4-4 shows three positions of the air injector inside the burner plenum (L_o) investigated in the CFD element of this study.

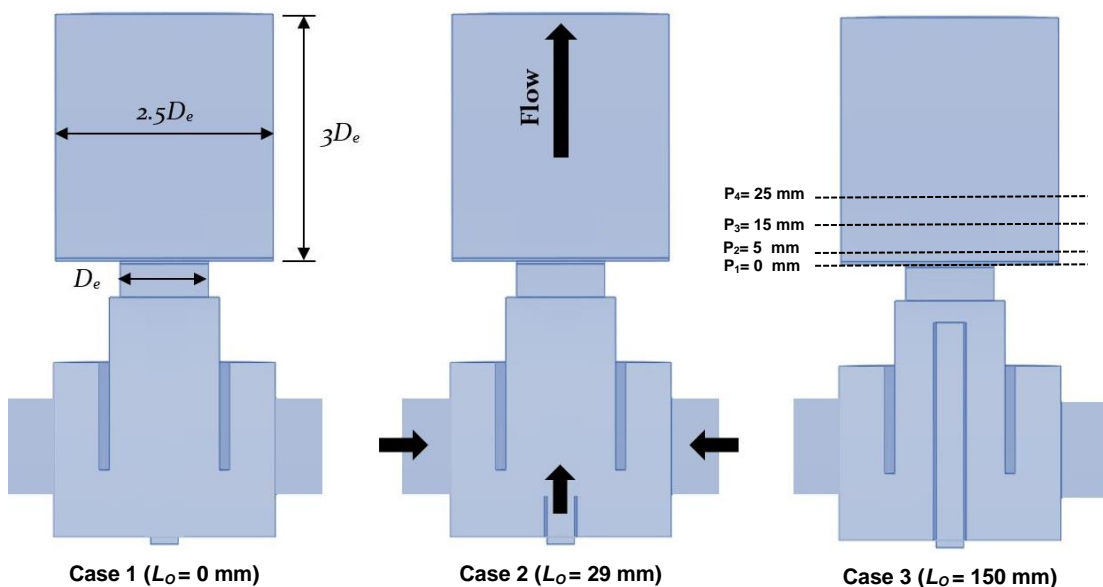


Figure 4-4: Different burner configurations investigated in the CFD campaign with a swirl number (S_g) of 0.913.

4.3.3 Mesh Generation

Before determining the setup to be adopted for the numerical solution, care was taken to construct a high-quality mesh to ensure an adequate convergence. Two kinds of grid exist in numerical analysis, structured and unstructured. The structured mesh is usually generating manually and consists of hexahedral elements. On the other hand, unstructured grids are creating automatically and can include several different element types, the majority being tetrahedrons [223]. A structured mesh typically provides the modeller with better control over the mesh generated and enables denser node concentrations in regions where better resolution is wanted. Every cell is used to define nodes where fluid properties are estimated.

The computational regions, see Figure 4-5, were meshed with well-refined structured grids, specially at the core of the flow field where a coherent structure exists. The solution is iterated at all nodes based on the values in the neighbouring nodes. Consequently, the higher the number of elements, the higher number of nodes and ultimately the more calculations needed, i.e., incurring greater computation costs. Increasing the mesh size reduces computational time, but higher mesh densities are essential to capture the details of the swirl flow and that means greater computational expense, see section 4.3.5 for the final mesh size adopted in this study.

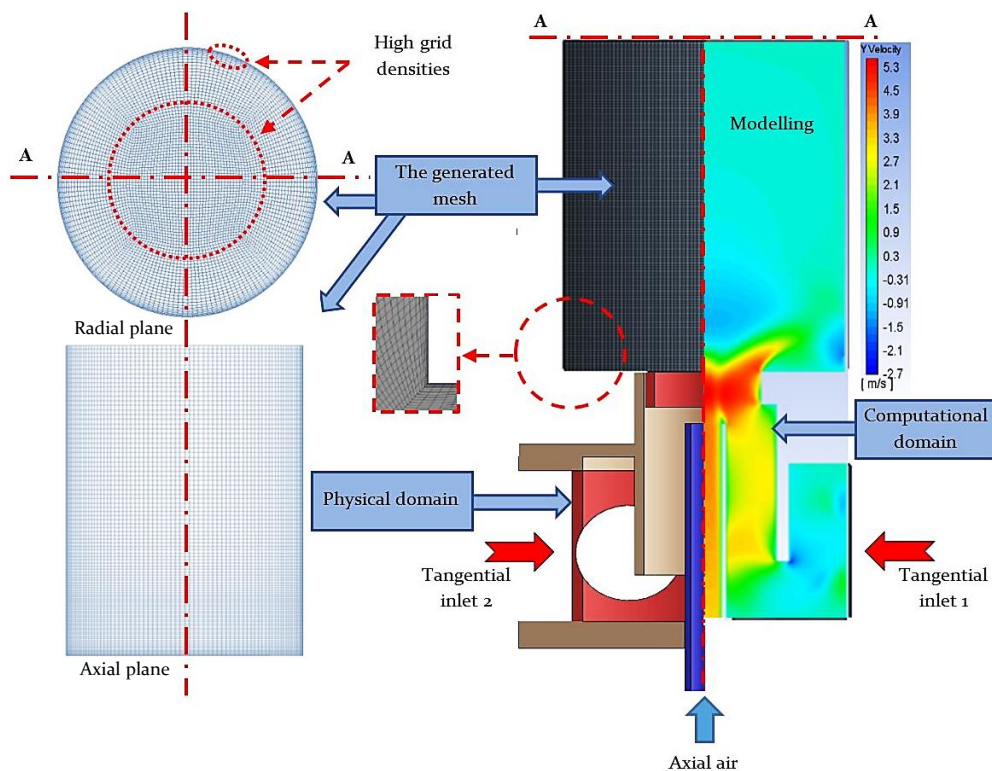


Figure 4-5: CFD computational mesh of the burner (not-to-scale).

4.3.4 Solution Convergence

Convergence was satisfactory with accurate results achieved for every case. In Ansys Fluent code, along the path towards convergence, the governing equations are solved through iterations that depend on the mesh size, the numerical method chosen and the physical problems being solved. Deciding if a solution is converging can be somewhat challenging. The solution convergence represents an indication of how well the solution satisfies the discrete form of the governing equations. In general, defining convergence by looking at residual values is only a small part of ensuring a valid solution. For a steady-state simulation, it is required to ensure that the numerical solution satisfies the following three conditions [223]:

- CFD convergence using scaled residual values. The residual is a crucial measure of the convergence of an iterative solution because it quantifies the error in the CFD solution of the system of governing equations. In other words, the residual measures the local imbalance of a conserved variable in every control volume. The normalised residuals of the critical simulation parameters (continuity, velocities, k , and ϵ) were monitored throughout the computations. For a CFD solution to converge, the normalised residuals must be typically less than 10^{-4} or 10^{-5} [223]. In this work, the absolute convergence criteria were set to 10^{-4} . Figure 4-6 presents the path of the scaled residual towards convergence for one of the CFD cases considered in the present work.

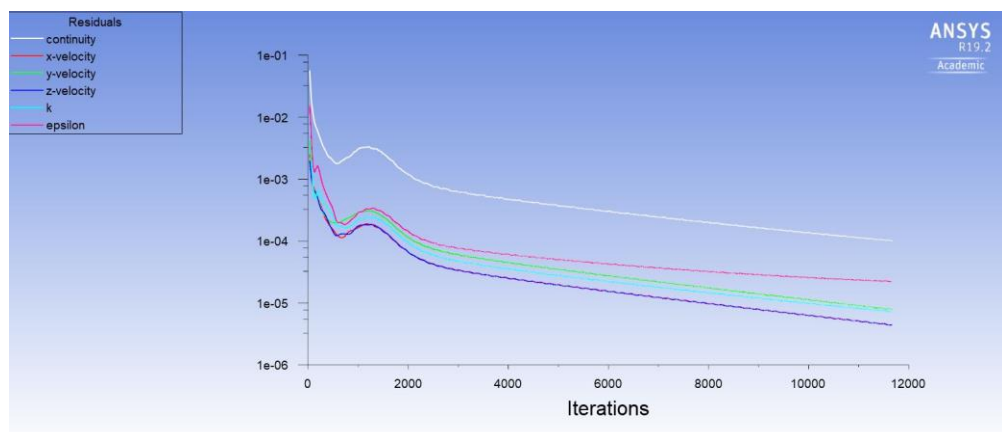


Figure 4-6: Scaled residuals versus number of iterations of the numerical solution adopted for one of the simulated cases.

- Monitoring certain points for values of interest have reached a steady solution. These values are essentially the main outputs from the simulation. In this study, the velocity magnitude at the centre of the nozzle and 5 mm

downstream of the burner exit were monitored. The designated point value, velocity magnitude, must converge to a steady value, see [Figure 4-7](#) for a 600 l/min tangential flow rate without axial air injection effects. Without convergence should the simulation run continue for an additional number of iterations, a different result would be obtained. Deciding whether these values have reached a steady solution is based on obtaining a single repeatable value. This step was repeated for all boundary conditions.

- The domain has an overall imbalances for all variables of less than 1% [\[223\]](#).

All the above criteria were used in this study to ensure convergent solutions for all configurations and boundary conditions studied, and according to these criteria accurate results were achieved.

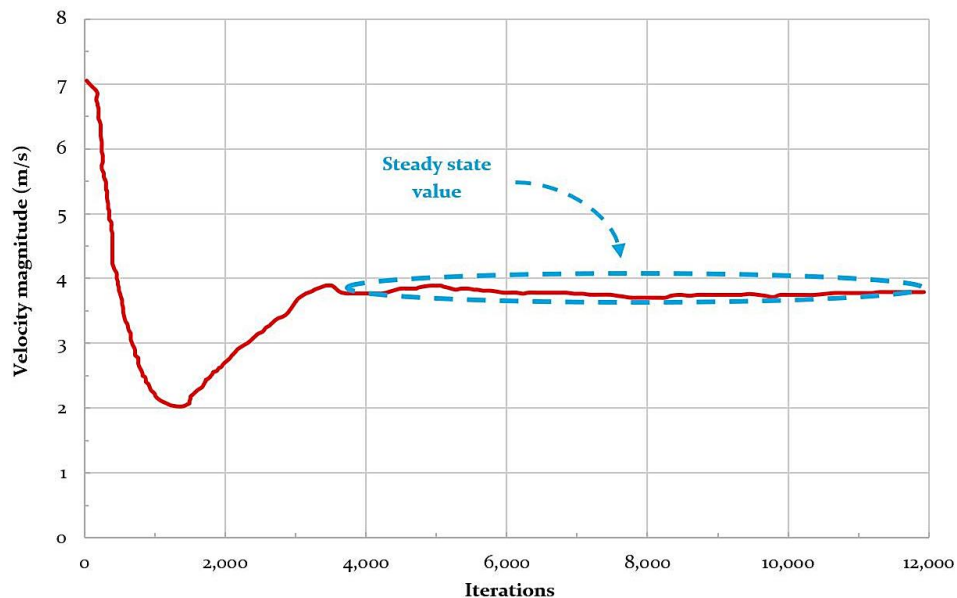


Figure 4-7: Velocity magnitude monitoring. Conditions: 600 l/min tangential flow rate without axial air injection.

4.3.5 Mesh Independence Analysis

A finely structured mesh was used and independent mesh analysis was performed by examining the mesh sensitivity and the provision of a mesh independent solution and get a valid result. The more accurate mesh and boundary conditions, the more accurate the "converged" solution will be. The convergence approach described in the previous section provides a single CFD solution based on initial mesh size. Although this converged CFD solution was based on scaled residuals values, monitor points and imbalances, making sure that the CFD solution is independent of the mesh

resolution is also crucial. Neglecting mesh independence analysis is a common reason for inaccurate results in CFD, and this process should be carried out at least once for each burner configuration so should a similar problem arise, the same mesh sizing can be applied. The sequence of the mesh sensitivity analysis carried out in this work required going throughout the following steps:

- **Step 1:** Running the first simulation based on initial mesh size ensuring the achievements of the numerical solution convergence requirements mentioned in Section 4.3.4. If convergence was not achieved, the mesh needed to be refined and then Step 1 repeated.
- **Step 2:** Once having determined the convergence criteria for the first CFD simulation, the mesh was globally refined to 0.5 of the initial mesh sizes to produce finer cells throughout the computational domain, and then the convergence criteria was again determined. Then the monitored point values (in this case the velocity magnitude) from Step 2 and Step 1 were compared. If they were the same (within the allowable limit), then the mesh for Step 1 was accurate enough to capture the result. If the value at Step 2 is not in satisfactory values of the Step 1 result, then this indicates that the solution is changing due to mesh resolution, and hence the solution is not yet independent of the mesh. In this case, moving to Step 3 is necessitated.
- **Step 3:** In this step, further refinement of the mesh was carried out. This process was repeated until a sufficiently accurate agreement was achieved between consecutive runs, which meant a mesh independent solution had been achieved. The CFD run was carried out with the lower number of elements, to reduce run time.

The mesh independence analysis (**Step 1-Step 3**) was employed to examine the grid quality for every configuration. [Table 4-2](#) shows the grid statistics for each region of the computational domain in this study.

Table 4-2: Mesh size statistics.

Entity	Value (mm)
Domain downstream the burner nozzle (max / min)	0.9 / 0.5
The flow core downstream the burner nozzle (max / min)	0.9 / 0.5
Domain at the burner nozzle (Max/wall)	0.5 / 0.4
The burner planum domain (Max/wall)	0.9 / 0.5
Average total number of elements within the computational domain	11,117,541

4.3.6 Operating and Boundary Conditions

After defining the fluid domain and the mesh size, the location of boundary conditions and values in terms of different input parameters needed to be specified. CFD simulations were conducted under isothermal (no combustion) conditions with no air preheating. A fixed tangential inlet blockage (insert) 25%-25% was employed to give a suitable swirl number ($S_g=0.913$) when a coherent structure existed in the flow. The velocity inlet boundary condition options of ANSYS Fluent were employed to define the scalar properties and the velocity of the flow at inlet boundaries of the burner (the tangential and the axial air jet inlets). Different flow conditions (inlet tangential flow rates) were selected at ambient temperature and pressure. The tangential flow rate value and the reason for selecting it will be discussed in detail in Section 4.4.1.

Regarding determination of the turbulence parameters at the inlet boundaries, a turbulence intensity of less than 1% is commonly supposed low, while and turbulence intensities more than 10% are presumed high [223]. The turbulence intensity of the flow at the inlets depends on the upstream history of the flow. The turbulence intensity of fully developed flow may be only a few percent higher than for under-developed and undisturbed flows. In this study, the core of the flow at inlet boundaries (tangential and axial air inlets) was assumed to be fully developed as there was a sufficient number of pipe length upstream of the inlets. The turbulence intensity values (I) at the tangential and the axial air inlets are directly proportional to the flow Reynolds number (Re), and the turbulence intensities at these boundaries were estimated from the empirical relation [223]:

$$I \equiv 0.16(Re_{D_H})^{-1/8} \quad (4.1)$$

Where: Re_{D_H} is the Reynolds number based on the hydraulic diameter D_H of the inlet boundaries. However, the exit flow was modelled utilising a pressure outlet boundary condition. At atmospheric pressure, and total backflow temperature of 300 K, and turbulent intensity of backflow of 5%; the hydraulic diameter is equal to the diameter of the computational domain downstream the burner nozzle [223].

4.3.7 Solution Method and Fluent Settings

All CFD calculations were done by Ansys Fluent R19.2 code. In this work, the RANS turbulence solution was achieved employing a segregate flow solver, which handled the many pressure velocity coupling algorithms. The realizable $k-\epsilon$ turbulence model [223] with standard wall functions was adopted in this study.

ANSYS Fluent provides the option of selecting from amongst four pressure-velocity coupling algorithms: SIMPLE, SIMPLEC (a variant of SIMPLE), Pressure Implicit with Splitting of Operators (PISO, an extension of the SIMPLE algorithm) and Coupled. For unsteady flows ANSYS Fluent used the Non-Iterative Time Advancement scheme (NITA) [224]. All these schemes, except the Coupled, are based on the predictor-corrector approach. The PISO pressure-velocity coupling scheme is a solution method recommended for steady-state and transient calculations on large skewed meshes, and is based to a high degree on the approximate relationship between the corrections for velocity and pressure [238]. One of the restrictions of the SIMPLE family of schemes is that new velocities and corresponding fluxes do not contribute to the momentum balance after the pressure-correction has been completed. Consequently, the computation must be repeated until the balance is satisfied [238]. To enhance the efficiency of this computation, the PISO algorithm performs two additional correction improvements: skewness correction and neighbour correction [223].

A suitable pressure scheme needs to be chosen to enable ANSYS Fluent to interpolate the pressure at faces when discretising the pressure gradient term in momentum. Different pressure schemes are available in ANSYS, first order, second order, PRESTO and body force weighted. The best option for swirl flow is the PRESTO interpolation scheme which is usually helpful when there are strong body forces present such as high swirl, or natural convection with high Rayleigh number [223].

Appropriate options need to be selected for the discretisation of momentum, turbulent kinetic energy, and turbulent dissipation rate. In this work, the QUICK scheme was employed for computing variables at a face for the momentum, turbulent dissipation rate, and turbulent kinetic energy [223], see Table 4-2.

Table 4-3: Numerical setup discretization for the RANS simulation of the isothermal swirl flows.

Simulations tools	Settings
Domain	Three-dimensional, the domain geometry is shown in Figure 4-4
Method	Finite volume
Discretisation	QUICK for momentum, turbulent kinetic energy and specific dissipation rates
Discretisation	Pressure staggering option (PRESTO) for pressure
Discretisation	PISO for pressure-velocity coupling
Discretisation	Steady state
Turbulence model	The realizable ($k-\varepsilon$) model

Regarding the solution control, the under-relaxation factors were selected to be equal to 0.7 and 0.3 for momentum and pressure, respectively. However, they were set to 0.8 for both the turbulent dissipation rate and the turbulent kinetic energy equations. All other parameters were set to 1. All the under-relaxation factors were selected to get a better and the smoother path of the scaled residual values throughout the path towards convergence.

4.4 Results and Discussion

This main section divides the results into two main subsections, the CFD modelling and the experimental work. The CFD subsection presented two aims. First, the progressive transition of coherent swirl structures from pre-breakdown flow reversal to a CRZ is discussed for low tangential flow rates. Second, the hydrodynamic effects of the axial air jet on the swirl flow characteristics. In comparison, the experimental work presented the effects of the axial air injection system on the flame stability map.

4.4.1 The CFD Campaign

4.4.1.1 The Onset of the Vortex Breakdown

This subsection will present the transition process from the axisymmetric flow to swirling flow under the effects of the axial air jet. In other words, the start of breakdown and the appearance of the CRZ. This is crucial to give a clear picture for the study of the effects of axial air injection on the swirl flow characteristics from low to high strength swirling flows.

As described in Chapter Two, and according to some authors [99], swirl burners provide controllable and flexible reverse flow zones (CRZ) with regions of high turbulence and shear characteristics that give good, stable combustion. A CRZ appears as an ovoid bubble of fluid that remains in the flow at a point just above the burner exit. It should be formed downstream, remaining coherent under a great variety of conditions. The vortex core does not remain stable, but starts precessing [91]. Its frequency remains constant as determined by flow conditions and the geometry of the burner [64]. However, axial air injection may affect the coherent structure of the swirl flow and hence the flame stability.

The swirl flow is considered axisymmetric until the onset of vortex breakdown. Previous literature in this context stated that the vortex breakdown and the development of a CRZ happen when the swirl number is equal to ($S \approx 0.6$) [88]. However, applying axial air injection to modify the burner resistance against the CIVB

flashback will affect the swirl number range by adding a pure axial momentum which can significantly degrade the swirl flow strength. As a result, the value of the axial air flow rate should be chosen carefully to avoid any negative impact on the coherent structure of the swirling flow.

Swirl strength linked to geometric swirl number is critical in the development and characteristics of the coherent structures of the swirling flow, its value can change locally according to the ratio of (tangential/axial) flowrates. Therefore, this number can vary when considerable amounts of air are injected axially. Figure 4-8 illustrates the effect of different axial air injection flowrates on the burner's local swirl number (S) at different inlet tangential flowrates. The local swirl number was evaluated for isothermal conditions where density is assumed to be constant, employing Equation 2.15 which is based on burner geometry, inlet conditions but neglecting pressure variations [92][96]. The inlet tangential flowrates varied from 200 l/min up to 1200 l/min while the axial air injection flowrates varied from zero to 300 l/min. The figure shows that the increase in the axial air injection rate leads to a decrease in the local swirl number for all tangential flowrates due to the pure axial momentum added by the axial air jet. It is also observed that the local swirl number will be the same magnitude ($S \approx 0.58$) for all values of tangential flowrates when the value of the axial air flow rate is equal to 25% of those flowrates, see the red dashed line. The zero value of the axial air flowrate represents the case of the burner without air jet effect, where the swirl number is the same ($S = S_g \approx 0.9$) regardless of the values of tangential flowrates.

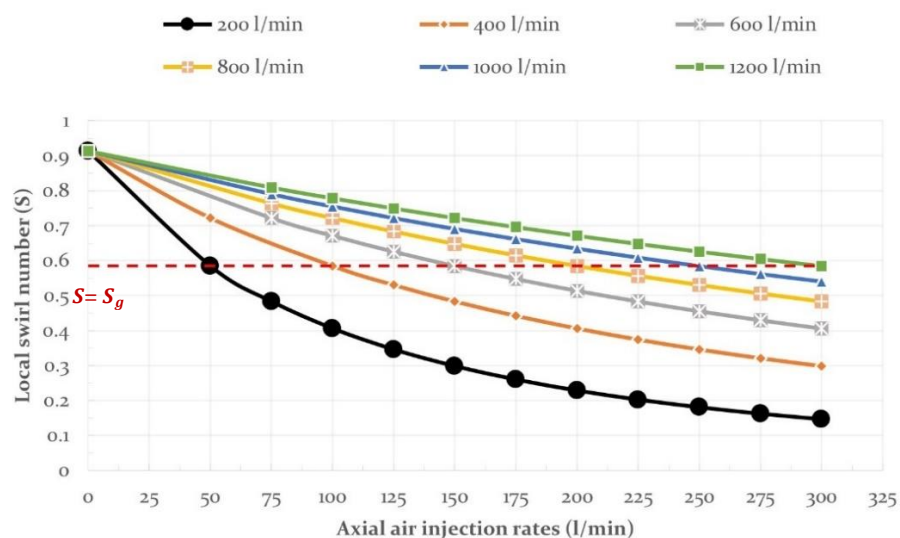


Figure 4-8: Local swirl numbers (S) at different axial air jet flowrates.

In this work, the central air injection will be kept at 50 l/min with a mean inlet axial velocity of $\bar{u} = 3.1$ m/s at atmospheric conditions. This value will be used with all tangential flowrates in this study to minimise swirl flow degradation. This value accounts for 10% of the minimum tangential mass flowrate. It was demonstrated that injecting air at 50 l/min via the central injector ensures a coherent structure of the axial air jet able to attain the required positive hydrodynamic effects on the swirl flow in the burner under consideration, see [Figure 4-9](#).

This figure shows the velocity vector coloured by the axial velocity in both axial and radial planes at burner exit for 400 l/min tangential flow rate under the effect of axial air injection. The coherent structure of the axial air jet is obvious at the centre of the burner nozzle. This coherent jet will achieve the desired effect on the swirl flow at the CRZ tip, especially the axial velocity component, which is one of the main reasons for CIVB flashback mechanism in swirl burners.

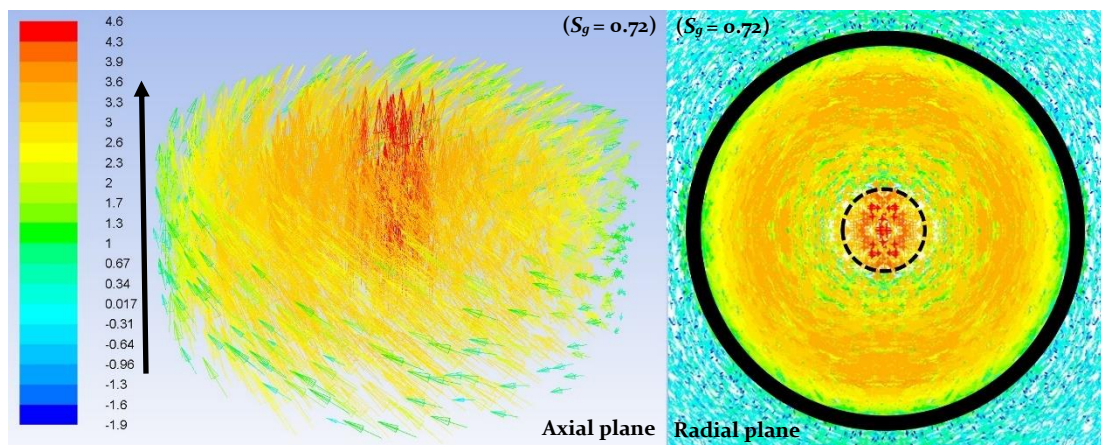


Figure 4-9: Velocity vectors coloured by axial velocity (m/s) at burner mouth for tangential flow rate (400 l/min) with 50 l/min axial air jet represented in both axial and radial planes.

To understand the onset of vortex breakdown under the effect of the axial air injection, CFD simulations were done for three low tangential flow rates (200, 300, and 400 l/min). [Figure 4-10](#), [Figure 4-11](#), and [Figure 4-12](#) illustrate the comparison of the axial velocity contours (isothermal condition) between the two main cases of with and without axial air injection, for different air injector positions (L_o) of 0, 29 and 150 mm, respectively, all with an inlet tangential flow rate of 200 l/min (Re at burner exit ≈ 4625 - 5781). The figures show that the axial air jet distorts the swirl flow for all injector positions (L_o) by affecting the vortex breakdown preventing the formation of the CRZ.

Figure 4-13, Figure 4-14 and Figure 4-15 illustrate axial velocity contours (isothermal condition) for a tangential flow rate of 300 l/min (Re at burner exit $\approx 6937 - 8094$) with and without axial air injection at the same three central injector positions (L_o) of 0, 29 and 150 mm, respectively. The same effects as previously for the axial air were observed at ($L_o=150$ mm). However, a weak CRZ appears in the flow downstream of the burner nozzle despite axial air jet effects at ($L_o=0$ and 29 mm). Upon increasing the inlet tangential flowrate to 400 l/min ($Re \approx 9250 - 10406$), the CRZ becomes more robust and coherent for the three burner configurations ($L_o=0, 29, 150$ mm) with and without axial air injection; this will be discussed in detail in the next section.

Regarding the local swirl number (S), it is noticed that the minimum value of ($S \approx 0.72$) is essential in the formation of the vortex breakdown under the effect of an axial air jet of 50 l/min for all three burner configurations ($L_o=0, 29, 150$ mm). This value of swirl number could be achieved when the tangential flowrate is equal to or greater than 400 l/min.

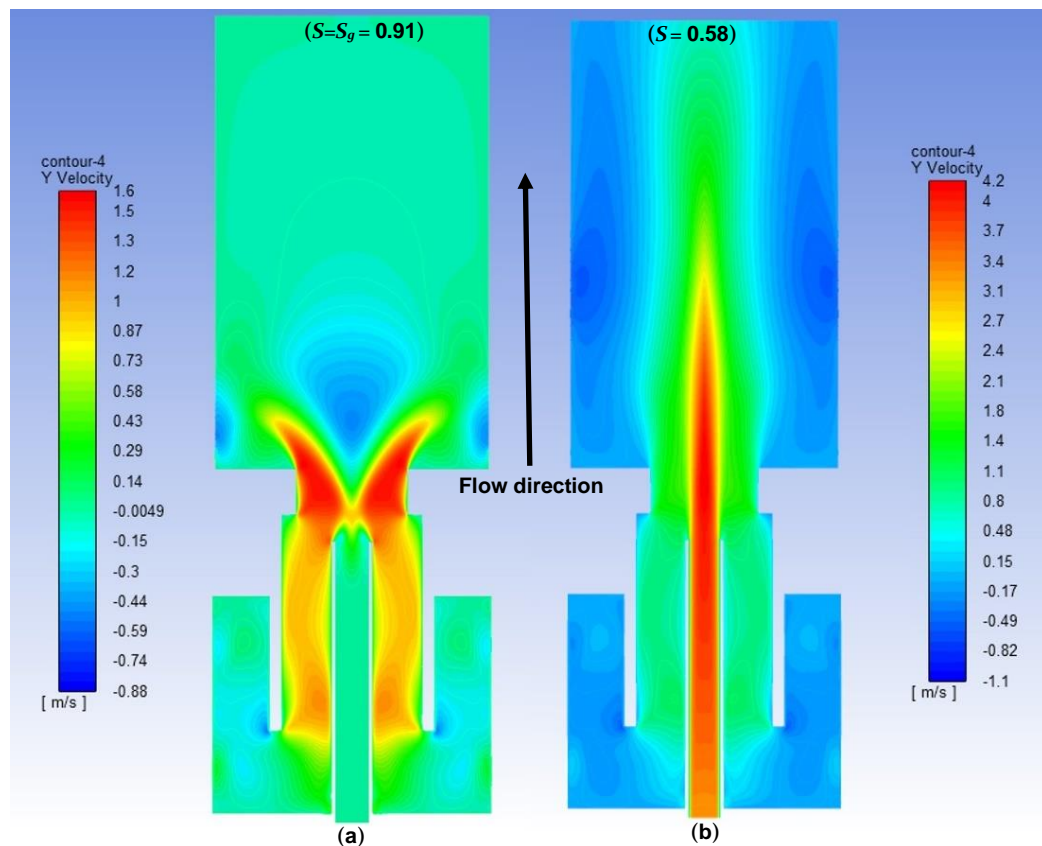


Figure 4-10: Axial velocity contours (m/s), isothermal flow, for (200 l/min) inlet tangential flow rate and $L_o=150$ mm (a) without axial air injection, and (b) with 50 l/min axial air injection.

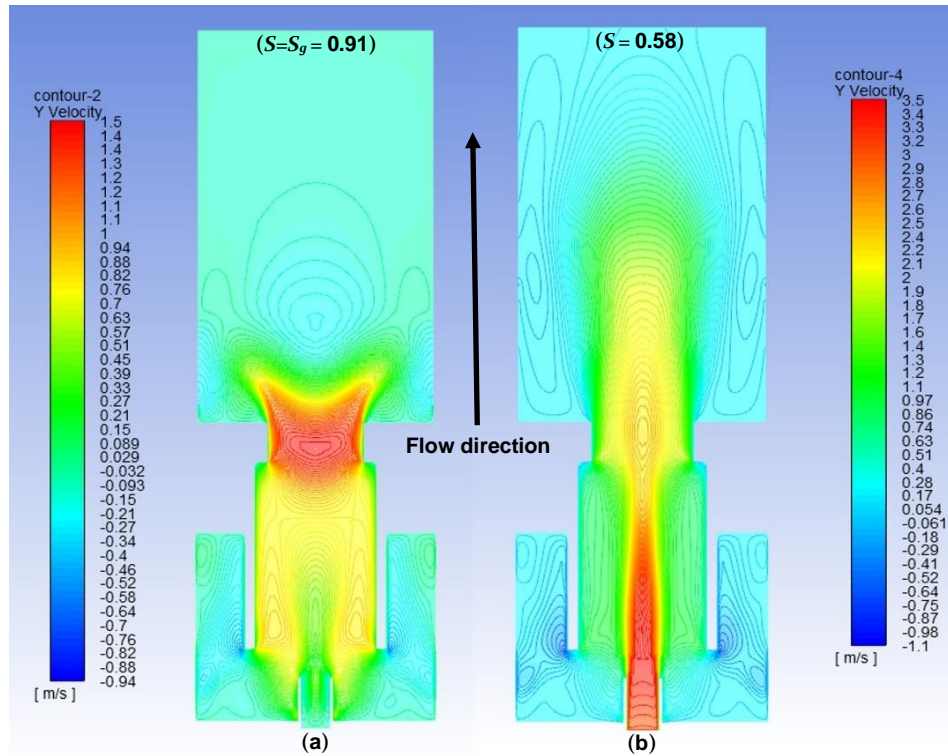


Figure 4-11: Axial velocity contours (m/s), isothermal flow, for (200 l/min) inlet tangential flow rate and $L_o=29$ mm (a) without axial air injection, and (b) with 50 l/min axial air injection.

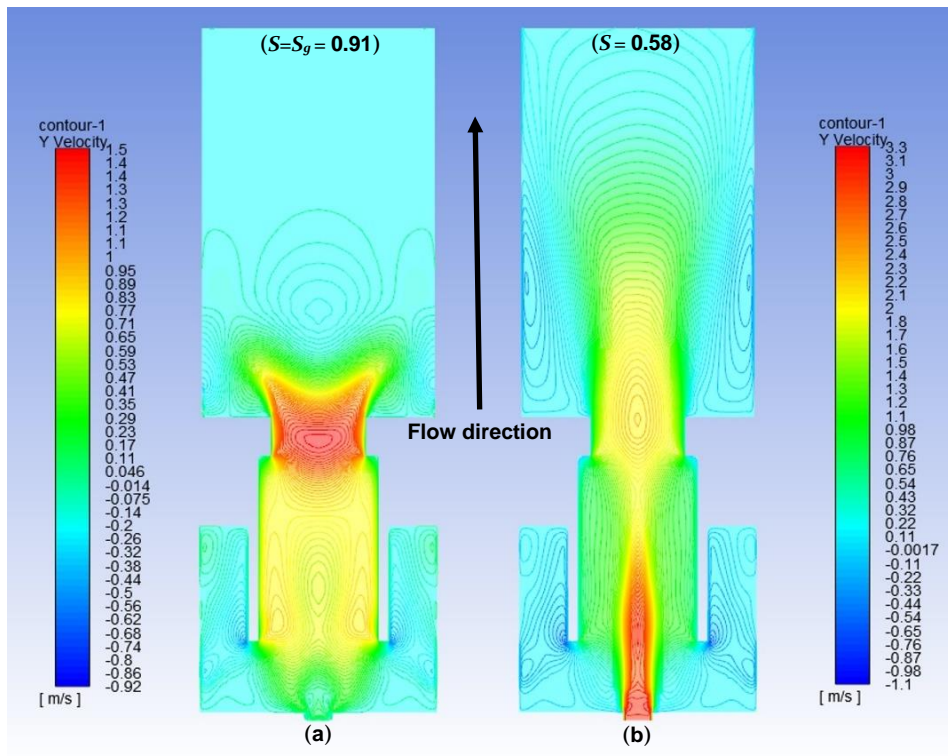


Figure 4-12: Axial velocity contours (m/s), isothermal flow, for (200 l/min) inlet tangential flow rate and $L_o=0$ mm (a) without axial air injection, and (b) with 50 l/min axial air injection.

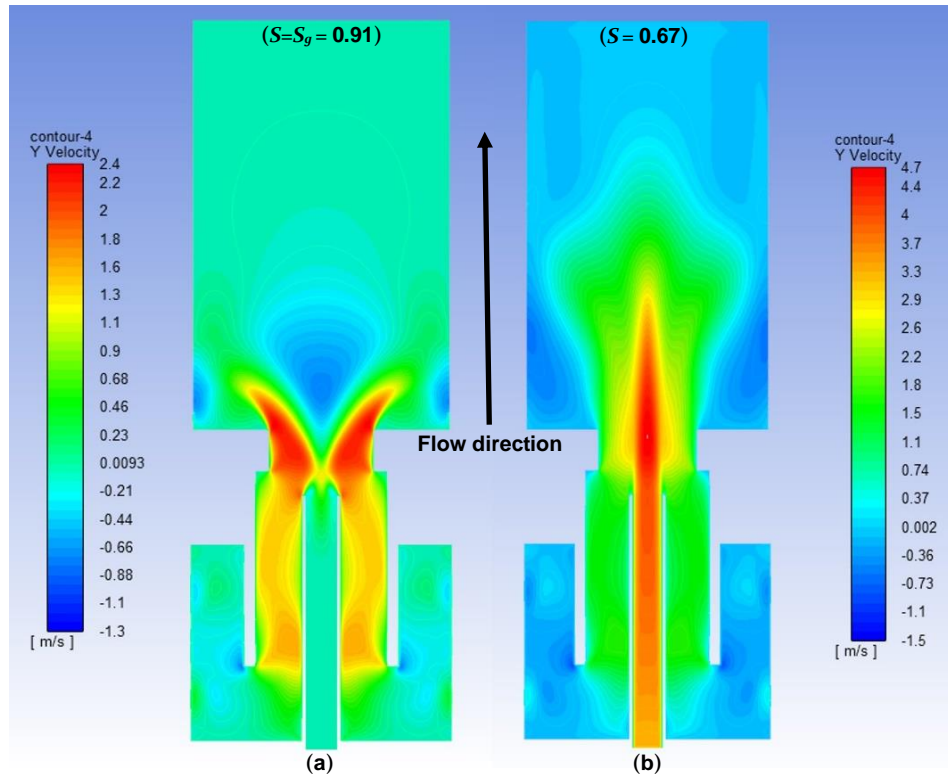


Figure 4-13: Axial velocity contours (m/s), isothermal flow, for (300 l/min) inlet tangential flow rate and $L_o = 150$ mm (a) without axial air injection, and (b) with 50 l/min axial air injection.

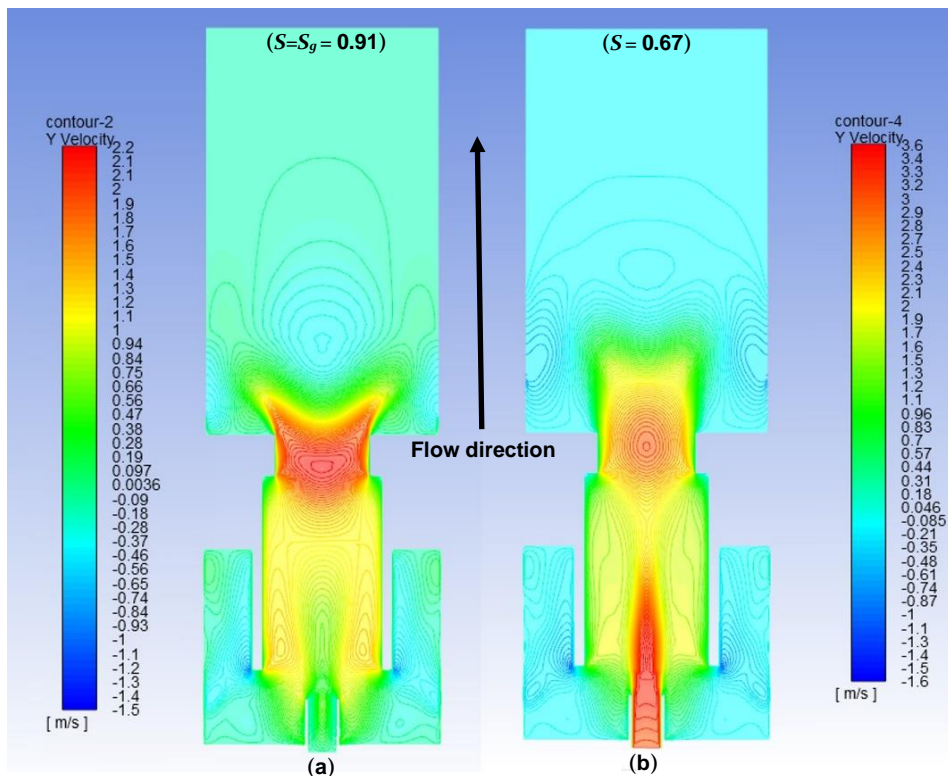


Figure 4-14: Axial velocity contours (m/s), isothermal flow, for (300 l/min) inlet tangential flow rate and $L_o = 29$ mm (a) without axial air injection, and (b) with 50 l/min axial air injection.

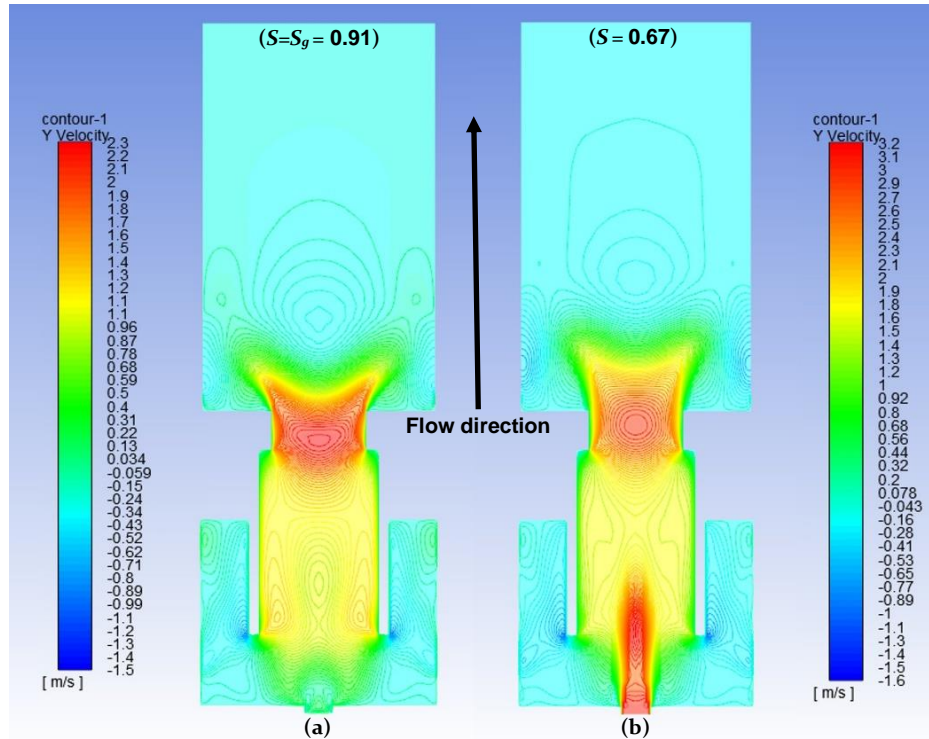


Figure 4-15: Axial velocity contours (m/s), isothermal flow, for (300 l/min) inlet tangential flow rate and $L_0=0$ mm (a) without axial air injection, and (b) with 50 l/min axial air injection.

4.4.1.2 The Hydrodynamic Effects of Axial Air Injection

Based on the findings reported in the previous section, the effect of 50 l/min are discussed here for a wide range of tangential flowrates (400, 600, 800, 1000, 1200 and 1400 l/min), which are equivalent to mean axial velocities at the tangential inlets of $\bar{u} = 2.31$ m/s, 3.43 m/s, 5.59 m/s, 5.76 m/s, 6.93 m/s and 7.86 m/s, respectively. These tangential flowrates provide a Reynolds number (Re) ($\pm 3\%$) at the burner exit of 10783, 15721, 20593, 25452, 30469, and 33532 respectively which is equivalent to $\phi = 0.58$, $\phi = 0.67$, $\phi = 0.71$, $\phi = 0.73$, $\phi = 0.77$ and $\phi = 0.8$, respectively. The CFD results were presented in terms of different levels downstream of burner dump plane i.e., plane located exactly at the burner exit. Different levels (P_y) were set out in the computational domain downstream the burner dump plane to illustrate the different required unknown variables in the swirl flow. These planes are $P_1=0$ mm, $P_2=5$ mm, $P_3=15$ mm and $P_4=25$ mm, return to [Figure 4-4](#).

4.4.1.2.1 CFD Result's Validation

Regarding CFD result's validation, computer aided decision making and insight into the physics of the engineering problems is essential. A personal computer (PC) became our companion in our research life, however, no matter how much we trusted

it a primary question needed to be answered. Validation and verification of the codes used are required before proceeding to a theoretical approach. It does not matter whether the validation case is similar exactly to the one being considered a very close model is needed in terms of physical behaviour and boundary conditions.

However, in this study, the CFD simulation gave a good agreement with the observed experimentally (physical model and boundary conditions) in parallel work by other researchers [63]. To get acceptable CFD results, this work was carried out via the following steps: the proper model, the geometrical representation was the same as the experimental work, the mesh was of high quality and the domain size was the same as for the real case. After the CFD solved the problem, a comparison step showed any discrepancy between the real data and the CFD results. This depended on the following points: the correct physical behaviour was achieved, and the difference should be of a significant level. However, in the worst case, it is enough to just report the discrepancy.

LDA measurements of published work were used to validate the CFD results [63]. For example, Figure 4-16, Figure 4-17 and Figure 4-18 show the comparison of the axial velocity values between the LDA and the CFD results. It was concluded from these three figures that CFD results regarding the axial velocity profile revealed very good agreement with the LDA measurements. Therefore, the numerical approach was used to provide more insights into the phenomena and processes.

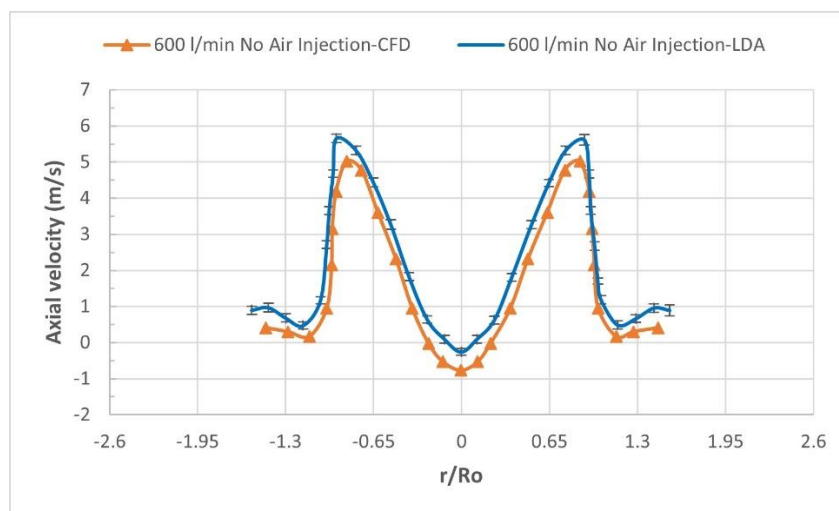


Figure 4-16: Comparison of axial velocity (m/s) measured by LDA with the CFD results for tangential flowrate of 600 l/min without axial air jet, $L_o=150$ mm at P_2 .

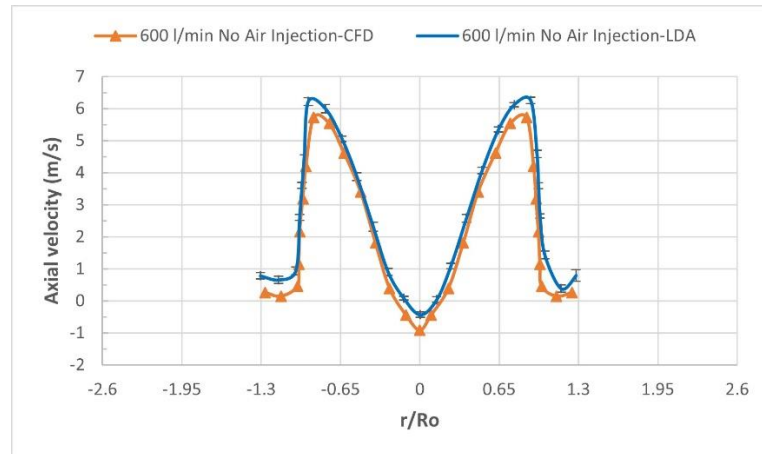


Figure 4-17: Comparison of axial velocity (m/s) measured by LDA with the CFD results for tangential flowrate of 800 l/min without axial air jet, $L_o=150$ mm at P_2 .

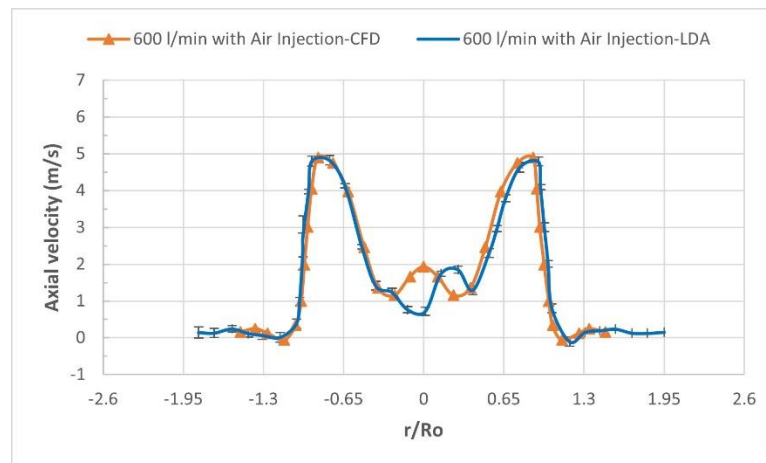


Figure 4-18: Comparison of axial velocity (m/s) measured by LDA with the CFD results for tangential flowrate of 600 l/min with 50 l/min axial air jet, $L_o=150$ mm at P_2 .

4.4.1.2.2 Effect of Axial Air Injection on the Axial Velocity

Central air injection affects the aerodynamic characteristics of the flow field downstream of the burner dump plane. It reduces the axial velocity defect (negative velocity regions) at the tip of the recirculation zone, which is one of the main reasons for CIVB flashback [185]. As a result, the stability map of the burner will be affected. Figure 4-19 - Figure 4-27 show the reduction of axial velocity defects for various burner configurations (different L_o) and tangential flowrates all measured at level ($P_2=5$ mm) downstream the burner dump plane: Figure 4-19 - Figure 4-21 ($L_o=150$ mm), tangential flowrates (400, 600, and 800 l/min); Figure 4-22 - Figure 4-24 ($L_o=29$ mm), tangential flowrates (400, 600, and 800 l/min), Figure 4-25 - Figure 4-27 ($L_o=0$ mm), tangential flowrates (400, 600, and 800 l/min).

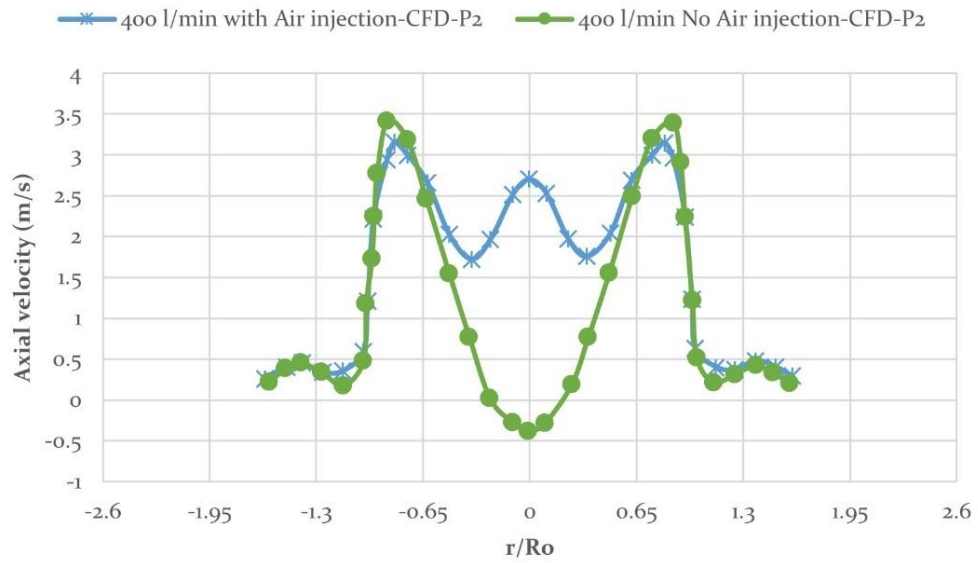


Figure 4-19: CFD results, the effect of axial air injection on the axial velocity defect downstream of the burner mouth, tangential flowrate 400 l/min, $L_o=150$ mm, at level $P_2=5$ mm.

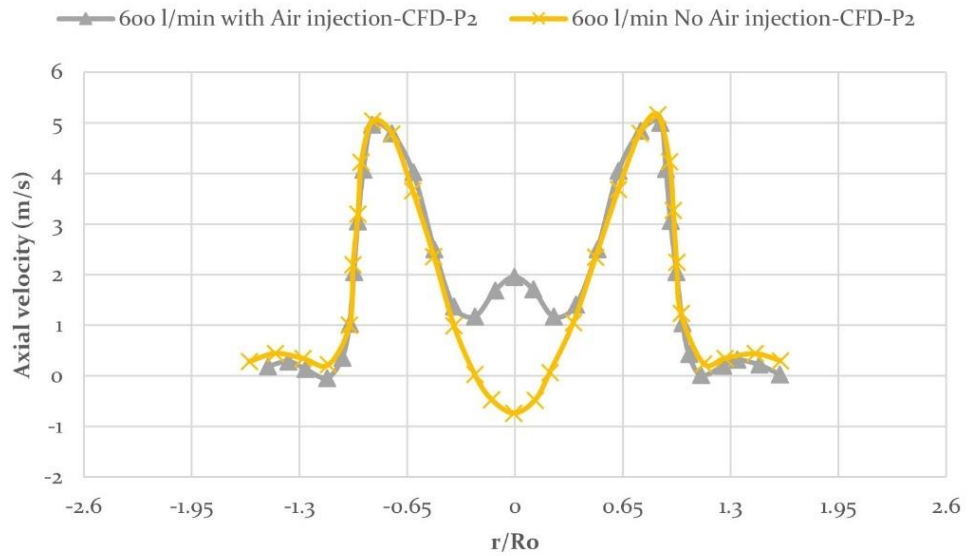


Figure 4-20: CFD results, the effect of axial air injection on the axial velocity defect downstream of the burner mouth, tangential flowrate 600 l/min, $L_o=150$ mm, at level $P_2=5$ mm.

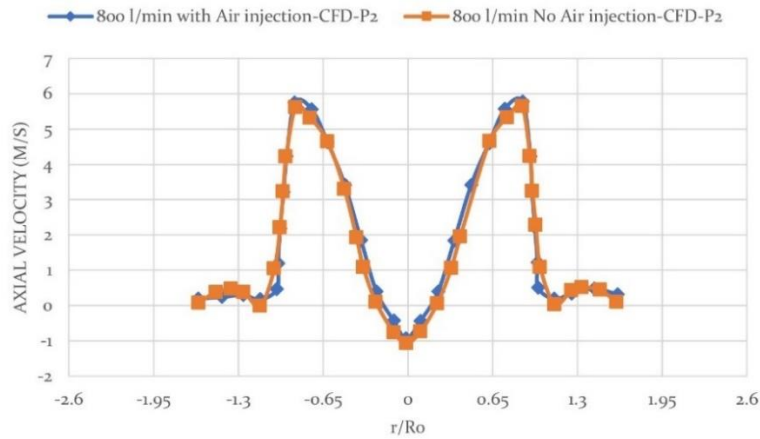


Figure 4-21: CFD results, the effect of axial air injection on axial velocity defect downstream of the burner mouth, tangential flowrate 800 l/min, $L_o=150$ mm, at level $P_2=5$ mm.

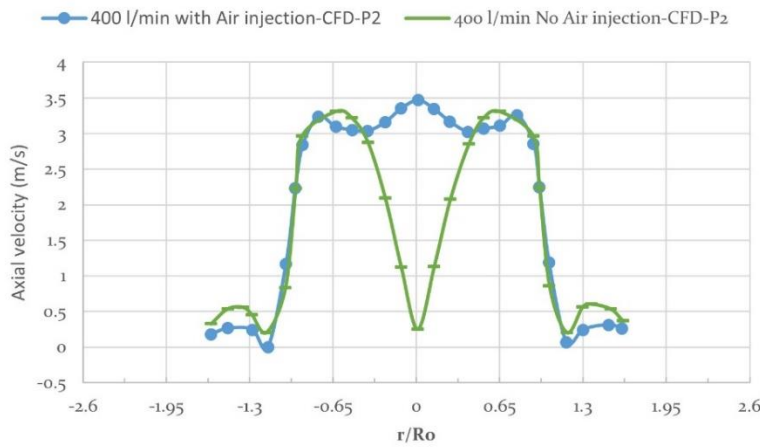


Figure 4-22: CFD results, the effect of axial air injection on the axial velocity defect downstream of the burner mouth, tangential flowrate 400 l/min, $L_o=29$ mm, at level $P_2=5$ mm.

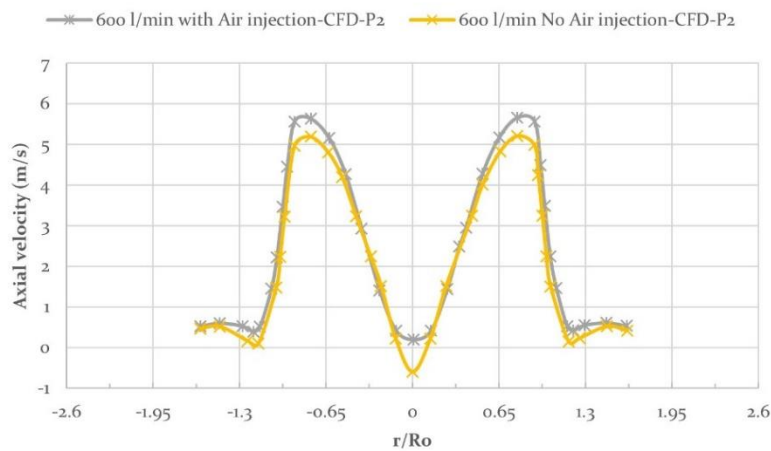


Figure 4-23: CFD results, the effect of axial air injection on the axial velocity defect downstream of the burner mouth, tangential flowrate 600 l/min, $L_o=29$ mm, at level $P_2=5$ mm.

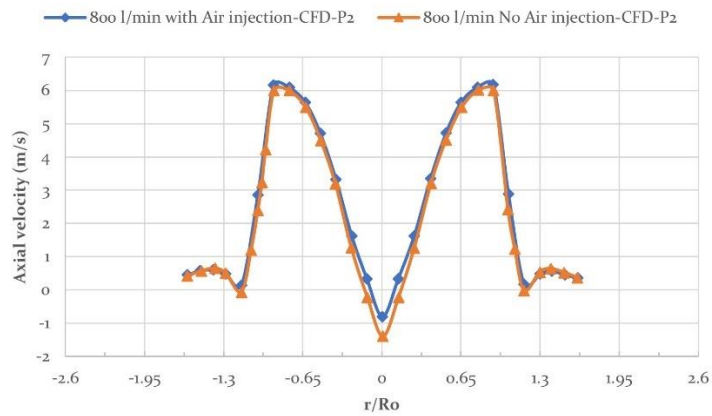


Figure 4-24: CFD results, the effect of axial air injection on the axial velocity defect downstream of the burner mouth, tangential flowrate 800 l/min, $L_o=29$ mm, at level $P_2=5$ mm.

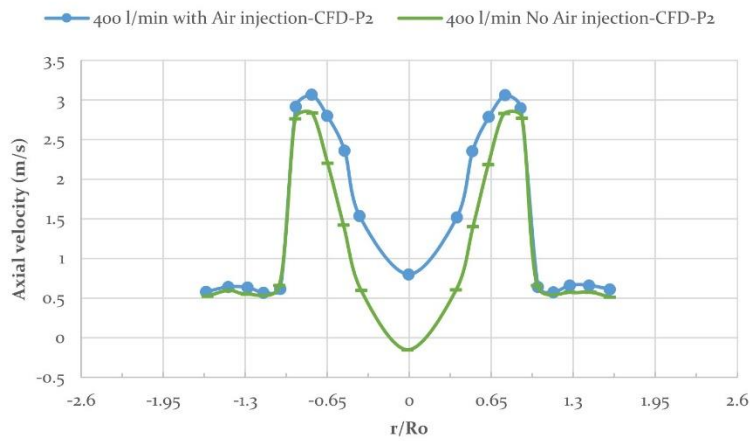


Figure 4-25: CFD results, the effect of axial air injection on the axial velocity defect downstream of the burner mouth, tangential flowrate 400 l/min, $L_o=0$ mm, at level $P_2=5$ mm.

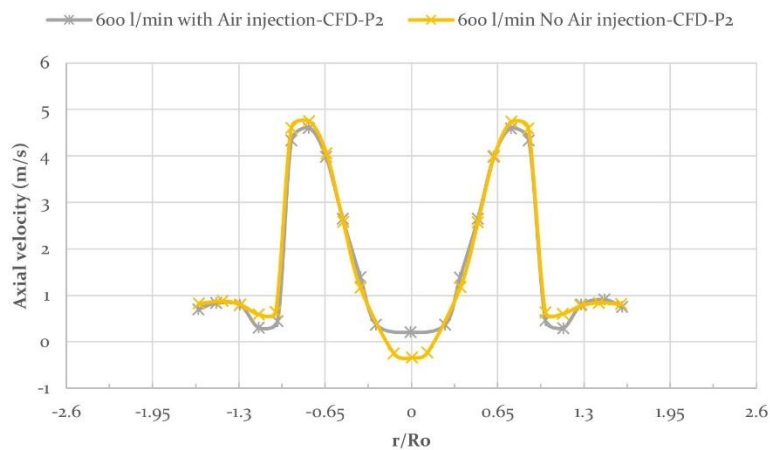


Figure 4-26: CFD results, the effect of axial air injection on the axial velocity defect downstream of the burner mouth, tangential flowrate 600 l/min, $L_o=0$ mm, at level $P_2=5$ mm.

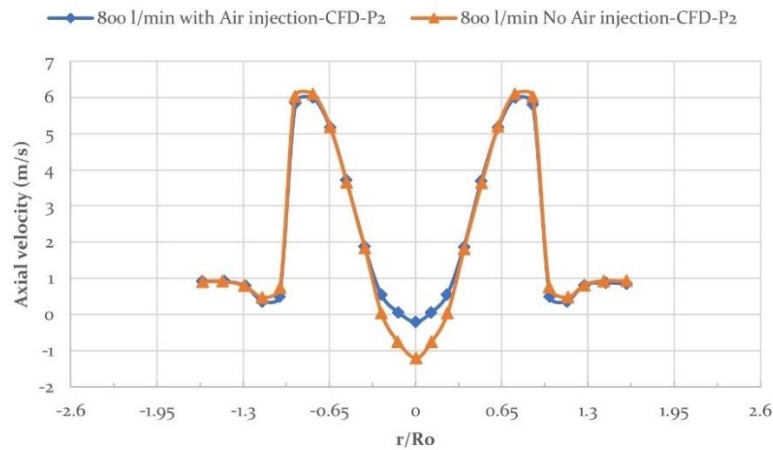


Figure 4-27: CFD results, the effect of axial air injection on the axial velocity defect downstream of the burner mouth, tangential flowrate 800 l/min, $L_o=0$ mm, at level $P_2=5$ mm.

A closer analysis of the axial velocity profiles approaching the exit dump plane, Figure 4-19 - Figure 4-27, show how the position of the central air injector is critical in re-establishing the recirculation zone to enhance flashback. As the central injector is closer to the dumping plane ($L_o=150$ mm, Figure 4-19, Figure 4-20 and Figure 4-21), the axial momentum of the former remains strong enough to push the CRZ back into the combustor, which is because the negative velocity seeks to reposition itself closer to the burner exit. Figure 4-28 compares all these effects for $L_o =150$ mm at the different tangential flowrates.

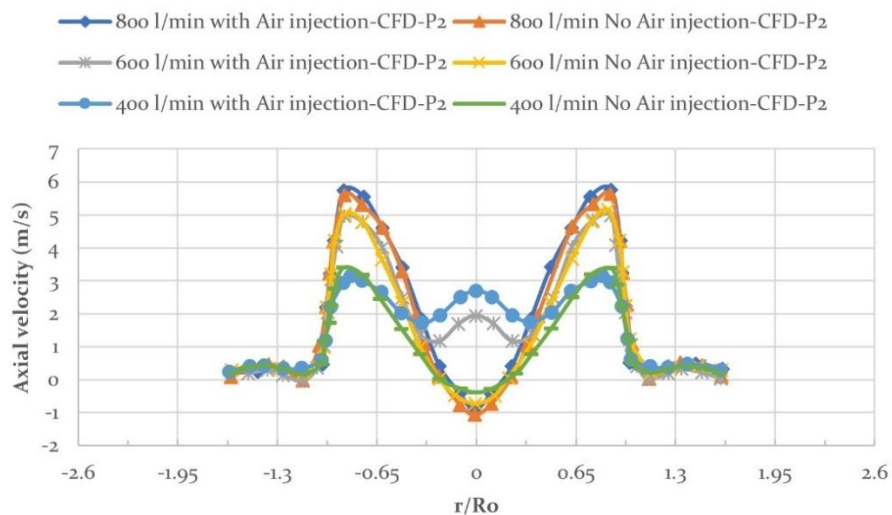


Figure 4-28: CFD results, the effect of axial air injection on the axial velocity defect downstream of the burner mouth $L_o=150$ mm, at level $P_2=5$ mm.

However, as the central injector is located closer to the baseplate ($L_o=29$ mm, Figure 4-22, Figure 4-23 and Figure 4-24 and $L_o=0$ Figure 4-25, Figure 4-26 and Figure 4-27) the negative profiles, like those without central air injection and with the clear presence of a CRZ, reappear, showing that the use of the central injection technique barely affects the axial position of the central recirculation zone. However, the effect of axial air injection on the centreline velocity defect became more evident at low flowrates as the air injector was moved downstream of the burner baseplate. On the other hand, as the injector is moved closer to the dump plane (i.e., $L_o=150$ mm, Figure 4-19, Figure 4-20 and Figure 4-21), negative profiles are eliminated along the central axis. See Figure 4-29 and Figure 4-30 for all these effects in one place when the axial air injector is located near the baseplate ($L_o=0$ and 29 mm).

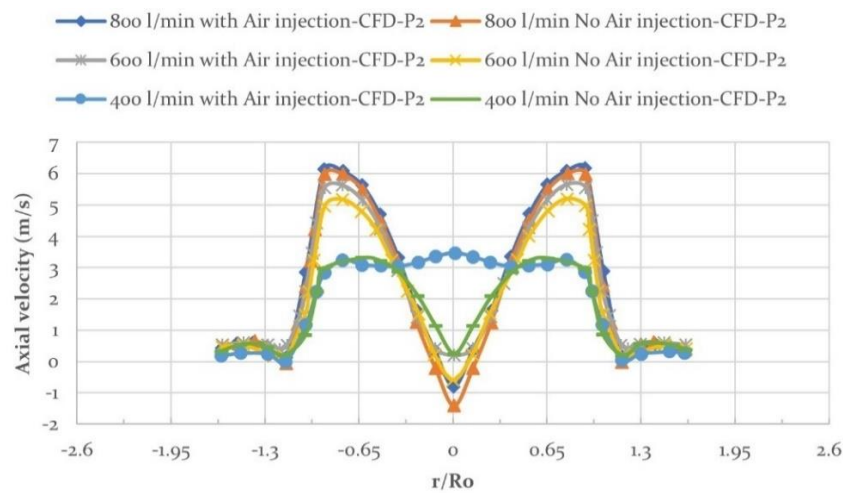


Figure 4-29: CFD results, the effect of axial air injection on the axial velocity defect downstream of the burner mouth $L_o=29$ mm, at level $P_2=5$ mm.

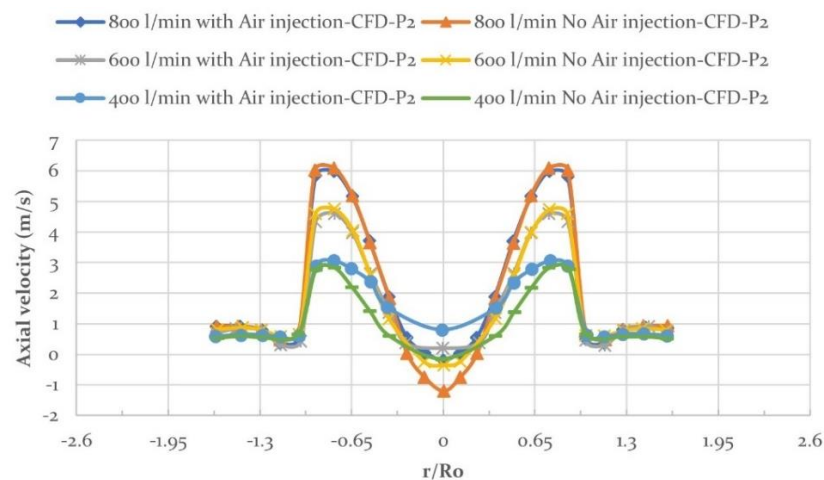


Figure 4-30: CFD results, the effect of axial air injection on the axial velocity defect downstream of the burner mouth $L_o=0$ mm, at level $P_2=5$ mm.

As previously mentioned, at moderate tangential flow rates, the amount by which the axial velocity defects are reduced, is quite clear due to the weak CRZ at these low flowrates. However, high tangential flowrates (1000- 1400 l/min) are barely effective in reducing the axial velocity defects at the tip of the central recirculation zone. As a result, there is little change in axial velocity profile under the effect of axial air injection as can be observed from Figure 4-31 - Figure 4-33. These findings suggest that the amount of axial air injection must be proportionate to the magnitude of the tangential flowrates that directly change the size and strength of the CRZ [88][121]. For instance, at low flowrates, the amount of axial air injection is around 10% of the total air to obtain the required effect in terms of flame flashback resistance while at high flowrates, the ratio is decreased to about 4%.

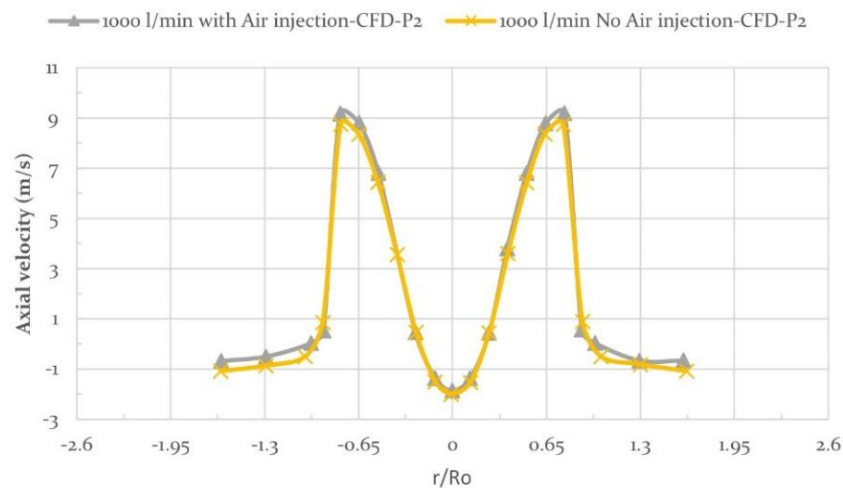


Figure 4-31: CFD results, effect of axial air injection on the axial velocity defect downstream of the burner mouth at 1000 l/min flowrate $L_o=150$ mm, $P_2=5$ mm.

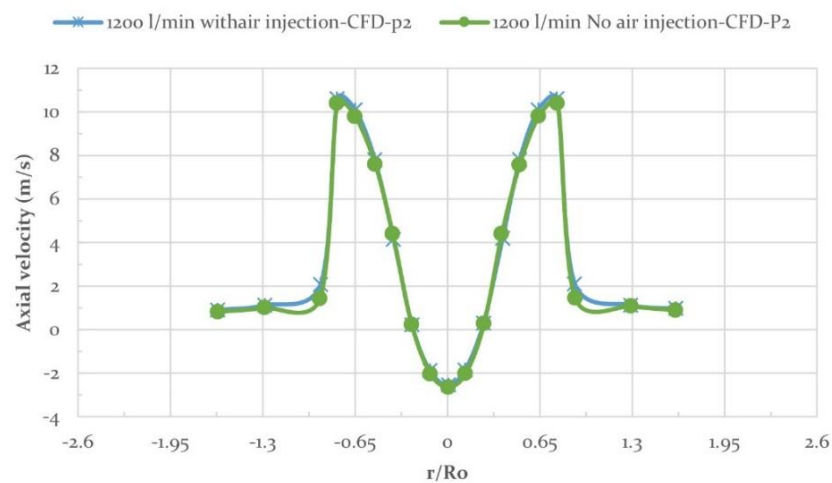


Figure 4-32: CFD results, effect of axial air injection on the axial velocity defect downstream of the burner mouth at 1200 l/min flowrate $L_o=150$ mm, $P_2=5$ mm.

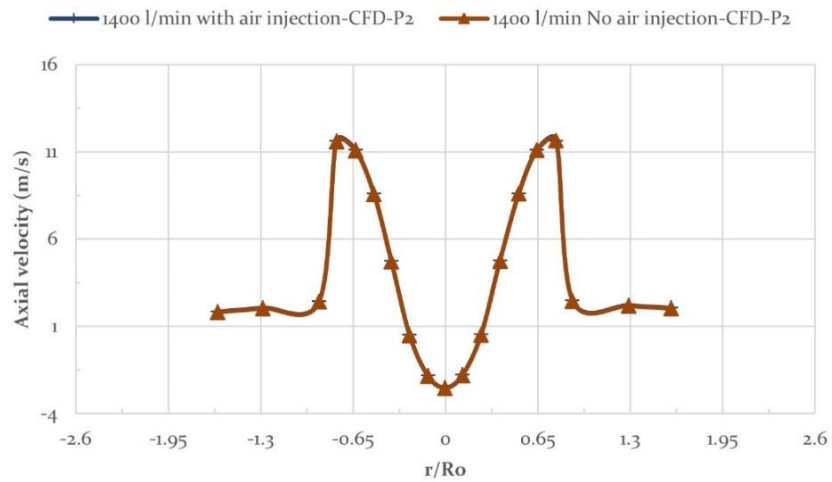


Figure 4-33: CFD results, effect of axial air injection on the axial velocity defect downstream of the burner mouth at 1400 l/min flowrate $L_o=150$ mm, $P_2=5$ mm.

The effect of axial air injection needs to be examined for different distances downstream of the burner dump plane to see how far the axial jet of 50 l/min is still effective. For example, Figure 4-34 shows the axial velocity values for moderate tangential flowrate (600 l/min) at different levels ($P_1=0$ mm, $P_2=5$ mm, $P_3=15$ mm, and $P_4=25$ mm) and axial position $L_o=150$ mm. The figure shows that the axial air injection effect is still active and almost the same at different distances downstream. Nevertheless, the impact of the axial air injection on axial velocity defects will be less and gradually vanish when moving further downstream the burner mouth, see Figure 4.35.

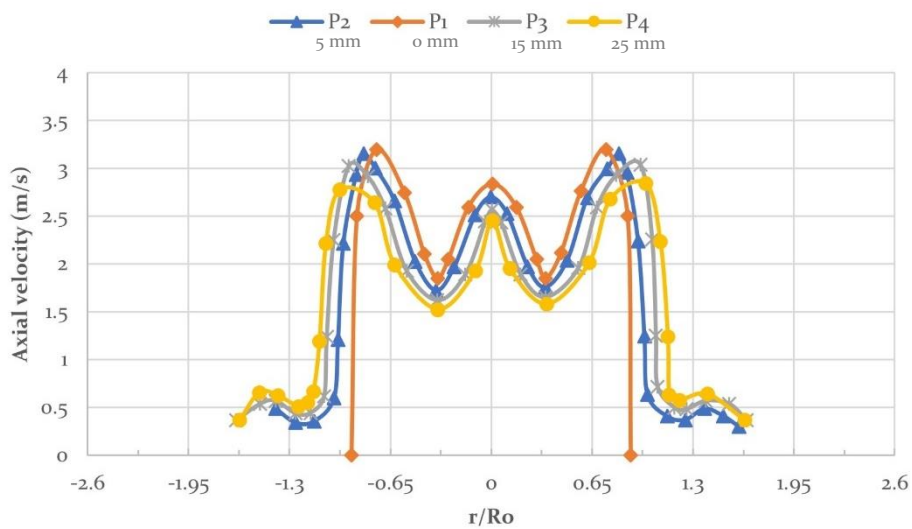


Figure 4-34: Axial velocity component at different distances from burner dump plane (P_j), 600 l/min, $L_o=150$ mm.

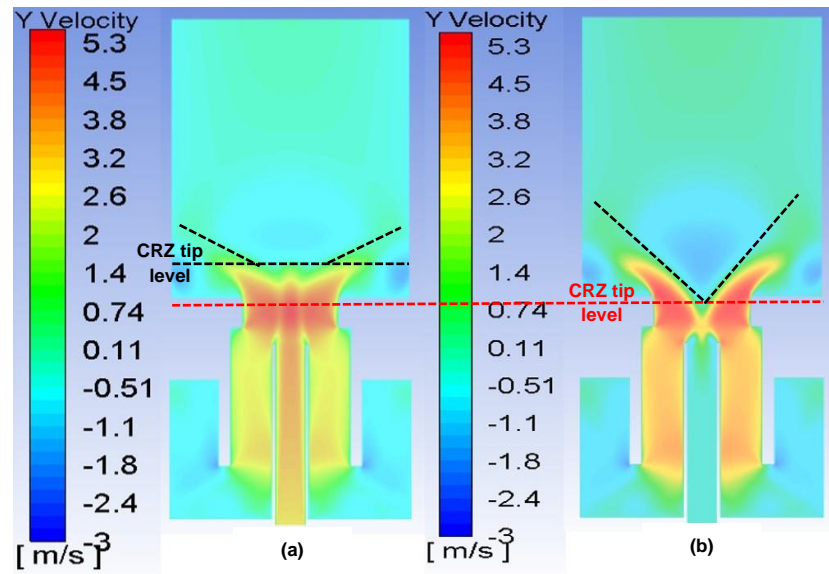


Figure 4-35: CFD results, Axial velocity contour for 600 l/min, $L_o=150$ mm (a) with air injection, (b) without air injection.

In [Figure 4-35](#), contours of the mean axial velocity with and without air injection are presented for the whole burner for the case of 600 l/min with $L_o=150$ mm. It is clear that the axial air pushed the CRZ downstream the burner mouth due to the hydrodynamics effect of the jet, affecting its size, shape and position by adding positive values to the negative axial velocity at the vortex core.

4.4.1.3 Effect of the Central Air Injection on the Flow Turbulence

The increase in turbulence plays an important role in flashback resistance. In turbulent flames, the high level of turbulence can develop flame speed, consequently the likelihood of flashback initiation [\[257\]](#). The relationship between turbulence intensity and turbulent flame speed is reported as follows [\[79\]](#):

$$S_T \propto S_L + u' \quad (4.2)$$

Where:

S_T : turbulent flame speed [m/s]

S_L : laminar flame speed [m/s]

u' : velocity fluctuations [m/s]

According to [Equation \(4.2\)](#), any increase in turbulence intensity will consequently be followed by an increase in turbulent flame speed. Therefore, if this increment occurs at some weak regions inside the swirling flow, particularly at the tip of the CRZ, there

is a strong chance of upstream flame propagation generated by turbulence effects in the flame. Hence, determining and correlating turbulence intensity with combustion instabilities, especially flame flashback, has significant potential. However, methods of measuring turbulence intensity depend mainly on the flow characteristics. Consequently, in this study, the CFD simulation describes the changes in turbulence intensity at the exit of the dumping plane. In ANSYS Fluent, the turbulence intensity, I , is defined as the ratio of the root-mean-square of the velocity fluctuations, u' , to the mean flow velocity, u_{avg} [223].

It must be understood that the position of the central injector plays an essential role in the final position of the CRZ, as the closer the injector is to the burner dump plane, the further away the CRZ is pushed into the combustion zone. Consequently, measurements of turbulence at the plane of interaction between the central jet and the CRZ were challenging to determine for each case. However, this CFD simulation was intended to determine the flow turbulence close to the dump plane ($P_1=5$ mm) as a parameter for flashback propagation/avoidance.

Predictions about turbulence changes related to the axial air injection effect will be presented in this section. Isothermal CFD simulation has been implemented to investigate turbulence characteristics at different inlet tangential flow rates for different burner configurations (L_o) under the effect of a central air jet.

Figure 4-36 presents the effect of central air injection on the turbulence intensity values at low flow rates. This influence is also felt at higher flow rates, as shown in Figures 4-37, Figures 4-38 and Figures 4-39. Nevertheless, this effect is reduced with increasing tangential flow rates as the CRZ moves to the level of P_2 .

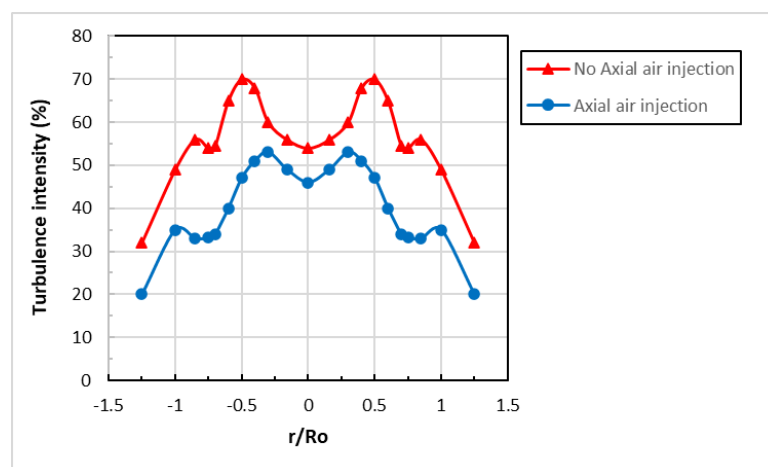


Figure 4-36: Effect of axial air injection on turbulence intensity values, 400 l/min, $L_o=150$ mm, $P_2=5$ mm.

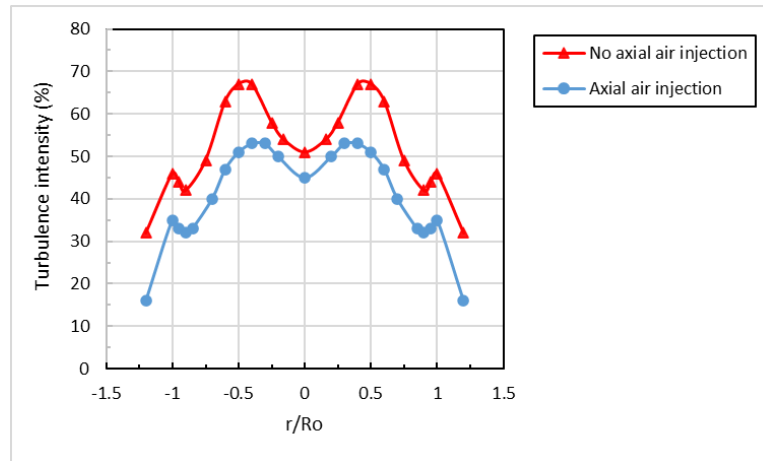


Figure 4-37: Effect of axial air injection on turbulence intensity values, 600 l/min, $L_o=150$ mm, $P_2=5$ mm.

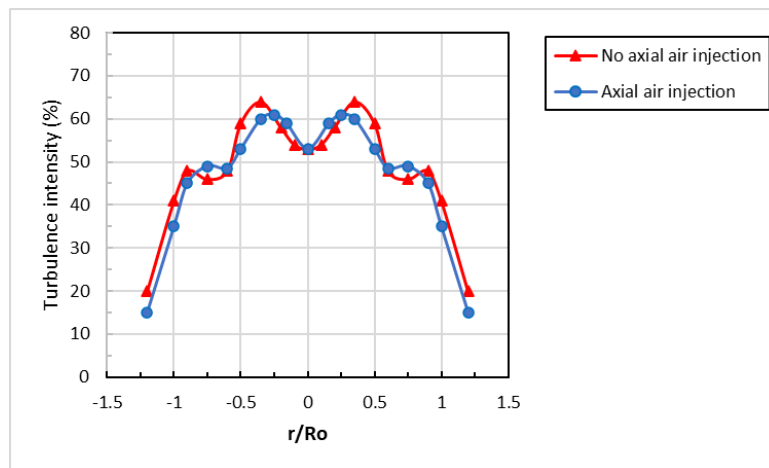


Figure 4-38: Effect of axial air injection on turbulence intensity values, 800 l/min, $L_o=150$ mm, $P_2=5$ mm.

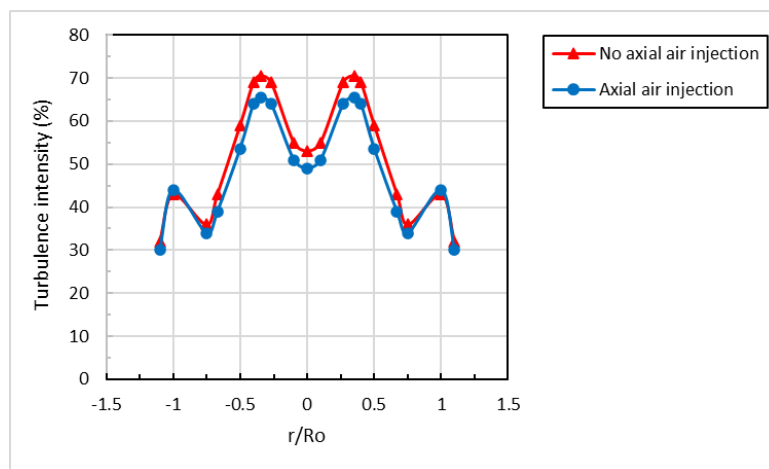


Figure 4-39: Effect of axial air injection on turbulence intensity values, 1000 l/min, $L_o=150$ mm, $P_2=5$ mm.

It appears that the effect of axial air injection, in general, is to decrease the turbulent intensity and variations of the turbulence intensity in the shear layers became more uniform and less intense. Higher values of turbulence intensity are located at the boundary of the central recirculation zone. Those values may have significant impacts on the propagation of the CRZ before CIVB flashback occurs. Therefore, to minimise the high turbulence in the CRZ makes it possible to govern flashback mechanisms, particularly CIVB.

Figure 4-40, Figure 4-41, Figure 4-42 and Figure 4-43 show the effect of the central air injector position (L_o) on the turbulence intensity values for different tangential flowrates at level $P_2=5$ mm. These figures show that the location of the central injector increases (i.e., $L_o=0$ and 29 mm) or reduces ($L_o=150$ mm) turbulence at the dump plane, as a consequence of the interactions of different magnitudes between geometry, central air injection and the tangential air flowrates.

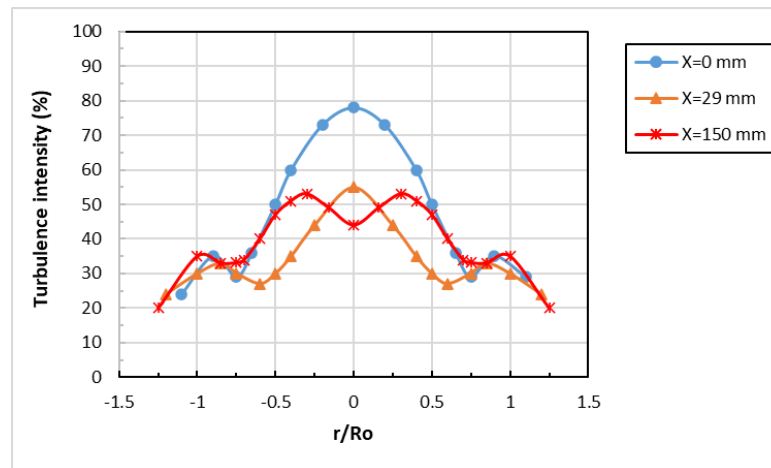


Figure 4-40: Effect of air injector position (L_o) on turbulence characteristics, 400 l/min and 50 l/min, $P_2=5$ mm, central air injection.

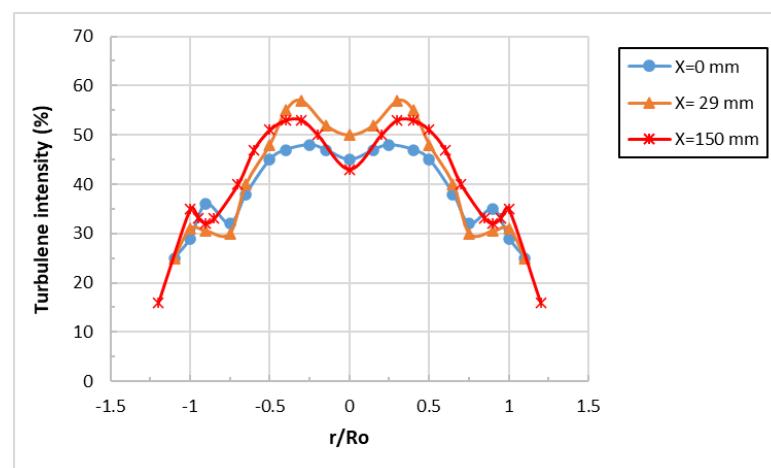


Figure 4-41: Effect of air injector position (L_o) on turbulence characteristics, 600 l/min and 50 l/min, $P_2=5$ mm, central air injection.

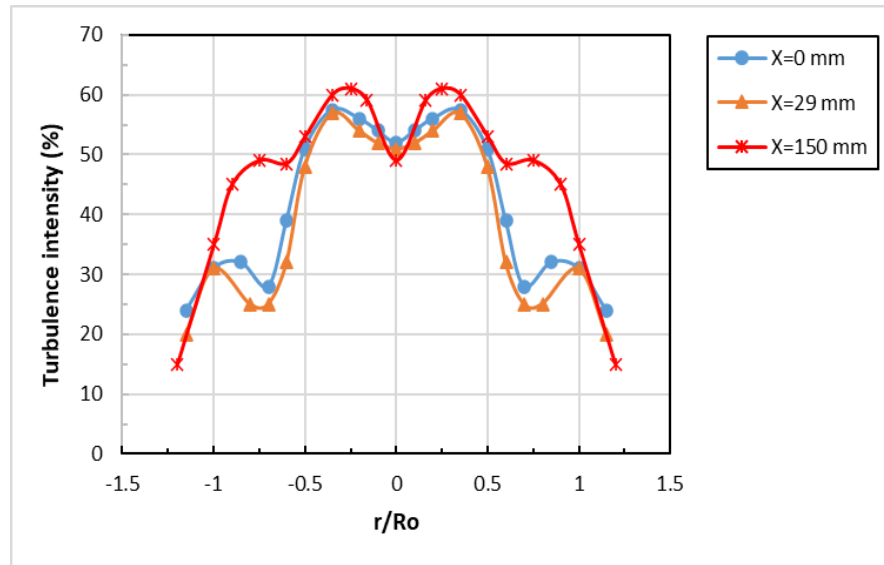


Figure 4-42: Effect of air injector position (L_o) on turbulence characteristics, 800 l/min and 50 l/min, $P_2=5$ mm, central air injection.

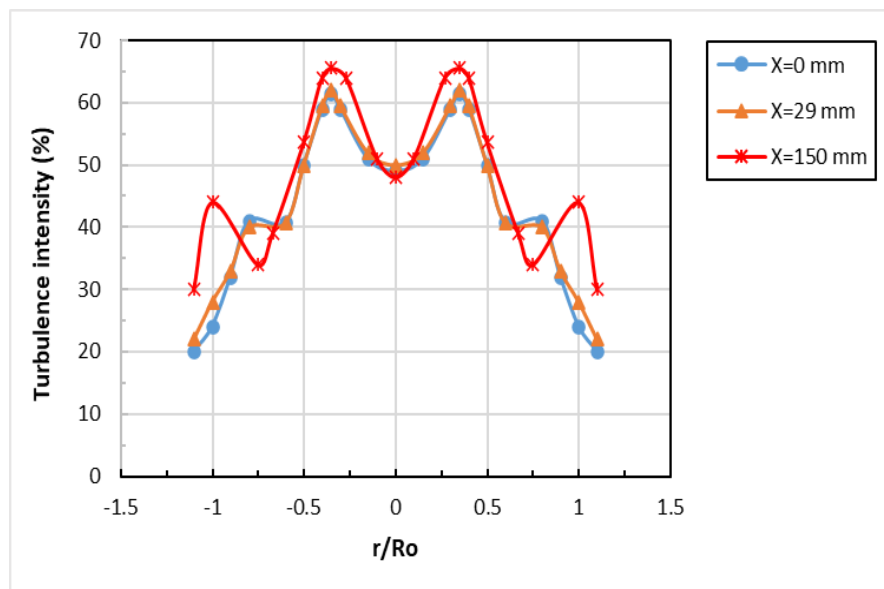


Figure 4-43: Effect of air injector position (L_o) on turbulence characteristics, 1000 l/min and 50 l/min, $P_2=5$ mm, central air injection.

Figure 4-44 shows turbulence map of the entire flow field for injector position ($L_o=150$ mm) with and without the effect of central air injection. It is clear from the results that the levels of turbulence caused by the central air injection are considerably lower than those without axial air.

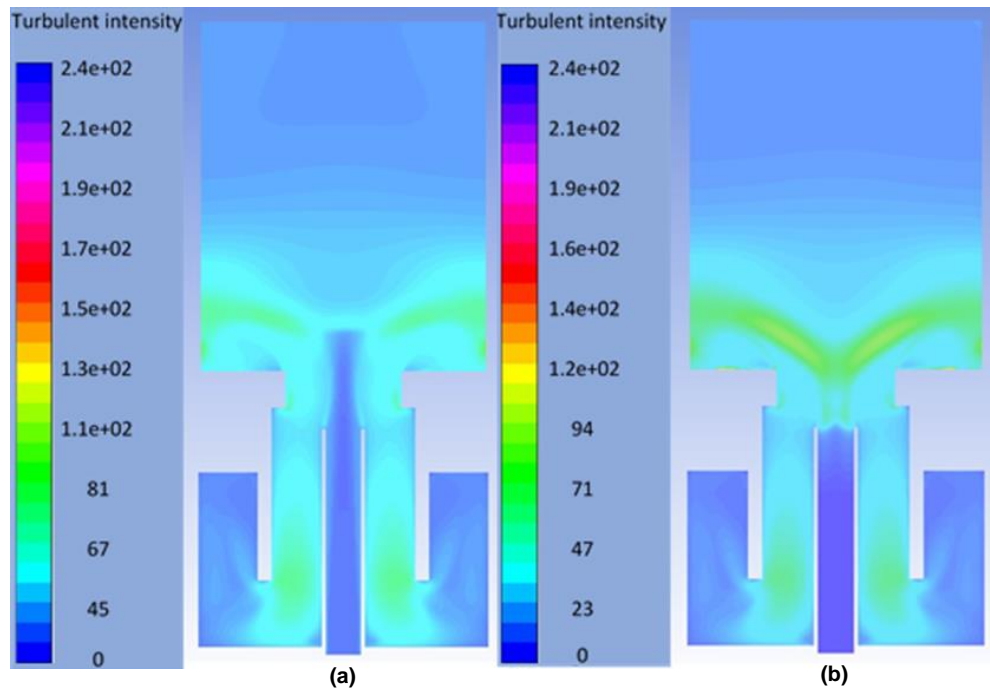


Figure 4-44: Turbulent intensity contours (600 l/min), $L_o=150$ mm (a) with central air injection; (b) without central air injection.

4.4.2 The Experimental Work

4.4.2.1 Central Air Injection Effects on Burner Operation

The flow field generated in GT swirl burners has an important impact on the performance of the combustion process. Many techniques can be used in developing conventional burner designs to ensure stable operation of GTs, environmental compatibility, high efficiency, reliability, and fuel variability and flexibility of GTs. The flow field manipulation technique that employs the central air injection discussed in the isothermal based CFD section will be extended to the burner stability map to link its hydrodynamic effects with burner operation. Therefore, the experimental work tested the impact of the 50 l/min axial air jet and the injector position ($L_o=0, 29$ and 150 mm) on the burner stability map.

4.4.2.2 Methodology

Provisional tests revealed that obtaining a stable swirling flame was difficult without a central injector or bluff body. Since only air was injected into the central region, this difficulty was more pronounced. Several experiments were undertaken to obtain a suitable start-up procedure to achieve a stable flame, eventually concluding that fuel must continuously be injected through the central injector during start-up for this burner geometry.

The blowoff point was when the flame zone was visibly lifting from the burner mouth. Flashback was defined as when the flame zone appeared to retreat towards the burner nozzle. Both envelopes, i.e., flashback and blowoff, were deduced and compared between cases. To check the accuracy of results, experiments were repeated five times, showing deviations not greater than 5%.

4.4.2.3 Central Air Injection Effects on Burner Operation

Initial studies were carried out to observe the impact of central air injection on burner operability. Figure 4-45 shows the relationship between flashback and blowoff limits at various equivalence ratios and tangential velocities for two conditions, with and without central air injection. These tests were conducted without a central injector to observe the effects caused by the injected airflow. Stable operation is to the right and left sides of the blowoff and flashback regions, respectively. Above these points unstable conditions were observed leading to a complete loss of the flame.

The improvement in operability is achieved by using central air injection which simulates the physical shape of a central injector, allowing wider range of operation ($0.55 > \phi < 0.7$) over a tangential velocity ranging from 2.5 m/s to 7.5 m/s. When there is no central air injection, operability limits are narrower ($0.48 > \phi < 0.57$) over a smaller tangential velocity range 2.5–4.0 m/s, after which no stable flame could be achieved.

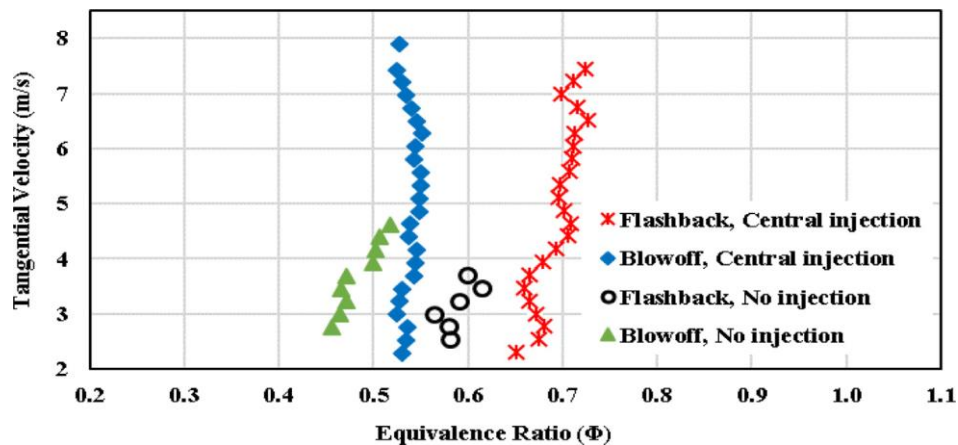


Figure 4-45: Burner stability operation region (effect of using central air injection), $L_o=0$ mm.

4.4.2.4 Effect of the Central Injector Position

The position of the central injector inside the burner plenum with respect to the baseplate was then mapped. The amount of central air injected is crucial in obtaining a stable flame. On the one hand, it should be robust and coherent enough to prevent

upstream flame propagation. On the other hand, its ratio to the tangential injection must be kept as low as possible to avoid both swirl strength deterioration and lack of mixing between reactants, i.e., excessive fuel dilution at the tip of the CRZ. It was found that the optimum amount of central air injection required to achieve a coherent air jet and avoid swirl strength degradation was ~ 50 l/min, this flowrate was maintained for all the experiments that followed within the scope of this thesis. This ratio represents 3–10% of the total mass flow rate at different inlet tangential flow rates.

Figure 4-46 shows the flame flashback trends for three different positions of the central injector with respect to the baseplate (the same position in the CFD predictions). When air is injected directly from the burner baseplate ($L_o=0$ mm), the flame flashback margin is around $\phi = 0.7$ for inlet tangential velocities ranging from 2.5 to 7.5 m/s. However, when the position of the central injector opening is parallel to the bottom edge of the tangential inlets ($L_o=29$ mm), flashback trends were affected significantly and shifted to a leaner region.

Furthermore, enhancement of flashback resistance is observed at $L_o=150$ mm where the stable operating regime became wider as both the air injection and sleeve promote flame stability. The flashback limit shifts to a richer region and higher flow rates (5.0 m/s tangential velocity). Interestingly, no flashback was observed beyond this point, see Figure 4-47. This outcome is of importance regarding the possibility of switching to higher power operation.

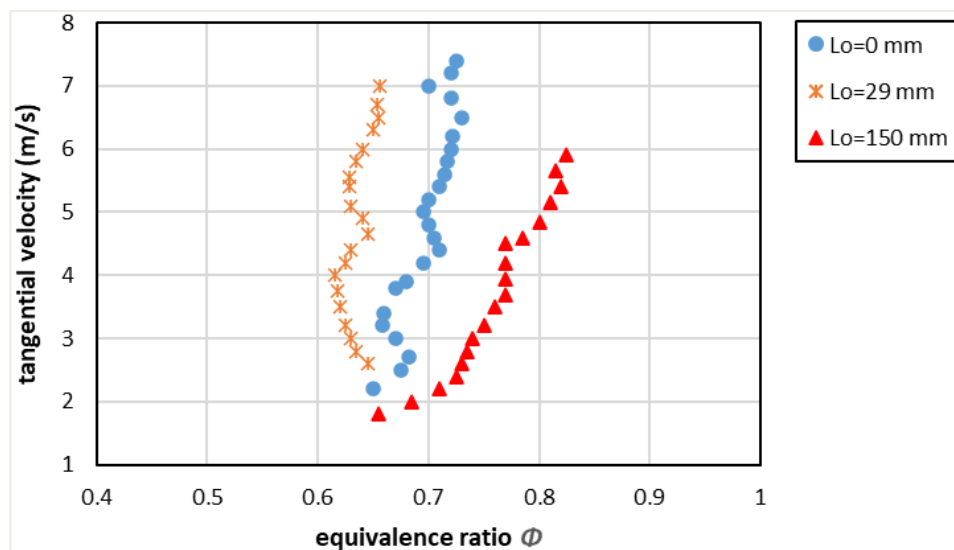


Figure 4-46: Flame flashback trends at different central injector positions (L_o).

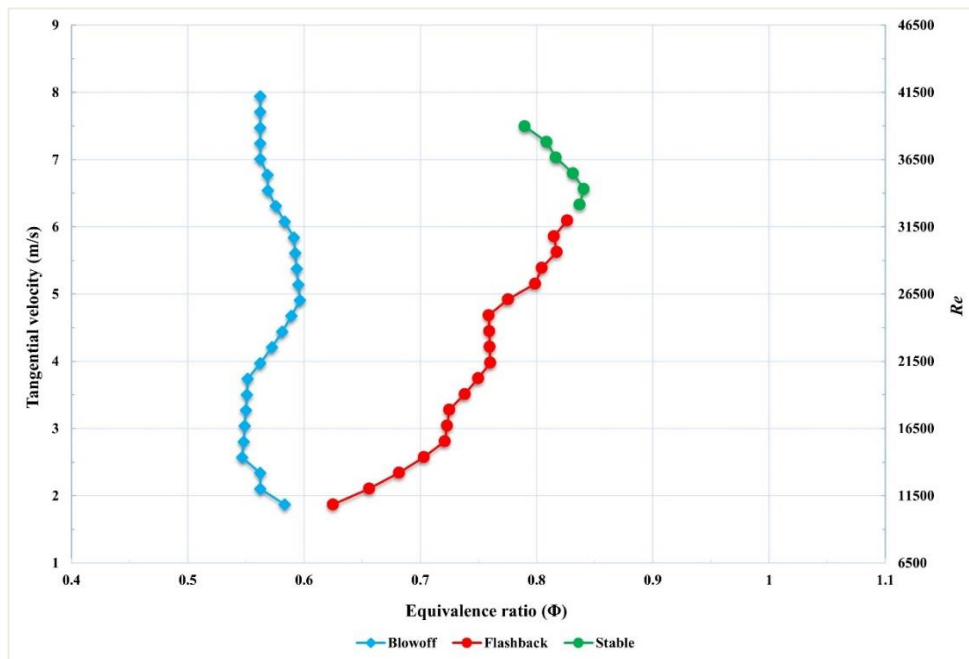


Figure 4-47: Stability map of the burner under the effect of 50 l/min axial air injection.

4.4.2.5 Central Air injection Combined with Best Central Injector Position

The previous results of the CFD and the stability map tests demonstrated a better hydrodynamic effects and resistance to flashback when using $L_o=150$ mm. Therefore, the $L_o=150$ mm configuration was employed for the remaining experiments, refer to Chapters Five and Six.

It was also noticed that the high flame flashback resistance potential of axial air injection can offer an exceptional flame re-stabilisation technique. This effect can be counted as a very positive outcome regarding avoiding the consequences that arise when a combustion system is subjected to various flame flashback mechanisms. Such techniques are essential particularly for the fuels with a high turbulent flame speed. Pure hydrogen or blends high in hydrogen will be able to operate more safely if central air injection is employed as a flame stabiliser method.

4.5 Chapter Summary and Conclusions

The turbulent swirl flow research community is keen to have a positive effect on the critical global concerns of energy security and environmental sustainability. This will require a constant and effective push towards the development of predictive and precise CFD models for sophisticated swirl burners that are based on rigorous

scientific observation. The close link between computation and laser diagnostics will be essential for the continuous improvement of GT combustion systems as more complex flames, chemistry, and flow structure are introduced. Using powerful CFD model like LES are expensive in terms of computational requirements compared to the classical models based on the RANS approach. Despite the fundamental theoretical questions relating to the RANS methods, it is possible to achieve very good results that are useable in practice. However, these calculations should always be complemented with qualitative comparison with published results of similar experiments, or test experiments performing to match the simulation. In the industrial sector, engineers are generally not interested in precise data, they want sufficiently accurate data matching real measurements: reasonable predictions at an acceptable computational cost - as with models based on the RANS method that have been tested against experimental data for validation.

This chapter presents a new alternative approach for avoiding flashback in swirl combustors, increasing operability, and leading to more flexible fuel usage with minimum retrofitting. Results confirm that using central injectors at the proper position combined with central air injection can enhance flame flashback resistance by pushing back into the combustor structures prone to CIVB flashback while reducing the velocity gradient at the exit of the burner. The position of the injector is imperative to decrease propagating turbulence that can impact the flashback regime. Nevertheless, this method alone could increase BLF flashback, as such stabilisation techniques force the flame to propagate via the wall boundary layer. Therefore, methods for increasing resistance to BLF flame flashback is required. As a result, the next chapter will discuss a new method to improve BLF flashback resistance by restructuring the fuel nozzle's internal surface.

Chapter 5

Improvement of BLF Flashback Resistance in Swirl Burners Using Nozzle with Scalloped Riblet Microstructure Surface

CHAPTER FIVE

5 IMPROVEMENT OF BLF FLASHBACK RESISTANCE IN SWIRL BURNERS USING NOZZLE WITH SCALLOPED RIBLET MICROSTRUCTURE SURFACE

"If I have been able to see further, it was only because

I stood on the shoulders of giants"

Isaac Newton, scientist (1642-1726)

5.1 Introduction

Flame flashback via wall boundary layer depends on many parameters such as the flow field characteristics, equivalence ratio, pressure, flow temperature, wall temperature, confinement type, the state of the boundary layer and the geometry of interior liners in the burner nozzle [189]. Flashback in the boundary layer was firstly studied by Lewis and von Elbe for laminar flames [187]. In this pioneering work, a relation between the velocity gradient at the wall and the ratio of the laminar flame speed to the quenching distance was suggested. This model was developed even further in terms of the pressure effects on the velocity gradient in laminar flames [80]. Some turbulent flame studies, [246] reported that the flashback limit could not be explained by the original concept of velocity gradient as proposed by the Lewis and von Elbe model due to the very thin boundary layer in turbulent cases [257]. Fine studied the relation between pressure and flashback in laminar and turbulent flames [258] and proposed that a turbulent flame near flashback stabilised in the laminar sublayer. He concluded that a turbulent flame could penetrate around three times closer to the wall than a laminar flame. The same ratio was suggested by others [259] in a study of turbulent wall flashback of hydrogen flames using a temperature-controlled rim burner. Hydrogen flames were used because their flame speeds are an order of magnitude greater than most fossil gaseous fuels, thus increasing their propensity to flashback. However, their flame speed varies with equivalence ratio, especially with rich mixtures. The geometry of the nozzle wall also plays an important role in upstream flame propagation during BL flashback, i.e., the interaction between nozzle wall and flame can directly affect the heat flux, which consequently changes the wall quenching distance [260]. The interaction between nozzle wall surface and

the parallel flow generates a viscous drag which produces an adverse pressure gradient, consequently promoting velocity gradients that could lead to flashback.

In swirl burners, the presence of a flame near the wall of the burner nozzle is usually affected by the flow characteristics upstream of the nozzle exit close to the boundary layer [160]. Influencing the boundary layer to modify BLF flashback resistance needs innovative research and this has included Boundary Layer stabilisation using biomimetic applications.

Microsurfaces for drag reduction and to increase resistance to boundary layer flashback have been well-reported [261]. A laminar boundary layer will transit to turbulent due to kinetic energy transmission from the free stream flow then the turbulent fluctuations will dissipate through viscous drag forces. The drag force is commonly categorized into pressure and skin friction drag. Thus, riblet microstructures generally reduce skin friction drag by effectively controlling the naturally occurring turbulent velocities, which leads to less momentum transfer and shear stress. In fully turbulent flows the thickness of the laminar sublayer is very small which means that the tips of the microsurfaces would penetrate the layer [262], thus allowing a grooved surface to play a role of damping turbulence and reducing drag [263].

Modifications in burner geometries and manipulation of swirling flows can develop the resistance versus flashback mechanisms in swirl burners. This chapter presents an experimental approach to enhancing BLF flashback resistance in swirl burners by changing the wall boundary layer characteristics using scalloped riblet structures on the nozzle wall. However, increasing resistance against CIVB flashback mechanisms can lead to augmentation of the propensity of other flashback mechanisms and so this chapter will study the combination of two techniques: the axial air injection system previously studied in Chapter Four that increase the resistance to CIVB, i.e., by repositioning a central injector and using central air injection, while simultaneously avoiding BLF flashback by using the technique proposed here.

5.2 Experimental Setup

Experiments were conducted under combustion and isothermal conditions. In the isothermal experiments, the effects of the scalloped riblet on the flow field characteristics were examined. While the effect on the stability map were tested in the combustion tests.

5.2.1 Swirl Burner and Experimental Facilities

The experimental setup is similar to that described in section 4.2.1 Chapter Four. The difference is based on investigating the effect of the burner nozzle with a microstructured surface for studies on BLF flame flashback, see [Figure 5-1](#). The outside diameter of the central fuel injector was 23 mm. The ratio of this diameter to the nozzle inside diameter is $X = 0.378$, which is enough to ensure BLF flashback, as demonstrated previously [\[264\]](#). The previous results of Chapter Four demonstrated better resistance to CIVB flashback when positioning the air injector at $L_o=150$ mm from the burner base plate. Therefore, this burner configuration was employed for these experiments.

The combustion experiments were undertaken under atmospheric pressure with no air preheating, using NG as fuel. This work was based on NG as a fuel as a safety precaution, but NG was suitable for validating the proposed combined technique (the axial air and the nozzle with microstructured surface) for use in systems fuelled with high hydrogen content blends which are particularly disposed to flashback due to their higher flame speeds.

The instantaneous velocity components and the turbulence intensity downstream of the burner mouth was measured during the isothermal tests by Laser Doppler Anemometry (LDA). The LDA system used was a one-component Flowlight LDA (Dantec) operated at backscatter mode, refer to section 3.2.3 in Chapter Three.

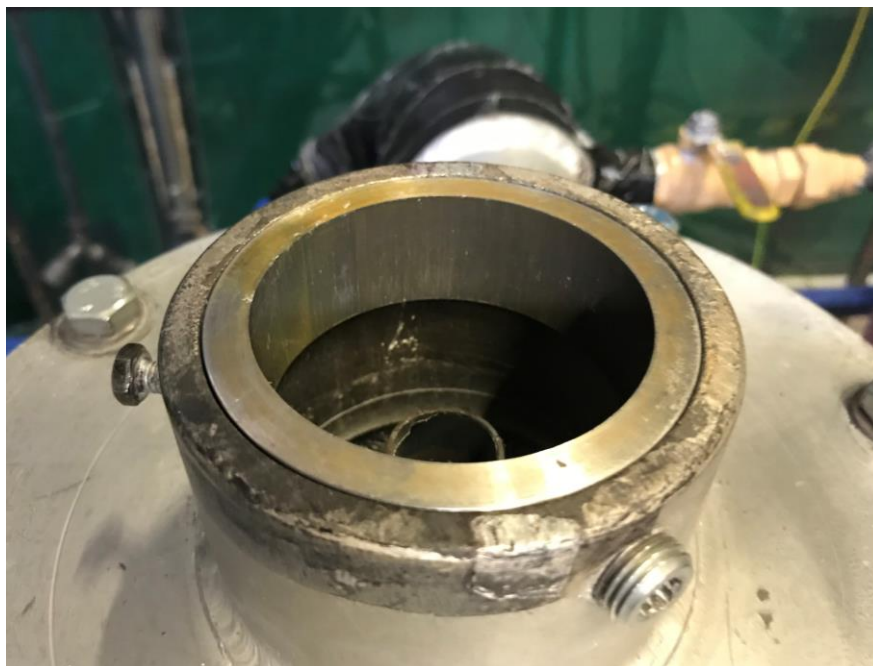


Figure 5-1: The tangential swirl burner with the new fitting (microstructured surface nozzle).

5.2.2 Nozzle Manufacturing

Achieving the aim of this study required applying riblet manufacturing process to the burner nozzle. The scalloped riblet microstructure was chosen based on a previous study of channel flow [265]. The results show that the geometry of the riblets has a significant effect on the streamwise velocity profile. That study concluded that the scalloped geometry was the best after numerical and experimental assessment of different geometries and their limitations. The most significant effect of scalloped riblets on the flow is represented by uniforming the flow near the wall and reducing the drag. The scallop riblets showed a good drag reduction of around 6.7 % [265]. Although swirl flows have more complicated structures than diffusion flow, the swirl flow near the wall is similar to other flow patterns. Consequently, scallop riblets as a liner to the burner nozzle, a geometry that could be manufactured using the manufacturing machines available at Cardiff University, were examined.

The height of the nozzle (h_n) was chosen to be no more than 25 mm. The construction of scalloped riblet on the nozzle wall was done according to the following steps: First, a stainless-steel burner nozzle was cut with inner diameter of 59 mm, and height of 50 mm. Then the nozzle was cut horizontally into two pieces 25 mm each; one part was milled to increase the inner diameter to 61 mm, the other piece was subject to WEDM to construct a patch of scalloped riblet on the inner wall of the nozzle, giving a final inner diameter of 61 mm. The two nozzles were inserted in the tangential swirl burner in the Combustion Laboratory of Cardiff University.

5.2.3 Wire Electrical Discharge Machining (WEDM)

The scalloped microstructure was applied on the inner wall of burner nozzle employing Wire Electrical Discharge Machining (WEDM) technology available at Cardiff University. The Electrical Discharge Machining (EDM) process, in general, has become the workhorse of the tool making industry for the precise machining of the workpiece that can conduct electricity. It can produce holes or cavities of the complex cross-section and to almost any depth in fully hardened steels or tungsten carbide with relative ease. In the context of the research presented here, this capability of structuring hard material is essential due to the expected applications in combustion systems, in which the burners operate under high temperature, pressure and acoustics level, especially during the flashback phenomenon [265].

EDM processes remove metal by discharging electric current from a pulsating DC power supply across a thin interelectrode gap between the tool and the workpiece. The gap is filled with a dielectric fluid, which becomes locally ionised at the point

where the interelectrode gap is the narrowest—generally, where a high point on the workpiece comes close to the high point on the tool. The ionisation of the dielectric fluid creates a conduction path in which a spark is produced. The spark produces a tiny crater in the workpiece by melting and vaporisation, and consequently, tiny, spherical “chips” are produced by resolidifying the melted quantity of workpiece material. Bubbles from discharge gases are also produced. In addition to machining the workpiece, the high temperature created by the spark also melts or vaporises the tool, creating tool wear. The dielectric is pumped through the interelectrode gap and flushes out the chips and bubbles while confining the sparks. Once the highest point on the workpiece is removed, a subsequent spark is created between the tool and the next highest point, and so on. Literally, hundreds of thousands of sparks may be generated per second [266].

WEDM strategy is promising to produce the structures required for this PhD study, see Figure 5-2. This process uses a consumable, electrically charged wire to affect very fine and intricate cuts. The process is particularly useful in cutting fine details in the workpiece. A wire drive system constantly presents fresh wire to work, so electrode wear is not a problem. Typical wire diameters range from 50 to 300 μm . Because the fresh wire is constantly brought to the cutting zone, the wear on the tool can be ignored, and accurate microscale features can be produced in relatively large areas. However, these wires will produce a kerf slightly larger than their diameter depending on the discharge power used. WEDM's can run for long periods without operator attention. Also, it can produce a sharp edge on the outside of a corner, but it will always leave a small radius on inner corners. The size of this radius is determined by the wire diameter plus the spark gap.

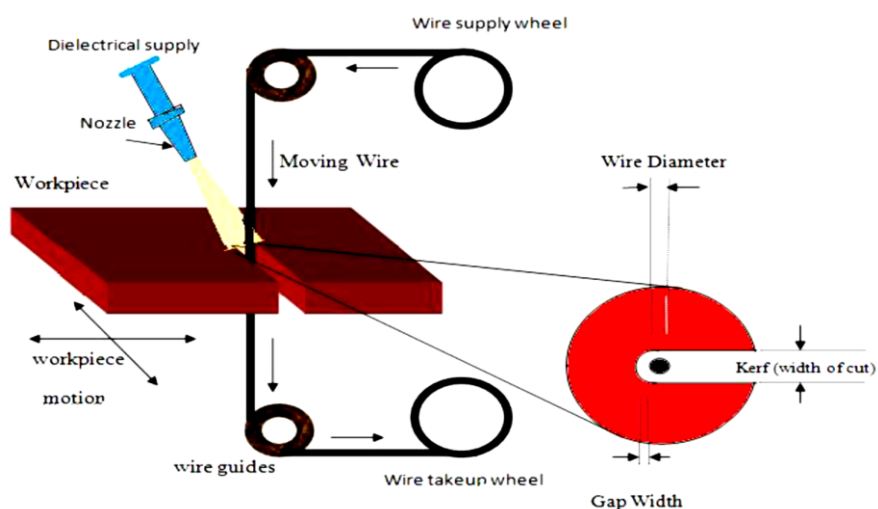


Figure 5-2: Working principles of WEDM. Reproduces from [265].

A jig was primarily designed to help build more complicated patterns more efficiently and cost-effectively. The construction of the scalloped riblet using WEDM showed that the length of the patch is significant to avoid manufacturing errors due to stresses, which leads to change in space and depth of the riblet between the top and bottom of the workpiece.

In order to validate the resulted surface profile on the nozzle wall, the light microscopy imaging technique has been used, see [Figure 5-3](#). This figure shows the surface profile image of the scalloped riblet microstructure on the nozzle wall.

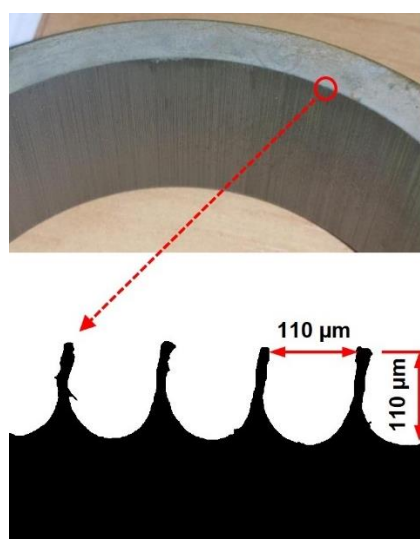


Figure 5-3: The geometry of scalloped riblet microstructure surface on the nozzle wall.

5.3 Results and Discussion

5.3.1 The Isothermal Tests

The LDA measurements of the isothermal flow were carried out to study the hydrodynamic effects of the scalloped riblet microstructure on the swirl flow field especially near the burner nozzle. Two configurations were tested, the smooth nozzle and the nozzle with scalloped riblets on the surface. These two nozzles were tested without axial air injection. It is challenging to directly measure the flow field characteristics adjacent to the burner nozzle wall because of the difficulty of laser access. Therefore, the turbulence profile and the velocity gradient were measured 5 mm downstream at the burner dump plane. This is a valuable way to describe the effect of the scallop riblet microstructure properties on flame flashback resistance. Tecplot 360 software was employed to plot the LDA results in terms of the axial velocity contour.

Two configurations were tested isothermally to examine the hydrodynamic effects of the scalloped riblet on the swirl flow characteristics: the smooth nozzle and the microstructured nozzle. By increasing the nozzle wall surface roughness employing scalloped riblet microspheres, the sudden variations from high-velocity values at the central axis of the nozzle to the low-velocity region near the wall are reduced, see Figure 5-4.

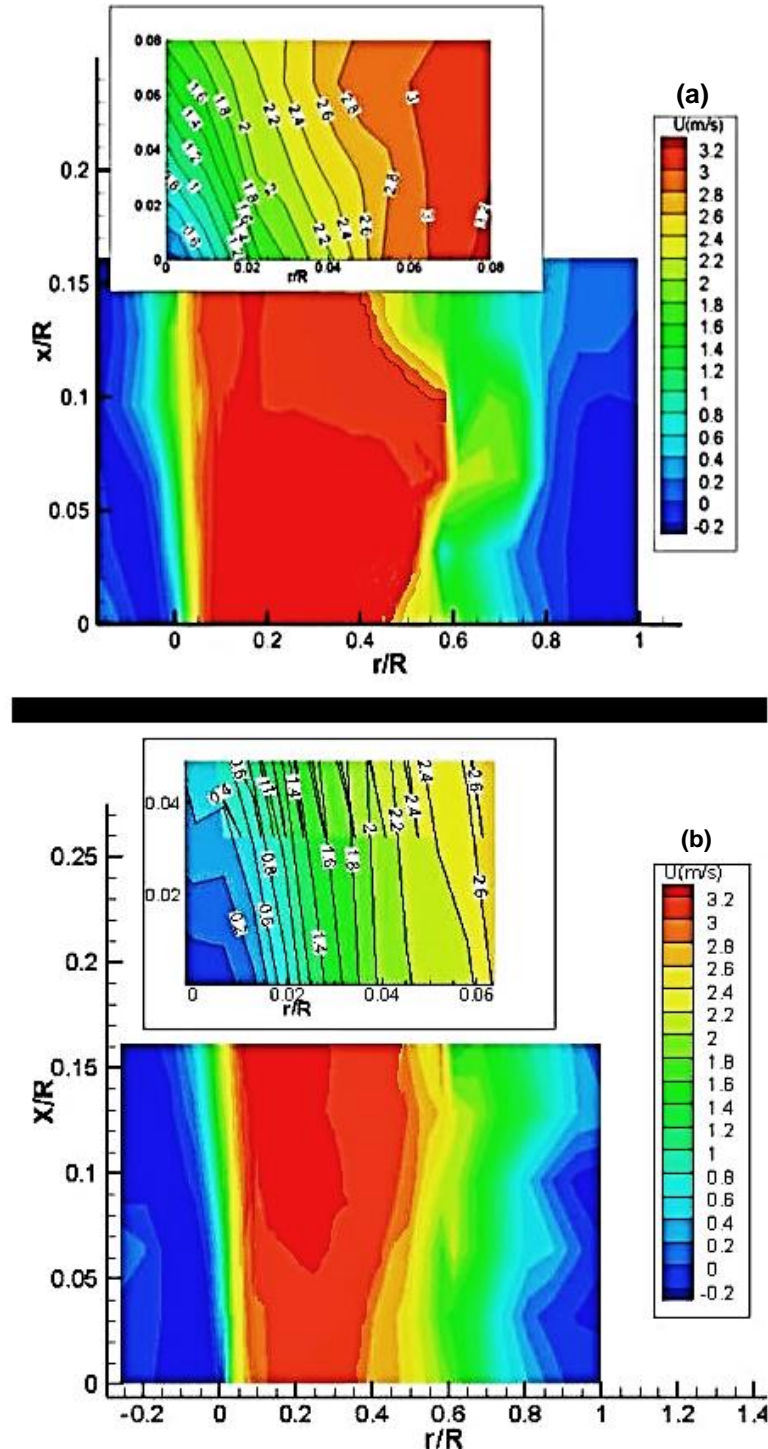


Figure 5-4: Axial velocity distribution downstream the burner rim (a) nozzle with scallop riblet, (b) smooth nozzle.

The effect is related to the reduction of the boundary layer, which is controlled by the microspheres. Scallop structures reduce the radial distance where the viscous wall effect on the flow and the high-velocity region is shifted closer to the wall. This shifting results in a modification of the flow structure in the thin shear layer downstream the nozzle exit. Consequently, lower gradients in the value of the velocity at the boundary layer region near the nozzle wall were achieved, overcoming the flashback event at this region, see [Figure 5-4](#). Moreover, the use of the microspheres also had a positive impact on the reduction of the turbulence generated close to the nozzle, see [Figure 5-5](#). This will certainly enhance the resistance against BLF and will be proved in the next section.

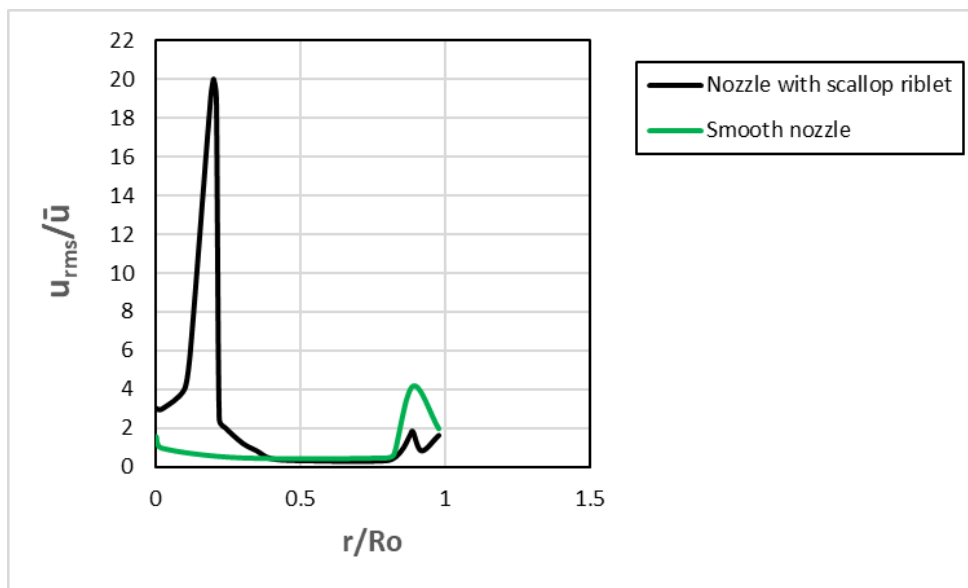


Figure 5-5: Effect of microstructure on turbulence intensity at the nozzle outlet.

5.3.2 The Combustion Tests

To completely understand the effect of the scalloped riblet on flame stability in swirl flow, it is necessary to ensure that the flame flashback mechanism is mainly BLF. Therefore, two flame flashback resistance techniques will be discussed here, i.e., central injector in the right position ($L_o=150$ mm) with no air injection, central air injection and the nozzle with microstructured surface. These techniques can work together to develop the flame flashback resistance for BLF and CIVB.

The first set of experiments was implemented at low flow rates to avoid the risk of severe flashback that could lead to damaging the system. The best procedure for burner operation under these conditions was to inject fuel first. This was done by shutting the air valve and allowing fuel injection through the air injector pipe. Then the

tangential premixed injection was started at a low flow rate with simultaneous decreasing of the central fuel injection. Once a stable flame is achieved the central fuel was shut down. At this point axial air injection can be started (if necessary) with simultaneous increasing of the tangential premixed mixture until a stable swirl flame was observed.

The blowoff point was determined when the flame zone was visibly lifted from the burner mouth. Flashback points were defined before the flame zone appeared to retreat into the plenum. Both envelopes, i.e., flashback and blowoff, were deduced and compared between cases. To check the accuracy of the results, experiments were repeated five times, showing deviations not greater than 5%.

Figure 5-6 illustrates a comparison between the flame structure of the smooth nozzle, Figure 5-6 (a), and the scalloped riblet microstructure nozzle, Figure 5-6 (b), at $\phi_{\text{stable}} = 0.79$.

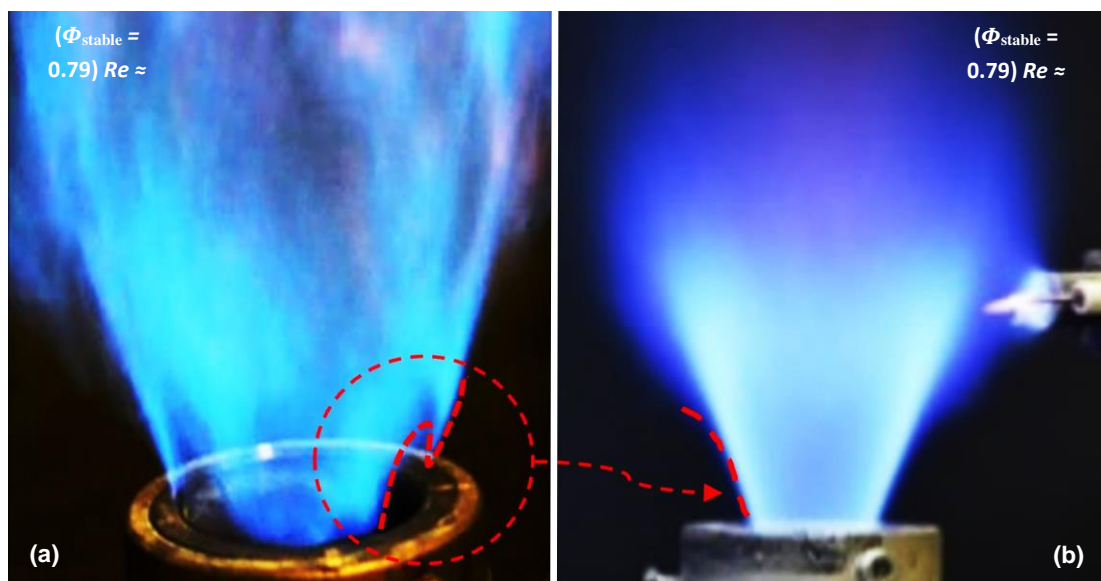


Figure 5-6: Effect of using scalloped riblet microstructure nozzle on the outer boundary layer propagation, no axial air injection.

For the smooth nozzle, Figure 5-6 (a), the function of the appropriate central fuel injector diameter (with no axial air) as a physical body performed high resistance against central upstream flow breakdown propagation imposes radial propagation of the flow. Consequently, the outer shear layer stabilised at the nozzle lip (or inside the nozzle) could be more likely onset the BLF when increasing equivalence ratios (ϕ). In most practical applications this contact between flame and nozzle lip has some consequences represented by life degradation of nozzle material due to continuous high temperatures in addition to the possibility of increasing pollutants level. At high

equivalence ratios (ϕ), the outer boundary layer between the shear layer and the nozzle wall starts an upstream propagation via low-velocity sublayer leading to flame BLF. However, for the scalloped riblet microstructure nozzle, the high axial momentum near the burner wall produced by the microstructure surface pushed the flame away from the burner rim towards the axial direction, see [Figure 5-6 \(b\)](#). This effect will undoubtedly reduce the possibility of the BLF when central fuel injectors (no axial air) or central air injection are used as flame stabilisation techniques. Moreover, the scalloped riblet microstructure nozzle flame looked more coherent than the smooth nozzle flame.

[Figure 5-7](#) shows the flame structure across different equivalence ratios at stable operation (ϕ_{stable}) for the microstructure flashback resistance scenario (no axial air), i.e., due to the scalloped riblet burner nozzle. The effect of the scalloped riblets is quite clear especially at high Reynolds number. Interestingly, the figure shows that flame behaviour remained unchanged across the stable operational region when using the scalloped riblet microstructure.

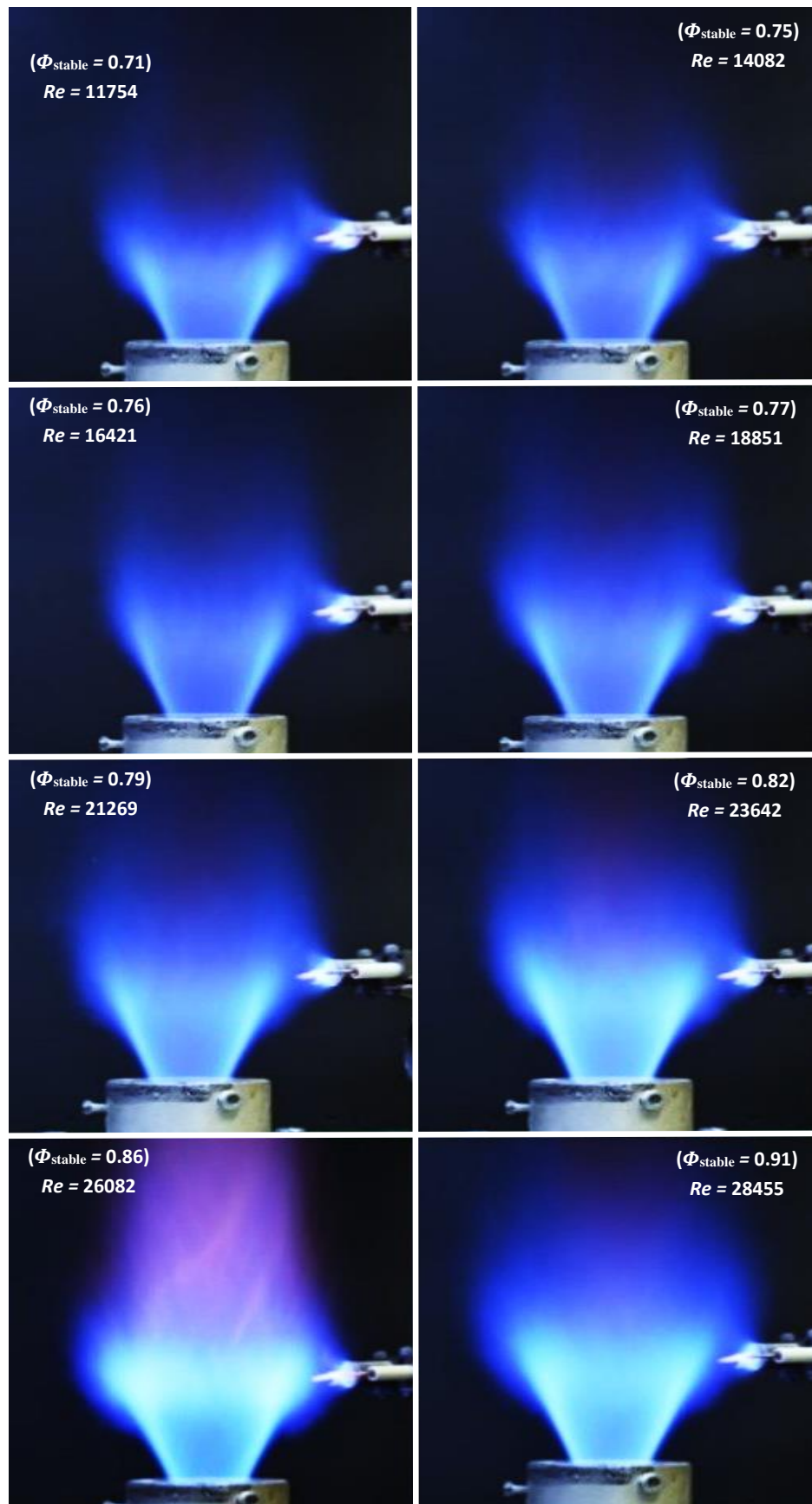


Figure 5-7: Flame structure of the scalloped riblet burner nozzle (no axial air) for stable operation at different Reynolds number (Re) and equivalence ratios (Φ).

5.3.2.1 The Scallop Riblet Combined with the Central Injector Flame Stabilization Techniques

The best position of the central injector is ($L_o=150$ mm) as discussed in Chapter Four. In this technique, the flashback mechanism is mainly BLF. The axial air injection rate is equal to zero, i.e., central fuel injector technique. In this section the stability map nozzle with scalloped riblet will be compared with a smooth nozzle under the same operation conditions. Both nozzle heights are equal to ($h_n=25$ mm). The term "microstructured nozzle" refers to the nozzle with a scalloped riblet surface.

Figure 5-8 shows the stability map for the microstructured nozzle with the flame flashback resistance scenario (flame images) for different equivalence ratios (Φ_{FB}), the flame images for blowoff case are also included in this figure across different equivalence ratio (Φ_{BO}).

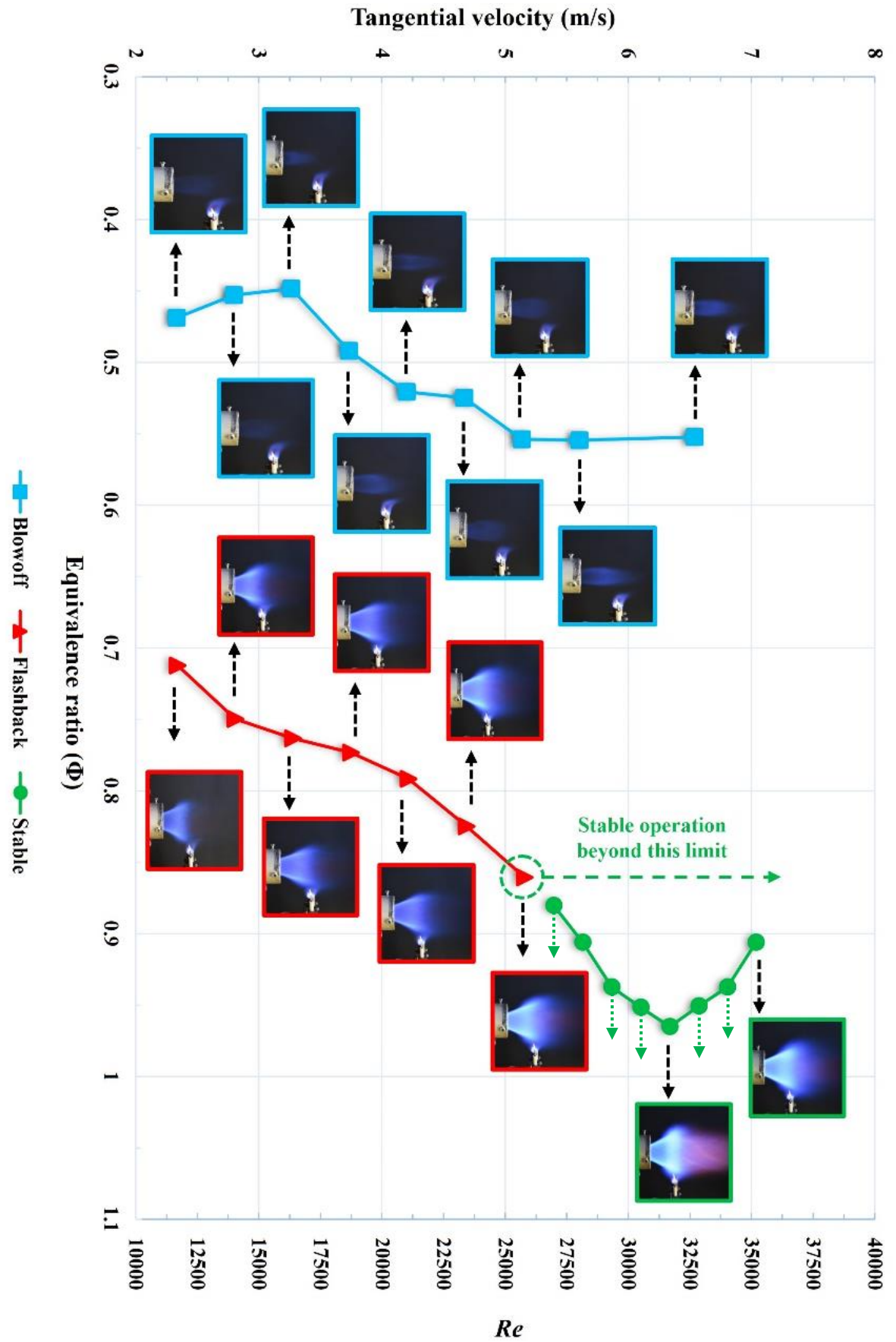


Figure 5-8: Flame stability map of the microstructured nozzle, $h_n=25$ mm - central injector technique (i.e., no axial air injection).

Figure 5-9 depicts the effect of the microstructured nozzle on the stability regime as compared with that of the smooth nozzle. It can be seen that the using of the microstructured nozzle in tackling flame flashback is promising. It expands the stability region to double in both directions (Re and ϕ) as compared with the smooth nozzle allowing the burner to work with high tangential velocities and a wide range of equivalence ratios. This opens a promising approach to flame stability of high hydrogen blend flames in gas turbines. The figure shows that the use of the microstructured nozzle achieved a wide range of stable operation limit across the region ($0.45 > \phi < 0.87$), and a tangential velocity ranging from 2.25 m/s to 7 m/s. Moreover, at higher flowrates the potential flame flashback resistance provided by the microstructured nozzle consolidated the flame stability, and no flashback was observed (see the green line).

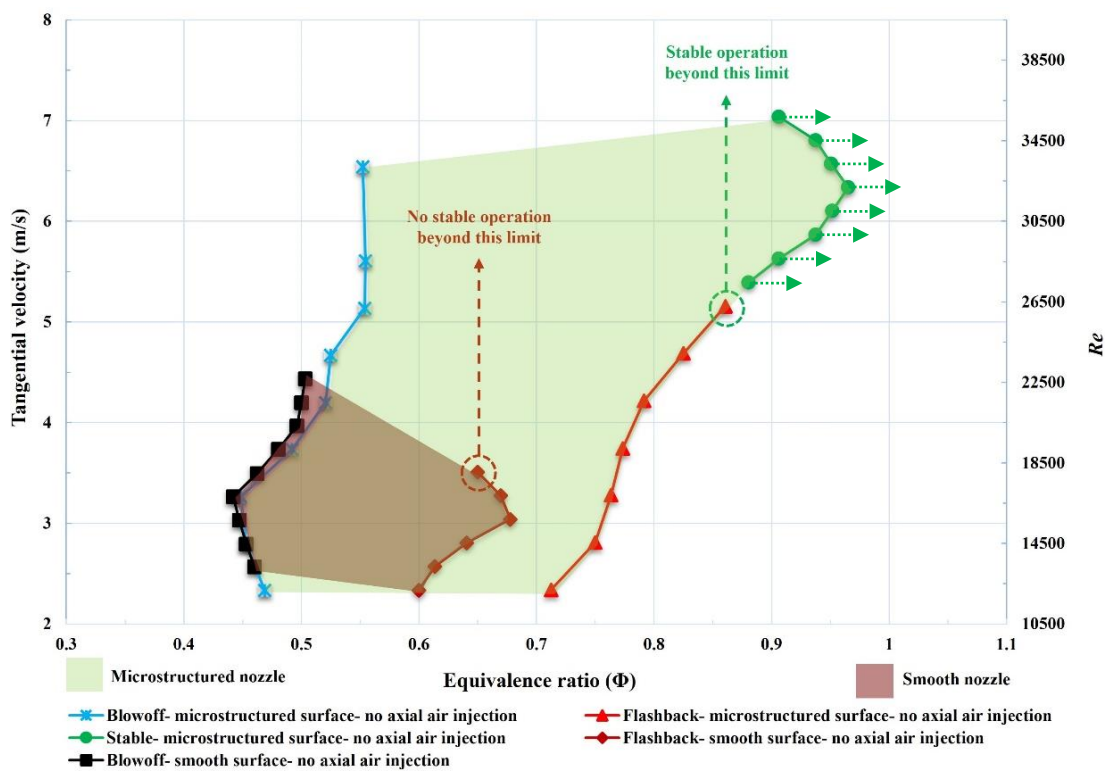


Figure 5-9: Effect of using microstructured nozzle on the stability map, $h_n=25$ mm – central injector technique (i.e., no axial air injection).

On the other hand, when using the smooth nozzle, the stability operation region was ($0.45 > \phi < 0.67$), and the maximum tangential velocity that could be achieved was just below 3.5 m/s. This could be attributed to the limitation

of nozzle surface resistance to BLF flashback at high tangential velocities. Higher values of tangential velocity led to outward radial propagation of the CRZ, which in turn pushes the high momentum flow region closer to the wall. Due to the lack of a damping mechanism BLF flashback can occur earlier in the case of the smooth nozzle. It is seen that the blowoff limit is almost the same for the two techniques at low tangential velocity.

5.3.2.2 Scallop Riblet Combined with Axial Injector Flame Stabilization Techniques

Axial air injection has confirmed its potential for flame flashback resistance, as proposed in Chapter Four. However, this resistance is mainly against CIVB. Further, it has been visually observed that the high momentum axial jet at the central axis forces the flame to propagate via the nozzle wall boundary. Consequently, another flashback damping mechanism for BLF flashback is also required see [Figure 5-10](#).

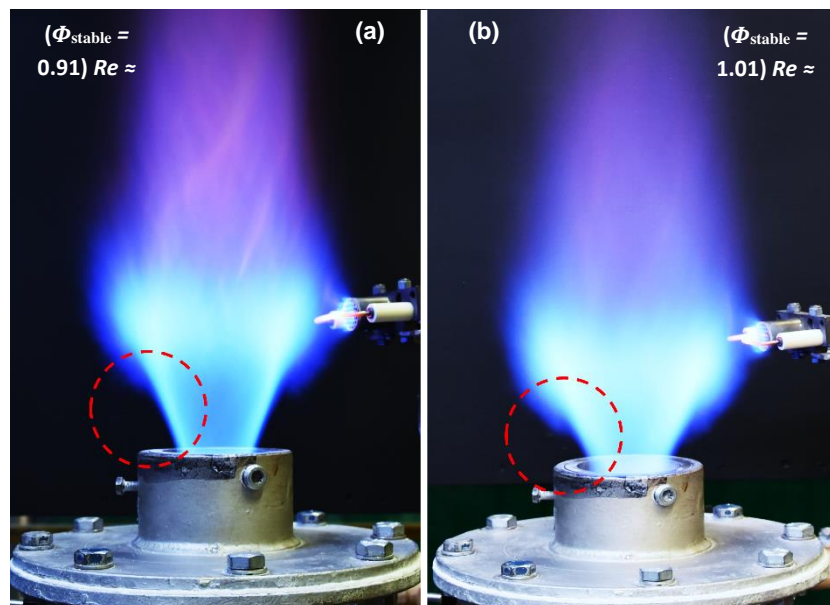


Figure 5-10: Flame shape of scalloped riblet microstructure nozzle; (a) without axial air, (b) with 50 l/min axial air injection.

[Figure 5-11](#) illustrates the stability region for the microstructured nozzle with the flame flashback resistance scenario (flame images) across different equivalence ratios (Φ_{FB}). The flame images for blowoff case are also included in this figure across different equivalence ratios (Φ_{BO}). It can be seen that as the flame approached flashback, the flame became attached to the nozzle, thus modifying the behaviour of the flow field. The effect is demonstrated when considering the change in the burner stability map when using the microstructured nozzle for additional flame stability.

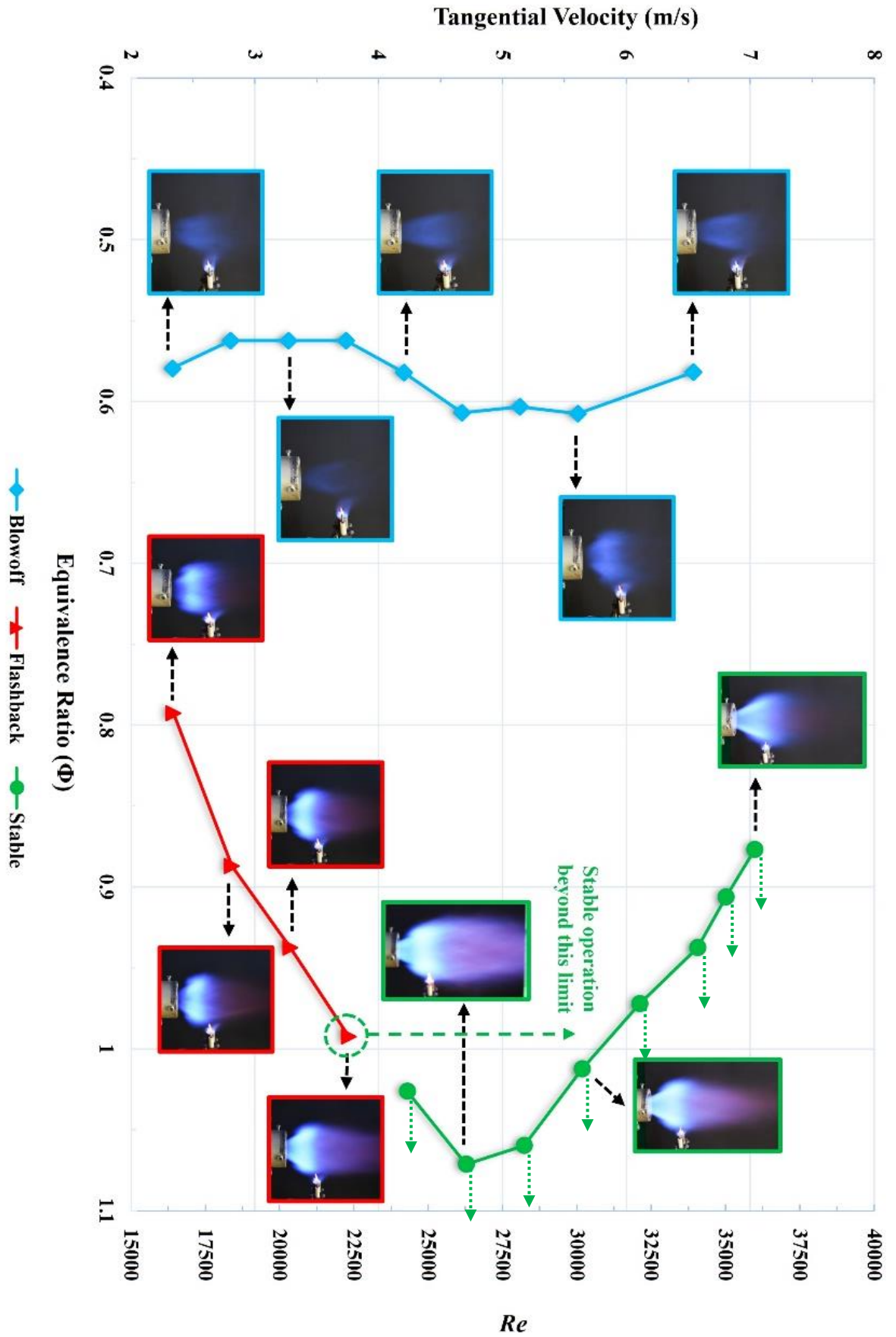


Figure 5-11: Flame stability map of the microstructured nozzle, $h_n=25$ mm - axial injector technique (50 l/min axial air jet).

Figure 5-12 shows a comparison between the two techniques. The figure shows the big difference in the stability region achieved by including the microstructured nozzle. A good improvement in flashback resistance is observed when the microstructured nozzle is used for additional stability. Flame flashback was observed for an inlet tangential velocity ranging from 2.1 to 3.7 m/s; beyond this limit, no flame flashback occurs, and operation is stable for higher equivalence ratios and high tangential flowrates.

However, for the smooth nozzle, at a tangential velocity of 1.8 m/s, blow off and flashback curves are approaching each other, leading to a narrow stability region. Upon raising the equivalence ratio and tangential velocity, the stability map became wider. Nevertheless, there are still some limits over which the flame cannot be stable, and flame flashback happens. The last conditions where flashback was observed were tangential velocity = 6 m/s, $\Phi = 0.83$; beyond these values, no flashback was observed.

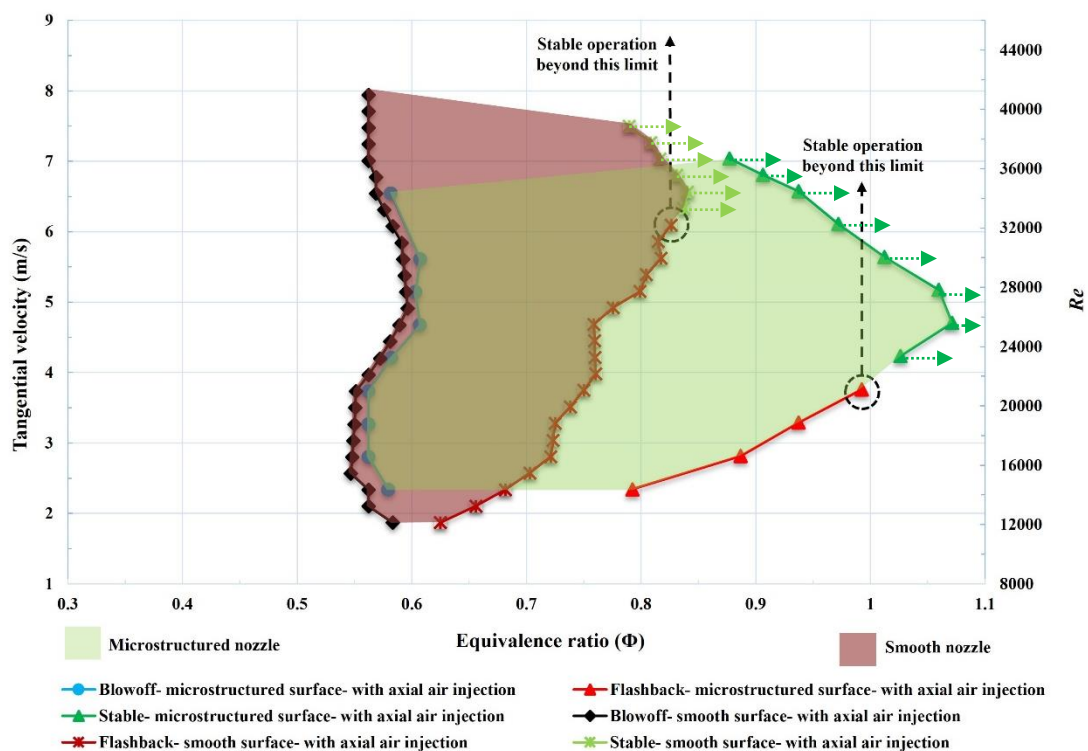


Figure 5-12: Effect of using microstructured nozzle on the stability map, $h_n=25$ mm – axial injector technique (50 l/min axial air jet).

5.3.2.3 Further observations on flame stability map

Here, a further observation is made regarding the stability map when using the microstructured nozzle concerning the stability map of the burner nozzle with

microstructured nozzle (no axial air injection) versus that for the smooth nozzle with 50 lpm axial air injection at best injector position.

It can be seen from Figure 5-13 that the stability map of the microstructured nozzle without axial air injection is wider in both lean and rich directions than that for the smooth nozzle with axial air injection. The improvement in operability caused by using the microstructured nozzle allows a wider operation range ($0.48 > \Phi < 0.87$) over a tangential velocity ranging from 2.5 m/s to 7 m/s. For the smooth nozzle with the axial air, operability limits are narrower ($0.48 > \Phi < 0.82$) over a smaller tangential velocity range of only 2.5–4.0 m/s, after which no stable flame could be achieved. It is also seen that no flashback was observed after a tangential velocity of 5 m/s ($Re=26000$) with the microstructured nozzle. However, this value is higher for the smooth nozzle under the effects of axial air, 6 m/s ($Re=31000$). This means that using the microstructured nozzle configuration alone without any other techniques can significantly impact the burner operability.

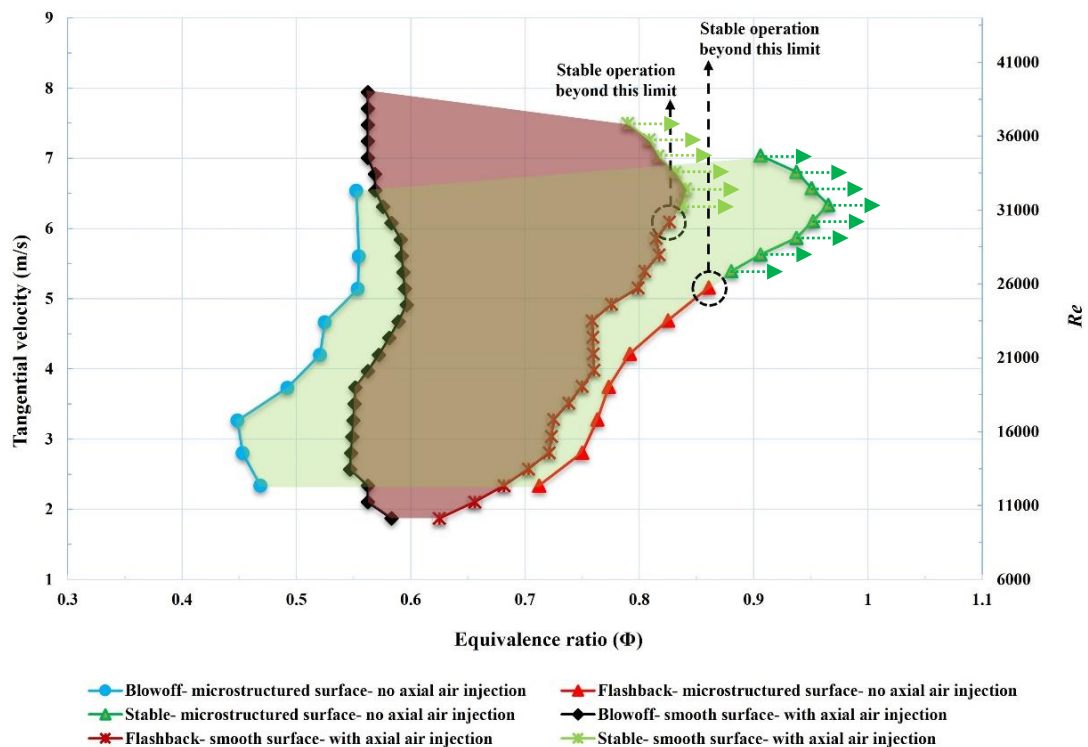


Figure 5-13: The stability map of the burner the microstructured nozzle (no axial air injection) versus that of the smooth nozzle with 50 lpm axial air injection.

This chapter demonstrates that it is possible to run premixed swirl burners with a wide range of gaseous fuel blends to substantially minimise flashback behaviour, thus permitting wider use of the technology to reduce NO_x emissions. However, no

CO/NO_x measurements have been done within this chapter's scope due to the limitation of the study program timescale.

5.4 Chapter Summary and Conclusions

Based on the previous results, it appears that the two flame flashback resistance techniques, i.e., central injector method with microstructured nozzle, and central air injection with microstructured nozzle, can work together to achieve high flame flashback resistance for BLF and CIVB flashback. However, different to previous studies, this chapter combined two different techniques increasing even further the final resistance compared to using these techniques separately. Using both combined techniques shift the operating envelope to richer conditions, and a much wider equivalence ratio can be achieved when the microstructured nozzle used. Thus, stable operation is achieved with the microstructured nozzle at more than double the central injector with no air injection. This outcome is of great importance because it opens the possibility of increasing power output without increasing the size and dimensions of the combustor. Moreover, since microstructured nozzle leads to wider operability margins, it enables smoother fuel switching, a technical problem that has become one of the important milestones for modern, flexible gas turbines using alternative fuels. Additionally, wider operation limits reduce power input fluctuations, which is an important parameter when operating gas turbines on a baseload basis.

The main conclusions of this chapter can be summarised as follows:

- Increasing resistance against boundary layer flame flashback needs enhancement of the surface characteristics of the interior wall of the nozzle which leads to the velocity gradient close to the nozzle wall to be higher than the critical velocity gradient, hence avoiding it being overcome by the turbulent flame speed in this region.
- The effect of the microstructured nozzle technique has been investigated regarding its effect on velocity gradient and hence flame flashback trends.
- Results showed that the microstructured nozzle configuration has excellent potential in increasing flame flashback resistance. This was seen visually and through increasing operation stability margins compared with the smooth nozzle.
- Using both improvement techniques (the central air injection and the microstructured nozzle) enhanced stability limits considerably, stability

margins increased in terms of both equivalence ratio and inlet tangential velocity.

- Regarding industrial applications, using such techniques is considered a possible commercial solution to simultaneously protect swirl combustors from CIVB and BLF flashback.

Chapter 6

Effects of Different Nozzle Configurations on Swirl Flow Topology And Flashback Propensity

CHAPTER SIX

6 EFFECTS OF DIFFERENT NOZZLE CONFIGURATIONS ON SWIRL FLOW TOPOLOGY AND FLASHBACK PROPENSITY

"We are stuck with technology when what we really want is just stuff that works"

Douglas Adams, English author (1952-2001)

6.1 Introduction

Gas turbine designers are simultaneously targeting improvement in thermal efficiency while reducing noxious emissions (NO_x), which poses a significant challenge as the two are usually controlled in opposite ways. From the available means to achieve these objectives, lean premixing (LPM) is an efficient technique that has been used to reduce NO_x emissions and increase power outputs. However, this technique requires further analysis to prevent instabilities such as extinction, flashback or thermoacoustic oscillations when introducing alternative fuels. These factors represent the deciding issues limiting the improvement of the gas turbine combustion systems which should be designed and developed to overcome these and other problems.

A well-designed gas turbine combustor will meet the requirements of a vast spectrum of gas turbine applications with regard to efficiency, reliability, fuel flexibility and environmental acceptability. Many techniques can be used in developing conventional gas turbine burner design to ensure stable operation with fuel variability and flexibility. The most common is to develop the aerodynamics of the swirling flow. Flashback is an instability that occurs with premixed combustion in gas turbines and can occur under a variety of conditions as the flame may stabilise where the fuel and oxidiser mix, upstream of the reaction zone, which could cause considerable damage to the combustion system and increase pollutant levels. The BLF and CIVB flashback mechanisms receive particular attention as they commonly occur in swirl combustors [246].

Many techniques can efficiently mitigate flashback: including geometric modifications or changing flow field patterns. These techniques range from using diffusive fuel injection to push the vortex breakdown downstream or employing bluff bodies as stabilisers in the swirling flow [79]. As discussed in Chapter Four, central air injection systems have been presented to mitigate the CIVB flashback in tangential swirl burners. It was found that using central air jets affects turbulence characteristics and the defect of negative axial velocity, and hence promotes CIVB flashback resistance with a wider operability limit. However, using such methods for the mitigation of the CIVB flashback mechanism will lead to BLF flashback. With BLF flashback, the geometry of the nozzle and the properties of its walls play an essential role in upstream flame propagation [193]. Furthermore, the interaction between nozzle wall surface and the parallel flow generates a viscous drag that produces an adverse pressure gradient, consequently promoting the velocity gradient. The degree of wall roughness is of particular importance in this context as it promotes heat transfer, hence decreasing or increasing the shear wall stress [160]. The contribution of the effect of the surface type on the mean velocity profile and hence the wall turbulent boundary layer is usually described by a roughness function which represents the difference in normalised velocity distribution between smooth and rough surfaces [267]. It is known that the shear stress can be reduced using micro surfaces extending from the wall, and such reduction leads to a better velocity gradient at the wall and a drag reduction in the flow [268]. In a more recent study, it was noticed that the high turbulent velocity fluctuation near the burner wall increases the tendency to flashback. Thus, to avoid flashback, it is required that the local premixed flow speed is higher than the flame speed. This concept is valid for all flashback mechanisms except for CIVB [269].

This chapter aims to expand the understanding of the role of different burner nozzle configurations (different nozzle heights) with/without different heights of micro-structured surfaces as a liner in improving system resistance to the main flashback mechanisms, CIVB and BLF. A stainless-steel woven mesh was employed to serve as a liner for the nozzle burner with different lengths (h_n) to examine the effects on swirl flow characteristics near the burner rim and the burner stability map. The isothermal experiments are conducted using Laser Doppler Anemometry (LDA) to measure the swirl flow characteristics close to the nozzle wall and downstream of the burner exit. The combustion experiments were done to determine the impact of these nozzle configurations on the stability map of the tangential swirl burner.

6.2 Experimental Setup

Tests to promote the stability of the previously designed 150-kW tangential swirl burner took place at Cardiff University's combustion laboratory. Burner details are illustrated in section 3.2.1 Chapter Three. The best central injector position $L_o=150$ mm has been used for this study, as discussed in Chapter Four. In addition, a 25%-25% insert was selected to provide suitable geometric swirl numbers ($S_g=0.9$) where vortex breakdown coherent structures exist in the flow. Two nozzle configurations with different lengths (h_n) were tested, the previous design with $h_n=25$ mm, and a second new design with $h_n=70$ mm. Both with a same inner diameter of 61 mm.

Producing a machined micro-structured surface (like the scallop riblet discussed in Chapter Five) can be costly and difficult or even impossible to introduce inside a circular nozzle. Here, a 316 stainless steel woven wire mesh with $150\ \mu\text{m}$ between valleys (as recommended elsewhere [265]) was employed to investigate the effect of the nozzle surface roughness in different heights (h_g) on the swirl flow and flashback resistance, as it presents some structural similarities to diamond and lotus geometries [193]. Three different lengths (h_g) of mesh strip, i.e., 25, 40, and 70 mm, were attached firmly to the internal wall of the nozzle as a liner to increase the roughness of its surface as shown in Figure 6-1. The main idea is to examine the effect of different grid height on the swirl flow characteristics. The liner thickness was scanned by Shared Labs Europe LTD [265]; Figure 6-2 shows the microstructure geometry and dimensions of the 316 stainless steel woven wire liner.

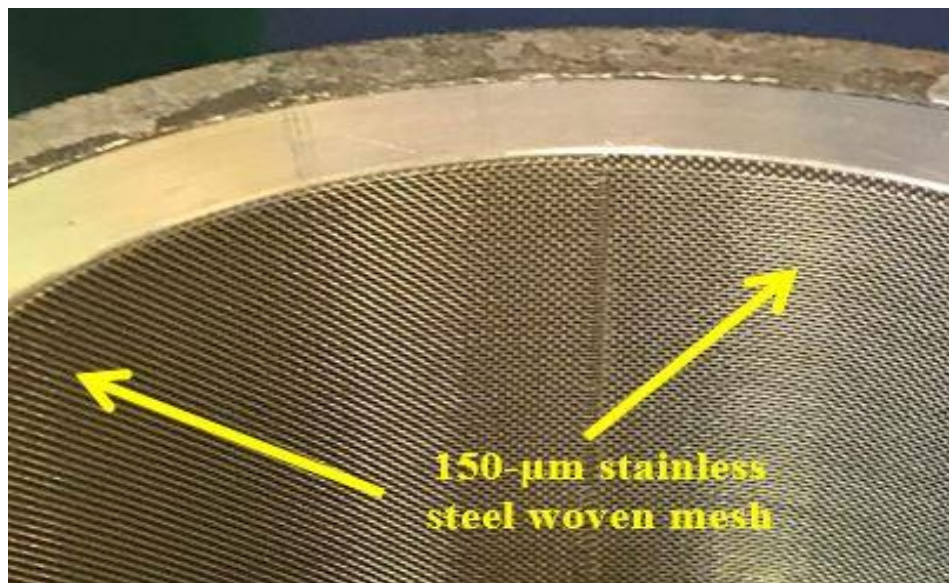


Figure 6-1: Nozzle inner surface with 316 stainless steel woven wire as a liner.

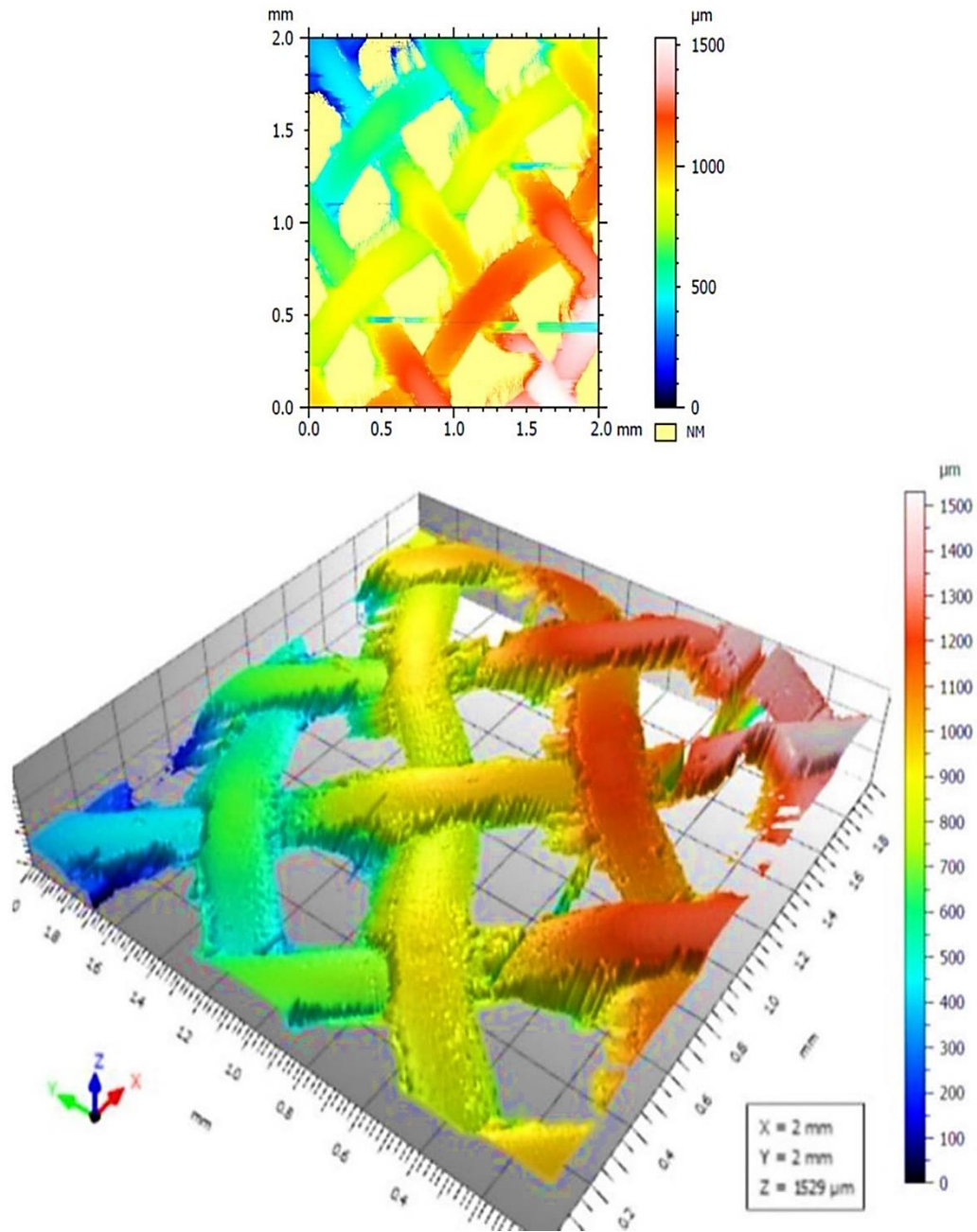


Figure 6-2: The geometry of the Microsurfaces.

6.3 Results and Discussion

6.3.1 The Isothermal Experiments

6.3.1.1 Effects on Axial Velocity Defect

The primary objective of this research was to observe the impact of different nozzle lengths (h_n) on the swirl flow characteristics under isothermal (no combustion) and atmospheric conditions. Average axial velocities (\bar{u}) and the velocity fluctuations (U_{rms})

were determined employing 1D LDA system to show the axial velocity and turbulence distribution at the burner dump plane (5 mm downstream the burner rim) for nozzle lengths $h_n=25$ and 70 mm. Two tangential flowrates 800 and 1000 l/min without central air jets were used to set different operating conditions. The term “smooth nozzle” is referring to the nozzle without microstructure grid. To check the accuracy of results, experiments were repeated three times.

Figure 6-3 shows the reduction in axial velocity defect (negative region) under a moderate inlet tangential flowrate (800 l/min) for two smooth nozzle lengths ($h_n=25$, 70 mm). It is apparent that the long nozzle ($h_n=70$ mm) is significantly more effective in reducing the axial velocity defect at the tip of the central recirculation zone (CRZ) which is one of the main causes of swirling flow instabilities particularly the CIVB.

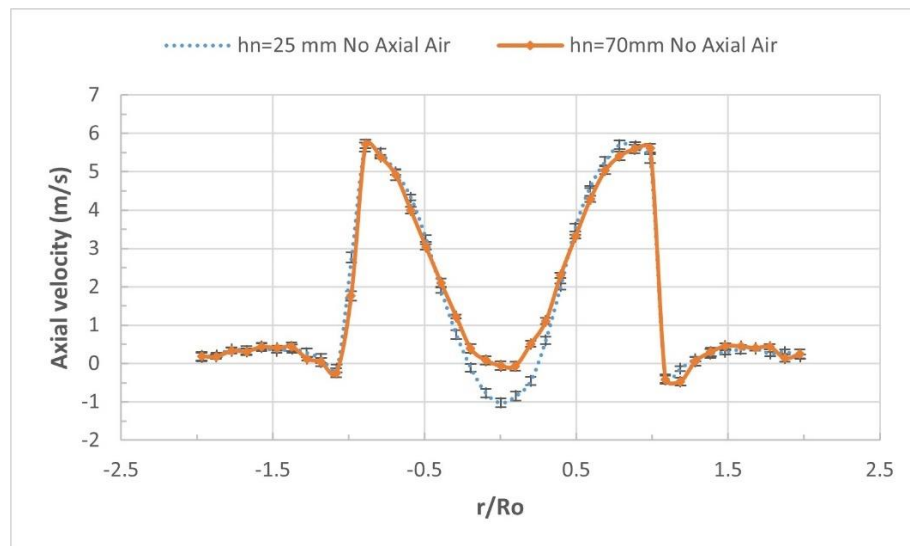


Figure 6-3: LDA results, axial velocity for different nozzle heights ($h_n=25$, 70 mm), 800 l/min tangential flowrate.

For the higher tangential inlet flowrate (1000 l/min), the effects of the long nozzle ($h_n=70$ mm) were more influential in reducing the velocity defect, as shown in Figure 6-4. The axial velocity defect is minimised by 50% at the CRZ tip under the effects of the long nozzle compared with the short nozzle ($h_n=25$ mm). This is a promising finding as the long nozzle will automatically self-correct the axial velocity defect at the CRZ tip without any other system by adding an axial momentum directly proportional to the tangential flowrate. These hydrodynamic effects undoubtedly promoted the stability limit of the burner, as demonstrated in Chapter Four.

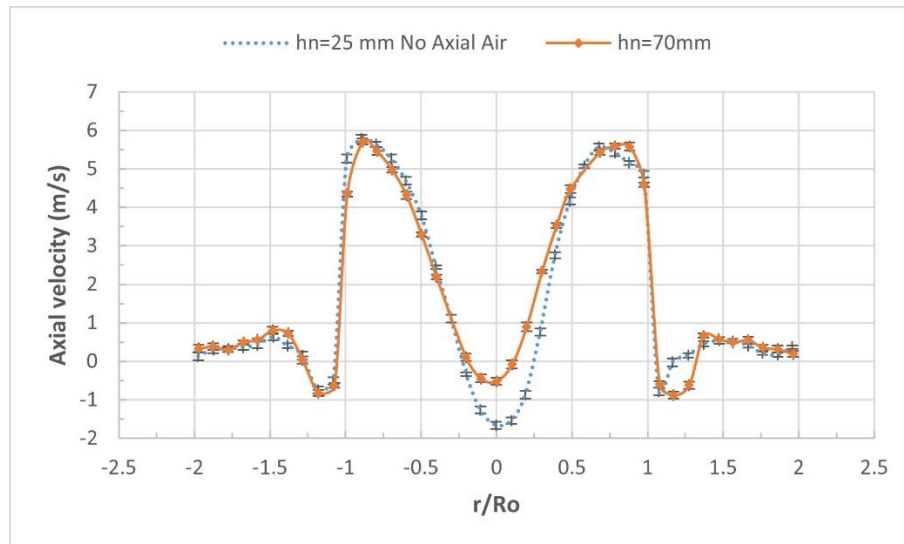


Figure 6-4: LDA results, axial velocity for different nozzle heights ($h_n=25, 70$ mm), 1000 l/min tangential flowrate.

6.3.1.2 Effects on Turbulence Intensity

Turbulent intensity at the dump plane was calculated from the experimental results by dividing the root mean square of the axial velocity fluctuations by the average axial velocity as measured by the LDA system. At the higher tangential inlet flowrate (1000 l/min), the long nozzle had a positive effect on the turbulence intensity, as illustrated in Figure 6-5. This was a very promising observation as actual gas turbine combustors operate on high flowrates under pressurised conditions. Moreover, the long nozzle ($h_n/R_o=2.3$) can be used as an alternative technique to the central air injection system especially for high inlet flowrate to promote resistance to CIVB flashback, reducing cost and complexity of the swirl burner.

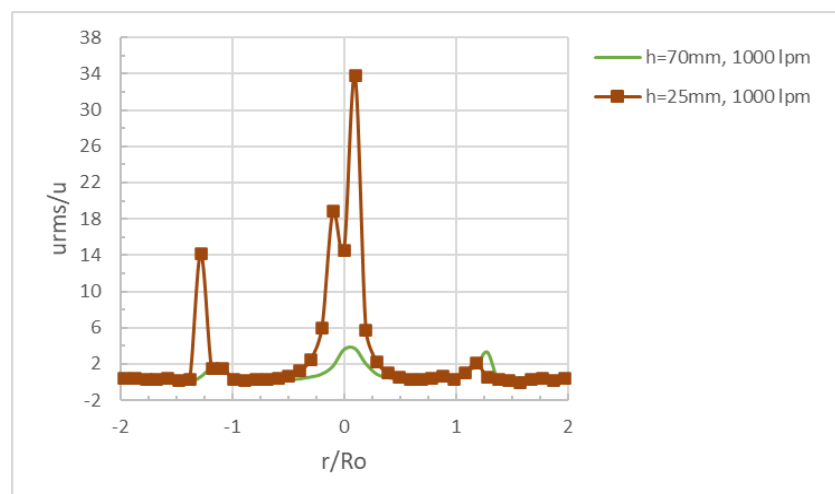


Figure 6-5: Turbulent intensity for different nozzle lengths (h_n) and different inlet tangential flowrates with air injection.

6.3.1.3 Effects of Nozzle with SST Woven Wire Grid in Different Lengths

To investigate the effects of internal burner nozzle surface roughness on the swirl flow characteristics near the wall, three lengths of 316 stainless steel woven wire, as described above, were used as nozzle liners, see Figure 6-1. The insertion lengths (h_g) were 25 mm, 40 mm, and 70 mm. The tests were performed for 800 l/min inlet tangential flowrate. The influence of the SST grids has been analyzed by other authors using numerical simulation but for channel flow. Another author [193][265] examined the grid for swirl burner, but the effect of different strip lengths is not studied yet.

For the long smooth nozzle without mesh lining, the wall effect is clear and is seen as a reduction in axial velocity due to viscosity and wall shear stress. On the other hand, when using woven wire meshes as lining regardless of length, limited the wall effects by maintaining the axial velocity at a relatively high value near the wall, see Figure 6-6.

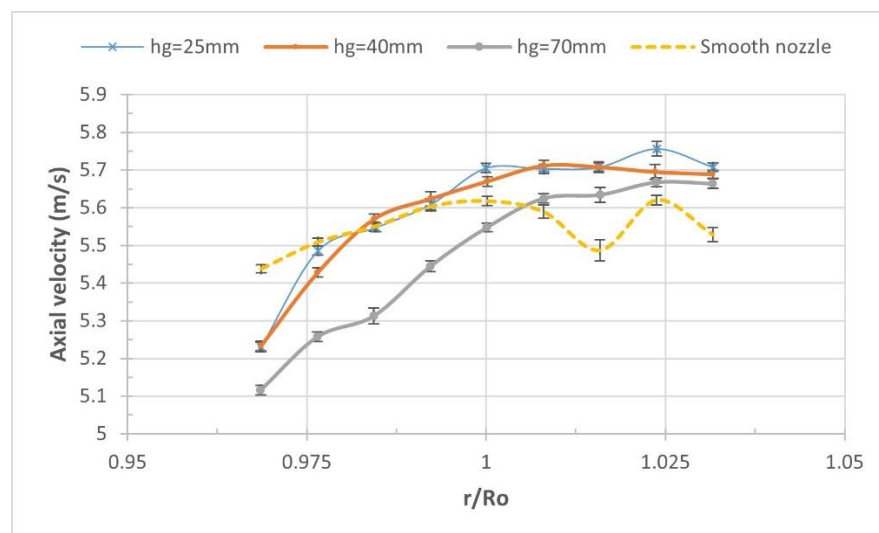


Figure 6-6: Axial velocity downstream the burner nozzle for different surface roughness length strip.

Such behaviour can be explained using the concept of antifouling surfaces, which use regular surface roughness patterns as a passive control of the boundary layer. Also, the length of the lining has only a small effect on overall velocity values. A wide strip of the mesh caused a drop in the flow while the narrower one did not produce such noticeable reduction in overall velocity. The better the reduction of the wall effect the greater the resistance to BLF flashback, which was achieved using the 25 mm wide strip. This approach of simply inserting a wire mesh into the burner looks quite promising since there is no need for a long and costly micro surfaced burner nozzle.

In Figure 6-7, the LDA axial velocity downstream the nozzle is plotted. The results show that the axial velocity gradient is affected by changing the length of the wire mesh liner. The results show that the velocity gradient in the radial direction was decreased with the 25 mm length of liner, which means that the high-velocity region was shifted towards the nozzle wall. The velocity gradient in the downstream direction shows some significant results regarding the impact of these structures on the flow. This result is important because it explains the improvement in BLF flashback resistance when using the shorter mesh. According to the Lewis von Elbe formula for laminar flame speed, a sharp velocity gradient increases the likelihood of flashback, where the flame attacks the low-velocity region near the wall to penetrate towards the premixing channels.

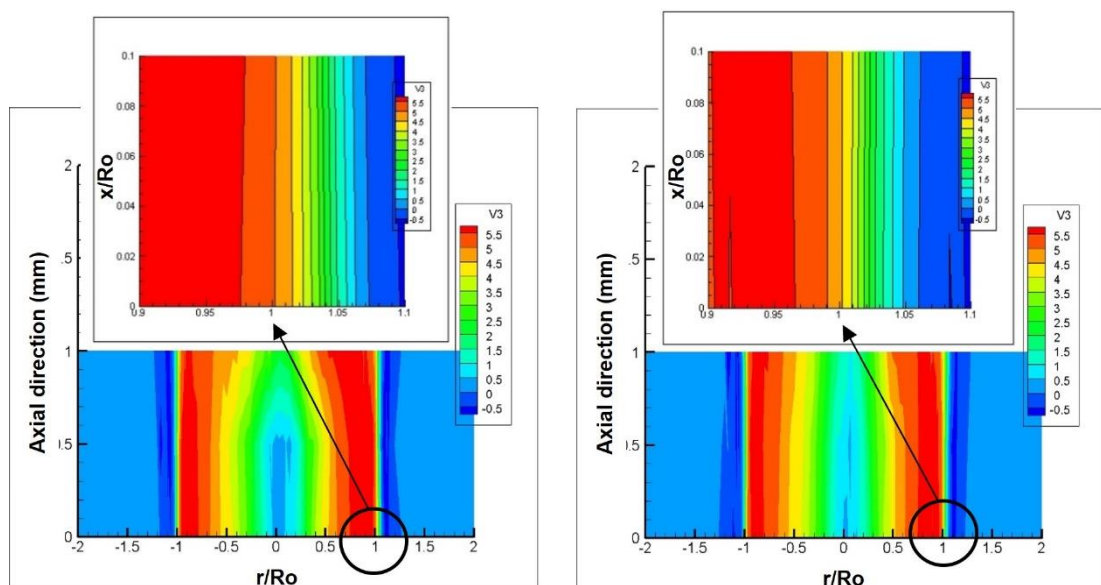


Figure 6-7: Contour of axial velocity downstream the dump plane (a) lining grid length (25 mm) (up left), (b) lining grid length (70 mm) (up right).

Velocity gradient measurements show that a wire mesh has a similar effect on the flow as the riblets. The wire mesh traps some fluid (air) in the texture (holes), which act as fluid bubbles that provide a fluidic bed for the flow, reducing the contact of high momentum flow with the wall.

6.3.2 The Combustion Tests

The hydrodynamic effect of the long nozzle suggests a better flame stability in the burner. Figure 6-8 shows the flame structure across different equivalence ratios at stable operation (ϕ_{stable}) for the long nozzle $h_n=70$ mm (no axial air).

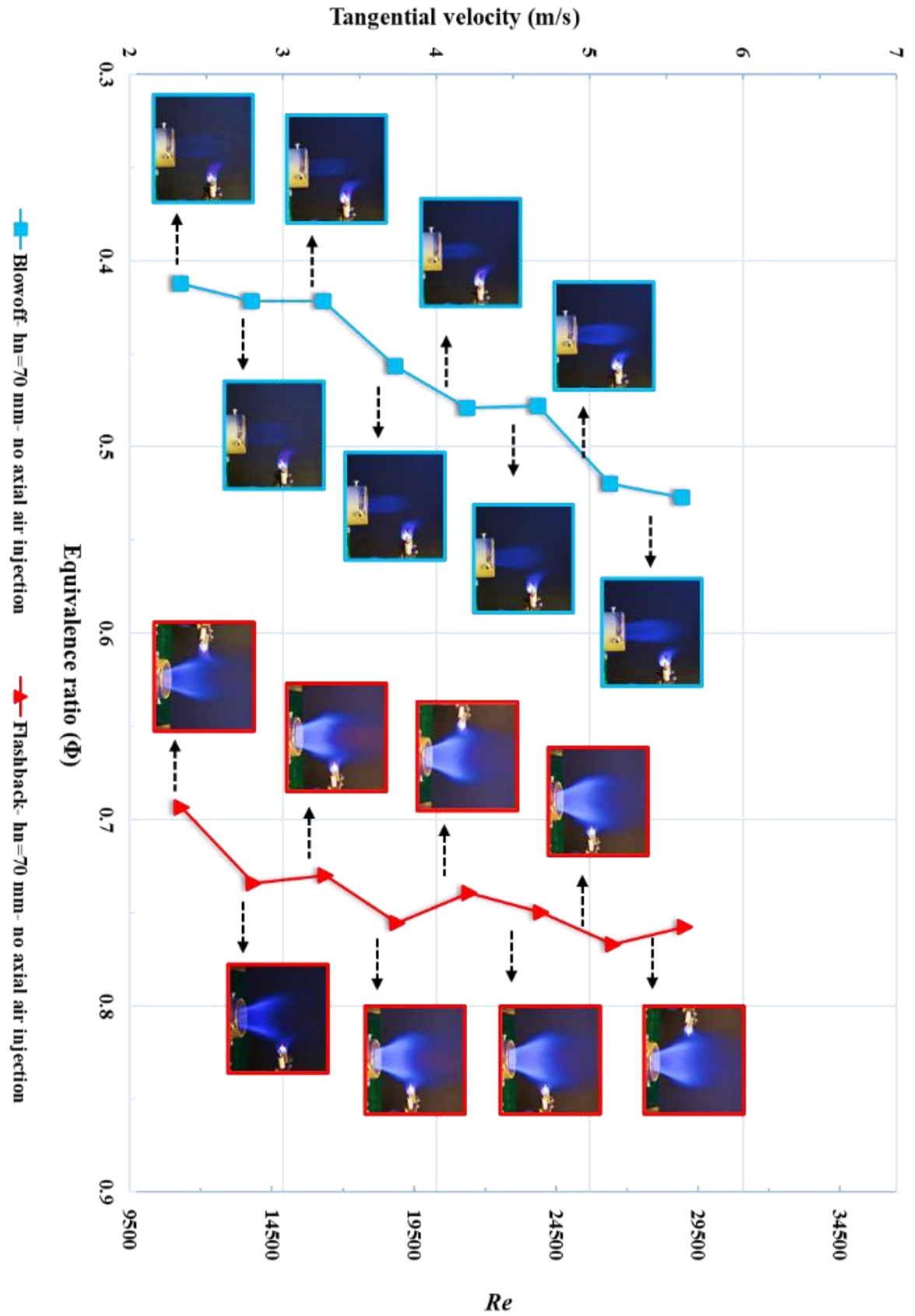


Figure 6-8: Flame stability map of the long nozzle, $h_n=70$ mm - central injector (i.e., no axial air injection).

Figure 6-9 shows the effect of the long nozzle on the stability regime as compared with the base case nozzle ($h_n=25$ mm). It expands the stability region in both directions (Re and Φ) as compared with the short nozzle allowing the burner to work with high tangential velocities and a wide range of equivalence ratios. The figure shows that the use of the long nozzle achieved a wide range of stable operation limit across the region ($0.42 > \Phi < 0.75$), and a tangential velocity ranging from 2.2 m/s to 5.6 m/s. It is also seen that the long nozzle affects the blowoff limit by shifting it further towards the lean region. On the other hand, when using the short nozzle (the base case), the stable operation region was ($0.45 > \Phi < 0.67$), and the maximum tangential velocity that could be achieved was just below 3.5 m/s. These results suggest that the best ratio of the nozzle length to its inner radius should not exceed ($h_n/R_o=2.3$) to have better flame stability.

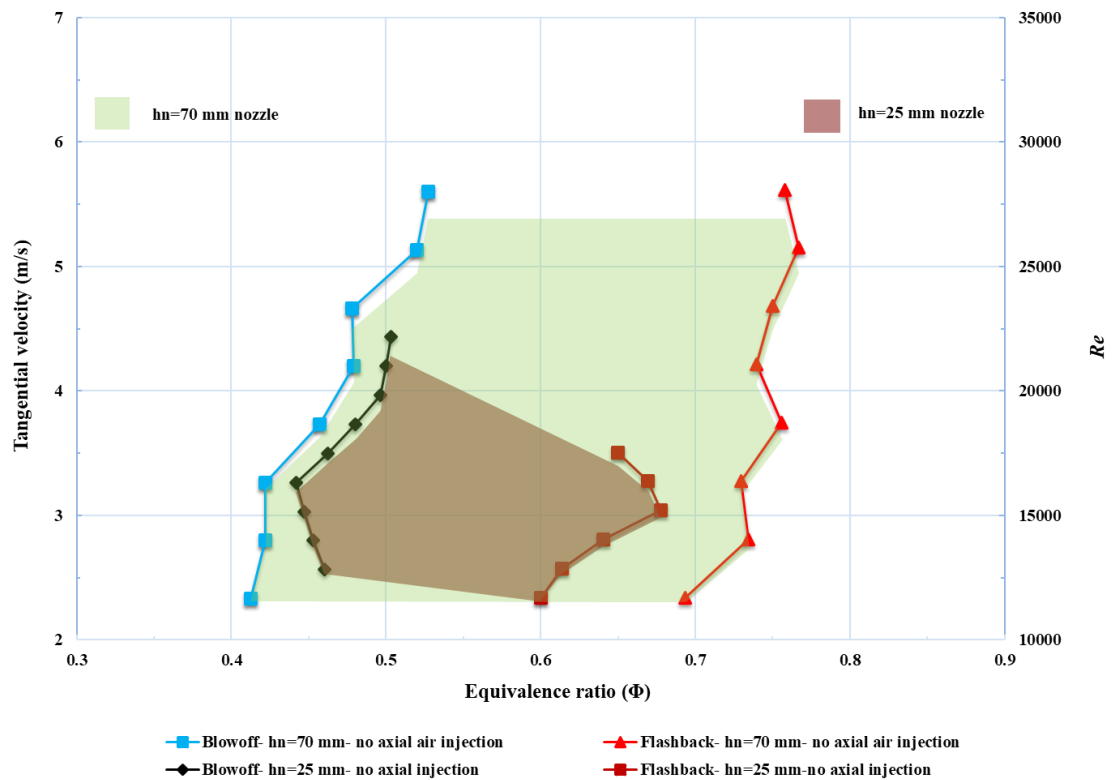


Figure 6-9: Effect of using the long nozzle on the stability map, $h_n=70$ mm – central injector technique (i.e., no axial air injection).

Figure 6-10 illustrates the flame structure across different equivalence ratios at stable operation (Φ_{stable}) for the long nozzle.

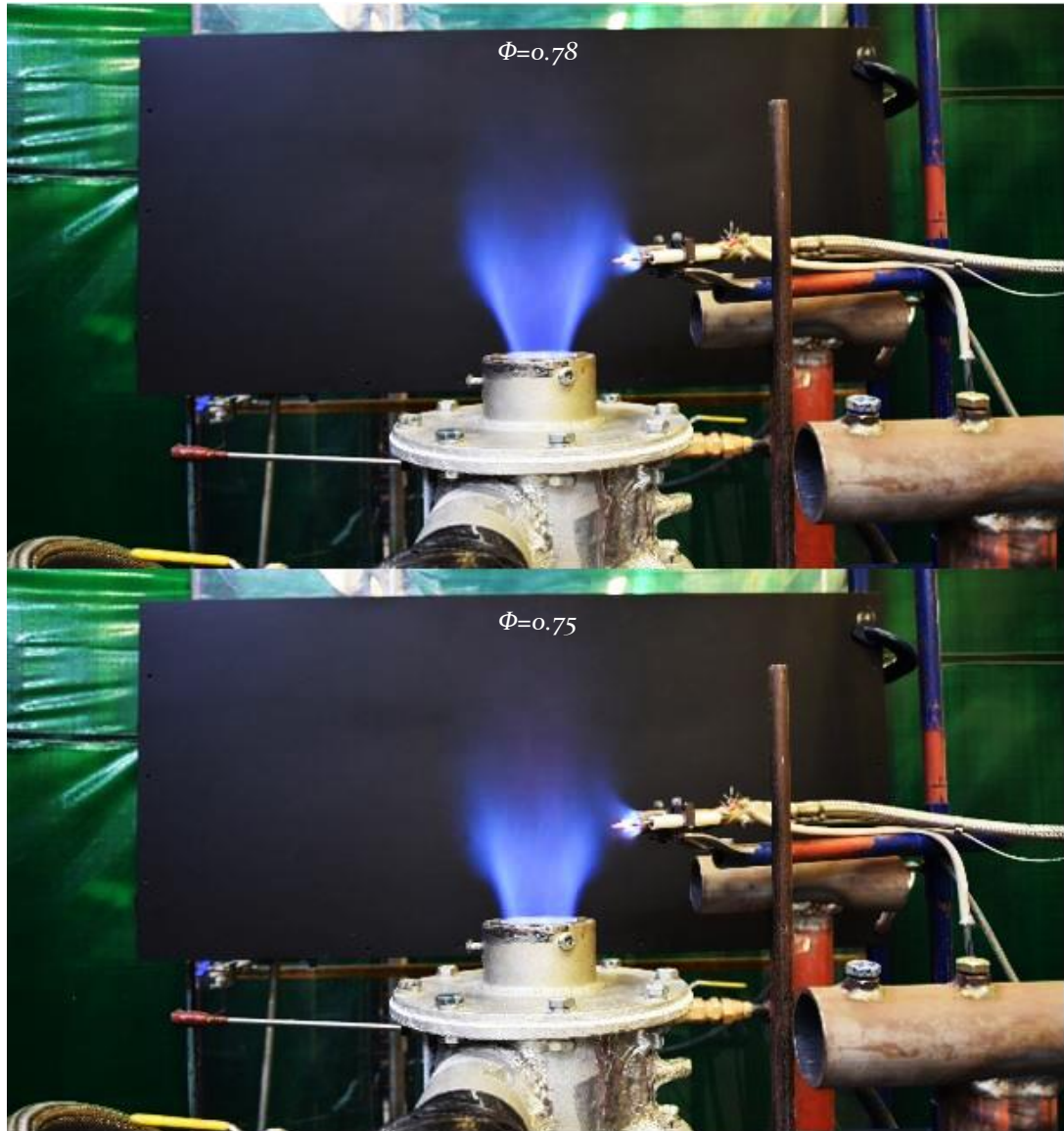


Figure 6-10: Flame structure for stable operation at equivalence ratios (Φ).

6.4 Chapter Summary and Conclusions

The swirl flow manipulation represents an essential technique used to improve the resistance of the swirl burner against different flashback mechanisms such as CIVB and BLF. This chapter aimed to increase the resistance to CIVB using different burner nozzle heights. On the other hand, using a stainless-steel micromesh strip was proved to be essential to tackle the BLF mechanism. The effects of different nozzle heights with and without an added microstructure, on the swirl flow characteristics were investigated experimentally using a 1D LDA system. Different strip lengths (hg) of stainless steel (SST) woven wire mesh were employed as liners on the smooth nozzle to change its surface roughness. It was found that long smooth nozzles ($h_n/R_o=2.3$)

led to promotion of stability in the swirl burner by minimising the axial velocity defect while decreasing turbulence downstream of the dump plane. Moreover, the average measurements show that the burner nozzles with micro-structured surfaces improved control of the BLF flashback and hence reduced outflow drag. It was found that the microstructure mesh alters the flow pattern near the wall by increasing the velocity adjacent to this region increasing resistance to BLF flashback.

Two different nozzle lengths ($h_n=25$ mm and 70 mm) have been tested regarding the promotion of CIVB flashback resistance in a tangential swirl burner. In the combustion experiments, it was observed that the long nozzle increased the resistance to CIVB flashback. On the other hand, a new technique inspired by biomimetic engineering has been developed and tested using two different strip lengths (h_g) of microspheres to improve burner performance regarding BLF flashback phenomena. It was found that the length of the micromesh is important, the shorter the better. A micromesh strip of length 25 mm gave better results than the longest one (70 mm), because the former produced a better shift in the velocity gradient close to the wall. The effect of the grid on the flame stability was not tested due to the safety precautions at the time.

The results showed that decreasing the turbulence in certain positions, such as the CRZ tip and near the nozzle's wall, resulted in several benefits, including an increase in the resistance of CIVB flashback and the BLF, respectively. However, increasing the turbulence within the CRZ improves the circulation and heat released, improving the flame stability. It was found that the turbulent kinetic energy levels increased by a factor of three as heat release increased [270].

Chapter 7

RESULTS

and

DISCUSSION

CHAPTER SEVEN

7 RESULTS AND DISCUSSION

"Experiments are mediators between nature and idea"

J. W. von Goethe, scientist (1749-1832)

7.1 Summary of Discussion

Swirling flows have been widely used for many years in such applications as combustion chambers of gas turbines (GTs), jet engines, turbomachines, and mixing tanks. Swirl combustors offer such superior flame stabilisation over a broad range of equivalence ratios that they are widely considered to have been the greatest single improvement in GT combustion. They not only enhance the intensity of the combustion process by improving mixing, but they also increase residence times and improve flame stabilisation. The high swirl levels generated produce vortex breakdown phenomena that create a Central Recirculation Zone (CRZ) and an off-centre, Precessing Vortex Core (PVC). The vortices produced and their breakdown increase flow turbulence and the shear processes, greatly enhancing the efficiency of combustion by stimulating mixing of fuel and air and making sure every molecule of fuel has numerous oxygen molecules in their proximity. The circulation and mixing of combustion gases with air entering the combustion zone also aids the ignition process.

Efficient configuration and operation of GT burners can be significantly facilitated by measurements attained from parallel experimental and modelling investigations. Such studies merge experimental and theoretical combustion aerodynamics with advanced computational fluid dynamics (CFD) and its development and use will decrease the cost of improvement programs noticeably. The turbulent combustion in GTs, in general, is the sequence of two central interactions, the very complicated hydrodynamics and the chemical reactions. This interaction can enhance or reduce the combustion turbulence and hence affect the combustion stability.

Flashback is an instability that takes place when a flame moves upstream away from its desired position in the direction of the pre-mixing zone and is particularly prevalent with lean premixed combustion. Flashback is an important factor in determining the dependability of low NO_x burners. In turbulent swirling flows mechanisms likely to

produce flashback include autoignition, combustion instabilities, vortex breakdown and Boundary Layer Flashback (BLF).

In swirl combustors common flashback mechanisms that have attracted special interest are Combustion Induced Vortex Breakdown (CIVB) and Boundary Layer Flashback (BLF) because they are a severe risk to the stability of operation, and can, in extreme conditions, result in system failure with consequential financial losses. Flashback is more likely to occur with fuels with higher flame speeds particularly blends with a high hydrogen content. Presently, this is judged to be a barrier to the production of GTs. This problem is considered a severe obstacle in developing GT combustors that can be switched to an alternative fuel, such as when the use of low pollutant blends becomes required for low emissions.

To better understand the various flashback mechanisms, intense numerical and experimental research is needed. Such investigations need to consider modifications to both system hardware and flow fields. A number of techniques are known to efficiently reduce Combustion Induced Vortex Breakdown Flashback and successfully fix the Central Recirculation Zone downstream of the burner by making a modification to system geometry and/or changing the patterns of flow. Placing a bluff body in the flow can act to stabilise the flow, while altering the pattern of fuel flow by changing the fuel injector can move the position of the vortex breakdown further downstream and so reduce the likelihood of Combustion Induced Vortex Breakdown.

Nevertheless, useful as these techniques are they cannot fully solve the problem of flashback and have potential drawbacks. Inserting a bluff body (or central injector) in the presence of high-temperature combustion processes for extended periods of time could produce material degradation and increase maintenance costs. The use of a central fuel injector could increase NO_x emissions and downgrade the fuel/air mixing process. The injection of air into the central core of the vortex to reduce negative axial velocity and turbulence characteristics is another possible way of mitigating CIVB flashback. In the present context this appears to have the significant benefits of avoiding any increase in pollutant levels while providing the required flame stabilisation.

The interactions between the hardware and the very turbulent swirling flows of the combustion system are important and should be considered when seeking methods to solve the problems of combustion stability issues. As a result, this research has investigated both numerically and experimentally the viability of various methods of retarding flame flashback in GT swirl combustors. In this experimental programme,

Flowlight LDA laser diagnostic system from DANTEC was used, while in the numerical studies the most recent ANSYS Fluent R19.2 CFD code were utilised to simulate the isothermal swirl flow in the tangential swirl burner under consideration.

This investigation targeted the hydrodynamic impact of air injected axially using a centrally located fuel injector to tackle the Combustion Induced Vortex Breakdown flashback mechanism. The effect was investigated numerically by changing the characterisation of the turbulence intensity and velocity profiles. The LDA average measurements were used to compare with the isothermal RANS based numerical simulation results as a validation approach.

The effect on the stability map of axial air injection was also reviewed. It is clear from the study of the flashback mechanisms with axial air injection that improving the swirling system against Combustion Induced Vortex Breakdown reduces resistance of the system to BLF. Thus, resistance to boundary layer flame flashback needs to be increased by some appropriate technique.

Increasing system resistance to BLF could be achieved via cooling of the wall or injection of air through small slits parallel to the burner walls to diluting the fuel mix close to the wall, though this would risk increasing NO_x emissions. BLF is sensitive to the velocity gradient at the wall as shown by the Lewis Von Elbe formula [265]. Consequently, in this work, a passive technique to control the velocity gradient near the burner nozzle wall has been investigated experimentally. A technique referred to as the sharkskin effects was used. Regular roughness of the skin caused by small protrusions on the surface referred to as riblets which reduce drag forces and, for example, enable a shark to swim faster. After reviewing published experimental studies, a scalloped riblet geometry was selected to manipulate the flow adjacent to the nozzle wall and hence improve the resistance to Boundary Layer Flashback. In these experiments, a scallop riblet microstructure geometry was used to change the surface roughness of the burner nozzle. It was found that applying scalloped riblet microstructure on nozzle surface changes the flow patterns close to the wall, delivering further resistance to Boundary Layer Flashback. The finish was applied to the burner nozzle using Wire Electrical Discharge Machining. Results show that using both techniques together (axial air injection and microstructured nozzle) show promise of a more comprehensive stable operation for swirl combustors, enabling them to burn a wider range of fuel mixes efficiently without high NO_x levels.

Then the work was extended using the LDA system to investigate the results of different burner nozzle heights on the characteristics of the swirl flow. Additionally, the

new biomimetic approach was tested using three different strip heights of microsurfaces as an internal insert applied onto the internal surface of the longest smooth nozzle to improve the burner resistance to Boundary Layer Flashback. In these experiments, a woven stainless-steel wire mesh liner was used to change the surface roughness of the burner nozzle. The wire diameter was 150 μm . It was found that using the microstructured mesh as a liner to the burner nozzle changes the flow patterns close to the wall, delivering further resistance to Boundary Layer Flashback.

7.2 Summary of Results

The most essential conclusions of this thesis are:

- Swirl combustors in general use are subject to a number of combustion instabilities but have the potential for stable operation subject to the formation of so-called coherent structures. Such combustors would have the potential to operate in the LPM mode with the possibility of undesirable instabilities with multiple fuels.
- Combustion Induced Vortex Breakdown is a source of flashback in swirl combustors, particularly when there is no centre-body or axial injection. Such upstream flame propagation can be initiated even if the velocity of the unburned mixture is greater than the flame speed. CIVB is associated with interaction between flow field turbulence and the heat released at the tip of the Central Recirculation Zone.
- Despite extensive investigations into the mechanisms of flame flashback, studies of the Combustion Induced Vortex Breakdown are still relatively few. CIVB was first observed and recorded in 2003 by [156][185], so investigations into CIVB represent state of the art research when compared to other flashback mechanisms. Despite much interest in this phenomenon, both theoretically and experimentally, there remains significant and important ambiguities and further investigations in this area are important and urgent.
- Here, 1D LDA investigative technique was used to determine the effect of changes in the configuration of the burner on the Combustion Induced Vortex Breakdown and boundary layer flashback mechanisms.
- Computational fluid dynamics codes used to model swirl flows often lack adequate validation, and the vast majority of work carried out on swirling flows has been done experimentally, a process that is both complicated and costly.

Despite the modern approaches to turbulent combustion modelling, the lack of precise and reliable turbulence closure models is still a leading obstacle in modelling complex, swirling, turbulent combustor flows. As a result, studying the hydrodynamics of the isothermal flow in swirl combustors can give primary predictions about the behaviour of combustor flows.

- Fuel injectors when placed centrally can provide significant flashback resistance and suppress Combustion Induced Vortex Breakdown. Such centrally placed injectors undergo significant life degradation as they are in contact with the flame. An effect which is likely to be increased when high hydrogen content blends are used, increasing maintenance costs. Additionally, central fuel injectors may increase pollutant levels and less effective mixing. Axial air injection, rather than fuel injection, used for flame stabilisation can provide solutions for at least some of the problems that arise when using central fuel injectors.
- The axial air jets will often mimic the shape of a central fuel injector and will cause considerable changes in the stability map. They produce wider operational stability, and the limits of stability increase regarding both equivalence ratio and inlet tangential velocity. Changes in the air jet diameter may give more flexibility of operation whereas central fuel injectors do not have this possibility.
- An extended region of operation obtained with central air injection allows the burner to operate at higher power than when a central fuel injector is used, hence it is possible to increase power to higher levels at a constant equivalence ratio, which is difficult for burners using central fuel injectors due to the limitations imposed by their stability maps.
- Greater resistance to flame back-propagation obtained when using axial air injection increases the possibility of flame re-stabilisation under flashback conditions. Slightly increasing axial air injection pushes the CRZ downstream and prevents the flame from propagating towards the burner plenum, which is impossible to achieve when using a central fuel injector.
- Defects in the axial velocity occurring in the central vortex core and leading to Combustion Induced Vortex Breakdown can be reduced significantly when axial air injection is used. An air jet also leads to a wider vortex core, with a consequent lower pressure gradient, hence reducing baroclinic torque effects which are considered as one of the factors that provoke CIVB.

- Axial air injection clearly and definitely effects the downstream flow characteristics. This is seen in the considerable reduction in turbulence levels, hence reduction in local turbulent flame speed. This reduction of turbulent flame speed, especially close to the burner exit plane, will enable the upcoming fresh mixture to compensate for the velocity effect that occurs at the tip of the CRZ providing the necessary velocity balance at this region.
- The relative positioning of burner base plate and air injector is critical for stable operation.
- Air injected from the level of the burner baseplate maintains flow coherence and is not so affected by tangential flow via the inlet. This allows the burner to work under reasonable conditions.
- Air injected downstream ($L_o=29$ mm, say), is directly subject to the tangential flow with its high level of momentum which induces pressure fluctuations and enhances turbulence intensity in this region, which can cause flashback to occur at a lower ϕ .
- Air injected further downstream ($L_o=150$ mm, say) significantly decreases the turbulence level and hence provides better flashback resistance and wider stability operation margins. The reason for that is at this position the air injector is protected by the burner sleeve and hence is less affected by the inlet tangential flow.
- Axial air injection rather than axial fuel injection can noticeably reduce maintenance costs. In addition, axial air injection better enables fuel switching due to its wider stability operation map.
- Measurement of axial turbulence intensity and velocity (using 1D LDA) based on instantaneous velocity seem to be useful tools to investigate the effect of different configuration on flashback limits.
- CFD simulation (using ANSYS Fluent R19.2) of the flow for different air injection rates and positions reveal a considerable change in turbulence level and velocity gradient not just close to the burner mouth but also for a significant distance downstream. This was evident when pushing the CRZ away from the burner exit plane with reduced turbulence intensity.
- Relative flow rates of centrally injected air and tangential inlet flow are very important and should be chosen carefully. This relation directly effects the size and velocity values of the CRZ and other coherent structures. The ratio will

depend on the required swirl structure: high axial injection could reduce the swirl strength to be less than $S=0.6$ which is the minimum swirl number required for vortex breakdown. On the other hand, very low axial injection could reduce its potential for flame stabilisation.

- The Precessing Vortex Core depends on axial injection: too great axial injection will reduce the Precessing Vortex Core, reduce the frequency of oscillation and lessen acoustic-combustion instabilities.
- Air injected at the central burner axis will generate a positive axial velocity gradient that enhances Combustion Induced Vortex Breakdown resistance. But a positive gradient at the centre produces negative velocity gradients close to the nozzle wall, resulting in Boundary Layer Flashback. This effect has been observed. Axial injection with large diameter fuel injectors will cause flame propagation via wall boundary layer.
- To attain the desired benefits from axial air injection, its effects on Boundary Layer Flashback need to be considered.
- To enhance BLF resistance in the burner, a scalloped riblet geometry was applied to the burner nozzle. A stainless-steel woven mesh with wire of diameter 150 μm was used as the liner.
- Using scalloped structures decreases the radial distance at which viscous wall effects on the flow and the high-velocity region ($u/U > 0.5$) are moved nearer the wall. This shift results in changes in the flow structure in the thin shear layer downstream of the nozzle exit, which assists in avoiding Combustion Induced Vortex Breakdown when used in combination with central air injection.
- Applying microstructures to the nozzles of burners via Wire Electrical Discharge Machining has its own difficulties. On the one hand, the access to the work piece is limited due to the mechanism of wire feeding. However, more complicated show little difference from simple geometries.
- Good enhancement in the radial velocity gradient was found when using the scalloped geometry. Furthermore, in the combustion tests, the scalloped geometry improved protection against boundary layer flashback.
- Velocity gradient measurements show that a wire mesh has a similar effect on the flow as the riblets. The wire mesh traps some fluid (air) in the texture

(holes), which act as fluid bubbles that provide a fluidic bed for the flow, reducing the contact of high momentum flow with the wall.

- Using micro meshes demonstrated their potential for Boundary Layer Flashback resistance. The structure changed the behaviour of the boundary sublayer in such a way that the velocity of the fresh mixture remains high even close to the wall which in turn increases the velocity gradient to above the critical value that can overcome turbulent flame speed.
- The use of a micromesh increases the operational stability map, the effects of which can be observed visually. The optimum conditions were obtained when using axial air injection and micromesh surfaces simultaneously.
- The microstructure use for flame stabilisation seems to be useful for commercial and industrial applications. However, considerable research is needed to predict the manufacturing cost of suitable microstructure geometry, with more detail of the flow control to be achieved.
- Regarding the different nozzle configurations, it was seen that longer nozzle increased the resistance to CIVB flashback. Using these techniques, i.e., a long flat nozzle ($h_n=70$ mm) gave substantial axial velocity defect reduction, while minimizing turbulent intensity and hence achieving swirl flow stability for a wider range of inlet flowrates.
- It was found that the height of the micromesh strip is important. A strip of micromesh of height 25 mm gave better results than the longest one (70 mm) as the former produced the best shift of the velocity gradient close to the wall and hence improve the resistance against BLF.

Chapter 8

Conclusions and Recommendations for Further Work

CHAPTER EIGHT

8 CONCLUSIONS AND RECOMMENDATIONS FOR FURTHER WORK

"The true subject of science is the beauty of the world"

Simone Weil, French philosopher (1909-1943)

8.1 CONCLUSIONS

The main conclusions of this thesis are:

- CFD codes utilising different software packages are used widely in industrial design for many reasons: CFD simulations are relatively convenient and easy to use, CFD is an inherently more flexible way to investigate a change in operating conditions as the change to the computer code is quicker and cheaper than designing and conducting experimental tests, which may require the redesign, manufacture, and testing of modified components.
- Air injected axially can be used for flame stabilisation and can provide solutions to the many difficulties that can occur if central fuel injectors and/or bluff bodies are used. Axial air injectors can produce wider regions of stable operation than can central fuel injectors. The major result is to push the Central Recirculation Zone downstream and avoid the high turbulence that may induce flashback.
- Combining axially injected air, with scallop riblet microstructure enhancements can expand stability limits considerably and enhance flame flashback resistance against Boundary Layer Flashback and Combustion Induced Vortex Breakdown.
- Using different nozzle heights could have the potential to control the swirling flow and hence the operability limit.

8.2 Recommendations for Further Work

The present research programme identified questions that were outside its scope but could be explored in further studies. Therefore, based on the present work, some related further studies should be considered. To investigate:

- The effect on flame stability and swirl structures of preheated, and/or pressurised mixture.
- The use of gas mixes other than air injected axially at different rates on flame stability.
- The effect of air injected axially on a range of fuels, in particular blends high in hydrogen.
- The effects of a variable diameter air jets on stability limits.
- How air injection affects combustion products and correlates with pollutant products such as NO_x, CO and UHC.
- How more modern (2-D and 3-D) laser diagnostic systems could improve system diagnostics compared to the 1-D laser system used here.
- How microstructure manufacturing, using techniques such as Electrical Discharge Machining (EDM) could produce more complex surface geometries for surfaces such as the entrance to the nozzle.
- How different injector positions define the turbulence intensity and affect the Precessing Vortex Core (PVC) to determine the effect of turbulence intensity on flame structure.
- How the presence and type of micro mesh impacts of the stabilisation mechanisms and the Precessing Vortex Core (PVC).
- Carry out more combustion tests using microstructures and micromesh for a wide range of fuel blends.
- Substitution of part of the NG used in this study by syngas to provide the opportunity of lowering the possible overall equivalence ratio in the combustion zone and to extend the operation range towards lower minimum power output without violating emission limits (CO and UHC), flame out or combustion instabilities.

Appendix
Photographs
and
Diagrams

APPENDIX : (PHOTOGRAPHS AND DIAGRAMS)

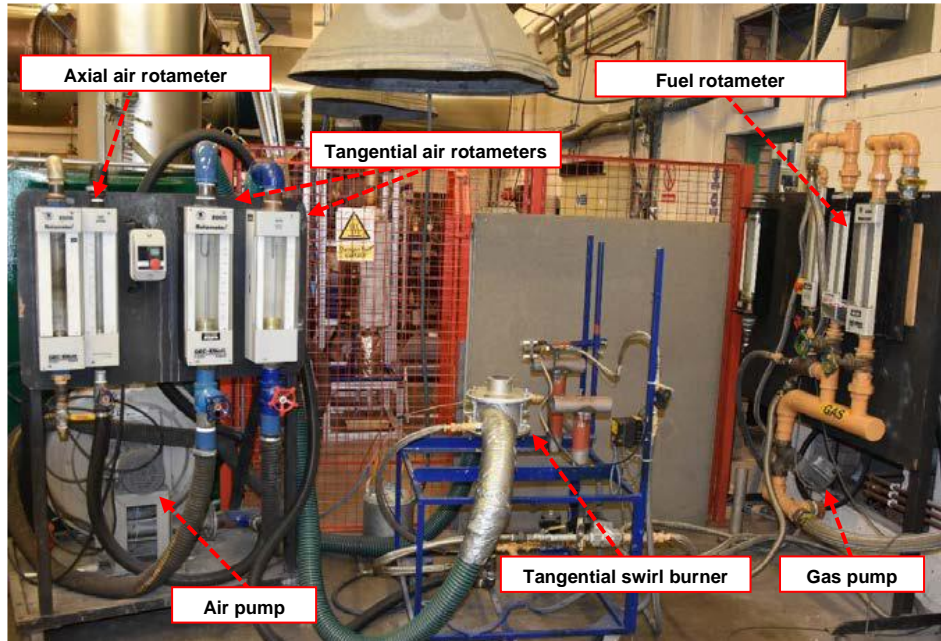


Figure A-1: Experimental setup, testing rig.

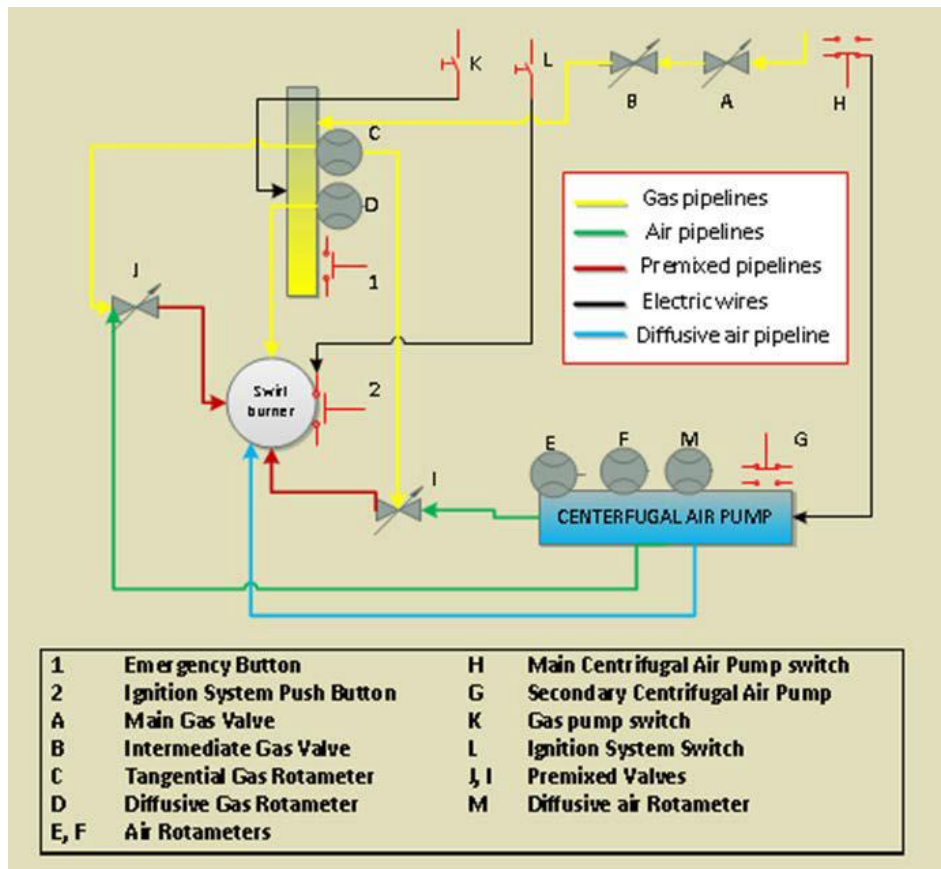


Figure A-2: The arrangement of the testing rig during the experiments.

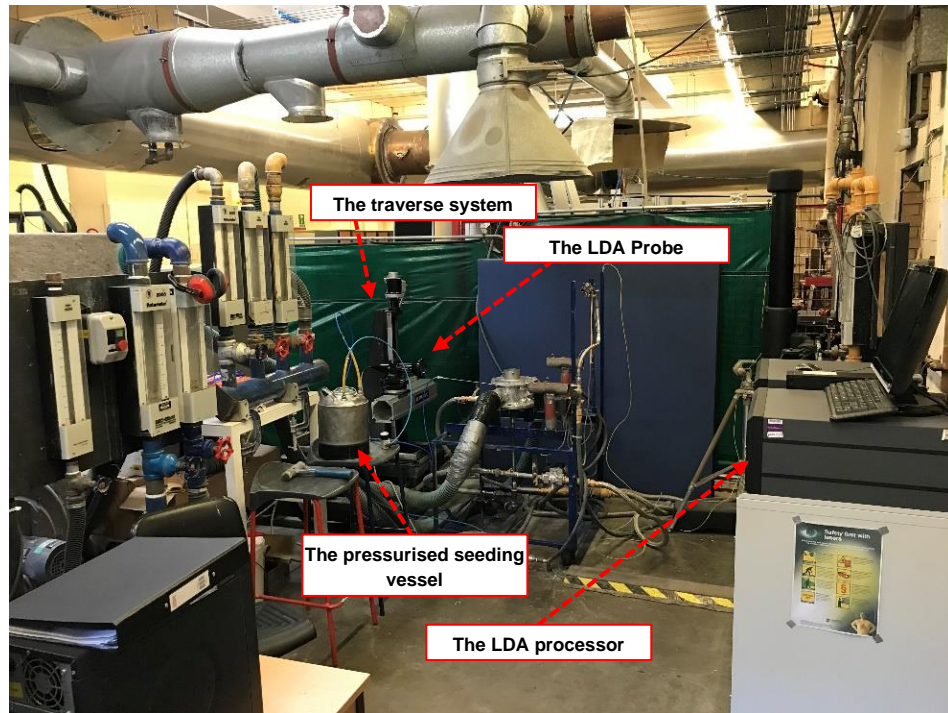


Figure A-3: The LDA setup.

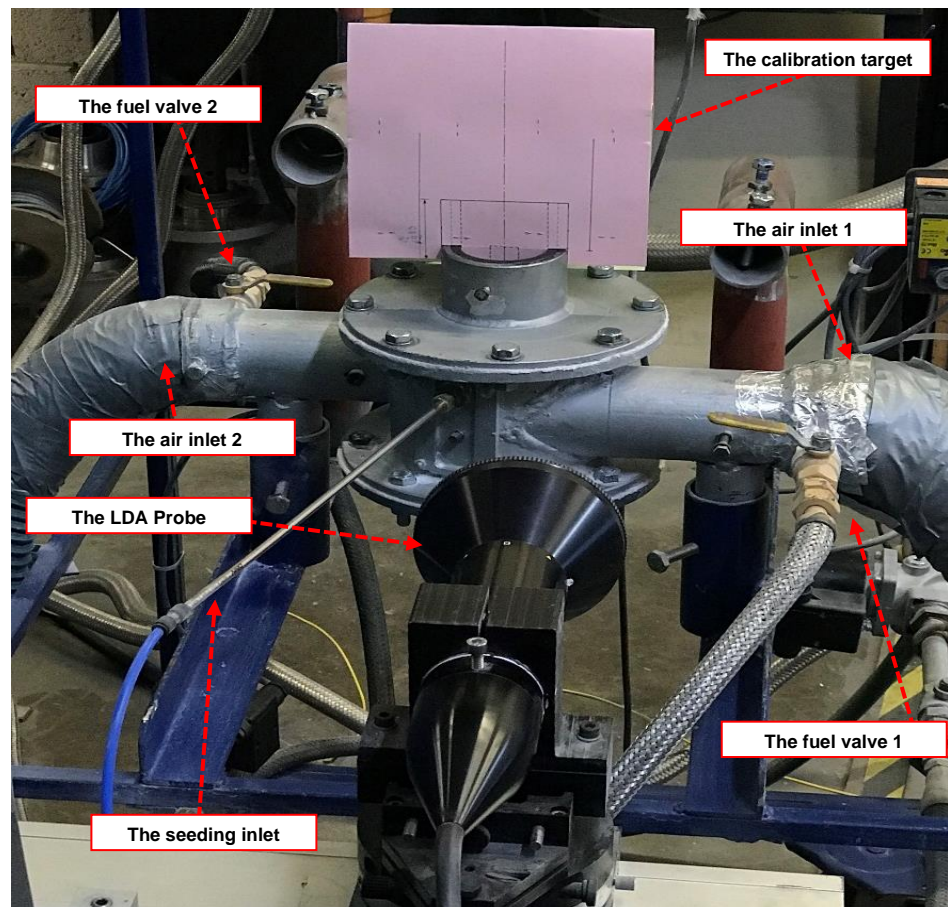


Figure A-4: Calibration of traverse movement.

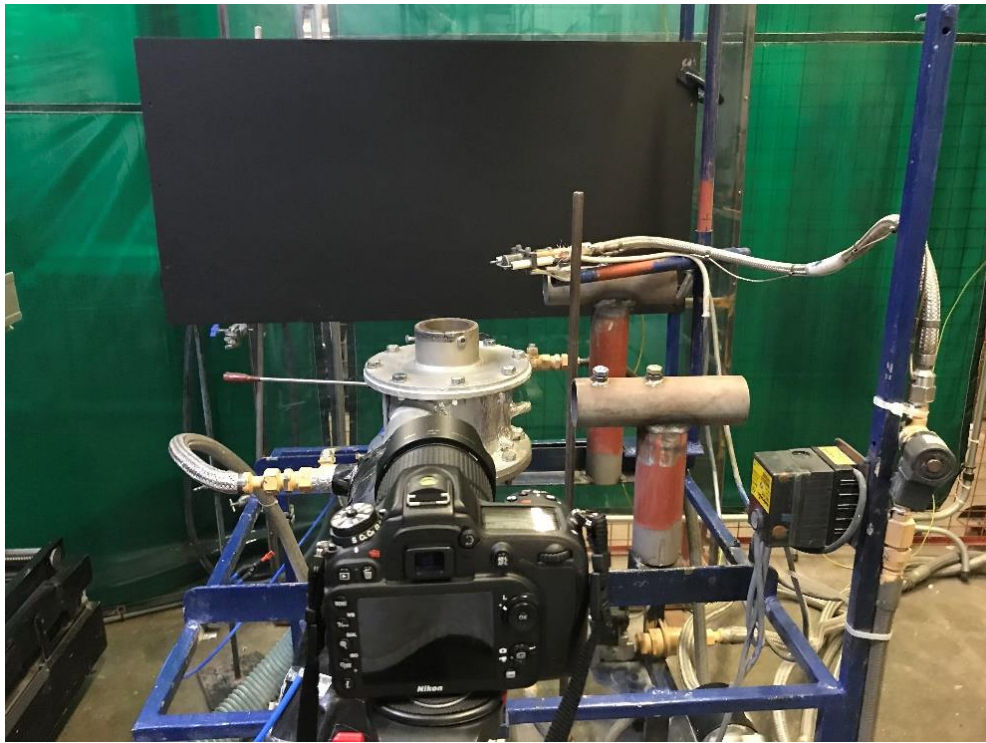


Figure A-5: Camera setup for flame imaging, Nikon 7200 DSLR camera.

REFERENCES

- [1] I. J. Andrews, "The Carboniferous Bowland Shale Gas Study: Geology and Resource Estimation," *British Geological Survey for Department of Energy and Climate Change, UK Government*, 2013. [Online]. Available: https://www.gov.uk/government/uploads/system/uploads/attachment_data/file/226874/BGS_DECC_BowlandShaleGasReport_MAIN_REPORT.pdf.
- [2] P. Whitelaw *et al.*, "An Evaluation of Shale Gas Potential in the Bowland Shale, UK Using Sequential High Water Pressure Pyrolysis and Methane Adsorption," in *AAPG International Conference and Exhibition, London, England*, 2017.
- [3] ExxonMobil, "2018 Outlook for Energy: A View to 2040," 2018. [Online]. Available: <https://corporate.exxonmobil.com/en/~media/Global/Files/outlook-for-energy/2018-Outlook-for-Energy.pdf>.
- [4] I. E. Agency, "World Energy Outlook Executive Summary," *OECD/IEA*, 2018. [Online]. Available: <https://webstore.iea.org/download/summary/190?fileName=English-WEO-2018-ES.pdf>.
- [5] E. & I. S. Department for Business, "Energy Trends March 2018.," *UK Government*, 2018. [Online]. Available: https://assets.publishing.service.gov.uk/government/uploads/system/uploads/attachment_data/file/712458/Energy_Trends_March_2018.pdf.
- [6] Defra, "Emissions of Air Pollutants in the UK, 1970 to 2016," *UK Government*, 2018. [Online]. Available: https://assets.publishing.service.gov.uk/government/uploads/system/uploads/attachment_data/file/778483/Emissions_of_air_pollutants_1990_2017.pdf.
- [7] Greg Chapman, "UK Energy: Changing Patterns of Power Generation," *British Geological Survey for Department of Energy and Climate Change, London, UK*, 2005. [Online]. Available: <https://www.bgs.ac.uk/downloads/start.cfm?id=97>.
- [8] E. & I. S. Department for Business, "Digest of UK Energy Statistics 2018," *UK Government*, 2018. [Online]. Available: https://assets.publishing.service.gov.uk/government/uploads/system/uploads/attachment_data/file/736148/DUKES_2018.pdf.
- [9] M. Wietschel and M. Ball, "The future of hydrogen – opportunities and challenges," *Int. J. of Hydrog. Energy*, vol. 34, pp. 615–627, 2009.
- [10] E. & I. S. Department for Business, "UK Energy Statistics, Q1 2018," *UK Government*, 2018. [Online]. Available: https://assets.publishing.service.gov.uk/government/uploads/system/uploads/attachment_data/file/720182/Press_Notice_June_18.pdf.
- [11] J. Moylan, "Hinkley Point: What is it and Why is it Important?," *BBC News*, 2016. [Online]. Available: <https://www.bbc.co.uk/news/business-36897180>.

- [12] E. & I. S. Department for Business, "UK Energy Brief in 2021," 2021. [Online]. Available: www.gov.uk/government/statistics/uk-energy-in-brief-2021.
- [13] A. Gani, "Government Cuts Tax Relief for Community Green Energy," *The Guardian*, 2015. [Online]. Available: <https://theecologist.org/2015/oct/30/government-cuts-tax-relief-community-green-energy>.
- [14] BP, "BP Energy Outlook 2018 Edition," *BP Energy Economics*, 2018. [Online]. Available: <https://www.bp.com/content/dam/bp/business-sites/en/global/corporate/pdfs/energy-economics/energy-outlook/bp-energy-outlook-2018.pdf>.
- [15] Oliver Wyman, "World Energy Trilemma 2017," *World Energy Council*, 2017. [Online]. Available: <https://www.worldenergy.org/wp-content/uploads/2017/11/Energy-Trilemma-Index-2017-Report.pdf>.
- [16] S. W. Leah Davis, Peter Daw, Michael Doust, Ross Hudson, "Delivering London's Energy Future," *Greater London Authority*, 2011. [Online]. Available: https://www.london.gov.uk/sites/default/files/gla_migrate_files_destination/Energy-future-oct11.pdf.
- [17] DBEIS, "Uk Energy in Brief 2014," *UK Government*, 2014. [Online]. Available: https://assets.publishing.service.gov.uk/government/uploads/system/uploads/attachment_data/file/350941/UK_Energy_in_Brief_2014_revised.pdf.
- [18] E. and I. S. Department for Business, "2016 UK Greenhouse Gas Emissions, Final Figures," *UK Government*, 2018. [Online]. Available: https://assets.publishing.service.gov.uk/government/uploads/system/uploads/attachment_data/file/680473/2016_Final_Emissions_statistics.pdf.
- [19] E. & I. S. Department for Business, "2019 UK Greenhouse Gas Emissions, Final Figures," 2021. [Online]. Available: https://assets.publishing.service.gov.uk/government/uploads/system/uploads/attachment_data/file/957887/2019_Final_greenhouse_gas_emissions_statistical_release.pdf.
- [20] F. and R. A. Department for Environment, "Guidance on How to Measure and Report Your Greenhouse Gas Emissions," *The Department for Environment, Food and Rural Affairs, UK Government*, 2009. [Online]. Available: https://assets.publishing.service.gov.uk/government/uploads/system/uploads/attachment_data/file/69282/pb13309-ghg-guidance-0909011.pdf.
- [21] NOAA, "Basics of the Carbon Cycle and the Greenhouse Effect," *U.S. Department of Commerce*, 2009. [Online]. Available: <https://www.esrl.noaa.gov/gmd/ccgg/basics.html>.
- [22] US EPA, "Inventory of U.S. Greenhouse Gas Emissions and Sinks, 1990-2016," *EPA 430-R-18-003*, 2018. [Online]. Available: https://www.epa.gov/sites/production/files/2018-01/documents/2018_complete_report.pdf.
- [23] National Atmospheric Emission Inventory, "Overview of Air Pollutantsle," 2016. [Online]. Available: <http://naei.beis.gov.uk/overview/ap-overview>.

- [24] DBEIS, "Energy Consumption in the UK," *UK Government*, 2018. [Online]. Available: https://assets.publishing.service.gov.uk/government/uploads/system/uploads/attachment_data/file/729317/Energy_Consumption_in_the_UK__ECUK__2018.pdf.
- [25] DBEIS, "Uk Energy in Brief 2017," *UK Government*, 2017. [Online]. Available: https://www.gov.uk/government/uploads/system/uploads/attachment_data/file/350941/UK_Energy_in_Brief_2014_revised.pdf.
- [26] ALSTOM, "The World's First Industrial Gas Turbine Set at Neuchâtel (1939)," *ASME*, 2007. [Online]. Available: https://www.asme.org/wwwasmeorg/media/ResourceFiles/AboutASME/Who_We_Are/Engineering_History/Landmarks/135-Neuchatel-Gas-Turbine.pdf.
- [27] P. Breeze, "Gas-Turbine Power Generation," in *Academic Press*, 1st Ed., Elsevier, 2016, pp. 65–75.
- [28] Global Market Insights, "Gas Turbine Market Outlook 2018-2024 Industry Trends Analysis Report," 2018. [Online]. Available: <https://www.gminsights.com/industry-analysis/gas-turbine-market>.
- [29] SIEMENS, "SGT-750 Gas Turbine Proven Technology," *Siemens AG 2015*, 2015. [Online]. Available: https://www.energy.siemens.com/hq/pool/hq/power-generation/gas-turbines/sgt-750/SGT-750_brochure.pdf.
- [30] A. H. L. and D. R. Ballal, *Gas Turbine Combustion Alternative Fuels and Emissions*. Taylor & Francis Group, 2010.
- [31] M. H. Baumgärtner and T. Sattelmayer, "Improvement of the turn-down ratio of gas turbines by autothermal on board syngas generation," *J. Glob. Power Propuls. Soc.*, vol. 1, pp. 55–70, Jun. 2017.
- [32] P. E. Rokke, J. E. Hustad, N. A. Rokke, and O. B. Svendsgaard, "Technology Update on Gas Turbine Dual Fuel, dry Low Emission Combustion system," in *Proceedings of ASME Turbo Expo 2003 Power for Land, Sea, and Air*, 2003, pp. 16–19.
- [33] M. Welch and B. Igboe, "Gas Turbine Fuel and Fuel Quality Requirements for use in Industrial Gas Turbine Combustion," *Proc. Second Middle East Turbomach. Symp.*, no. March, p. 10, 2013.
- [34] T. Lieuwen, V. Mcdonell, and E. Petersen, "Fuel Flexibility Influences on Premixed Combustor Blowout, Flashback, Autoignition, and Stability," in *ASME Turbo Expo 2006: Power for Land, Sea and Air*, 2006, pp. 1–15.
- [35] D. J. Abbott, J. P. Bowers, and S. R. James, "The Impact of Natural Gas Composition Variations on the Operation of Gas Turbines for Power Generation," in *The Future of Gas Turbine Technology 6th International Conference*, 2012, no. October, p. 1.
- [36] GE, "Specification for Fuel Gases for Combustion in Heavy-Duty Gas Turbines," *GE Power Systems*, 2002. [Online]. Available: <http://citeseerx.ist.psu.edu/viewdoc/download?doi=10.1.1.143.6392&rep=rep1&type=pdf>.

- [37] T. Lieuwen, V. McDonell, E. Petersen, D. Santavicca, and T. Sattelmayer, "Burner Development and Operability issues Associated with Steady Flowing Syngas Fired Combustion," *Combust. Sci. Technol.*, vol. 180, no. 6, pp. 1–15, 2006.
- [38] D. M. Jarvie, R. J. Hill, T. E. Ruble, and R. M. Pollastro, "Unconventional shale-gas systems: The Mississippian Barnett Shale of north-central Texas as one model for thermogenic shale-gas assessment," *Am. Assoc. Pet. Geol. Bull.*, vol. 91, no. 4, pp. 475–499, 2007.
- [39] M. Welch, M. Welch, and B. M. Igoe, "Combustion, Fuels and Emissions for Industrial Gas Turbines," *Asia Turbomach. Pump Symp.*, 2016.
- [40] A. S. Alsaegh, F. Amer Hatem, and A. Valera-Medina, "Visualisation of Turbulent Flows in a Swirl Burner under the effects of Axial Air Jets," *Energy Procedia*, vol. 142, pp. 1680–1685, 2017.
- [41] Y. Huang and V. Yang, "Dynamics and stability of lean-premixed swirl-stabilized combustion," *Prog. Energy Combust. Sci.*, vol. 35, no. 4, pp. 293–364, 2009.
- [42] N. K. Rizk and H. C. Mongia, "Semi-analytical Correlations for NO_x, CO, and UHC Emissions," *ASME*, vol. 115, no. 3, p. 612, 1992.
- [43] Clean Air Technology Center, "Nitrogen Oxides (NO_x), Why and How They Are Controlled," *U.S. Environmental Protection Agency*, 1999. [Online]. Available: <http://www.epa.gov/ttn/catc1/dir1/fnoxdoc.pdf>.
- [44] N. A. Hussein, A. Valera-Medina, and A. S. Alsaegh, "Ammonia- hydrogen combustion in a swirl burner with reduction of NO_x emissions," *Energy Procedia*, vol. 158, pp. 2305–2310, Feb. 2019.
- [45] B. Major, "Cost Analysis of NO_x Control Alternatives for Stationary Gas Turbines," *ONSITE SYCOM Energy Corporation, U.S. Department of Energy*, 1999. [Online]. Available: https://www.energy.gov/sites/prod/files/2013/11/f4/gas_turbines_nox_cost_analysis.pdf.
- [46] F. and R. A. Department for Environment, "Emissions of air pollutants in the UK – Nitrogen oxides (NO_x)," 2022. [Online]. Available: <https://www.gov.uk/government/statistics/emissions-of-air-pollutants/emissions-of-air-pollutants-in-the-uk-nitrogen-oxides-nox>.
- [47] G. M. Satish Gadde, Jianfan Wu, Anil Gulati, "Syngas Capable Combustion Systems Development for Advanced Gas Turbines," in *ASME Turbo Expo 2006: Power for Land, Sea and Air*, 2006.
- [48] S. Leibovich, "The Structure of Vortex Breakdown," *Annu. Rev. Fluid Mech.*, vol. 10, no. 1, pp. 221–246, Jan. 1978.
- [49] P. Chiesa, G. Lozza, and L. Mazzocchi, "Using Hydrogen as Gas Turbine Fuel," *Vol. 3 Turbo Expo 2003*, no. January 2005, pp. 163–171, 2003.
- [50] Tim C. Lieuwen, *Unsteady Combustor Physics*. Cambridge University Press, 2012.

- [51] R. S. Cant and E. Mastorakos, *An Introduction to Turbulent Reacting Flows*. Imperial College Press, 2008.
- [52] D. G. Lilley, "Swirl Flows in Combustion: A Review," *AIAA J.*, vol. 15, no. 8, pp. 1063–1078, 1977.
- [53] L. Guedot, G. Lartigue, and V. Moureau, "Modeling and Analysis of the Interactions of Coherent Structures with a Spray Flame in a Swirl Burner," in *Turbulence and Interactions Proceedings of the TI 2015 conference, Corsica, France*, 2015.
- [54] P. M. Anacleto, E. C. Fernandes, M. V. Heitor, and S. I. Shtork, "Swirl Flow Structure and Flame Characteristics in a Model Lean Premixed Combustor," *Combust. Sci. Technol.*, vol. 175, no. 8, pp. 1369–1388, 2003.
- [55] V. N. Kurdyumov, E. Fernández, and A. Liñán, "Flame Flashback and Propagation of Premixed Flames Near a Wall," *Proc. Combust. Inst.*, vol. 28, no. 2, pp. 1883–1889, 2000.
- [56] T. Sattelmayer, C. Mayer, and J. Sangl, "Interaction of Flame Flashback Mechanisms in Premixed Hydrogen-Air Swirl Flames," *J. Eng. Gas Turbines Power*, vol. 138, no. January, pp. 1–13, 2014.
- [57] W. M. Flegel, E. A. Haney, R. S. Elliott, J. T. Kamino, and D. N. Ernst, "Making Single-Mode Preforms by the MCVD Process," *AT&T Tech. J.*, vol. 65, no. 1, pp. 56–61, 1986.
- [58] S. M. Correa, "Power Generation and Aeropropulsion Gas Turbines: From Combustion Science to Combustion Technology," in *Twenty-Seventh Symposium (International) on Combustion/The Combustion Institute*, 1998, pp. 1793–1807.
- [59] S. Hoffmann, P. Habisreuther, and B. Lenze, "Development and assessment of correlations for predicting stability limits of swirling flames," *Chem. Eng. Process.*, vol. 33, no. 5, pp. 393–400, 1994.
- [60] D. Froud, A. Beale, T. O'Doherty, and N. Syred, "Studies of helmholtz resonance in a swirl burner/furnace system," in *Symposium (International) on Combustion /The Combustion Institute*, 1996, vol. 26, no. 2, pp. 3355–3362.
- [61] A. J. Griffiths, N. Syred, and W. Fick, "A Review of Biomass and Associated Work at Cardiff Relating to Small Scale Heat and Power Systems," *IFRF Combust. J.*, no. Article 200002, p. 40, 2000.
- [62] N. Peters, *Turbulent Combustion*. Cambridge: Cambridge University Press, 2000.
- [63] F. Hatem, "Flashback Analysis and Avoidance in Swirl Burners," PhD Thesis, Cardiff University, 2017.
- [64] A. Valera-Medina, "Coherent Structure and Their Effects on Process Occuring in Swirl Combustors," PhD Thesis, cardiff University, 2009.
- [65] P. Sayad, "Operational Stability of Lean Premixed Combustion in Gas Turbines An Experimental Study on Gaseous Alternative Fuels," PhD Thesis, Lund University, 2016.

- [66] S. R. Turns, *An Introduction to Combustion: Concepts and Application*. McGraw-Hill, New York, 2013.
- [67] J. R. Dawson, "An Investigation into Naturally Excited Helmholtz Oscillations in a Swirl Burner/Furnace System," Phd Thesis, Cardiff University, 2000.
- [68] K. P. Vanoverberghe, "Flow, Turbulence and Combustion of Premixed Swirling Jet Flames," Phd Thesis, Katholieke Universiteit Leuven, Belgium, 2004.
- [69] R. G. Abdel-Gayed, D. Bradley, and F. K. K. Lung, "Combustion regimes and the straining of turbulent premixed flames," *Combust. Flame*, vol. 76, no. 2, pp. 213–218, 1989.
- [70] S. J. Shanbhogue, S. Husain, and T. Lieuwen, "Lean blowoff of bluff body stabilized flames: Scaling and dynamics," *Prog. Energy Combust. Sci.*, vol. 35, no. 1, pp. 98–120, 2009.
- [71] T. J. Poinsoot and D. P. Veynante, "T. J. Poinsoot 1 and D. P. Veynante 2 1," *Encyclopedia of Computational Mechanics*. John Wiley & Sons, Ltd, pp. 1–42, 2004.
- [72] Y. Nada, K. Matsumoto, and S. Noda, "Liftoff heights of turbulent non-premixed flames in co-flows diluted by CO₂/N₂," *Combust. Flame*, vol. 161, no. 11, pp. 2890–2903, 2014.
- [73] V. K. Arghode, A. K. Gupta, and K. M. Bryden, "High intensity colorless distributed combustion for ultra low emissions and enhanced performance," *Appl. Energy*, vol. 92, pp. 822–830, 2012.
- [74] T. Kim and Y. Kim, "Interactive transient flamelet modeling for soot formation and oxidation processes in laminar non-premixed jet flames," *Combust. Flame*, vol. 162, no. 5, pp. 1660–1678, 2015.
- [75] K. C. Oh and H. D. Shin, "The effect of oxygen and carbon dioxide concentration on soot formation in non-premixed flames," *Fuel*, vol. 85, no. 5–6, pp. 615–624, 2006.
- [76] S. Li, W. Li, M. Xu, X. Wang, H. Li, and Q. Lu, "The experimental study on nitrogen oxides and so₂ emission for oxy-fuel circulation fluidized bed combustion with high oxygen concentration," *Fuel*, vol. 146, pp. 81–87, 2015.
- [77] F. Liu, H. Guo, G. J. Smallwood, and Ö. L. Gülder, "The chemical effects of carbon dioxide as an additive in an ethylene diffusion flame: Implications for soot and NO_x formation," *Combust. Flame*, vol. 125, no. 1–2, pp. 778–787, 2001.
- [78] K. Ramohalli, S. Jones, and R. Bashar, "Some Experimental Data on Liftoff Characteristics of Turbulent Jet Flames," *Combust. Sci. Technol.*, vol. 36, no. 3–4, pp. 199–203, 1983.
- [79] T. Lieuwen, V. McDonell, D. Santavicca, and T. Sattelmayer, "Burner development and operability issues associated with steady flowing syngas fired combustors," *Combust. Sci. Technol.*, vol. 180, no. 6, pp. 1169–1192, 2008.
- [80] T. Sattelmayer, C. Mayer, and J. Sangl, "Interaction of Flame Flashback Mechanisms in Premixed Hydrogen–Air Swirl Flames," *J. Eng. Gas Turbines Power*, vol. 138, no. 1, p. 011503, 2015.

- [81] V. Yakhot, S. A. Orszag, S. Thangam, T. B. Gatski, and C. G. Speziale, "Development of turbulence models for shear flows by a double expansion technique," *Phys. Fluids A Fluid Dyn.*, vol. 4, no. 7, pp. 1510–1520, 1992.
- [82] D. Bradley, M. N. Hamid, and M. Lawes, "Lewis Number Effects On Turbulent Burning Velocity," in *Twentieth Symposium (International) on Combustion/The Combustion Institute*, 1984, pp. 505–512.
- [83] F. C. Gouldin, "Combustion intensity and burning rate integral of premixed flames," *Symp. Combust.*, vol. 26, no. 1, pp. 381–388, 2007.
- [84] J. M. DUCLOS and D. VEYNANTE, "A Comparison of Flamelet Models for Premixed Turbulent Combustion," *Combust. Flame*, vol. 95, pp. 101–117, 1993.
- [85] and J. B. T. García-Armingol, A. Sobrino, "Stability ranges of fully and partially premixed syngas flames," in *Proceedings of the European Combustion Meeting*, 2013.
- [86] and G. R. T. Poinso, D. Veynante, A. Trouve, "Turbulent flame propagation in partially premixed flames," in *Proceeding of the Summer Program*, 1996.
- [87] R. W. Schefer and P. J. Goix, "Mechanism of flame stabilization in turbulent, lifted-jet flames," *Combust. Flame*, vol. 112, no. 4, pp. 559–567, 1998.
- [88] N. Syred, "A review of oscillation mechanisms and the role of the precessing vortex core (PVC) in swirl combustion systems," *Prog. Energy Combust. Sci.*, vol. 32, no. 2, pp. 93–161, 2006.
- [89] N. Syred, M. Abdulsada, A. Griffiths, T. O'Doherty, and P. Bowen, "The effect of hydrogen containing fuel blends upon flashback in swirl burners," *Appl. Energy*, vol. 89, no. 1, pp. 106–110, 2012.
- [90] M. Abdulsada, A. Griffiths, N. Syred, S. Morris, and P. Bowen, "Effect of Swirl Number and Fuel Type Upon the Combustion Limits in Swirl Combustors," in *Proceedings of ASME Turbo Expo 2011 GT2011*, 2011.
- [91] and D. J. L. Syred, N., A.K. Gupta, *Swirl Flow*. Abacus Press, 1984.
- [92] N. Syred and J. M. Beer, "Combustion in swirling flows: A review," *Combust. Flame*, vol. 23, 1974.
- [93] S. E.-D. H. F El-Mahallawy, *Fundamentals and Technology of Combustion*. Elsevier Science, 2002.
- [94] Y. Huang and V. Yang, "Dynamics and stability of lean-premixed swirl-stabilized combustion," *Prog. Energy Combust. Sci.*, vol. 35, no. 4, pp. 293–364, 2009.
- [95] M. Abdulsada, "Flashback and blowoff characteristics of gas turbine swirl combustor," PhD, Cardiff University, 2011.
- [96] W. Fick, "Characterisation and Effects of the Precessing Vortex Core," PhD, cardiff University, 1998.
- [97] J. M. B. and N. A. Chigier, *Combustion Aerodynamics*. London: Applied Science Publishers LTD, 1972.

- [98] P. Sayad, A. Schönborn, and J. Klingmann, "Experimental investigations of the lean blowout limit of different syngas mixtures in an atmospheric, premixed, variable-swirl burner," *Energy and Fuels*, vol. 27, no. 5, pp. 2783–2793, 2013.
- [99] Y. M. Al-Abdeli and A. R. Masri, "Recirculation and flowfield regimes of unconfined non-reacting swirling flows," *Exp. Therm. Fluid Sci.*, vol. 27, no. 5, pp. 655–665, 2003.
- [100] M. Dular and R. Bachert, "The issue of strouhal number definition in cavitating flow," *Stroj. Vestnik/Journal Mech. Eng.*, vol. 55, no. 11, pp. 666–674, 2009.
- [101] O. Lucca-Negro and T. O'Doherty, "Vortex breakdown: A review," *Prog. Energy Combust. Sci.*, vol. 27, no. 4, pp. 431–481, 2001.
- [102] J. Lewis, "The Behaviour of Swirling Flames Under Variable Fuel Composition," PhD Thesis, Cardiff University, 2014.
- [103] C. Syred, W. Fick, A. J. Griffiths, and N. Syred, "Cyclone gasifier and cyclone combustor for the use of biomass derived gas in the operation of a small gas turbine in cogeneration plants," *Fuel*, vol. 83, pp. 2381–2392, 2004.
- [104] A. Valera-Medina, N. Syred, and A. Griffiths, "Visualisation of isothermal large coherent structures in a swirl burner," *Combust. Flame*, vol. 156, no. 9, pp. 1723–1734, 2009.
- [105] N. S. A. Bagdanavicius and N. S. A. Griffiths, "Premixed Swirl Combustion and Flashback Analysis with Hydrogen/Methane Mixtures," in *AIAA 47th Aerospace Sciences Meeting. Florida*, 2010, no. 4-7 January, p. 1169.
- [106] I. Chterev *et al.*, "Flame and flow topologies in an annular swirling flow," *Combust. Sci. Technol.*, vol. 186, no. 8, pp. 1041–1074, 2014.
- [107] A. Bagdanavicius, P. J. Bowen, D. Bradley, M. Lawes, and M. S. Mansour, "Stretch rate effects and flame surface densities in premixed turbulent combustion up to 1.25 MPa," *Combust. Flame*, vol. 162, no. 11, pp. 4158–4166, 2015.
- [108] M. G. fuLL, "Vortex breakdown," *Annu. Rev. Fluid Mech.*, vol. 4, no. 1, pp. 195–218, 1972.
- [109] S. Leibovich, "the Structure of Vortex Breakdown," *Annu. Rev. Fluid Mech.*, vol. 265, no. 1969, pp. 75–97, 1983.
- [110] S. Leibovich, "Vortex stability and breakdown - Survey and extension," *AIAA J.*, vol. 22, no. 9, pp. 1192–1206, 1984.
- [111] M. P. ESCUDIER and J. KELLER, "Recirculation in Swirling Flow: A Manifestation of Vortex Breakdown," *AIAA J.*, vol. 23, no. 1, pp. 111–116, 1985.
- [112] M. Vanierschot and E. Van den Bulck, "Hysteresis in flow patterns in annular swirling jets," *Exp. Therm. Fluid Sci.*, vol. 31, no. 6, pp. 513–524, 2007.
- [113] B. Schuermans, V. Bellucci, F. Guethe, F. Meili, P. Flohr, and C. O. Paschereit, "A Detailed Analysis of Thermoacoustic Interaction Mechanisms in a Turbulent Premixed Flame," in *Proceeding of ASME Turbo Expo 2004, Vienna, Austria*, 2004, pp. 539–551.

- [114] D. Mourtazin and J. Cohen, "The effect of buoyancy on vortex breakdown in a swirling jet," *J. Fluid Mech.*, vol. 571, pp. 177–189, 2007.
- [115] E. Serre and P. Bontoux, "Vortex breakdown in a three-dimensional swirling flow," *J. Fluid Mech.*, vol. 459, pp. 347–370, 2002.
- [116] C. O. Paschereit and E. Gutmark, "Control of High-Frequency Thermoacoustic Pulsations by Distributed Vortex Generators," *AIAA J.*, vol. 44, no. 3, pp. 550–557, 2006.
- [117] J. Dawson, "An investigation into naturally excited Helmholtz oscillations in a swirl burner/furnace system," PhD, Cardiff University, Wales, UK, 2000.
- [118] P. J. Smith, L. D. Smoot, and D. G. Sloan, "Modeling of swirl in turbulent flow systems," *Prog. Energy Combust. Sci.*, vol. 12, no. 3, pp. 163–250, 1986.
- [119] N. A. BEÉR, J. M. & CHIGIER, *Combustion Aerodynamics*. Applied Science, 1972.
- [120] and S. N. Gupta A.K., Lilley D.G., *Swirl Flow*. Abacus Press, 1984.
- [121] A. Valera-Medina, N. Syred, P. Kay, and A. Griffiths, "Central recirculation zone analysis in an unconfined tangential swirl burner with varying degrees of premixing," *Exp. Fluids*, vol. 50, no. 6, pp. 1611–1623, 2011.
- [122] J. O. N. Runyon, "Gas Turbine Fuel Flexibility: Pressurized Swirl Flame Stability, Thermoacoustics, and Emissions," PhD Thesis, Cardiff University, 2017.
- [123] A. K. Gupta, J. M. Beér, and J. Swithenbank, "Concentric Multi-annular Swirl Burner: Stability Limits and Emission Characteristics," *Proc. Combust. Inst.*, vol. 16, no. 1, pp. 79–91, 1977.
- [124] P. A. DELLENBACK, D. E. METZGER, and G. P. NEITZEL, "Measurements in Turbulent Swirling Flow Through an Abrupt Axisymmetric Expansion," *AIAA J.*, vol. 26, no. 6, pp. 669–681, 1988.
- [125] D. Froud, T. O'Doherty, and N. Syred, "Phase Averaging of the Precessing Vortex Core in a Swirl Burner Under Piloted and Premixed Combustion Conditions," *J. Power Energy, Part A*, vol. 210, pp. 383–395, 1996.
- [126] N. Syred, W. Fick, T. O'Doherty, and A. J. Griffiths, "The Effect of the Precessing Vortex Core on Combustion in a Swirl Burner," *Combust. Sci. Technol.*, vol. 125, no. 1–6, pp. 139–157, 1997.
- [127] P. M. Anacleto, E. C. Fernandes, M. V. Heitor, and S. I. Shtork, "Swirl Flow Structure and Flame Characteristics in a Model Lean Premixed Combustor," *Combust. Sci. Technol.*, vol. 175, no. 8, pp. 1369–1388, 2003.
- [128] S. Wang, V. Yang, G. Hsiao, S. Y. Hsieh, and H. C. Mongia, "Large-eddy Simulations of Gas-turbine Swirl Injector Flow Dynamics," *J. Fluid Mech.*, vol. 583, pp. 99–122, 2007.
- [129] L. Selle *et al.*, "Compressible Large Eddy Simulation of Turbulent Combustion in Complex Geometry on Unstructured Meshes," *Combust. Flame*, vol. 137, no. 4, pp. 489–505, 2004.

- [130] S. Roux, G. Lartigue, T. Poinso, U. Meier, and C. Bérat, "Studies of mean and unsteady flow in a swirled combustor using experiments, acoustic analysis, and large eddy simulations," *Combust. Flame*, vol. 141, no. 1–2, pp. 40–54, 2005.
- [131] P. Wang, X. S. Bai, M. Wessman, and J. Klingmann, "Large eddy simulation and experimental studies of a confined turbulent swirling flow," *Phys. Fluids*, vol. 16, no. 9, pp. 3306–3324, 2004.
- [132] B. Guo, T. A. G. Langrish, and D. F. Fletcher, "Simulation of turbulent swirl flow in an axisymmetric sudden expansion," *AIAA J.*, vol. 39, no. 1, pp. 96–102, 2012.
- [133] S. Terhaar, "Identification and Modeling of Coherent Structures in Swirl-Stabilized Combustors at Dry and Steam-Diluted Conditions," PhD, Technische Universität Berlin, 2015.
- [134] T. Sarpkaya, "On stationary and travelling vortex breakdowns," *J. Fluid Mech.*, vol. 45, no. 3, pp. 545–559, 1971.
- [135] T. C. Lieuwen and V. Yang, *Combustion Instabilities in Gas Turbine Engines: Operational Experience, Fundamental Mechanisms, and Modeling*. AIAA, Prog Astronautics Aeronautics. U.S.A., 2005.
- [136] S. V. Alekseenko, P. A. Kuibin, V. L. Okulov, and S. I. Shtork, "Helical vortices in swirl flow," *J. Fluid Mech.*, vol. 382, pp. 195–243, 1999.
- [137] N. Syred, T. O'doherty, and D. Froud, "The Interaction of the Precessing Vortex Core and Reverse Flow Zone in the Exhaust of a Swirl Burner," *Proc. Inst. Mech. Eng. Part A J. Power Energy*, vol. 208, no. 1, pp. 27–36, 1994.
- [138] T. O'doherty, D. Froud, C. J. Bates, and N. Syred, "Characteristics of a Power Station Boiler," *Proc. Inst. Mech. Eng. Part A J. Power Energy*, vol. 208, no. 2, pp. 89–101, 1994.
- [139] R. CHANAUD, "Observations of Oscillatory Motion in Certain Swirling Flows," *Journal Fluid Mech.*, vol. 21, p. 111, 1962.
- [140] M. García-Villalba, J. Fröhlich, and W. Rodi, "Identification and analysis of coherent structures in the near field of a turbulent unconfined annular swirling jet using large eddy simulation," *Phys. Fluids*, vol. 18, no. 5, pp. 1–18, 2006.
- [141] L. Selle, L. Benoit, T. Poinso, F. Nicoud, and W. Krebs, "Joint use of compressible large-eddy simulation and Helmholtz solvers for the analysis of rotating modes in an industrial swirled burner," *Combust. Flame*, vol. 145, no. 1–2, pp. 194–205, 2006.
- [142] K. Oberleithner *et al.*, "Three-dimensional coherent structures in a swirling jet undergoing vortex breakdown: Stability analysis and empirical mode construction," *J. Fluid Mech.*, vol. 679, pp. 383–414, 2011.
- [143] M. Stöhr, I. Boxx, C. D. Carter, and W. Meier, "Experimental study of vortex-flame interaction in a gas turbine model combustor," *Combust. Flame*, vol. 159, no. 8, pp. 2636–2649, 2012.
- [144] M. Stöhr, C. M. Arndt, and W. Meier, "Effects of Damköhler Number on Vortex-flame Interaction in a Gas Turbine Model Combustor," *Proc. Combust. Inst.*, vol. 34, no. 2, pp. 3107–3115, 2013.

- [145] S. K. Dhanuka, J. E. Temme, J. F. Driscoll, and H. C. Mongia, "Vortex-shedding and mixing layer effects on periodic flashback in a lean premixed prevaporized gas turbine combustor," *Proc. Combust. Inst.*, vol. 32 II, no. 2, pp. 2901–2908, 2009.
- [146] A. Coghe, G. Solero, and G. Scribano, "Recirculation phenomena in a natural gas swirl combustor," *Exp. Therm. Fluid Sci.*, vol. 28, no. 7, pp. 709–714, 2004.
- [147] I. Boxx, C. D. Carter, M. Stöhr, and W. Meier, "Study of the mechanisms for flame stabilization in gas turbine model combustors using kHz laser diagnostics This article is part of the Topical Collection on Application of Laser Techniques to Fluid Mechanics 2012," *Exp. Fluids*, vol. 54, no. 5, 2013.
- [148] M. K. El_Hossaini, "Review of the New Combustion Technologies in Modern Gas Turbines," in *Progress in Gas Turbine Performance*, IntechOpen, 2013.
- [149] A. H. Lefebvre, *GAS Turbine Combustion*, Third edit. CRC press, 1998.
- [150] R. C. and H. M. Haynes J, Janssen J, "Advanced Combustion Systems for Next Generation Gas Turbines," *United States. Dept. Energy, Washington, D.C.; Oak Ridge, Tenn.*, 2006.
- [151] M. DP, *Fundamentals of Combustion*. Prentice-Hall Of India Pvt. Limited, 2008.
- [152] M. Flamme, "New combustion systems for gas turbines (NGT)," *Appl. Therm. Eng.*, vol. 24, no. 11–12, pp. 1551–1559, 2004.
- [153] G. Baumgartner, L. R. Boeck, and T. Sattelmayer, "Experimental Investigation of the Transition Mechanism From Stable Flame to Flashback in a Generic Premixed Combustion System With High-Speed Micro-Particle Image Velocimetry and Micro-PLIF Combined With Chemiluminescence Imaging," *J. Eng. Gas Turbines Power*, vol. 138, no. 2, p. 021501, 2015.
- [154] M. Utschick and T. Sattelmayer, "Flame Holding in the Premixing Zone of a Gas Turbine Model Combustor After Forced Ignition of H₂–Natural Gas–Air Mixtures," *J. Eng. Gas Turbines Power*, vol. 139, no. 4, p. 041504, 2016.
- [155] L. Rosentsvit *et al.*, "Extension of the Combustion Stability Range in Dry Low NO_x Lean Premixed Gas Turbine Combustor Using a Fuel Rich Annular Pilot Burner," *J. Eng. Gas Turbines Power*, vol. 136, no. 5, p. 051509, 2013.
- [156] S. Zhu and S. Acharya, "Flame Dynamics With Hydrogen Addition at Lean Blowout Limits," *J. Eng. Gas Turbines Power*, vol. 136, no. 5, p. 051506, 2013.
- [157] J. Fritz, M. Kr, and T. Sattelmayer, "Flashback Limits For Combustion Induced Vortex Breakdown In A Swirl Burner," *ASME TURBO EXPO 2002, Amsterdam, Netherlands*, 2002.
- [158] C. Eichler and T. Sattelmayer, "Premixed flame flashback in wall boundary layers studied by long-distance micro-PIV," *Exp. Fluids*, vol. 52, no. 2, pp. 347–360, 2012.
- [159] V.-Z. Marco Osvaldo, S. Nicholas, V.-M. Agustín, and D. la R.-U. Daniel, "Flashback Avoidance in Swirling Flow Burners," *Ing. Investig. y Tecnol.*, vol. 15, no. 4, pp. 603–614, 2015.

- [160] D. Ebi and N. T. Clemens, "Experimental investigation of upstream flame propagation during boundary layer flashback of swirl flames," *Combust. Flame*, vol. 168, pp. 39–52, 2016.
- [161] T. G. Reichel, S. Terhaar, and O. Paschereit, "Increasing Flashback Resistance in Lean Premixed Swirl-Stabilized Hydrogen Combustion by Axial Air Injection," *J. Eng. Gas Turbines Power*, vol. 137, no. 7, p. 071503, 2014.
- [162] B. Dam, G. Corona, M. Hayder, and A. Choudhuri, "Effects of syngas composition on combustion induced vortex breakdown (CIVB) flashback in a swirl stabilized combustor," *Fuel*, vol. 90, no. 11, pp. 3274–3284, 2011.
- [163] P. Sayad, A. Schönborn, M. Li, and J. Klingmann, "Visualization of Different Flashback Mechanisms for H₂/CH₄ Mixtures in a Variable-Swirl Burner," *J. Eng. Gas Turbines Power*, vol. 137, no. 3, p. 031507, 2014.
- [164] A. J. De Rosa, S. J. Peluso, B. D. Quay, and D. A. Santavicca, "The Effect of Confinement on the Structure and Dynamic Response of Lean-Premixed, Swirl-Stabilized Flames," *J. Eng. Gas Turbines Power*, vol. 138, no. 6, p. 061507, 2015.
- [165] J. Lewis, A. Valera-Medina, R. Marsh, and S. Morris, "Augmenting the Structures in a Swirling Flame via Diffusive Injection," *J. Combust.*, vol. 2014, pp. 1–16, 2014.
- [166] M. Abdulsada, N. Syred, A. Giles, and P. J. Bowen, "Tangential Velocity Effects and Correlations for Blow-Off and Flashback in a Generic Swirl Burner and the Effect of a Hydrogen containing Fuel," in *51st AIAA Aerospace Sciences Meeting including the New Horizons Forum and Aerospace Exposition*, 2013, no. January, pp. 1–15.
- [167] and R. K. N. Syred, C. Wong, R.-M. v, J. Dawson, "Characterisation of the Occurrence of the Precessing Vortex Core in Partially Premixed and Non-Premixed Swirling Flow," *Present. 12th Int. Symp. Appl. Laser Tech. to Fluid Mech. (12th 2004 Lisbon, Port., 2004*.
- [168] J. O'Connor, V. Acharya, and T. Lieuwen, "Transverse combustion instabilities: Acoustic, fluid mechanic, and flame processes," *Prog. Energy Combust. Sci.*, vol. 49, pp. 1–39, 2015.
- [169] S. Candel, D. Durox, T. Schuller, J.-F. Bourgouin, and J. P. Moeck, "Dynamics of Swirling Flames," *Annu. Rev. Fluid Mech.*, vol. 46, no. 1, pp. 147–173, 2013.
- [170] P. Strakey, T. Sidwell, and J. Ontko, "Investigation of the effects of hydrogen addition on lean extinction in a swirl stabilized combustor," *Proc. Combust. Inst.*, vol. 31 II, no. 2, pp. 3173–3180, 2007.
- [171] J. P. Longwell, E. E. Frost, and M. A. Weiss, "Flame Stability in Bluff Body Recirculation Zones," *Ind. Eng. Chem.*, vol. 45, no. 8, pp. 1629–1633, 1953.
- [172] S. L. Plee and A. M. Mellor, "Characteristic time correlation for lean blowoff of bluff-body-stabilized flames," *Combust. Flame*, vol. 35, pp. 61–80, 1979.
- [173] K. Radhakrishnan, J. B. Heywood, and R. J. Tabaczynski, "Premixed turbulent flame blowoff velocity correlation based on coherent structures in turbulent flows," *Combust. Flame*, vol. 42, no. C, pp. 19–33, 1981.

- [174] D. R. Noble, Q. Zhang, A. Shareef, J. Tootle, A. Meyers, and T. Lieuwen, "Syngas Mixture Composition Effects Upon Flashback and Blowout," in *Proceedings of ASME Turbo Expo. 2006. Barcelona, Spain: ASME.*, 2006.
- [175] T. Lieuwen, V. McDonnell, E. Petersen, and D. Santavicca, "Fuel Flexibility Influences on Premixed Combustor Blowout, Flashback, Autoignition, and Stability," *J. Eng. Gas Turbines Power*, vol. 130, no. 1, p. 011506, 2008.
- [176] T. Lieuwen, S. Shanbhogue, S. Khosla, and C. Smith, "Dynamics of Bluff Body Flames Near Blowoff," in *45th AIAA Aerospace Sciences Meeting and Exhibit, ed: American Institute of Aeronautics and Astronautics*, 2007.
- [177] B. Roy Chowdhury and B. M. Cetegen, "Experimental study of the effects of free stream turbulence on characteristics and flame structure of bluff-body stabilized conical lean premixed flames," *Combust. Flame*, vol. 178, pp. 311–328, 2017.
- [178] D. E. Cavaliere, J. Kariuki, and E. Mastorakos, "A comparison of the blow-off behaviour of swirl-stabilized premixed, non-premixed and spray flames," *Flow, Turbul. Combust.*, vol. 91, no. 2, pp. 347–372, 2013.
- [179] J. De Vries and E. L. Petersen, "Autoignition of methane-based fuel blends under gas turbine conditions," *Proc. Combust. Inst.*, vol. 31 II, no. 2, pp. 3163–3171, 2007.
- [180] A. Lantz, R. Collin, M. Aldén, A. Lindholm, J. Larfeldt, and D. Lörstad, "Investigation of Hydrogen Enriched Natural Gas Flames in a SGT-700/800 Burner Using OH PLIF and Chemiluminescence Imaging," *J. Eng. Gas Turbines Power*, vol. 137, no. 3, p. 031505, 2014.
- [181] M. Kröner, T. Sattelmayer, J. Fritz, F. Kiesewetter, and C. Hirsch, "Flame propagation in swirling flows - Effect of local extinction on the combustion induced vortex breakdown," *Combust. Sci. Technol.*, vol. 179, no. 7, pp. 1385–1416, 2007.
- [182] B. Dam, N. Love, and A. Choudhuri, "Flashback propensity of syngas fuels," *Fuel*, vol. 90, no. 2, pp. 618–625, 2011.
- [183] D. Beerer, V. McDonnell, P. Therkelsen, and R. K. Cheng, "Flashback and Turbulent Flame Speed Measurements in Hydrogen/Methane Flames Stabilized by a Low-Swirl Injector at Elevated Pressures and Temperatures," *J. Eng. Gas Turbines Power*, vol. 136, no. 3, p. 031502, 2013.
- [184] M. Kröner, J. Fritz, and T. Sattelmayer, "Flashback Limits for Combustion Induced Vortex Breakdown in a Swirl Burner," in *ASME TURBO EXPO 2002, Amsterdam, The Netherlands*, 2002.
- [185] M. K. Kröner and T. S. Jassin Fritz, "Flashback In A Swirl Burner With Cylindrical Premixing Zone," in *Proceedings of ASME TURBO EXPO 2001, New Orleans, Louisiana*, 2001.
- [186] A. N. Lipatnikov and J. Chomiak, "Molecular transport effects on turbulent flame propagation and structure," *Prog. Energy Combust. Sci.*, vol. 31, no. 1, pp. 1–73, 2005.
- [187] B. Lewis and G. von Elbe, "Stability and Structure of Burner Flames," *J. Chem. Phys.*, vol. 11, no. 2, pp. 75–97, 1943.

- [188] K. Wohl, "Quenching, flash-back, blow-off-theory and experiment," in *4th Symposium (Int.) on Combustion. 1953. Pittsburgh, PA: The combustion Institute*, 1953, pp. 68–89.
- [189] C. Eichler and T. Sattelmayer, "Experiments on Flame Flashback in a Quasi-2D Turbulent Wall Boundary Layer for Premixed Methane-Hydrogen-Air Mixtures," *J. Eng. Gas Turbines Power*, vol. 133, no. 1, p. 011503, 2010.
- [190] Y.-C. Lin, S. Daniele, P. Jansohn, and K. Boulouchos, "Turbulent Flame Speed as an Indicator for Flashback Propensity of Hydrogen-Rich Fuel Gases," *J. Eng. Gas Turbines Power*, vol. 135, no. 11, p. 111503, 2013.
- [191] K. Yamazaki and H. Tsuji, "An experimental investigation on the stability of turbulent burner flames," *8th Symp. Combust. Combust. Inst. Calif.*, pp. 543–553, 1961.
- [192] B. Fine, "The flashback of laminar and turbulent burner flames at reduced pressure," *Combust. Flame*, vol. 2, no. 3, pp. 253–266, 1958.
- [193] M. Al-Fahham, A. V. Medina, F. A. Hatem, S. Bigot, A. S. Alsaegh, and R. Marsh, "Experimental study to enhance resistance for boundary layer flashback in swirl burners using microspheres," in *Proceedings of the ASME Turbo Expo*, 2017.
- [194] S. L. Plee and A. M. Mellor, "Reply to comments by C. M. Coats on 'Review of flashback reported in prevaporizing/premixing combustors,'" *Combust. Flame*, vol. 32, pp. 193–203, 1978.
- [195] D. J. Beerer and V. G. McDonnell, "Autoignition of Hydrogen and Air Inside a Continuous Flow Reactor With Application to Lean Premixed Combustion," *J. Eng. Gas Turbines Power*, vol. 130, no. 5, p. 051507, 2008.
- [196] M. Konle, A. Winkler, F. Kiesewetter, J. Wäsle, and T. Sattelmayer, "CIVB Flashback Analysis with Simultaneous and Time Resolved PIV-LIF Measurements," in *13th Int Symp on Applications of Laser Techniques to Fluid Mechanics Lisbon, Portugal*, 2006.
- [197] A. Umemura and K. Tomita, "Rapid flame propagation in a vortex tube in perspective of vortex breakdown phenomena," in *Proceedings of ASME Turbo Expo 2006. Barcelona, Spain*, 2006.
- [198] F. Kiesewetter, M. Konle, and T. Sattelmayer, "Analysis of Combustion Induced Vortex Breakdown Driven Flame Flashback in a Premix Burner With Cylindrical Mixing Zone," *J. Eng. Gas Turbines Power*, vol. 129, no. 4, p. 929, 2007.
- [199] M. Konle and T. Sattelmayer, "Interaction of heat release and vortex breakdown during flame flashback driven by combustion induced vortex breakdown," *Exp. Fluids*, vol. 47, no. 4–5, pp. 627–635, 2009.
- [200] J. Lewis, A. Valera-medina, S. Morris, and R. Marsh, "The Use Of Co2 To Improve Stability And Emissions Of An Igcc Combustor," in *Proceedings of ASME Turbo Expo 2014, Düsseldorf, Germany*, 2014.
- [201] A. Valera-Medina, N. Syred, P. Bowen, and A. Crayford, "Studies of Swirl Burner Characteristics, Flame Lengths and Relative Pressure Amplitudes," *J. Fluids Eng.*, vol. 133, no. 10, p. 101302, 2011.

- [202] A. Valera-Medina, N. Syred, and P. Bowen, "Central Recirculation Zone Visualization in Confined Swirl Combustors for Terrestrial Energy," *J. Propuls. Power*, vol. 29, no. 1, pp. 195–204, 2012.
- [203] D.L. Darmofal, "The Role of Vorticity Dynamics in Vortex Breakdown," in *AIAA, Fluid Dynamics Conference, 24th: Orlando, FL*, 1993.
- [204] R. L. Panton, *Incompressible flow*. New York: John Wiley & Sons, Inc., 1996.
- [205] S. Burmberger and T. Sattelmayer, "Optimization of the Aerodynamic Flame Stabilization for Fuel Flexible Gas Turbine Premix Burners," *J. Eng. Gas Turbines Power*, vol. 133, no. 10, p. 101501, 2011.
- [206] C. Mayer, J. Sangl, T. Sattelmayer, T. Lachaux, and S. Bernero, "Study on the Operational Window of a Swirl Stabilized Syngas Burner Under Atmospheric and High Pressure Conditions," *J. Eng. Gas Turbines Power*, vol. 134, no. 3, p. 031506, 2012.
- [207] R. Balachandran, "Dynamics of bluff-body stabilised flames subjected to equivalence ratio oscillations," in *Proceedings of the European Combustion Meeting 2011, Cardiff, Great Britain*, 2011.
- [208] B. Shaffer, Z. Duan, and V. McDonell, "Study of Fuel Composition Effects on Flashback Using a Confined Jet Flame Burner," *J. Eng. Gas Turbines Power*, vol. 135, no. 1, p. 011502, 2012.
- [209] G. Baumgartner and T. Sattelmayer, "Experimental Investigation of the Flashback Limits and Flame Propagation Mechanisms for Premixed Hydrogen-Air Flames in Non-Swirling and Swirling Flow," in *Proceedings of ASME Turbo Expo, San Antonio, Texas, USA*, 2013.
- [210] P. Sayad, A. Schönborn, M. Li, and J. Klingmann, "Visualization of Different Flashback Mechanisms for H₂/CH₄ Mixtures in a Variable-Swirl Burner," *J. Eng. Gas Turbines Power*, vol. 137, no. 3, p. 031507, 2015.
- [211] F. A. Hatem, A. S. Alsaegh, M. Al-Faham, A. Valera-Medina, C. T. Chong, and S. M. Hassoni, "Enhancing flame flashback resistance against Combustion Induced Vortex Breakdown and Boundary Layer Flashback in swirl burners," *Appl. Energy*, vol. 230, no. September, pp. 946–959, 2018.
- [212] C. M. Arndt, M. Severin, C. Dem, M. Stöhr, A. M. Steinberg, and W. Meier, "Experimental analysis of thermo-acoustic instabilities in a generic gas turbine combustor by phase-correlated PIV, chemiluminescence, and laser Raman scattering measurements," *Exp. Fluids*, vol. 56, no. 4, pp. 1–23, 2015.
- [213] M. Molière, "Stationary gas turbines and primary energies: A review of fuel influence on energy and combustion performances," *Int. J. Therm. Sci.*, vol. 39, no. 2, pp. 141–172, 2000.
- [214] K. K. Gupta, A. Rehman, and R. M. Sarviya, "Bio-fuels for the gas turbine: A review," *Renew. Sustain. Energy Rev.*, vol. 14, no. 9, pp. 2946–2955, 2010.
- [215] I. Gökalp and E. Lebas, "Alternative fuels for industrial gas turbines (AFTUR)," *Appl. Therm. Eng.*, vol. 24, no. 11–12, pp. 1655–1663, 2004.
- [216] G. L. Juste, "Hydrogen injection as additional fuel in gas turbine combustor. Evaluation of effects," *Int. J. Hydrogen Energy*, vol. 31, no. 14, pp. 2112–2121, 2006.

- [217] R. Jones, J. Goldmeier, and B. Monetti, "Addressing Gas Turbine Fuel Flexibility," *GE Energy*, vol. GER-4601, 2011.
- [218] United Kingdom Health and Safety Executive, "Gas Safety (Management) Regulations 1996 – GS(M)R; 1996. [cited 18 May 2014]." [Online]. Available: <http://www.legislation.gov.uk/ukxi/1996/551/contents/made>.
- [219] E. M. R S Cant, *An Introduction to Turbulent Reacting Flows*. Imperial College Press, 2008.
- [220] A. Sharma and S. Jayanti, "CFD Modeling of Oxygen-Enhanced Combustion," in *Oxygen-Enhanced Combustion*, 2nd Editio., Boca Raton, FL, CRC Press, 2013.
- [221] Dantec Dynamics, *Turbulence Handbook for Experimental Fluid Mechanics Professionals*. Dantec Dynamics, 2009.
- [222] J. Turnbull, "A Novel Approach to Reduce the Computation Time for CFD; Hybrid LES–RANS Modelling on Parallel Computers," PhD Thesis, School of Engineering, Cranfield University, 2003.
- [223] ANSYS Inc, "ANSYS Fluent Theory Guide," 2016.
- [224] S. V. Patankar, *Numerical Heat Transfer and Fluid Flow*. Taylor and Francis, 1980.
- [225] W. Hübner, J. Volkert, N. Grosjean, M. Michard, L. Graftieaux, and C. Tropea, "Combining LDA and PIV for turbulence measurements in unsteady swirling flows," *Meas. Sci. Technol.*, vol. 8, no. 12, pp. 1523–1532, 1997.
- [226] A. Sayma, *Computational Fluid Dynamics*. Ventus Publishing ApS, 2012.
- [227] W. T. Su, X. Bin Li, F. C. Li, X. Z. Wei, Z. Y. Zheng, and X. Zhang, "Comparisons of les and RANS computations with PIV experiments on a cylindrical cavity flow," *Adv. Mech. Eng.*, 2013.
- [228] F. Xing, Y. Huang, M. Zhao, and J. Zhao, "The Brief Introduction of Different Laser Diagnostics Methods Used in Aeroengine Combustion Research," *J. Sensors*, vol. 2016, pp. 1–13, 2016.
- [229] M. Riethmuller, L. David, and B. Lecordier, "Particle Image Velocimetry," in *Laser Velocimetry in Fluid Mechanics*, A. Boutier, Ed. ISTE Ltd, 2012, pp. 160–281.
- [230] Z. Shi, Y. Hardalupas, and A. M. K. P. Taylor, "Laser-induced plasma image velocimetry," *Exp. Fluids*, vol. 60, no. 1, p. 0, 2019.
- [231] C. Tropea, "Laser doppler anemometry: Recent developments and future challenges," *Meas. Sci. Technol.*, vol. 6, no. 6, pp. 605–619, 1995.
- [232] DANTIC DYNAMICS, "Measurement principles of LDA," 2018. [Online]. Available: <https://www.dantecdynamics.com/measurement-principles-of-lda>.
- [233] A. Bagdanavicius, "Premixed Combustion of Alternative Fuels Under Varying Conditions of Temperature and Pressure," PhD Thesis, Cardiff University, 2010.
- [234] E. P. Hassel and S. Linow, "Laser diagnostics for studies of turbulent combustion," *Meas. Sci. Technol.*, vol. 11, no. 2, 2000.

- [235] A Melling, "Tracer Particles and Seeding for Particle Image Velocimetry," *Meas. Sci. Technol.*, vol. 8, no. 12, p. 1406, 1997.
- [236] J. F. F. Cameron Tropea, Alexander L. Yarin, *Springer Handbook of Experimental Fluid Mechanics*. 2007.
- [237] ANSYS, "Structural nonlinearities, User's guide for revision 5.5." 1997.
- [238] H. K. Versteeg and W. Malaskechera, *An Introduction to Computational Fluid Dynamics: The Finite Volume Method*. Longman Group Ltd, 1995.
- [239] Shelil N, "Flashback Studies with Premixed Swirl Combustion," PhD Thesis, Cardiff University, 2009.
- [240] N. K. Aluri, "Numerical Modelling of Turbulent Premixed Combustion for Gas Turbine Conditions with Incorporation of Molecular Transport Effects," University of Siegen, 2007.
- [241] D. Corson, R. Jaiman, and F. Shakib, "Industrial application of RANS modelling: capabilities and needs," *Int. J. Comput. Fluid Dyn.*, vol. 23, no. 4, pp. 337–347, Apr. 2009.
- [242] N. Syred, "40 years with Swirl, Vortex, Cyclonic Flows, and Combustion," in *49th AIAA Aerospace Sciences Meeting*, 2011.
- [243] S. P. Muppala and S. P. M. Vasudevan, "RANS studies of hydrogen-enrichment premixed turbulent flames," *IOP Conf. Ser. Mater. Sci. Eng.*, vol. 1080, no. 1, p. 012046, Feb. 2021.
- [244] H. SCHLICHTING, *Boundary-Layer Theory*. McGRAW-HILL, 1970.
- [245] C. Heeger, R. L. Gordon, M. J. Tummers, T. Sattelmayer, and A. Dreizler, "Experimental analysis of flashback in lean premixed swirling flames: Upstream flame propagation," *Exp. Fluids*, vol. 49, no. 4, pp. 853–863, 2010.
- [246] E. Tangermann, M. Pfitzner, M. Konle, and T. Sattelmayer, "Large-eddy simulation and experimental observation of combustion-induced vortex breakdown," *Combust. Sci. Technol.*, vol. 182, no. 7, pp. 505–516, 2010.
- [247] A. A. Chaparro and B. M. Cetegen, "Blowoff characteristics of bluff-body stabilized conical premixed flames under upstream velocity modulation," *Combust. Flame*, vol. 144, no. 1–2, pp. 318–335, 2006.
- [248] K. S. Kedia and A. F. Ghoniem, "The blow-off mechanism of a bluff-body stabilized laminar premixed flame," *Combust. Flame*, vol. 162, no. 4, pp. 1304–1315, 2015.
- [249] S. Chaudhuri, S. Kostka, M. W. Renfro, and B. M. Cetegen, "Blowoff dynamics of bluff body stabilized turbulent premixed flames," *Combust. Flame*, vol. 157, no. 4, pp. 790–802, 2010.
- [250] A. Nauert, P. Petersson, M. Linne, and A. Dreizler, "Experimental analysis of flashback in lean premixed swirling flames: Conditions close to flashback," *Exp. Fluids*, vol. 43, no. 1, pp. 89–100, 2007.
- [251] T. Reichel, "Experimental Investigation of Flame Stability of Swirl-Stabilized , Lean Pre- mixed Hydrogen Flames," 2014.

- [252] M. Konle, F. Kiewewetter, and T. Sattelmayer, "Simultaneous high repetition rate PIV-LIF-measurements of CIVB driven flashback," *Exp. Fluids*, vol. 44, no. 4, pp. 529–538, 2008.
- [253] A. E. E. Khalil and A. K. Gupta, "Velocity and turbulence effects on high intensity distributed combustion," *Appl. Energy*, vol. 125, pp. 1–9, 2014.
- [254] A. E. E. Khalil and A. K. Gupta, "Toward ultra-low emission distributed combustion with fuel air dilution," *Appl. Energy*, vol. 148, no. x, pp. 187–195, 2015.
- [255] A. E. E. Khalil and A. K. Gupta, "Hydrogen addition effects on high intensity distributed combustion," *Appl. Energy*, vol. 104, pp. 71–78, 2013.
- [256] N. Syred, F. A. Hatem, A. Valera-Medina, and P. J. Bowen, "Experimental investigation of the Effect of Air Diffusive injection on premixing swirl flames," *55th AIAA Aerosp. Sci. Meet.*, no. January, pp. 1–10, 2017.
- [257] S. Taamallah, K. Vogiatzaki, F. M. Alzahrani, E. M. A. Mokheimer, and M. A. Habib, "Erratum to ' Fuel fl exibility , stability and emissions in premixed hydrogen-rich gas turbine combustion : Technology , fundamentals , and numerical simulations ' [Appl Energy 154 (2015) 1020 – 1047]," *Appl. Energy*, vol. 219, no. January, p. 426, 2018.
- [258] C. Degroot and J. M. Floryan, "Drag Reduction Due to Streamwise Grooves in Turbulent Channel Flow," no. August 2020, 2016.
- [259] L.N.KhitrinP.B.MoinD.B.SmirnovV.U.Shevchuk, "Peculiarities of laminar- and turbulent-flame flashbacks," *Symp. Combust.*, vol. 10, no. 1, pp. 1285–1291, 2007.
- [260] A. Gruber, J. H. Chen, D. Valiev, and C. K. Law, "Direct numerical simulation of premixed flame boundary layer flashback in turbulent channel flow," pp. 516–542, 2012.
- [261] S. Martin and B. Bhushan, "Journal of Colloid and Interface Science Modeling and optimization of shark-inspired riblet geometries for low drag applications," *J. Colloid Interface Sci.*, vol. 474, pp. 206–215, 2016.
- [262] ZHANGDe-yuanLUOYue-haoLIXiangCHENHua-wei, "Numerical simulation and experimental study of drag-reducing surface of a real shark skin," *J. Hydrodyn. Ser. B*, vol. 23, no. 2, pp. 204–211, 2011.
- [263] S. Martin, And, and B. Bhushan, *Fluid flow analysis of a shark-inspired microstructure*. 2014.
- [264] N. Syred, R. Marsh, F. A. Hatem, P. J. Bowen, and A. Valera-Medina, "Experimental Investigation of the Effects of Central Fuel Injectors on Premixed Swirling Flames," pp. 1–8, 2015.
- [265] M. A. H. Al-fahham, "School of Engineering," 2017.
- [266] R. A. W. Benjamin W. Niebel , A. B. D., *Modern Manufacturing process Engineering*. 1989.
- [267] R. A. Antonia and P. Krogstad, "Turbulence structure in boundary layers over different types of surface roughness," *Fluid Dyn. Res.*, vol. 28, no. 2, pp. 139–157, 2001.

- [268] C. T. DeGroot, C. Wang, and J. M. Floryan, "Drag Reduction Due to Streamwise Grooves in Turbulent Channel Flow," *J. Fluids Eng.*, vol. 138, no. 12, p. 121201, 2016.
- [269] V. Hoferichter, C. Hirsch, and T. Sattelmayer, "Prediction of Confined Flame Flashback Limits Using Boundary Layer Separation Theory," *J. Eng. Gas Turbines Power*, vol. 139, no. 2, p. 021505, 2016.
- [270] V. TANGIRALA, R. H. CHEN, and J. F. DRISCOLL, "Effect of Heat Release and Swirl on the Recirculation within Swirl-Stabilized Flames," *Combust. Sci. Technol.*, vol. 51, no. 1–3, pp. 75–95, Jan. 1987.